



University
of Glasgow

Oni, Taiwo Oluwasesan (2015) Numerical investigation of heat transfer and fluid flow in tubes induced with twisted tape inserts. PhD thesis.

<http://theses.gla.ac.uk/6237/>

Copyright and moral rights for this thesis are retained by the author

A copy can be downloaded for personal non-commercial research or study, without prior permission or charge

This thesis cannot be reproduced or quoted extensively from without first obtaining permission in writing from the Author

The content must not be changed in any way or sold commercially in any format or medium without the formal permission of the Author

When referring to this work, full bibliographic details including the author, title, awarding institution and date of the thesis must be given.

Numerical Investigation of Heat Transfer and Fluid Flow in Tubes Induced with Twisted Tape Inserts

A thesis submitted for the degree
of Doctor of Philosophy

in the
School of Engineering
of the
University of Glasgow

By

Taiwo Oluwasesan ONI

B.Eng., M.Eng.

Systems, Power & Energy Research Division
School of Engineering
University of Glasgow UK

March, 2015

Copyright © 2015 by Taiwo Oni

All Rights Reserved

Dedication

This work is prayerfully dedicated to God, my parents, my wife & children and all those whose contributions in various forms have made my pursuits in life a success.

Declaration

This dissertation is the result of my own work. Any published ideas or techniques from other works are fully acknowledged in accordance with the standard referencing practices.

.....

Taiwo O. Oni

March, 2015

Abstract

Heat energy is important to all aspects of life. Various industries including food processing plants, chemical processing plants, thermal power plants, refrigeration and air conditioning equipments, petrochemical plants, etc. are faced with the problems of effective utilization, conservation and recovery of heat. The production of heat exchangers involves huge investments for capital and operation costs. In view of this, it has become important to design heat exchangers that will be efficient and also save energy, cost and materials. Different techniques known as heat transfer enhancement are employed to achieve this. Of these techniques, the tube-insert technology is applied in the present research.

No prior work on heat transfer and fluid flow in a tube induced with twisted tape insert with emphasis on cuts with different geometrical shapes but equal area has been reported. Hence, in the present work, heat transfer and fluid flow of water in tubes induced with twisted tape inserts with different-shape-equal-area cuts is investigated numerically.

The present studies pay attention to the thermo-hydraulic characteristics of laminar, transitional and turbulent flows of water through different tube designs fitted individually with twisted tape of different design under uniform wall heat flux. The numerical simulation in this work is carried out by using Fluent software. The RANS-based RNG $\kappa - \varepsilon$ model is employed for the turbulent flow because it is found to give a more accurate result than other turbulence models. Since transitional flow is not fully turbulent, the transitional variant of the SST $\kappa - \omega$ model is applied for the simulation of the transitional flow. The analyses quantify the improvement in the heat transfer, friction factor and thermal performance index in each of the tube

systems and these results are used to ascertain the system that gives the best performance. Correlations are also proposed for the Nusselt number and friction factor.

The results indicates that the superior fluid mixing provided by the alternate-axis triangular cut twisted tape is one of the reasons why it offers heat transfer enhancement and thermal performance factor that is higher than those that are offered by other induced tubes. Interestingly, the enhancement in heat transfer increases as the size of the cuts on the tape and the width of the tape increase but decreases as the pitch of the tape increases. The enhancement of heat transfer affects the start and the end of the transition to turbulent flow. Transition to turbulent flow occurs and ends earliest in the tube system with the highest heat transfer enhancement.

Investigation is also performed on the combined forced and free convection heat transfer in an inclined tube for laminar, transitional and turbulent flows. The induced tube is inclined at different angles ($15^\circ \leq \theta \leq 90^\circ$) with respect to the horizontal. Importantly, the heat transfer enhancement of the tube systems under mixed convection is higher than those under forced convection, and the enhancement for the mixed convection increases as the inclination angle increases.

Acknowledgement

Firstly, I thank God who has never lost a battle and who will not lose a battle on any matter on my life. He has been showing forth His light and will continue to show it in my life (Amen). The divine intervention really manifested. Nobody is like unto thee, O Lord. You are glorious in holiness, fearful in praises, and doing wonders. (Exo. 15:11)

I wish to express my matchless and sincere gratitude to my supervisor, Dr Manosh C. Paul. He was there for me. His constant encouragement, constructive criticisms, stimulating comments, inspiring determination, regular audience, and leadership quality, to mention a few, contributed meaningfully to the success of the programme.

The financial sponsorship provided for me by the Tertiary Education Trust Fund (TETFund) Abuja, the funding agency for the sponsorship, is tenaciously appreciated.

Words are inadequate to convey my profound appreciation to my employer, Ekiti State University Ado-Ekiti, Nigeria for the study leave approved for me and other enabling supports provided for me to undergo the programme. I also place on record all forms of official and personal assistance extended to me by staff of Mechanical Engineering Department and Faculty of Engineering of Ekiti State University Ado-Ekiti.

I remember my nuclear family, particularly my beloved spouse, Mrs R. O. Oni, who took charge of our matrimonial home throughout the period of my unavoidable “absence” from home. She carried a lot of responsibilities from my shoulders to let me concentrate on this research. I sincerely salute all her prayers, efforts and words of encouragement. Moreover, I cherish the care and concern of my children - Ayodeji, Oluwafunmilayo, Ayokunle,

Ayomisikusibe and Oluwafunmilola. They were able to endure my absence from home.

I am matchlessly grateful to my beloved parents who presented me in this life, struggled for me and made a phenomenal and difficult sacrifice in those days to ensure that I advance in my academic programme. I owe you much that I cannot possibly express. Also, I convey my peerless appreciation to my mother-in-law for all the unquantifiable supports I received from her.

I would like to express my appreciation to all members of academic staff, IT staff, technical staff and administrative staff of the School of Engineering, University of Glasgow for their efforts in sustaining the vision of the University.

I extend special appreciation to Professor W.O. Adebayo and Professor J. Kayode of Ekiti State University Ado-Ekiti for their fantastic contribution in making the programme a reality.

My immeasurable appreciation is dispatched to all those (either known or unknown to me) who raised prayers for me and my family towards the success of the programme.

Gratitude is due to my brothers, sisters, neighbours, members of my extended family and other too numerous to be mentioned who stood by me.

Finally, I would like to thank my colleagues: Al Waaly, Blaid Alganash, Goutam Saha and others for their words of encouragement.

Contents

Dedication	ii
Declaration	iii
Abstract	iv
Acknowledgement.....	vi
Contents	viii
List of Figures.....	xiii
List of Tables.....	xx
List of Symbols.....	xxi
List of Acronyms	xxiv
Chapter 1	1
INTRODUCTION.....	1
Chapter 2	7
LITERATURE REVIEW	7
2.1 Experimental Studies on Forced Convection in Tubes with Twisted Tape Inserts	8
2.1.1 Experimental laminar flow	8
2.1.2 Experimental transitional flow.....	11
2.1.3 Experimental turbulent flow	12
2.2 Computational Investigations on Forced Convection in Tubes with Twisted Tape Inserts.....	17
2.2.1 Computational laminar flow.....	17
2.2.2 Computational turbulent flow	19
2.3 Experimental and Numerical Works on Mixed Convection in Tubes..	21
2.3.1 Experimental works.....	22
2.3.2 Numerical works	23

2.4	Objectives of the Thesis.....	24
2.5	Layout of the Thesis	25
 Chapter 3.....		31
NUMERICAL METHODS		31
3.1	Introduction	31
3.2	Governing Equations	31
3.3	Turbulence Modelling	34
3.3.1	Standard $\kappa - \varepsilon$ model.....	36
3.3.2	RNG $\kappa - \varepsilon$ model	37
3.4	Transitional Modelling	39
3.4.1	Shear-Stress Transport (SST) $\kappa - \omega$ model	39
3.4.2	Standard $\kappa - \omega$ model.....	41
3.5	Boundary Conditions	42
3.6	Enhanced Wall Treatment	44
3.7	Numerical Techniques	46
 Chapter 4.....		48
NUMERICAL INVESTIGATION OF HEAT TRANSFER AND LAMINAR FLOW CHARACTERISTICS IN DIVERSE TUBE DESIGNS		48
4.1	Introduction	48
4.2	Model Geometry	49
4.3	Grid Resolution	51
4.4	Computational Results and Discussions	54
4.4.1	Flow field	54
4.4.2	Velocity contour	55
4.4.3	Temperature profile	57
4.4.4	Pressure distribution	58

4.4.5 Heat transfer assessment	60
4.4.6 Friction factor	63
4.4.7 Thermal performance factor	65
4.5 Correlations for the heat transfer and fluid flow.....	66
4.6 Conclusion	67
Chapter 5.....	90
NUMERICAL SIMULATION OF TURBULENT HEAT TRANSFER AND FLUID FLOW IN DIFFERENT TUBE DESIGNS.....	90
5.1 Introduction	90
5.2 Computational Domains	91
5.3 Grid Generation	92
5.4 Validation with Experimental Works	95
5.5 Results and Discussions	97
5.5.1 Flow field	97
5.5.2 Velocity contour	99
5.5.3 Temperature contours	100
5.5.4 Pressure contour	101
5.5.5 Turbulent kinetic energy	102
5.5.6 Heat transfer	104
5.5.7 Friction factor	106
5.5.8 Thermal performance factor	108
5.6 Comparison of the quantity of material and thermal performance of the different domains	109
5.7 Investigations of the Effects of Variations in the Tape Geometry of TATCT	110
5.8 Grid Generation for the Variations in the Tape Geometries of TATCT	111

5.9	Results for the Variations in the Tape Geometries of TATCT.....	113
5.9.1	Effect on the flow field	113
5.9.2	Effect on velocity vector	114
5.9.3	Effects on the heat transfer	115
5.9.4	Effects on friction factor	117
5.9.5	Effects on the thermal performance factor.....	118
5.10	Implication of Various Tape Geometries on Production Cost and Thermal Performance.....	120
5.11	Correlations for the Heat Transfer and Fluid Flow	121
5.12	Conclusion	122
Chapter 6.....		162
NUMERICAL STUDY OF THERMAL-HYDRAULIC CHARACTERISTICS IN THE TRANSITION REGIME IN AN INDUCED TUBE		162
6.1	Introduction	162
6.2	Flow Model	163
6.3	Grid independence Test	163
6.4	Comparison of Different Models.....	164
6.5	Computational Results and Discussions	165
6.5.1	Temperature contours	166
6.5.2	Velocity contour	166
6.5.3	Turbulent kinetic energy	167
6.5.4	Turbulent intensity	168
6.5.5	Heat transfer	169
6.5.6	Friction factor	170
6.5.7	Correlation for the transitional flow	173
6.6	Conclusion	174

Chapter 7.....	187
INVESTIGATION OF MIXED CONVECTION HEAT TRANSFER IN A FLOW THROUGH AN INDUCED TUBE	187
7.1 Introduction	187
7.2 Model Geometry	188
7.3 Grid Sensitivity Analysis	188
7.4 Computational Results and Discussions	189
7.4.1 Turbulent kinetic energy	190
7.4.2 Surface temperature	191
7.4.3 Temperature inside the domain	193
7.4.4 Outlet velocity and outlet temperature	193
7.4.1 Heat transfer	194
7.4.2 Friction factor	196
7.5 Conclusion	197
Chapter 8.....	212
CONCLUSIONS AND SUGGESTIONS FOR FURTHER RESEARCH	212
8.1 Conclusions	212
8.2 Suggestions for Future Research	214
REFERENCES	216

List of Figures

Figure 1.1: Configuration of a twisted tape.	6
Figure 2.1: Plain twisted tapes showing (a) plain tape without a tube ^[68] , (b) regularly-spaced plain twisted tape with a tube ^[10] , (c) continuous plain twisted tape with a tube ^[66] and (d) twin co-twisted tapes and twin counter twisted tapes ^[68]	28
Figure 2.2: Modified twisted tape for (a) trapezoidal cuts ^[64] , (b) square cuts ^[65] , (c) serrated cuts ^[66] , (d) oblique-tooth cuts ^[69] and (e) edgefold ^[87]	29
Figure 2.3: (a) Spirally corrugated tube ^[61] (a) start, pitch and lead of a spirally corrugated tube ^[61]	30
Figure 4.1: Tube.	70
Figure 4.2: Twisted tape.	70
Figure 4.3: Different types of twisted tape insert used for the domains: (a) PTT, (b) ECT, (c) CCT, (d) TCT, (e) AECT, (f) ACCT (g) ATCT.	71
Figure 4.4: Computational domains with twisted tape inserts for (a) TPT, (b) TECT, (c) TCCT, (d) TTCT, (e) TAECT, (f) TACCT and (g) TATCT.	72
Figure 4.5: Geometries of the cuts on the tapes for (a) elliptical cut, (b) circular cut and (c) triangular cut.	73
Figure 4.6: Sectional view of a computational domain for the tube induced with a plain twisted tape.	73
Figure 4.7: Temperature across the cross-section at the exit of (a) PT, (b) TPT, (c) TECT, (d) TCCT, (e) TTCT, (f) TAECT, (g) TACCT and (h) TATCT for $Re = 1820$ with different grids.	74
Figure 4.8: Velocity across the cross-section at the exit of (a) PT, (b) TPT, (c) TECT, (d) TCCT, (e) TTCT, (f) TAECT, (g) TACCT and (h) TATCT for $Re = 1820$ with different grids.	76
Figure 4.9: Streamlines across the domain cross-section at axial location $0.866m$ of (a) PT, (b) TPT, (c) TECT, (d) TCCT, (e) TTCT, (f) TAECT, (g) TACCT and (h) TATCT for $Re=1820$	78
Figure 4.10: Vector plot appended on contour of velocity for PT (A), TPT (B), TECT (C), TCCT (D), TTCT (E), TAECT (F), TACCT (G) and TATCT (H)	

for $Re=1820$ at axial location (a) $0.5m$, (b) $0.516m$, (c) $0.6m$, (d) $0.673m$ and (e) $0.7m$	79
Figure 4.11: Contour plots of temperature for PT (A), TPT (B), TECT (C), TCCT (D), TTCT (E), TAECT (F), TACCT (G) and TATCT (H) for $Re=1820$ at axial location (a) $0.5m$, (b) $0.516m$, (c) $0.6m$, (d) $0.673m$ and (e) $0.7m$. .	83
Figure 4.12: Contour plots of pressure for PT (A), TPT (B), TECT (C), TCCT (D), TTCT (E), TAECT (F), TACCT (G) and TATCT (H) for $Re=1820$ at axial location (a) $0.5m$, (b) $0.516m$, (c) $0.6m$, (d) $0.673m$ and (e) $0.7m$	84
Figure 4.13: Validation of Nusselt number of the plain tube.	85
Figure 4.14: Validation of Nusselt number of the tube induced with plain twisted tape insert.	85
Figure 4.15: Effect of different twisted tape on Nusselt number with Reynolds number.	86
Figure 4.16: Validation of friction factor of the plain tube.	86
Figure 4.17: Validation of friction factor of the tube induced with plain twisted tape insert.	87
Figure 4.18: Effect of different twisted tape on friction factor with Reynolds number.	87
Figure 4.19: Effect of different twisted tape on thermal performance factor with Reynolds number.	88
Figure 4.20: Comparison between simulated and predicted results for Nusselt number of laminar flow.	88
Figure 4.21: Comparison between simulated and predicted results for friction factor of laminar flow.	89
Figure 5.1: Temperature across the cross-section at the exit of (a) PT, (b) TPT, (c) TECT, (d) TCCT, (e) TTCT, (f) TAECT, (g) TACCT and (h) TATCT for $Re=20000$ for different grids.	127
Figure 5.2: Velocity across the cross-section at the exit of (a) PT, (b) TPT, (c) TECT, (d) TCCT, (e) TTCT, (f) TAECT, (g) TACCT and (h) TATCT for $Re=20000$ for different grids.	129

Figure 5.3: Turbulent kinetic energy across the cross-section at the exit of (a) PT, (b) TPT, (c) TECT, (d) TCCT, (e) TTCT, (f) TAECT, (g) TACCT and (h) TATCT for $Re=20000$ for different grids.....	131
Figure 5.4: Validation with experimental works for PT.....	133
Figure 5.5: Validation with experimental works for TPT.	133
Figure 5.6: Streamlines across the domain cross-section at axial location $0.866m$ of (a) PT, (b) TPT, (c) TECT, (d) TCCT, (e) TTCT, (f) TAECT, (g) TACCT and (h) TATCT for $Re=20000$	134
Figure 5.7: Streamlines for turbulent flow inside the domains of (a) PT, (b) TPT, (c) TECT, (d) TCCT, (e) TTCT, (f) TAECT, (g) TACCT and (h) TATCT.	135
Figure 5.8: Vector plot appended on velocity contour of velocity for PT (A), TPT (B), TECT (C), TCCT (D), TTCT (E), TAECT (F), TACCT (G) and TATCT (H) for $Re=20000$ at axial location (a) $0.5m$, (b) $0.516m$, (c) $0.6m$, (d) $0.673m$ and (e) $0.7m$	136
Figure 5.9: Contour plots of temperature for PT (A), TPT (B), TECT (C), TCCT (D), TTCT (E), TAECT (F), TACCT (G) and TATCT (H) for $Re=20000$ at axial location.....	140
Figure 5.10: Contour plots of pressure for PT (A), TPT (B), TECT (C), TCCT (D), TTCT (E), TAECT (F), TACCT (G) and TATCT (H) for $Re=20000$ at axial location (a) $0.5m$, (b) $0.516m$, (c) $0.6m$, (d) $0.673m$ and (e) $0.7m$	141
Figure 5.11: Contour plots of turbulent kinetic energy for PT (A), TPT (B), TECT (C), TCCT (D), TTCT (E), TAECT (F), TACCT (G) and TATCT (H) for $Re=20000$ at axial location (a) $0.5m$, (b) $0.516m$, (c) $0.6m$, (d) $0.673m$ and (e) $0.7m$	142
Figure 5.12: Effect of different twisted tape on Nusselt number vs. Reynolds number.	143
Figure 5.13: Validation of friction factor of plain tube.	143
Figure 5.14: Validation of friction factor of tube induced with plain twisted tape insert.	144
Figure 5.15: Effect of different twisted tape on friction factor vs. Reynolds number.	144

Figure 5.16: Effect of different twisted tape on thermal performance factor vs. Reynolds number.	145
Figure 5.17: Comparison of the quantity of material and the thermal performance of the different domains.	145
Figure 5.18: Geometries of the alternate-axis triangular cut twisted tape of (a) TATCT, (b) TATCT _{w1} , (c) TATCT _{w2} , (d) TATCT _{a1} , (e) TATCT _{a2} , (f) TATCT _{y1} and (g) TATCT _{y2}	146
Figure 5.19: Temperature across the cross-section at the exit of (a) TATCT, (b) TATCT _{w1} , (c) TATCT _{w2} , (d) TATCT _{a1} , (e) TATCT _{a2} , (f) TATCT _{y1} and (g) TATCT _{y2} for $Re=20000$ for different grids.	147
Figure 5.20: Velocity across the cross-section at the exit of (a) TATCT, (b) TATCT _{w1} , (c) TATCT _{w2} , (d) TATCT _{a1} , (e) TATCT _{a2} , (f) TATCT _{y1} and (g) TATCT _{y2} for $Re=20000$ for different grids	148
Figure 5.21: Turbulent kinetic energy (TKE) across the cross-section at the exit of (a) TATCT, (b) TATCT _{w1} , (c) TATCT _{w2} , (d) TATCT _{a1} , (e) TATCT _{a2} , (f) TATCT _{y1} and (g) TATCT _{y2} for $Re=20000$ for different grids.	149
Figure 5.22: Streamlines across the cross-section at axial location $0.866m$ of (a) TATCT, (b) TATCT _{w1} , (c) TATCT _{w2} , (d) TATCT _{a1} , (e) TATCT _{a2} , (f) TATCT _{y1} and (g) TATCT _{y2} for $Re=20000$	150
Figure 5.23: Streamlines for turbulent flow inside the domains of (a) TATCT, (b) TATCT _{w1} , (c) TATCT _{w2} , (d) TATCT _{a1} , (e) TATCT _{a2} , (f) TATCT _{y1} and (g) TATCT _{y2}	151
Figure 5.24: Velocity vector plots for turbulent flow inside the domains of (a)TATCT, (b) TATCT _{w1} , (c) TATCT _{w2} , (d) TATCT _{a1} , (e) TATCT _{a2} , (f) TATCT _{y1} and (g) TATCT _{y2}	152
Figure 5.25: Effect of variations in (a) tape width, (b) area of cut on tape and (c) tape pitch of TATCT on Nusselt number vs. Reynolds number. ...	153
Figure 5.26: Effect of variations in tape geometries of TATCT on Nusselt number vs. Reynolds number.	154
Figure 5.27: Effect of variations in (a) width of tape, (b) area of cut on tape and (c) pitch of tape of TATCT on friction factor vs. Reynolds number.	155

Figure 5.28: Effect of variations in tape geometries of TATCT on friction factor vs. Reynolds number.	156
Figure 5.29: Effect of variations in (a) width of tape, (b) area of cut on tape and (c) pitch of tape of TATCT on thermal performance factor vs. Reynolds number.	157
Figure 5.30: Effect of variations in tape geometries of TATCT on thermal performance factor vs. Reynolds number.....	158
Figure 5.31: Implication of the various tape geometries on its production cost and the thermal performance.	159
Figure 5.32: Comparison between numerical and predicted results for Nusselt number.	160
Figure 5.33: Comparison between numerical and predicted results for friction factor of turbulent flow.	161
Figure 6.1: Grid resolution study for the SST $\kappa - \omega$ of TATCT showing the results of temperature and velocity at different locations for $Re = 2300$	176
Figure 6.2: Grid resolution study for the SST $\kappa - \omega$ of TATCT showing the results of temperature and velocity at different locations for $Re = 4650$.177	
Figure 6.3: Comparison of various models with Grid 3 of TATCT showing the results of temperature and velocity at different locations for $Re = 2300$.178	
Figure 6.4: Comparison of various models with Grid 3 of TATCT showing the results of temperature and velocity at different locations for $Re = 4650$. 179	
Figure 6.5: Contour plots of temperature across the TATCT cross-section at axial location $0.866m$ for (a) $Re=2150$, (b) $Re=2300$, (c) $Re=4400$ and (d) $Re=4650$	180
Figure 6.6: Contour plots of velocity across the TATCT cross-section at axial location $0.866m$ for (a) $Re=2150$, (b) $Re=2300$, (c) $Re=4400$ and (d) $Re=4650$	181
Figure 6.7: Contour plots of the turbulent kinetic energy (TKE) across the TATCT cross-section at axial location $0.866m$ for (a) $Re=2150$, (b) $Re=2300$, (c) $Re=4400$ and (d) $Re=4650$	182

Figure 6.8: Turbulent kinetic energy across the TATCT cross-section for different Reynolds number at different axial locations.	183
Figure 6.9: Contour plots of turbulent intensity across the TATCT cross-section at axial location $0.866m$ for (a) $Re=2150$, (b) $Re=2300$, (c) $Re=4400$ and (d) $Re=4650$	183
Figure 6.10: Turbulent intensity across the TATCT cross-section for different Reynolds number at different axial locations.	184
Figure 6.11: Nusselt number vs Reynolds number for TATCT, TACCT and TAECT showing laminar, transition and turbulent regimes.....	184
Figure 6.12: Friction factor vs Reynolds number for TATCT, TACCT and TAECT showing laminar, transition and turbulent regimes.....	185
Figure 6.13: Comparison between simulated and predicted results for Nusselt number of transitional flow.	185
Figure 6.14: Comparison between simulated and predicted results for friction factor of transitional flow.	186
Figure 7.1: Model geometry of TATCT inclined at an angle.	199
Figure 7.2: Grid independence test of laminar flow of mixed convection for (a) temperature and (b) velocity across the cross-section at the exit of TATCT inclined at 60°	199
Figure 7.3: Grid independence test of turbulent flow of mixed convection for (a) temperature, (b) velocity and (c) turbulent kinetic energy across the cross-section at the exit of TATCT inclined at 60°	200
Figure 7.4: Grid independence test of transitional flow of mixed convection for (a) temperature and (b) velocity across the cross-section at the exit of TATCT inclined at 60°	201
Figure 7.5: Turbulent kinetic energy for turbulent flow ($Re = 20000$) inside the TATCT for (a) forced convection, and mixed convection at inclination angle of (b) 15° , (c) 30° , (d) 60° , (e) 90°	201
Figure 7.6: Surface temperature variation with dimensionless length for various Reynolds numbers of laminar flow.	202
Figure 7.7: Surface temperature variation with dimensionless length for various Reynolds numbers of transitional flow.....	203

Figure 7.8: Surface temperature variation with dimensionless length for various Reynolds numbers of turbulent flow. 204

Figure 7.9: Contour plots of temperature for laminar flow ($Re = 1820$) inside through TATCT for (a) forced convection, and mixed convection at inclination angle of (b) 15° , (c) 30° , (d) 60° , (e) 90° 205

Figure 7.10: Contour plots of temperature for transitional flow ($Re = 2150$) inside through TATCT for (a) forced convection, and mixed convection at inclination angle of (b) 15° , (c) 30° , (d) 60° , (e) 90° 206

Figure 7.11: Contour plots of temperature for turbulent flow ($Re = 20000$) inside through TATCT for (a) forced convection, and mixed convection at inclination angle of (b) 15° , (c) 30° , (d) 60° , (e) 90° 207

Figure 7.12: Average outlet velocity at various inclinations for various Reynolds numbers of (a) laminar flow, (b) transitional flow and (c) turbulent flow..... 208

Figure 7.13: Effect of inclination on normalised outlet temperature for various Reynolds numbers of (a) laminar flow, (b) transitional flow and (c) turbulent flow..... 209

Figure 7.14: Impact of inclination on Nusselt number for various Reynolds numbers of (a) laminar flow, (b) transitional flow and (c) turbulent flow. 210

Figure 7.15: Impact of inclination on friction factor for various Reynolds numbers of (a) laminar flow, (b) transitional flow and (c) turbulent flow. 211

List of Tables

Table 4.1: Number of cells for grid resolution study for the laminar flow	.69
Table 4.2: Thermo-hydraulic values of different induced tubes for the laminar flow at $Re = 2000$69
Table 5.1: Cells for grid resolution study for the turbulent flow 124
Table 5.2: Amount of material for different domains 124
Table 5.3: Description of the various geometries of the alternate-axis triangular cut twisted tape (ATCT) used for the domain TATCT 125
Table 5.4: Thermo-hydraulic values of different induced tubes for the turbulent flow at $Re = 20000$ 125
Table 5.5: Cells for grid resolution study for various domains of TATCT for the turbulent flow 126
Table 5.6: Amount of material for various geometries of the alternate-axis triangular cut twisted tape (ATCT) used for the TATCT 126

List of Symbols

Roman Symbols

$C_{1\varepsilon}, C_{2\varepsilon}, C_{3\varepsilon}, C_{\mu}$	Model constant
C_p	Specific heat capacity at constant pressure ($J/kg.K$)
c	Clearance between the edge of tape and tube (m)
D	Diameter of tube (m)
f	Darcy friction factor
g	Gravitational acceleration (m/s^2)
F_1, F_2	Blending function
G_{κ}	Generation of turbulence kinetic energy due to the mean velocity gradients
G_{ω}	Generation of specific dissipation rate
G_b	Generation of turbulence kinetic energy due to buoyancy
Gr	Grashof number
h	Heat transfer coefficient ($W/m^2.K$)
I	Intensity of turbulence
k	Thermal conductivity ($W/m.K$)
L	Length of tube (m)
\dot{m}	Mass flow rate (kg/s)
m_1	Major diameter of elliptical (m)
m_2	Minor diameter of elliptical (m)
m	Radius of circular cut (m)
Nu	Average Nusselt number

p	Pressure (N/m^2), perimeter of cut on twisted (m)
Pr	Prandtl number
q''	Heat flux (W/m^2)
r	Radius of tube (m)
Re	Reynolds number
S_i	Source term
s	Length of a side of triangular cut (m)
sr	Space ratio
t	Time (s)
T	Temperature (K)
u_i, u_j, u, v, w	Velocity component in Cartesian coordinate (m/s)
V	Velocity vector (m/s)
w	Width of twisted tape (m)
x_i, x_j, x, y, z	Cartesian coordinate (m)
y	Pitch of twisted tape (m)

Greek Symbols

α_κ	Eddy diffusivity (m^2/s)
α	Correction factor
β_1, β_2	Model constant
β	Thermal expansion coefficient (K^{-1})
δ_{ij}	Kronecker delta
δ	Thickness of tape (m)
ε	Dissipation rate of Turbulent kinetic energy (m^2/s^3)
η	Thermal performance factor

θ	Angle of inclination with respect to horizontal direction
κ	Turbulent kinetic energy (m^2/s^2)
λ	Free stream direction
μ_t	Dynamic turbulent viscosity (kg/ms)
μ	Dynamic viscosity (kg/ms)
ν_t	Kinematic turbulent viscosity (m^2/s)
ν	Kinematic viscosity (m^2/s)
ρ	Density (kg/m^3)
σ_ε	Turbulent Prandtl numbers for ε
σ_κ	Turbulent Prandtl numbers for κ
σ_ω	Turbulent Prandtl numbers for ω
φ	Solution variable
\emptyset	Fluid thermal property
ω	Specific dissipation rate (s^{-1})

Subscripts

b	Bulk
eff	Effective
f	fluid
i	Inlet
m	Mean
o	Reference
p	Plain tube
t	Turbulent
w	Wall

List of Acronyms

ACCT	Alternate-axis circular cut twisted tape
AECT	Alternate-axis elliptical cut twisted tape
ATCT	Alternate-axis triangular cut twisted tape
CCT	Circular cut twisted tape
CFD	Computational fluid dynamics
PTT	Plain twisted tape
PT	Plain tube
ECT	Elliptical cut twisted tape
RANS	Reynolds-averaged Navier-Stokes
RNG	Renormalisation group
SIMPLE	Semi-Implicit Method for Pressure-Linked Equations
SST	Shear-stress transport
TACCT	Tube with alternate-axis circular cut twisted tape
TAECT	Tube with alternate-axis elliptical cut twisted tape
TATCT	Tube with alternate-axis triangular cut twisted tape
TCCT	Tube with circular cut twisted tape
TCT	Triangular cut twisted tape
TECT	Tube with elliptical cut twisted tape
TPT	Tube with plain twisted tape
TTCT	Tube with triangular cut twisted tape

Chapter 1

INTRODUCTION

Heat is a form of energy which is transferred whenever there is difference in the temperature between a system and its surrounding. The research on heat transfer has been receiving important attention since long time ago, and has found applications in several areas such as cooling of electronic devices, manufacturing systems and solar energy systems [1].

There exists three modes of heat transfer namely conduction, convection and radiation. Conduction is the transfer of heat from a substance of more energetic to another substance of less energetic particle as a result of interactions between the particles. The transfer of heat between a solid surface and an adjacent moving fluid is referred to as convection. In radiation, heat is emitted by a substance in the form of electromagnetic waves due to changes in electronic configurations of the atoms [1, 2].

Convection is subdivided into three classes: free convection, forced convection and mixed convection. In free convection, motion of fluid is due to variation of gravitational body force associated with variation of fluid density. In forced convection, fluid motion is caused by an externally applied force. The process of heat transfer in which both mechanisms of free and forced convections participate simultaneously is term mixed convection [2, 3].

Heat energy is indispensable to man for his survival and this has made man to be occupied by the quest for its effective utilization in commercial

industrial and domestic activities. In order to reduce the aggregate financial resources that go into producing this heat energy, it has become important to design heat exchanger equipment that is more efficient in performance and at the same time to reduce or save energy, cost and material. In this regard, heat transfer becomes a significant process. A report by Wang and Sunden [4] indicated that heat transfer enhancement technology results in reduction of the heat exchanger size, which generally leads to less capital cost. The effective usage of heat often governs the operation and economic design of process plants [5].

The technique of improving heat transfer rate is known as heat transfer enhancement or augmentation or intensification [6, 7]. These techniques are widely applied in such areas as air-cooled finned tube heat exchangers in the process industries, in all vehicles for radiators and internal heat exchangers, in domestic applications such as radiators in rooms, heat rejection cycles or refrigeration systems and condensing central heating exchangers [4, 8-10]. The performance of heat exchanger equipment which is an essential unit in efficient extraction, recovery, utilization and conversion of heat can be improved further by a number of intensification methods [11, 12].

Methods of enhancement (or intensification) of heat transfer can be classified as passive method, active methods and compound methods [13-15]. In enhancement of heat transfer by passive methods, direct input of external power is not required. These methods make use of geometrical or surface modifications, such as extended surfaces and rough surfaces, to the flow channel, or incorporate additional devices such as twisted tape inserts, displaced enhancement devices and coiled tubes. The active methods of enhancing heat transfer require direct application of external power. These methods include surface vibration, mechanical aids,

electromagnetic fields, etc. Because of their complexity and need for external power, they have not shown much potential and hence have found limited applications. The combination of different methods acting at the same time to enhance heat transfer is known as compound method of heat transfer enhancement. Some examples of these methods are internally-finned tube with twisted tape insert and spirally corrugated tube with twisted tape insert.

Heat transfer rate can be improved by introducing a disturbance in the fluid flow that breaks the viscous and thermal boundary layers. The dominant resistance to heat flow across a primary surface has to be broken for any heat exchanger to allow more heat to be transferred. The dominant resistance can be broken in two ways: increasing the heat transfer coefficient or by increasing the heat transfer area. By increasing the velocity of the flow parallel to the tube or the tube axis the heat transfer coefficient is increased as presented by Lane and Heggs [8], Liao and Xin [16] and Manglik and Bergles [17]. Tube insert technology - i.e., insertion of tape inside a tube - is used in this work to break the dominant resistance.

The tube insert technology enjoys some advantages that have made it become a reliable technique for intensification of heat transfer. For example, the tape can be inserted into and withdrawn the tube without a need for expertise which makes its installation easy. Also, its cost of production is low when compared to other heat transfer enhancement techniques that incorporate fins, spring, heatex wire matrix, etc. as inserts. Moreover, its maintenance cost is low compared to other techniques. Furthermore, significant reduction in size of a heat exchanger can be achieved when a twisted tape is employed in the heat exchanger for a specified duty. In addition, the configuration of the twisted tape is

simpler than heatex wire matrix, spring, fins, etc. and thus makes twisted tape attractive for fouling duties [6, 7, 18, 19].

A twisted tape is generally in the category of swirl flow device [20] and can be manufactured from a thin metallic strip made in a variety of materials. Its geometrical characteristics, as demonstrated in its general configuration shown in Figure 1.1, are described by the tape width w , (which is less than the tube diameter to allow for installation of the tape on the tube), the tape thickness δ , and twist pitch γ . Details of these geometrical characteristics are provided in subsequent Chapters.

The enhancement of heat transfer in the tube insert technology is attributed to some factors namely the reduction in hydraulic diameter (which increases the heat transfer coefficient), secondary motion and its resulting swirl mixing generated by the twisted tape (which improves the convective coefficient), the partitioning and blockage of the tube flow cross section by the tape (which leads to higher flow velocities) and the helically-twisting flow (which creates an effectively longer flow path) [21]. In application of a twisted tape, there is a trade-off between the heat transfer and pressure drop. Various research works have shown that twisted tapes with proper designs offer the promotion of heat transfer rate a with reasonable penalty in pressure drop which ultimately yields savings in energy and cost [6, 22].

As a consequence of the importance attached to improving the performance of heat exchanger, researchers have, over the past several years, concerned themselves with the analysis of laminar, transition and turbulent heat transfer and fluid flows. Reynolds in 1833 has described the motion of a fluid changing from laminar to turbulent flow as transitional flow [23]. Many researchers have reached a conclusion that the value of the

flow rate at which laminar flow can no longer be maintained can vary significantly [24-26]. The dynamical state of a system is controlled by Reynolds number such that there is a linearly stable fixed point for all Reynolds number and laminar or turbulence state such that when the Reynolds number is less than the critical Reynolds number the state of the flow is laminar but when the Reynolds number is greater than the critical Reynolds number the state is turbulent. A critical value of $Re = 2100$ was suggested by Reynolds [27] for the upper limit of laminar flow. Thereafter, Reynolds [28] himself observed that by taking great care in minimising external disturbances to the flow, the laminar state could be maintained to $Re \approx 12,000$. Through a good design of pipe entrances, Pfenniger [29] and Ekman [30] were able to maintain laminar pipe flow up to a $Re = 10,000$ and $Re = 40,000$ respectively. The analysis done by Meseguer & Trefethen [31] indicated $Re = 10^7$ for the upper limit of laminar flow. All these observations indicate that there exists no critical Reynolds number for the start of turbulent flow [24, 32, 33].

Most of the previous investigations on heat transfer enhancement were conducted on plain tubes and induced tubes for laminar, transitional and turbulent flows. However, there is very little emphasis on transitional flow for tubes induced with modified twisted tape. For clarity purpose, a twisted tape 'modified' means that cuts are made on the twisted-tape. These cuts can be trapezoidal cuts, square cuts, louvered strips and edge-fold, etc. The details of this are illustrated in Chapter 2. Also, the aspect of mixed convection in induced tube for laminar, transitional and turbulent flows has virtually been neglected. Therefore, one of the areas in which attention is focussed in this thesis is the enhancement of heat transfer in induced tubes for laminar, transitional and turbulent flows.

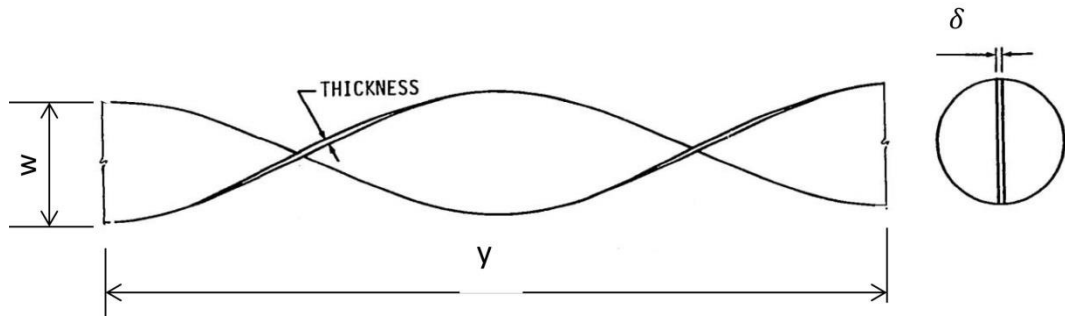


Figure 1.1: Configuration of a twisted tape.

Chapter 2

LITERATURE REVIEW

Studies regarding the augmentation of heat transfer rate have been in progress for some times to yield a better result for performance of heat exchangers. The use of extended surfaces, corrugated tubes and twisted tape inserts are some of the means of enhancing or augmenting heat transfer coefficients. Thermal enhancers are frequently used in such applications to avoid additional exchangers, which can lead to significant cost saving. For example, air-cooled finned tube heat exchangers in the process industries, in all vehicles for radiators and internal heat exchangers, in domestic applications such as radiators in rooms, heat rejection cycles or refrigeration systems and condensing central heating exchangers [4, 7, 8].

Several experimental and numerical studies involving augmentation techniques in tubes induced with plain twisted tape and modified twisted tape inserts are examined in this Chapter. By plain twisted tape is meant there is no cut or modification introduced on it. Variations in characteristics of the tape such as twist ratio, space ratio, tape length, height-to-diameter ratio are applied to some of these studies, and they have produced valuable results. In an attempt to improve fluid mixing inside a flow system, varieties of modifications have been made to plain twisted-tape. These modifications are the cuts (portrayed in Figure 2.2) made on the plain twisted-tape inserts (shown in Figure 2.1(a)), and are explained in details in the present Chapter.

2.1 Experimental Studies on Forced Convection in Tubes with Twisted Tape Inserts

Some of the previous experimental works on forced convection flow are presented below.

2.1.1 Experimental laminar flow

An early study of twisted tape insert was on the experiment performed by Royds [34] to examine the concept that the spiral motion given to a fluid flowing through a tube increased the heat transmission in the tube. Different tests of air cooling with different values of inlet temperature up to 811K, and different twisted twist ratios in the range $2.36 \leq y/w \leq 19.24$ were considered. The heat transfer obtained in the tube with twisted tape was up to 140% of that in the tube without tape. Thereafter, Colburn and King [35] and Kirov [36] experimentally made known their observations on the related work.

The first set of experimental finding for twisted tapes in laminar flow of viscous fluids was given by Hong and Bergles [37] in which a correlation for predicting the Nusselt Number in fully-developed swirl flows of water and glycol in electrically-heated tubes were presented. The augmentation of heat transfer due to twisted tapes in laminar flow for non-Newtonian liquids were experimentally x-rayed by Marner and Bergles [38, 39], Nazmiev [40], Manglik et al. [41] and Dasmahapatra and Raja Rao [42] and have been found to have a reasonable agreement with established correlations.

Saha et al. [43] carried out experimental work to investigate the heat transfer and pressure drop characteristics on laminar flow in a circular tube

fitted with regularly-spaced plain twisted-tape elements connected by thin circular rods, shown in Figure 2.1(b). The heat transfer and pressure drop characteristics were governed by Reynolds number between 500 and 2300, Prandtl number between 4 and 5.5, twist ratio between 3.18 and ∞ , space ratio between 2.5 and 10. The twist ratio is the ratio of the length of a segmented twist tape to the inner diameter of tube while the space ratio (sr) is the ratio of distance between two tapes to the inner diameter of the tube. Heat transfer data were obtained in an electrically-heated test section. Results of the experiments showed that the Nusselts number and friction coefficient increase with decreasing twist ratio and decreasing space ratio. It also showed that for the same values of Reynolds number, twist ratio and space ratio, the heat transfer and the friction coefficient in the regularly-spaced plain twisted tape are higher than those in full-length or continuous plain twisted tape as displayed in Figure 2.1(c).

Maner and Bergles [44] carried out a study on augmentation of highly viscous laminar heat transfer inside tubes with constant wall temperature with polybutene 20 as the test fluid. The experimental investigation was carried out on three test sections: a plain tube, an internally finned tube, and a tube with twisted-tape insert. Isothermal pressure drop, non-isothermal pressure drop, and heat transfer data were obtained over a wide range of Reynolds number 15.1-5.75 and Prandtl number 1260-8130. Results showed that friction factors obtained for the internally finned tube was 1.69 times those of the plain tube while the tube with twisted tape gave a friction factor in multiple of 3.38 that of the plain tube. Improvement in heat transfer coefficient recorded for heating was 3 to 4 times those of the plain tubes; they were 1.5 to 2.25 times for cooling.

In an experiment on laminar flow conducted by Sivashanmuham and

Sundaram [45], it was reported that an enhancement of about 44.7% in heat transfer was obtained over that of a heat exchanger without a twisted tape. Of all the different twist ratio used for the experiment, the highest enhancement was obtained in the tape with the least twist ratio. The enhancement of heat transfer in their findings was found to decrease exponentially as the Reynolds number increases.

Experiments were carried out by Al-Fahed et. al [46] in a single shell-and-tube heat exchanger to analyse the heat transfer and pressure drop in plain tube, microfinned tube and twisted tape insert-tube in laminar region under a uniform wall temperature. They observed that the twisted tape insert-tube gave a better heat transfer enhancement over the microfinned tube. It was their recommendation that twisted tape insert-tube with tight fit should be used in designing heat transfer exchanger due to its higher heat transfer enhancement over the loose-fit tape.

In the work of Saha et al. [10], heat transfer and flow friction characteristics of swirl flow in a circular tube fitted with twisted-tape elements which are regularly spaced was experimentally analysed. By varying the width of tape, diameter of rods between successive tape elements and phase-angle between successive tape elements, it was reported that the results obtained in connecting successive tapes with rods was not as good as when the tape was pinched. Also, it was observed that increasing the width of the tape is beneficial to the system.

By considering laminar flow of water in the Prandtl number range $205 \leq Pr \leq 518$ under uniform heat flux condition, Saha and Dutta [47] experimentally reported on heat transfer enhancement provided by short-length regularly-spaced twisted tape insert. The Nusselt number and

friction factor for full-length twisted tape are higher than those for the short-length twisted tape. Based on the constant pumping power, the enhancement in the full-length twisted tape for tighter twist was found to be less than that for the short-length twisted tape.

2.1.2 Experimental transitional flow

Heat transfer and pressure drop data in the transitional flow regime of water flowing in a horizontal circular smooth tube and an enhanced tube were measured by Meyer and Oliver [23]. The results indicated that transition occurs earlier with enhanced tubes than with a smooth tube and that the more the enhancement, the earlier the transition will occur.

The thermo-hydraulic behaviour of helical wire coils fitted inside a round tube was investigated in laminar, transitional and turbulent flows by García et al. [48]. They found that the induced tube behaves as a smooth tube at low Reynolds numbers and accelerates transition to critical Reynolds numbers. They also discovered that within the transition region, the heat transfer rate in the induced tube can be increased up to 2 times that of the smooth tube.

In the later work, García et al. [49] carried out experimental study on wire coils inserted in a smooth tube under uniform heat flux conditions and in the flow range $10 \leq Re \leq 2500$. They reported that the transition from laminar flow to turbulent flow took place at the Reynolds number range $1000 \leq Re \leq 1300$, the transition is continuous without the pressure drop fluctuations, and the heat transfer was increased by the wire coils.

2.1.3 Experimental turbulent flow

The experimental investigation which was published by Evans and Sarjant [50] and Kreith and Margolis [51] seems to be the pioneering work on heat transfer enhancement in turbulent flow in tubes fitted with twisted tape. Later on, experiments on turbulent flows of water in plain tubes induced with twisted tapes were conducted by Ibragimov et al. [52], Lopina and Bergles [53] and Brevi et al. [54]. In all these studies, a reasonable enhancement of up to 50% was obtained.

Klepper [55], Zozulya and Shkuratov [56], Migay and Golubev [57], Algifri and Bhardwaj [58] and Burfoot and Rice [59] experimentally reported that the pressure drops obtained in short lengths of twisted tapes placed intermittently along the length of a tube was less than those in full-length twisted tapes. They added that the reduction in the pressure drop was due to decrease in swirl in the full-length twisted tapes. However, the reduction in the pressure loss is at the expense of the heat transfer enhancement.

Augmentation of convective heat transfer inside tubes with three-dimensional internal extended surfaces and twisted-tape inserts was researched into by Liao and Xin [16]. The experiments were carried out to investigate the characteristics of the heat transfer and friction factor inside tubes with three-dimensionally internal fins and continuous twisted-tape inserts as well as with the segmented twisted-tape inserts. The experiments were carried out with water, ethylene glycol and turbine oil as working fluids. The Stanton number of the finned tube with continuous twisted-tape was enhanced up to 5.8 times of the smooth tube while the friction factor was enhanced almost 6.5 times of an empty smooth tube.

When the continuous tape insert was replaced with segmented tape insert, a decrease in both the friction factor and the Stanton number was observed.

An experimental study on the effect of gap width between horizontal tube and twisted tape on the pressure drop in turbulent water flow was carried out by Al-Fahed [60] on nine different twisted tapes comprising three different twist ratios with each of them having three different tape widths. The results showed that the pressure drop was increasing and decreasing as the tape width increases. The same trends of results were obtained when the twist ratio was increased. It was the believe of the author [60] that similar anomalous trend would be shown by the results of the heat transfer.

Zimparov [11] experimentally obtained heat transfer and pressure drop results for two three-start spirally corrugated tubes (Figure 2.3 [61]) combined with twisted-tape inserts. A smooth tube was used for standardising the experimental set-up and for comparing the enhancement in heat transfer fluid friction. For each of the two tubes, the characteristics parameters: height of corrugation, pitch of corrugation, and spiral angle were constant while the twist ratios were varied. The experiment was conducted in the range of Reynolds number 3000 to 60,000 and revealed that the friction coefficients and heat transfer coefficients were higher in enhanced tubes than in smooth tubes operating under the same conditions. The heat transfer efficiency (i_E), i.e. the ratio between the heat transfer for enhanced tube and the value for a smooth tube was between 1.0 and 1.2 when twisted tape alone was used. For an internally-grooved or corrugated tube alone, $1.5 \leq i_E \leq 2.0$. In the case of compound enhancement (i.e twisted tape and internally-grooved tube were used together), $2.5 \leq i_E \leq 3.3$.

Thereafter, Zimparov [62] conducted an experiment to investigate heat transfer and friction pressure drop for two single-start spirally corrugated tubes (Figure 2.3 [61]) combined with five twisted-tape inserts with different relative pitches. The same Reynolds number range of 3000 to 60,000 was used as in the previous work, but the characteristics parameters (height-to-diameter ratio and relative pitch) were different. Higher heat transfer coefficients and friction factor than those of the smooth tubes operating under the same conditions were recorded. However, the work did not state which of the two corrugated tubes (three-start and single-start) has a higher enhancement as the tubes used in the two works have different characteristic parameters.

According to the findings of the experimental work of Kumar and Prasad [63], the heat transfer in a solar water heater with a twisted tape can be increased by between 18 and 70% when compared with solar water heater without twisted tape. The report also showed that the pressure drop can be increased by between 87 and 132%, as compared to plain solar water heater operating within the same conditions. Moreover, the thermal performance was found to increase by about 30%. The author [63] has adduced the enhancement to the swirl flow induced by the twisted tape as well as the turbulence promoted by the twisted tape. It was discovered that beyond Reynolds number (Re) of 12000, the increase in the thermal performance of the solar collector system is monotonous. However, the system performed better in the lower range of $Re \approx 12,000$.

Murugesan et al. [64] experimentally discussed heat transfer and pressure drop characteristics of turbulent flow with Reynolds number in the range of 2000 - 12000 in a circular tube fitted with trapezoidal-cut twisted tape insert (Figure 2.2(a)). The trapezoidal-cut twisted tape used has twist

ratios of 6.4 and 4.4. The trapezoidal-cut were taken alternately on both top and bottom of the tape. In order to ensure standard experimental results, the experimental data obtained from the plain tube were verified with the standard correlation. The results of the comparison made between the tube fitted with trapezoidal-cut twisted tape and the plain tube showed that there was a significant increase in heat transfer coefficient and friction factor for the tape with trapezoidal-cut. It was found that the Nusselt number for the trapezoidal-cut twisted tape with twist ratios 4.4 and 6.0 were 1.72 and 1.37 times respectively better than that of plain tube. The friction factor for the trapezoidal-cut twisted tape with twist ratios 4.4 and 6.0 were 2.85 and 1.97 respectively times that of the plain tube. The authors formulated an empirical correlation which depicted that the experimental data fell within $\pm 5\%$ variation in Nusselt number and $\pm 6\%$ variation in friction factor. In the later work of Murusegan et al. [65], there was an examination of experimental investigation on heat transfer and thermal enhancement factor characteristics of a double pipe heat exchanger fitted with plain twisted tube and square-cut twisted-tape (Figure 2.2(b)) for twist ratios 2.0, 4.4 and 6.0 with Reynolds number between 2000 and 12000 and using water as working fluid. The square-cuts were taken alternatively on both top and bottom of the tape. Over the flow regime considered, the Nusselt number for the tube induced with square-cut twisted tape of twist ratios 2.0, 4.4 and 6.0 were respectively 1.08, 1.067 and 1.055 times those induced with plain twisted tape. The frictional factor for the tube with square-cut twisted tape of twist ratios 2.0, 4.4 and 6.0 were respectively 1.09, 1.12 and 1.15 times of those for the tube with plain twisted-tape insert. Empirical correlations were derived for the experiment. The predicted values agreed with experimental data within $\pm 6\%$ for Nusselt number and $\pm 8\%$ for the friction factor.

In the range of Reynolds number range of 5000-25000, heat transfer augmentation attributed to serrated twisted tape (Figure 2.2(c)) was found to be about 1.25 - 1.67 times that in the tube fitted with smooth twisted tape and 2.5 - 4.8 times that in the plain tube. These were the results of experimental study conducted by Chang et al. [66] in their work on turbulent heat transfer and pressure drop in tube fitted with serrated twisted tape. The serrations on the two sides of the twisted tape with twist ratio of 1.56, 1.88, 2.81 or ∞ are the square-sectioned ribs with the identical rib-pitch and rib-height. This shows that the tube fitted with serrated twisted tape inserts produced a better heat transfer enhancement than the tube fitted with smooth walled twisted tape.

By employing backward louvered strip and forward louvered strip, each with various inclined angles of 15° , 25° and 30° inserted in a double pipe heat exchanger, Eiamsa-ard et al. [67] were able to compare turbulent flow heat transfer and pressure loss in a louvered-strip fitted tube and plain tube. The average Nusselt number and pressure drop for backward louvered strip were 263% and 233% respectively over the plain tube. The average Nusselt number and pressure drop for forward louvered strip were 284% and 413% respectively over the plain tube. The thermal enhancement was found to increase with an increase in angle of inclination of the strips.

Single twisted tape (Figure 2.1(a)), twin counter twisted tape and co-twisted tapes (Figure 2.1(d)) were employed by Eiamsa-ard et al. [68] to produce single swirl flow, counter swirl flow and co-swirl flows respectively. Their experimental results indicated that the tapes with counter swirl gave higher heat transfer rate than the ones with single swirl flow and co-swirl flow. Specifically, the heat transfer for the counter

twisted tape is 12.5% to 44.5% and 17.8% to 50% higher than those for the single twisted tape and co-twisted tape respectively. At constant pumping power, the tapes with counter swirl has higher thermal performance factor than those with single swirl flow and co-swirl flow. The experimental results are in good agreement with the empirical correlations developed.

The characteristics of turbulent heat transfer and pressure drop in rectangular and square ducts having corrugated internal surfaces accompanied by twisted-tape inserts with and without oblique teeth (Figure 2.2(d)) was reported by Saha [69]. Based on the same pumping power, the combined effect of the axial corrugation together with twisted-tapes resulted in superior overall heat transfer enhancement over those of the individual effects. It was also discovered that the tape without oblique gave lesser thermal performance factor than the one with oblique teeth.

2.2 Computational Investigations on Forced Convection in Tubes with Twisted Tape Inserts

The contributions that numerical techniques have made to investigation on fluid flow and heat transfer cannot be overemphasised. Some of the several numerical works that have been done to study heat transfer and flow characteristics of tubes fitted with various forms of twist-tape inserts are expounded below.

2.2.1 Computational laminar flow

The publications of Date and Singham [70] was recorded as part of the early works on numerical study of heat transfer enhancement of laminar

flow through tubes with twisted tape inserts. The tubes were subjected to uniform heat flux and the numerical results indicated an increase in both heat transfer and pressure drop. Du Plessis and Kroger [71-73] numerically observed the advantage of applying twisted tape insert for promoting heat transfer in constant-property laminar flows and also presented correlations for Nusselt number and friction factor.

The numerical evaluation of Manglik and Bergles [74] defining the lower bound of heat transfer enhancement in tubes induced with twisted tape and that of Date and Saha [75] which took into consideration short-length twisted tape both observed the positive impact of the twisted tape on heat transfer.

In the presentation of Date and Saha [76], laminar flow and heat transfer characteristics in a tube fitted with regularly spaced twisted-tape elements were numerically predicted by solving the Navier-Stokes equation and the energy equation. The predicted friction factor agreed well with the experimental data of Saha et al [43] while the Nusselt number agreed well with the experimental data only for small spaces between the tape elements.

In their work, Sivashanmugam et al. [77] analysed CFD simulation for the heat transfer augmentation in a circular tube fitted with regularly spaced helical twist inserts in laminar flow conditions under constant heat flux. The results obtained indicated that the Nusselt number and friction factor for the tube fitted with the helical twist inserts are higher than that of the tube that is not fitted with helical twist inserts. Also, as the twist ratio of the tape increases, the Nusselt number decreases. Their results also showed that the simulated results of the Nusselt number and friction factor

for the plain and the fitted tube are in good agreement with the theoretical results.

In an attempt to predict data that cover a wide range of twist ratio, Prandtl number and Reynold number, Ray and Date [78] published numerical work on characteristics of laminar heat transfer of water of Prandtl number $Pr < 5$ under constant heat flux condition. Correlations were proposed and were found to be in good agreement with experimental results. A numerical study was carried out by Guo et al. [79] on laminar flow of water through a tube induced with a twisted tape showed that the tape increased the convective heat transfer in the tube.

Kumar and Kumar [80] numerically investigated the heat transfer and friction factor characteristics of laminar flow for water. The twisted tape provided additional heat transfer enhancement to that provided by the rib in the duct. The enhancement became higher for smaller rib spacing of the duct and lower twist ratio of the twisted tape.

The theory of enhancement in heat transfer to reduce flow resistance and improve temperature uniformity was numerically reported by Zhang [81]. The numerical results showed that the heat transfer coefficient in the laminar flow of water through the tube fitted with twisted tape is higher than that of the plain tube.

2.2.2 Computational turbulent flow

One of the early works on numerical investigation of heat transfer enhancement of turbulent flow through tubes fitted with twisted tape inserts was presented by Date [82]. Ever since then, several authors have attempted to carry out further numerical examinations. Gupte and Date

[83] evaluated Nusselt number and friction factor for swirl flow generated by twisted tape of twist ratios ∞ , 5.302, 5.038, and 2.659 in annuli. An increase in Nusselt number and friction factor were obtained over those of the plain tubes. Numerical investigation was carried out by Yadav and Padalkar [84] to investigate the turbulent heat transfer enhancement characteristics of air flow inside a circular tube with a partially decaying and partly swirl flow. The flow in the induced tubes produced heat transfer that is higher than that in the plain tube.

Chiu and Jang [85] numerically and experimentally carried out analyses to study thermal-hydraulic characteristics of air flow inside a circular tube with longitudinal strip inserts (both with and without holes) and twisted-tape inserts at three different angles (15.3° , 24.4° and 34.3°). The numerical simulations were carried out by using the finite volume method to solve the governing equations. The numerical predictions were in reasonable agreement with the experimental results. The heat transfer coefficient and the pressure drop in the tube with the longitudinal strip inserts (without holes) were 7-16% and 100-170% respectively higher than those of plain tubes. The heat transfer coefficient and the pressure drop were 13-28% and 140-220% respectively higher than those of the plain tubes. The heat transfer coefficient and the pressure drop of the tubes with twisted-tape inserts were 13-61% and 150-370% respectively higher than those of plain tubes.

Physical behaviour of the thermal and fluid flow in a tube fitted with loose-fit twisted-tape in the turbulent flow regime was published by Eiamsa-ard et al [86]. The effect of the clearance between the edge of the tape and the tube wall to the diameter of the tube on the Nusselt number, friction factor and thermal performance factor were numerically investigated for

twisted-tape at two different twist ratios of 2.5 and 5.0 by applying different turbulent models. The result of the simulation showed that the twisted tape with the least clearance ratio (c/D) produced the highest heat transfer enhancement as well as best thermal performance index.

In their own contribution, Cui and Tian [87] numerically and experimentally investigated the heat transfer characteristics and pressure drop in a circular tube induced with edgefold-twisted-tape insert (Figure 2.2(e)) and another tube induced with a plain twisted-tape inserts. The investigation was carried out by adopting the RNG $\kappa - \varepsilon$ turbulence model. It was revealed that the Nusselt number and friction factor of the tube induced with edgefold twisted tape were higher than those of the tube induced with a plain twisted-tape insert. The results of the simulation also revealed that the experimental results and numerical results are in a good agreement with a variation of 1.6% - 3.6% in the Nusselt number and 8.2% - 13.6% in the friction factor.

2.3 Experimental and Numerical Works on Mixed Convection in Tubes

The phenomenon of mixed convection heat transfer is utilized in a wide range of different engineering applications. Through a better understanding of the processes involved, the performances of various industrial applications can be improved and optimized [88, 89]. The significance of mixed convection has incited many investigations and research activities, under different boundary and operating conditions, in the literature.

2.3.1 Experimental works

Combined convection for laminar flow of water through a horizontal circular duct was investigated both numerically and experimentally under a uniform wall heat flux by Piva et al. [90]. The results indicated that the buoyancy effects manifested in that the pressure drop and the heat transfer were found to increase up to 22% and 150% respectively as a result of the buoyancy effect.

Patil and Babu [3], with the aim of investigating the importance of non-dimensional parameters like Prandtl number, Richardson number and Reynolds number in free and mixed convection regions, carried out an experiment on the laminar flow of mixed convection of water and ethylene glycol through a plain square duct under uniform wall temperature conditions. It was deduced that the intensity of free convection and magnitude of Richardson number decreased as the Reynolds number increased. Not only that, the average Nusselt number in the mixed convection was higher than that in pure forced convection. For a given Reynolds number, the average Nusselt number increased as the Richardson number and the Prandtl numbers of the fluids were increased.

Buoyancy-driven flow, transition of flow and the accompanying heat transfer process in a combined convection of air through an inclined rectangular duct was experimentally studied by Lin and Lin [91]. Through the results, it was concluded that the presence of the buoyancy augmented the heat transfer. The start of thermal instability moved upstream for a larger negative inclined angle and/or a higher Grashof number and delayed for a larger positive inclined angle and/or a higher Reynolds number. It was also observed that increasing the Grashof number or decreasing the

Reynolds number caused the flow to change from a transitional to turbulent state.

Chong et al. [92] conducted experiment to study the effect of inclination angles on the heat transfer characteristics of laminar and transition mixed convection of air in inclined rectangular ducts at seven different orientations ($-90^\circ \leq \theta \leq 90^\circ$). The results obtained showed that the heat transfer first increased with the inclination angles up to a maximum and then decreased. With the further increase in Reynolds number, the Nusselt number was not dependent of the inclination angles. It was also observed that the friction factor decreased with the increase of inclination angle up to a certain value as the Reynolds number increased. Thereafter, the friction factor became independent of the inclination angles.

2.3.2 Numerical works

For the first time, Abdelmeguid and Spalding [93] applied a two-equation model to perform numerical predictions of turbulent flow and heat transfer in a horizontal, vertical and inclined pipes under the effects of buoyancy, and with the wall subjected to uniform heat flux. Their findings showed that for Grashof number less than some critical Grashof number, the effect of buoyancy on turbulence is modest whereas for Grashof number greater than critical Grashof number, both the averaged flow and the heat transfer are affected by the buoyancy.

The problem of mixed convection flows in a horizontal cylinder rotating in air was experimentally and numerically carried out by Farouk and Ball [94]. Differences in the heat transfer and flow characteristics obtained from the rotating cylinders were observed and compared with those for the

stationary cylinder. Also, the mean Nusselt number of the rotating cylinder was higher than that of the stationary cylinder.

Nguyen et al. [95] numerically explored laminar mixed convection flow of air in a vertical tube subjected to a uniform heat flux. It was observed that the heat transfer increased due to the buoyancy effects. Also, the buoyancy forces have important effects on the axial velocity temperature of the fluid, particularly in the region near the tube wall.

Mixed convection around fixed and rotated circular cylinder was numerically studied by Jalil et al. [96]. From their results, they concluded that the average Nusselt number for the flow over the fixed cylinder decreased as the free stream direction (λ) was increased at constant value of Richardson number. As Richardson number was increased, the average Nusselt number was found to have increased for $\lambda \leq 135^\circ$ but decreased for $\lambda > 135^\circ$ as Grashof number increased. For the rotated cylinder, the Nusselt number increased with rotation over most of the cylinder surfaces for all directions of the free stream direction.

2.4 Objectives of the Thesis

From the literature review presented above, it is confirmed that some investigations have been carried out by some researchers with the aim of ascertaining improvement in heat transfer and fluid flow. Most of these investigations were conducted on plain tubes and induced tubes for laminar, transitional and turbulent flows. However, there has not been a report on heat transfer and fluid flow for plain tube induced with twisted tape insert with emphasis on cuts with different geometrical shapes but equal area (that is they are different-shape-equal-area cuts). Not only that, there is very little emphasis on transitional flow for tubes induced

with modified twisted tape. Moreover, the aspect of mixed convection on induced tube for laminar, transitional and turbulent flows has virtually been neglected in spite of its importance in practical applications.

Accordingly, the objectives of carrying out this study are given as follows:

- To investigate the thermo-hydraulic performance of laminar, transitional and turbulent flows under forced convection of water through tubes induced individually with different twisted tape inserts.
- To assess the impacts which the variations in tape width, tape pitch and perimeter of cuts on the twisted tape have on the heat transfer and turbulent forced convective flow of water through induced tubes.
- To examine the thermo-hydraulic performance of laminar, transitional and turbulent flows under mixed convection of water through tubes induced twisted tape inserts.
- To investigate the effect of inclination angle on the thermo-hydraulic performance of laminar, transitional and turbulent mixed convection of water through induced tubes.

2.5 Layout of the Thesis

In view of the goals stated in §2.4, the outline of the thesis is highlighted below:

Chapter 1 presents a general background on the different modes of heat

transfer. It explains the techniques of enhancing heat transfer and its area of applications.

Chapter 2 explores a review of the literature of previous research that is related to enhancement of heat transfer by means of tube insert technology. It looks into numerical and experimental studies of heat transfer enhancement in tubes with plain twisted tape as well as those with modified twisted tape. Moreover, it explains numerical and experimental studies of heat transfer enhancement of mixed convection in tubes. The objectives of the present investigation are also mentioned.

The mathematical formulations which are used in the numerical investigation are given in Chapter 3. Explanation is provided on governing equations for an incompressible fluid flow and heat transfer with different models viz standard $\kappa - \varepsilon$, RNG $\kappa - \varepsilon$, SST $\kappa - \omega$ and standard $\kappa - \omega$ models. In addition, the boundary conditions and numerical techniques are unveiled.

In Chapter 4, laminar heat transfer and fluid flow characteristics in tubes induced individually with different twisted tape is investigated. Correlations are also proposed for the Nusselt number and friction factor by means of non-linear regression analysis.

By employing RNG $\kappa - \varepsilon$ model, the thermo-hydraulic characteristic of turbulent heat transfer and fluid flow performed on induced tubes is expounded in Chapter 5. Correlations are proposed for the Nusselt number and friction factor. Furthermore, the effects of tape width, tape pitch and size cuts on the tapes on the performance of the tube system are considered.

In Chapter 6, investigation on heat transfer and fluid flow in transition

regime are carried out on divers induced tubes. The start and end of transition in each of the tubes is numerically provided by transitional variant of the SST $\kappa - \omega$.

A numerical study of heat transfer in a combined forced and free convection for laminar, transitional and turbulent flows through an induced tube is presented in Chapter 7. The effects of buoyancy force and inclination angle on the performance of the flow system is given.

Finally, Chapter 8 summarizes the findings of this study and gives suggestions for further research.

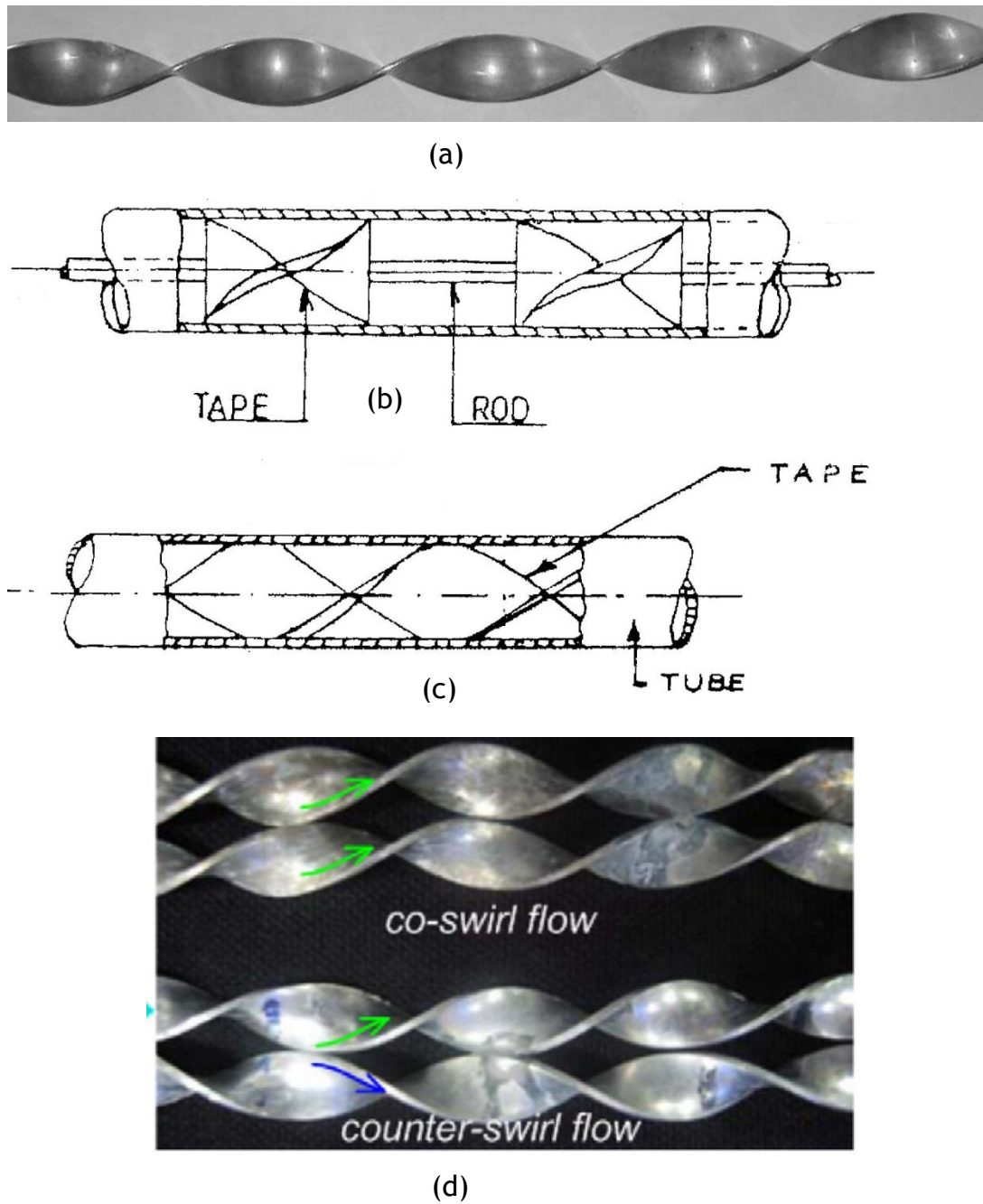


Figure 2.1: Plain twisted tapes showing (a) plain tape without a tube ^[68], (b) regularly-spaced plain twisted tape with a tube ^[10], (c) continuous plain twisted tape with a tube ^[66] and (d) twin co-twisted tapes and twin counter twisted tapes ^[68].

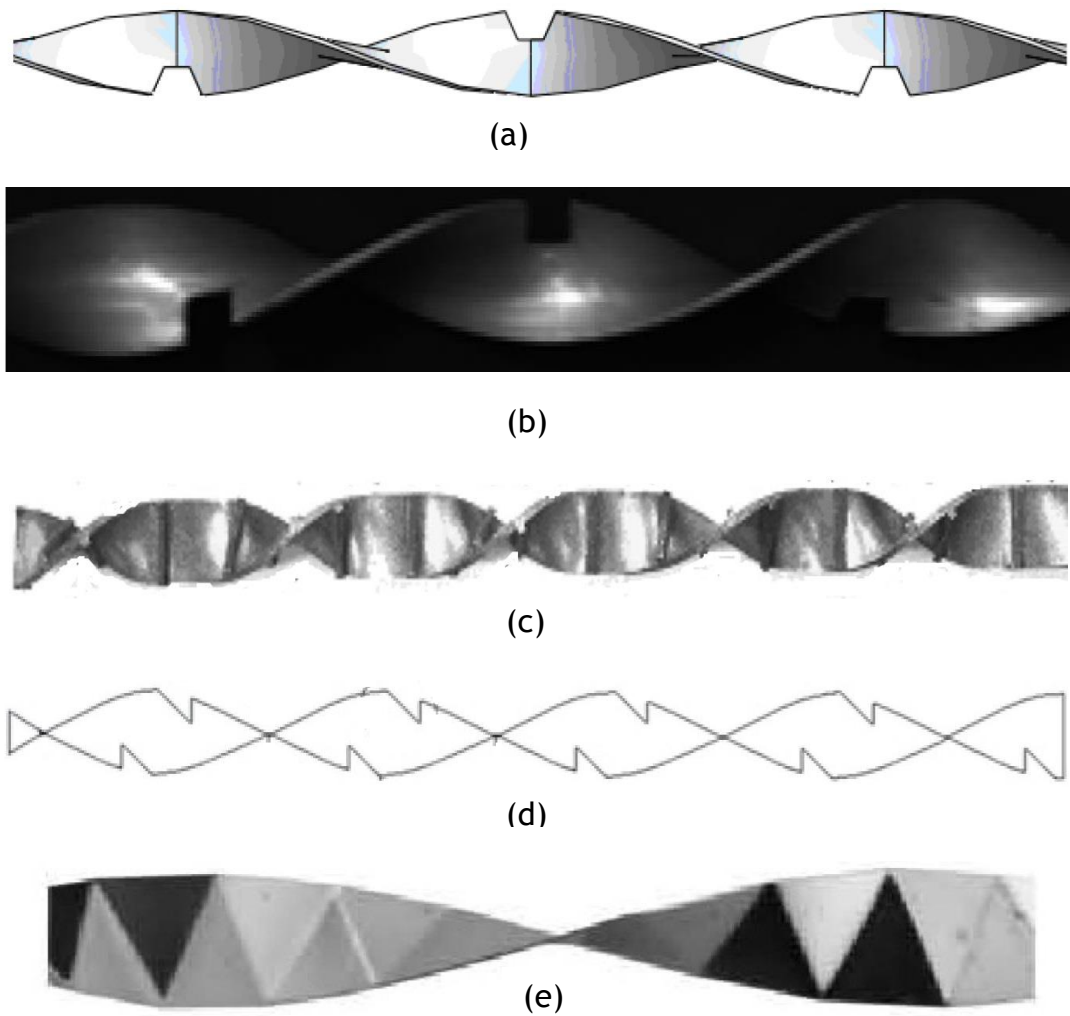


Figure 2.2: Modified twisted tape for (a) trapezoidal cuts ^[64], (b) square cuts ^[65], (c) serrated cuts ^[66], (d) oblique-tooth cuts ^[69] and (e) edgefold ^[87].

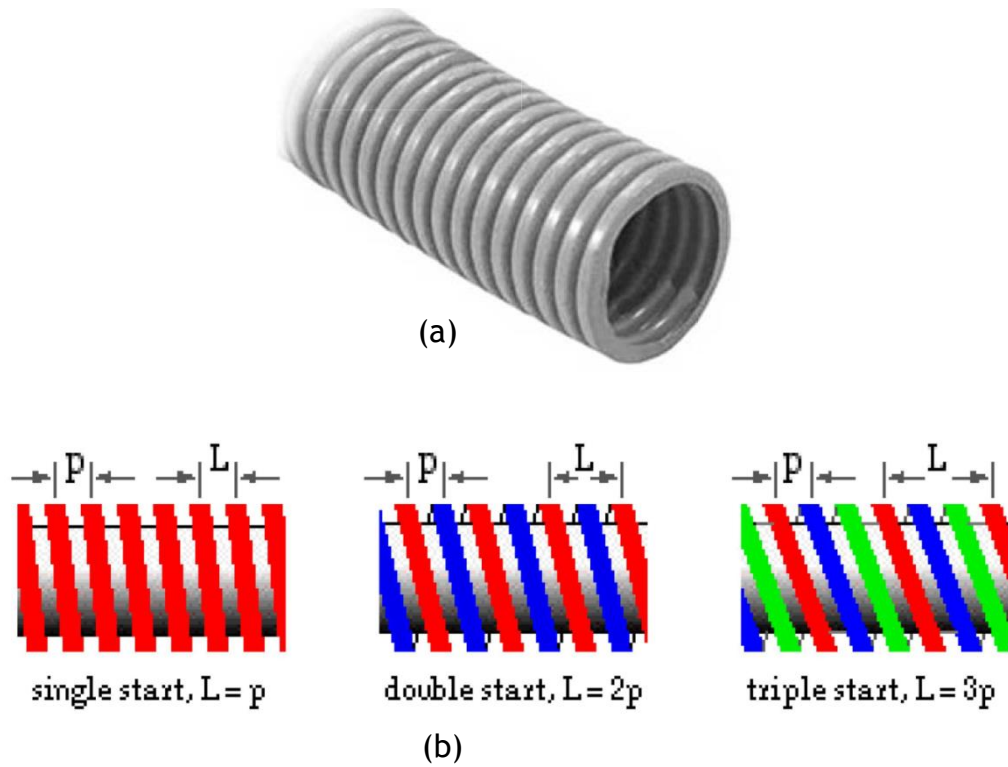


Figure 2.3: (a) Spirally corrugated tube ^[61] (a) start, pitch and lead of a spirally corrugated tube ^[61].

Note: p = pitch; L = lead

Chapter 3

NUMERICAL METHODS

3.1 Introduction

Simulation procedures based on computational fluid dynamics are necessary instrument in applications that have to do with fluid flow and heat transfer. The range of these applications is broadening. The methods employed in the present work for the numerical investigation of thermo-hydraulic behaviour of water in tubes of different designs are discussed in this Chapter. The governing equations as well as the modelling equations are presented and the numerical techniques employed are explained.

3.2 Governing Equations

Since the working fluid, water, is assumed to be Newtonian, the flow of the fluid can be described by the Navier-Stokes equations [97]. Therefore, the heat transfer and fluid flow under consideration are governed by the Navier-Stokes and energy transport equations. The working fluid is considered to be incompressible, and thermal radiation, chemical reaction and compression work are negligible.

The Navier-Stokes equations, developed by Stokes and Navier, represent the general behaviour of the fluid. They are continuity, momentum and energy equations [98, 99] as given below:

Continuity equation:

$$\nabla \cdot \mathbf{V} = 0 \quad (3.1)$$

Momentum equation:

$$\frac{\partial(\rho \mathbf{V})}{\partial t} + \nabla \cdot (\rho \mathbf{V} \mathbf{V}) = -\nabla p + \nabla \cdot \mu(\nabla \mathbf{V}) \quad (3.2)$$

Energy equation:

$$\rho C_p \left(\frac{\partial T}{\partial t} + \nabla \cdot \mathbf{V} T \right) = \nabla \cdot (k \cdot \nabla T) \quad (3.3)$$

where ρ is the density, k is the thermal conductivity, μ is the dynamic viscosity, p is the pressure, T is the temperature, \mathbf{V} is the velocity vector and C_p is the heat capacity at constant pressure.

The calculations for the forced convection are performed by making use of temperature-dependent functions for the fluid properties, expressed later in Equations (3.40) to (3.44). For the convective heat transfer with buoyancy influence (known as mixed convection), a constant formulation for properties is used for the fluid, except for the density which is taken as a function of the local-to-reference temperature difference and approximated [100] by

$$\rho = \rho_0 [1 - \beta(T - T_0)] \quad (3.4)$$

The Boussinesq approximation is employed for the mixed convection and therefore the momentum equations of the mixed convection take the following forms [89]:

$$\begin{aligned} & \frac{\partial(\rho u)}{\partial t} + \frac{\partial(\rho u u)}{\partial x} + \frac{\partial(\rho u v)}{\partial y} + \frac{\partial(\rho u w)}{\partial z} = \\ & -\frac{\partial p}{\partial x} + \mu \left(\frac{\partial^2 u}{\partial x^2} + \frac{\partial^2 u}{\partial y^2} + \frac{\partial^2 u}{\partial z^2} \right) + g \cos \theta (\rho - \rho_0) \end{aligned} \quad (3.5)$$

$$\begin{aligned} \frac{\partial(\rho v)}{\partial t} + \frac{\partial(\rho v u)}{\partial x} + \frac{\partial(\rho v v)}{\partial y} + \frac{\partial(\rho v w)}{\partial z} = \\ -\frac{\partial p}{\partial y} + \mu \left(\frac{\partial^2 v}{\partial x^2} + \frac{\partial^2 v}{\partial y^2} + \frac{\partial^2 v}{\partial z^2} \right) + g \sin \theta (\rho - \rho_0) \end{aligned} \quad (3.6)$$

$$\begin{aligned} \frac{\partial(\rho w)}{\partial t} + \frac{\partial(\rho w u)}{\partial x} + \frac{\partial(\rho w v)}{\partial y} + \frac{\partial(\rho w w)}{\partial z} = \\ -\frac{\partial p}{\partial z} + \mu \left(\frac{\partial^2 w}{\partial x^2} + \frac{\partial^2 w}{\partial y^2} + \frac{\partial^2 w}{\partial z^2} \right) \end{aligned} \quad (3.7)$$

where u , v and w are the velocity components.

With the Boussinesq model, the buoyancy term in the momentum equations (3.6) and (3.7) above is approximated [99] by

$$(\rho - \rho_0)g \approx -\rho_0\beta(T - T_0)g \quad (3.8)$$

where ρ is the density (kg/m^3), ρ_0 is the reference density (kg/m^3), calculated from the reference temperature $T_0(K)$, T is the fluid temperature (K), p is the pressure (Pa), μ is the dynamic viscosity (Ns/m^2), g is the gravitational acceleration, θ is the angle of inclination and β is the thermal expansion coefficient of the fluid (K^{-1}).

The above conservation Equations (3.1) to (3.3) and (3.5) to (3.7) are solved directly for laminar flow but for turbulent flow the μ and k are substituted by μ_{eff} and k_{eff} respectively [101, 102] and defined by

$$\mu_{eff} = \mu + \mu_t = \mu + \rho C_\mu \frac{\kappa^2}{\varepsilon} \quad (3.9)$$

and

$$k_{eff} = k + k_t = k + C_p \frac{\mu_t}{Pr_t} \quad (3.10)$$

where μ_t , k_t and Pr_t are the turbulent dynamic viscosity, turbulent thermal conductivity and turbulent Prandtl number respectively.

3.3 Turbulence Modelling

The predictions of turbulent flows can be based on the time-averaged properties of turbulence. The process of time-averaging gives rise to fluctuating temperature and velocities in the conservation equations. These small-scale turbulent fluctuations do not have to be directly simulated. To achieve this, the Navier-Stokes equations are rendered tractable by employing the Reynolds Averaged Navier-Stokes (RANS) equations.

In RANS averaging, the instantaneous solution variables $\varphi(u, p, T)$ in the Navier-Stokes equations are decomposed into mean $\varphi(\bar{u}, \bar{p}, \bar{T})$ and fluctuating components $\varphi'(u', p', T')$, mathematically written as

$$\varphi = \bar{\varphi} + \varphi' \quad (3.11)$$

A time averaging of the expression in Equation (3.11) is then taken by applying the time averaging operations $\overline{\varphi'} = 0$ and $\overline{\bar{\varphi} + \varphi'} = \bar{\varphi}$. The Reynolds-Averaged Navier-Stokes (RANS) equation for mass conservation can now be written in the tensor form as

$$\frac{\partial}{\partial x_i} (u_i) = 0 \quad (3.12)$$

The momentum equation for the time-averaged Navier-Stokes equation is given in the tensor form as:

$$\rho \frac{Du_i}{Dt} = -\frac{\partial p}{\partial x_i} + \frac{\partial}{\partial x_j} \left(\mu \frac{\partial u_i}{\partial x_j} - \rho \overline{u'_i u'_j} \right) + S_i \quad (3.13)$$

where S_i is the source term representing the gravitational term.

Note that the overbar on the velocity components is not shown in the above equations but these represent the time-averaged quantities and not the instantaneous quantities.

The additional terms $(-\rho \overline{u'_i u'_j})$ that now appear in the above equation are known as the Reynolds stresses or turbulent stresses and they are formed by the action of the fluctuating velocity components. The Reynolds-averaged approach to turbulence modelling requires that the Reynolds stresses be appropriately modelled in order to close it. This is done by employing Boussinesq equation [98, 103]. In applying Boussinesq approach, the term $-\overline{u'_i u'_j}$ is written as

$$-\overline{u'_i u'_j} = \nu_t \left(\frac{\partial u_i}{\partial x_j} + \frac{\partial u_j}{\partial x_i} \right) - \frac{2}{3} k \delta_{ij} \quad (3.14)$$

Substituting equation (3.14) into equation (3.13), the time-averaged momentum equation becomes

$$\rho \frac{Du_i}{Dt} = -\frac{\partial p}{\partial x_i} + \frac{\partial}{\partial x_j} \tau_{ij} + S_i \quad (3.15)$$

where

$$\tau_{ij} = \mu \frac{\partial u_i}{\partial x_j} + \rho \left(\nu_t \left(\frac{\partial u_i}{\partial x_j} + \frac{\partial u_j}{\partial x_i} \right) - \frac{2}{3} k \delta_{ij} \right) \quad (3.16)$$

The time-averaged energy equation can be written as

$$\frac{\partial T}{\partial t} + \frac{\partial}{\partial x_j} (u_i T) = \frac{\partial}{\partial x_j} \left(\frac{k_{eff}}{\rho C_p} \frac{\partial T}{\partial x_j} - \overline{u_j' T'} \right) \quad (3.17)$$

The term $\overline{u_j' T'}$ in Equation (3.18) is approximated as

$$\overline{u_j' T'} = -\alpha_t \frac{\partial T}{\partial x_j} = -\frac{\nu_t}{\sigma_t} \frac{\partial T}{\partial x_j} \quad (3.18)$$

where σ_t is the turbulent Prandtl number, α_t is the eddy diffusivity and ν_t is the kinematic turbulent viscosity.

The RANS equations mentioned above contain additional unknown variables such as turbulent viscosity, and turbulence models are needed to determine these variables in terms of known quantities. Before a turbulence model is chosen, some factors such as the physics encompassed in the flow, the level of accuracy required, computational resources that are available and established practice for a specific class of problem have to be considered. The discussion on the different turbulence models used in this work is discussed below.

3.3.1 Standard $\kappa - \varepsilon$ model

The standard $\kappa - \varepsilon$ model is a two-equation turbulence model proposed by Launder and Spalding [104]. It is a high-Reynolds number model. The two terms on which the model is based are the turbulent kinetic energy (κ) and dissipation rate of turbulence kinetic energy (ε). The turbulent kinetic energy (κ) is derived from an exact equation by assuming that the effect of the molecular viscosity of the flow is negligible while the turbulence dissipation rate (ε) is obtained by employing physical reasoning [99]. The transport equations, turbulent viscosity and model constants for the standard $\kappa - \varepsilon$ models [99] are given below:

Turbulence kinetic energy equation:

$$\frac{\partial}{\partial t}(\rho\kappa) + \frac{\partial}{\partial x_i}(\rho\kappa u_i) = \frac{\partial}{\partial x_j} \left[\left(\mu + \frac{\mu_t}{\sigma_\kappa} \right) \frac{\partial \kappa}{\partial x_j} \right] + G_k + G_b - \rho\varepsilon \quad (3.19)$$

Dissipation rate of turbulence kinetic energy equation:

$$\begin{aligned} \frac{\partial}{\partial t}(\rho\varepsilon) + \frac{\partial}{\partial x_i}(\rho\varepsilon u_i) = & \frac{\partial}{\partial x_j} \left[\left(\mu + \frac{\mu_t}{\sigma_\varepsilon} \right) \frac{\partial \varepsilon}{\partial x_j} \right] + \\ & C_{1\varepsilon} \frac{\varepsilon}{\kappa} (G_k + C_{3\varepsilon} G_b) - C_{2\varepsilon} \rho \frac{\varepsilon^2}{\kappa} \end{aligned} \quad (3.20)$$

where G_k is the generation of turbulence kinetic energy due to the mean velocity gradients; G_b is the generation of turbulence kinetic energy due to buoyancy; $C_{1\varepsilon}, C_{2\varepsilon}, C_{3\varepsilon}$ are model constants; the quantities σ_κ and σ_ε are the turbulent Prandtl numbers for κ and ε respectively.

Turbulent viscosity is given as:

$$\mu_t = \rho C_\mu \frac{\kappa^2}{\varepsilon} \quad (3.21)$$

The values of the model constants used in equations (3.19) and (3.20) for the standard κ - ε model are $C_{1\varepsilon} = 1.44$, $C_{2\varepsilon} = 1.92$, $C_\mu = 0.09$, $\sigma_\kappa = 1.0$ and $\sigma_\varepsilon = 1.3$ [99].

3.3.2 RNG $\kappa - \varepsilon$ model

Renormalization Group theory (RNG) $\kappa - \varepsilon$ model was proposed by Yaglom and Orszag [105] and this two-equation model was derived from the instantaneous Navier-Stokes equations using a statistical technique called renormalization group theory [106]. It takes into account low-Reynolds number effect. Like the standard $\kappa - \varepsilon$ model, it is based on model transport equations for the turbulence kinetic energy (κ) and its dissipation

rate (ε). It improves the accuracy of flows by the reason of an additional term in its transport equation for turbulence dissipation rate (ε).

The transport equations, turbulent viscosity and model constants for the RNG $\kappa - \varepsilon$ models [99] are given below:

Turbulence kinetic energy equation:

$$\frac{\partial}{\partial t}(\rho\kappa) + \frac{\partial}{\partial x_i}(\rho\kappa u_i) = \frac{\partial}{\partial x_j} \left[\alpha_\kappa \mu_{eff} \frac{\partial \kappa}{\partial x_j} \right] + G_k + G_b - \rho\varepsilon \quad (3.22)$$

Dissipation rate of turbulence kinetic energy equation:

$$\begin{aligned} \frac{\partial}{\partial t}(\rho\varepsilon) + \frac{\partial}{\partial x_i}(\rho\varepsilon u_i) = & \frac{\partial}{\partial x_j} \left[\alpha_\varepsilon \mu_{eff} \frac{\partial \varepsilon}{\partial x_j} \right] + C_{1\varepsilon} \frac{\varepsilon}{\kappa} (G_k + C_{3\varepsilon} G_b) \\ & - C_{2\varepsilon} \rho \frac{\varepsilon^2}{\kappa} - R_\varepsilon \end{aligned} \quad (3.23)$$

where G_k is the generation of turbulence kinetic energy due to the mean velocity gradients; G_b is the generation of turbulence kinetic energy due to buoyancy; $C_{1\varepsilon}, C_{2\varepsilon}, C_{3\varepsilon}$ are model constants; R_ε is a term which is related to the mean strain and turbulence quantities; the quantities α_κ and α_ε are the inverse effective Prandtl numbers for κ and ε respectively.

The turbulent viscosity (μ_t) for the RNG $\kappa - \varepsilon$ model is as given in Equation (3.21) above but the values of its model constants in equations (3.22) and (3.23) are $C_{1\varepsilon} = 1.42$, $C_{2\varepsilon} = 1.68$, $C_\mu = 0.0845$, $\sigma_\kappa = 0.7194$ and $\sigma_\varepsilon = 0.7194$ [99].

3.4 Transitional Modelling

The RANS equations of continuity, momentum and energy used for the simulation of the transitional flow [107] are given in Equations (3.24) to (3.26). They are

Continuity equation:

$$\frac{\partial}{\partial x_i} (u_i) = 0 \quad (3.24)$$

Momentum equation:

$$\frac{\partial(\rho u_i)}{\partial t} + \rho \left(u_i \frac{\partial u_j}{\partial x_i} \right) = - \frac{\partial p}{\partial x_i} + \frac{\partial}{\partial x_i} \left((\mu + \mu_t) \frac{\partial u_j}{\partial x_i} \right) \quad (3.25)$$

Energy equation:

$$\rho C_p \left(\frac{\partial T}{\partial t} + u_i \frac{\partial T}{\partial x_i} \right) = - \frac{\partial}{\partial x_i} \left(k_{eff} \frac{\partial T}{\partial x_i} \right) \quad (3.26)$$

where u = velocity (m/s), p = pressure (m/s^2), μ = dynamic viscosity (Ns/m^2), μ_t = turbulent viscosity (m^2/s^2), ρ = density (kg/m^3), C_p = specific heat at constant pressure ($J/kg.K$), k_{eff} = effective thermal conductivity = $k + k_{eff}$ ($W/m.K$), T = temperature (K).

The transportation equations and modelling equations for the transitional flow are elaborated in the subsequent section.

3.4.1 Shear-Stress Transport (SST) $\kappa - \omega$ model

The Shear-Stress Transport (SST) $\kappa - \omega$ model, developed by Menter [108], effectively mix the formulation of the free-stream independence of the $\kappa - \varepsilon$ model in the far field with the formulation of the $\kappa - \omega$ model in the

near-wall-region. It is based on transport equation of turbulence kinetic energy (κ) and specific dissipation rate (ω). Since transitional flow is not fully turbulent, the transitional variant of the SST $\kappa - \omega$ is used for this study. The turbulent viscosity (μ_t) needed as input to the RANS equations is provided by the transport equations of the SST $\kappa - \omega$ model are given [99, 107] as

$$\frac{\partial}{\partial t}(\rho\kappa) + \frac{\partial}{\partial x_i}(\rho\kappa u_i) = \frac{\partial}{\partial x_j} \left[\left(\mu + \frac{\mu_t}{\sigma_\kappa} \right) \frac{\partial \kappa}{\partial x_j} \right] + G_\kappa - \beta_1 \kappa \omega \quad (3.27)$$

$$\begin{aligned} \frac{\partial}{\partial t}(\rho\omega) + \frac{\partial}{\partial x_i}(\rho\omega u_i) = & \frac{\partial}{\partial x_j} \left[\left(\mu + \frac{\mu_t}{\sigma_\omega} \right) \frac{\partial \omega}{\partial x_j} \right] + G_\omega - \beta_2 \omega^2 \\ & + 2(1 - F_1) \sigma_{\omega,2} \frac{1}{\omega} \frac{\partial \kappa}{\partial x_j} \frac{\partial \omega}{\partial x_j} \end{aligned} \quad (3.28)$$

where G_κ is the generation of turbulence kinetic energy, G_ω is the generation of specific dissipation rate, the quantities σ_κ and σ_ω are the turbulent Prandtl numbers for κ and ω respectively, $\sigma_{\omega,2}$ is a model constant and F_1 is the blending function.

To obtain transitional model from the SST $\kappa - \omega$ model, a low-Reynolds correction factor (α) is applied to the turbulent viscosity μ_t . The correction factor depresses the rate of generation of turbulence [99]. Hence, the turbulent viscosity for the SST $\kappa - \omega$ model is presented as

$$\mu_t = \frac{\rho\kappa}{\omega} \frac{1}{\max \left[\frac{1}{\alpha}, \frac{S \cdot F_2}{a_1 \omega} \right]} \quad (3.29)$$

The model constant α , known as low-Reynolds correction factor, in Equation (3.29) is given as

$$\alpha = \alpha_{\infty} \left(\frac{\alpha_0 + Re_t/R_k}{1 + Re_t/R_k} \right) \quad (3.30)$$

where S is the absolute value of shear strain rate, F_2 is the blending function. The model constants are $\beta_1 = 0.072$, $\beta_2 = 0.072$, $\sigma_{\omega,2} = 1.168$, $a_1 = 0.31$, $\alpha_{\infty} = 1$, $\alpha_0 = \beta_i/3$, $\beta_i = 0.072$ and $Re_t = \rho\kappa/\mu\omega$ and $R_k = 6$.

3.4.2 Standard $\kappa - \omega$ model

The standard $\kappa - \omega$ model is based on the Wilcox model [109] and it incorporates modification of low -Reynolds-number effect. Like the SST $\kappa - \omega$ model, it is based on transport equation of turbulence kinetic energy (κ) and specific dissipation rate (ω). Since the flow being considered is not fully turbulent, the transitional variant of standard $\kappa - \omega$ is also applied for the simulation. The transport equations for the standard $\kappa - \omega$ model are given [99, 107] as

$$\frac{\partial}{\partial t}(\rho\kappa) + \frac{\partial}{\partial x_i}(\rho\kappa u_i) = \frac{\partial}{\partial x_j} \left[\left(\mu + \frac{\mu_t}{\sigma_{\kappa}} \right) \frac{\partial \kappa}{\partial x_j} \right] + G_{\kappa} - \beta_1 \kappa \omega \quad (3.31)$$

$$\frac{\partial}{\partial t}(\rho\omega) + \frac{\partial}{\partial x_i}(\rho\omega u_i) = \frac{\partial}{\partial x_j} \left[\left(\mu + \frac{\mu_t}{\sigma_{\omega}} \right) \frac{\partial \omega}{\partial x_j} \right] + G_{\omega} - \beta_2 \omega^2 \quad (3.32)$$

where G_{κ} and G_{ω} are as defined in § 3.4.1 above and the model constants $\beta_1 = 0.072$ and $\beta_2 = 0.072$.

The turbulent viscosity (μ_t) in the standard $\kappa - \omega$ model is written as

$$\mu_t = \frac{\rho\kappa}{\omega} \quad (3.33)$$

To obtain transitional model from the standard $\kappa - \omega$ model, a low-Reynolds correction factor (α) is applied to the turbulent viscosity. The

rate of generation of turbulence is depressed by the low-Reynolds correction factor [99].

Thus, Equation (3.33) becomes

$$\mu_t = \alpha \frac{\rho \kappa}{\omega} \quad (3.34)$$

The coefficient α in Equation (3.33) and the model constant therein are defined in Equation (3.30) above.

3.5 Boundary Conditions

In carrying out the numerical simulations in this work, the flow is considered to be incompressible and steady. The surface of the tube wall of diameter, D and length, L is under uniform heat flux condition, that is

$$-k \left(\frac{\partial T}{\partial x} \right)_{r=D/2} = q'' \quad (3.35)$$

where k is the thermal conductivity ($W/m^2 K$) and r is the radius of the tube (m).

A no slip condition is also applied to the tube wall, i.e. $u_i = 0$. At the inlet of the tube, a velocity to give the desired Reynolds number is specified by

$$Re = \frac{\rho v D}{\mu} \quad (3.36)$$

where Re is the Reynolds number and ρ and μ are the density and the dynamic viscosity of the fluid respectively.

The calculations for the thermal properties are taken at the inlet temperature of $301K$. At the outlet, a pressure outlet condition is used, a backflow temperature is specified and the gauge pressure is set to zero.

Other flow quantities are extrapolated from the interior domain by the solver in Fluent software [99].

For the turbulent flow, the intensity of turbulence (I) is given by the expression [99]

$$I = 0.16Re^{-0.125} \quad (3.37)$$

For the mixed convection, the Grashof number (Gr) is defined [110, 111] as

$$Gr = \frac{g\beta(T_o - T_i)^3}{\nu^2} \quad (3.38)$$

where ν is the kinematic viscosity of fluid (m^2/s).

The equations used for the temperature-dependent functions of the thermal properties of the fluid is of the form

$$\phi = \sum_{i=1}^{i=n} \alpha + \beta_i T_f^i; \quad i > 0 \quad (3.39)$$

where ϕ is the thermal properties of the flow; α and β are constants and T_f is the fluid temperature.

The temperature-dependent functions for the fluid properties (specific heat capacity, C_p ; Prandtl number, Pr ; density, ρ ; thermal conductivity, k and kinematic viscosity, ν) of the fluid (water) for $278K \leq T_f \leq 363K$, as provided by Kays and Crawford, [112] are:

$$C_p = (10.01128 - 5.135 \times 10^{-2}T_f + 1.492117 \times 10^{-4}T_f^2 - 1.427 \times 10^{-7}T_f^3) \times 10^3 \quad (3.40)$$

$$Pr = 899.99 - 7.78920T_f + 2.2641337 \times 10^{-2}T_f^2 - 2.204026 \times 10^{-5}T_f^3 \quad (3.41)$$

$$\rho = 330.116 + 5.91516T_f - 1.631041 \times 10^{-2}T_f^2 + 1.3323 \times 10^{-5}T_f^3 \quad (3.42)$$

$$k = -12.15974 + 0.1181916T_f - 3.6632142 \times 10^{-4}T_f^2 + 3.8084136 \times 10^{-7}T_f^3 \quad (3.43)$$

$$\nu = 1.083828 \times 10^{-4} - 9.330538 \times 10^{-7}T_f + 2.7027447 \times 10^{-9}T_f^2 - 2.6243211 \times 10^{-12}T_f^3 \quad (3.44)$$

3.6 Enhanced Wall Treatment

Wall is the common boundary encountered in confined flow problems and the presence of walls affect turbulent flows. In as much as walls are the main source of turbulence, the near-wall modelling has an effect on the accuracy of numerical solutions. It is in the near wall region that the solution variables have large gradients, and the momentum and other scalar transports occur most vigorously. Therefore, the successful prediction of wall-bounded turbulent flows is determined by an accurate representation of the flow in the near-wall region [98, 99, 113].

If the near-wall mesh is fine enough to be able to resolve the laminar sublayer, then the enhanced wall treatment will be identical to the traditional two-layer zonal model. The restriction that the near-wall mesh must be sufficiently fine everywhere might impose a large computational requirement. Then, one would like to have a near-wall formulation that can be used with coarse meshes as well as fine meshes. Enhanced wall

treatment possesses the accuracy of the standard two-layer approach for fine near-wall meshes and also will not significantly reduce accuracy for wall-function meshes [99]. It is therefore adopted for this study.

In order to extend the applicability of enhanced wall treatment throughout the near wall region, Fluent [99] has provided the following functions as suggested by Kader [114].

The mean velocity is calculated from the relation:

$$v^+ = e^\Gamma v_{lam}^+ + e^{\frac{1}{\Gamma}} v_{turb}^+ \quad (3.45)$$

where the factor e^Γ is written as

$$\Gamma = -\frac{a(x^+)^4}{1 + bx^+} \quad (3.46)$$

where $a = 0.01$ and $b = 5$

The general equation for the derivative $\frac{dv^+}{dx^+}$ is written as

$$\frac{dv^+}{dx^+} = e^\Gamma \frac{dv_{lam}^+}{dx^+} + e^{\frac{1}{\Gamma}} \frac{dv_{turb}^+}{dx^+} \quad (3.47)$$

The mean temperature is calculated from the relation:

$$T^+ = \frac{(T_w - T_p) \rho C_p \mu^*}{\dot{q}} = e^\Gamma T_{lam}^+ + e^{\frac{1}{\Gamma}} T_{turb}^+ \quad (3.48)$$

Where the factor Γ is written as

$$\Gamma = -\frac{a(Prx^+)^4}{1 + bPr^3x^+} \quad (3.49)$$

3.7 Numerical Techniques

To find solutions to the equations of motion, it is necessary to generate their discrete equivalents. The finite volume method is used to discretise the governing partial differential equations encountered in this work. The finite method sub-divides the calculation domain into a set of control volumes wherein lies the computational nodes. The equations of motion are integrated over a control volume, meaning that momentum and mass are conserved locally within it and also in the calculation domain. The discretisation is carried out with second order upwind scheme, introduced by Warming and Beam [115], by which the unknown quantities at the cell faces are computed through a Taylor series expansion of the cell centred solution about the cell centroid. The Taylor series expansion transforms the partial differential equations into numerical equations that describe the derivatives of a variable as the differences between values of the variable at various points in space and time [116].

As a way of incorporating the effects of pressure into the solution for the momentum equation, the SIMPLE (Semi-Implicit Pressure Linked Equations) algorithm introduced by Patankar and Spalding[117] was used to couple the calculations of pressure and velocity. This was done indirectly by the use of the continuity equation. This equation can be integrated over a control volume in the same way as the momentum equations. To initiate the SIMPLE calculation, a pressure field p^* is guessed. The discretised momentum equations are then solved using the guessed pressure to obtain velocity components u^*, v^* . The difference between the actual and assumed pressure, known as corrected pressure p' is then applied to achieve a better approximation of the pressure field by adopting the

relation $p = p' + p^*$. The velocity components are corrected to get u, v and then the discretised equation of a scalar quantity are solved using the updated results of u, v, p [98]. Fluent software [99] is used to obtain iterative solution of these equations. The solution convergence is met when the difference between normalised residual of the algebraic equation and the prescribed value is less than 10^{-5} .

Chapter 4

NUMERICAL INVESTIGATION OF HEAT TRANSFER AND LAMINAR FLOW CHARACTERISTICS IN DIVERSE TUBE DESIGNS

4.1 Introduction

Heat transfer and fluid flow characteristics have been numerically investigated for laminar flows in plain tubes and several induced tubes. The results from these investigations shall be applicable to numerous systems such as in automobile industries, process industries and refrigeration industries, among others. Applications of laminar flows are found in air flow over an aircraft wing in which as the wing moves forward through the air, the boundary layer at first flows smoothly over the streamlined shape of the airfoil. In addition, laminar flow is utilised by a laminar flow reactor (LFR) to study chemical reactions and process mechanisms. In commercial settings, heated or refrigerated air is kept from passing through doorways by making use of air curtains. Laminar flow hoods are used to exclude contaminants from sensitive processes in science, electronics and medicine [118, 119].

In an attempt to improve upon the thermal performance of these systems various techniques have been utilised among which is inducing a plain tube with twisted tape insert and modifying the tape. Even though these works

have received much attention, yet there is a gap in the sense that none of the works has reported on tapes having cuts of the same size but with different geometry.

In the light of the above, the objective of this Chapter is to investigate the heat transfer and flow characteristics in different tube designs under laminar flow condition. This objective is met by means of numerical simulations with various Reynolds numbers between 830 and 2000 in tubes induced with different tape which have cuts of the same size but with different shape. Moreover, investigation is conducted to ascertain which of the tube designs give the best performance. In addition, appropriate correlations are developed in order to predict the heat transfer and flow characteristics in the tube systems.

4.2 Model Geometry

The geometry of the model specifies the shape and size of the region of interest. The geometries, created in GAMBIT [120], are made up of tubes induced individually with different twisted tape. The tube geometry, shown in Figure 4.1, has dimensions of length (l) of 1000mm and internal diameter (D) of 19mm . The twisted tape inserts runs through the entire length of the tube and has a width (w), thickness (δ) and pitch (y) of 18mm , 1mm and 54mm respectively as shown in Figure 4.2. These dimensions were selected based on the experimental work of Wongcharee and Eiamsa-ard [121] which is one of the sources used to validate the numerical results of this work.

The different twisted tape inserts are shown in Figure 4.3. They are plain twisted tape (PTT), elliptical cut twisted tape (ECT), circular cut twisted tape (CCT), triangular cut twisted tape (TCT), alternate-axis elliptical cut twisted tape (AECT), alternate-axis circular cut twisted tape (ACCT) and

alternate-axis triangular cut twisted tape (ATCT). The alternate-axis twisted tapes were obtained from modification of the twisted tapes without alternate-axis by cutting twist lengths of the tape without alternate-axis and arranging each plane at an angle of 90° relative to the adjacent plane.

The domains with different twisted tape inserts are shown in Figure 4.4. The tubes are sliced so that the tapes inside of them can be seen. They are respectively tube with plain twisted tape (TPT), tube with elliptical cut twisted tape (TECT), tube with circular cut twisted tape (TCCT), tube with triangular cut twisted tape (TTCT), tube with alternate-axis elliptical cut twisted tape (TAECT), tube with alternate-axis circular cut twisted tape (TACCT) and tube with alternate-axis triangular cut twisted tape (TATCT).

Figure 4.5 depicts the three different geometrical shapes chosen as the cuts on the tapes. The cuts have different geometrical shapes viz ellipse, circle, and triangle but the same area (A) of 56.54mm^2 . For the ellipse, the dimensions are $m_1 = 16.36\text{mm}$, $m_2 = 4.40\text{mm}$; the circle has $m = 8.48\text{mm}$; the triangle has $s = 12.52\text{mm}$. A sectional view of a domain for the tube induced with a plain twisted tape (TPT) is shown in Figure 4.6. The twist ratio of the tape is the ratio $y/w = 3$ (i.e. $54\text{mm}/18\text{mm}$). The clearance (c) which is the distance between the edge of tape and the tube wall is 0.5mm , i.e. $((D - w)) / 2 = (19\text{mm} - 18\text{mm})/2$. The space ratio ($sr = 2c/D$) defined as the ratio of the clearance between the edge of the tape and the tube wall to the tube diameter which translates to 0.052. The same values of y , w , y/w , D , c and sr are used for the other domains (TECT, TCCT, TTCT, TAECT, TACCT and TATCT). The effect of the change in each of these variables on the heat transfer, fluid flow and thermal performance on are elaborated in Chapter 5.

4.3 Grid Resolution

Grid independence tests were conducted in order to know the grid which will be appropriate in obtaining numerical solutions of high accuracy. Four different grids were used for each domain as shown in Table 4.1. In carrying out the grid resolution study, temperature and velocity across the cross-section at the exit of each domain for Reynolds number of 1820 were plotted and shown in Figure 4.7 and Figure 4.8 respectively. The closeness of the computational results to exact solutions depends on the number of cells the domain is divided into.

Figure 4.7 shows the results of the temperature for the grid resolution test. In the PT (frame (a)), there is a variation of 2.9%, 3.4% and 3.4% in comparing the values of temperature obtained in the grids with the total number of cells 476554, 512420 and 614904 respectively with that in the grid with the number of cells 461178. The TPT (frame (b)) indicates a variation of 2.6%, 3.8% and 3.8% in comparing the values of temperature in the grids the number of cells 944154, 1015216 and 1218259 respectively with that in the grid with the number of cells 913594. For the TECT (frame (c)), there is a variation of 2.7%, 3.0% and 3.01% in comparing the values of temperature in the grids with the number of cells 1159966, 1247298 and 1496758 respectively with that in grid with the number of cells 1122468. In the TCCT (frame (d)), there is a variation of 2.7%, 3.01% and 3.01% in comparing the values of the temperature in the grids with the number of cells 1254681, 1349142 and 1618970 respectively that in the grid with the number of cells 1214178. The TTCT (frame (e)) shows a discrepancy of 2.6%, 2.9% and 3.01% in comparing the values of temperature in the grids with the number of cells 1277931, 1374099 and 1648919 respectively with that in the grid with the number of the cells 1236639.

As can also be seen in Figure 4.7, the TAECT (frame (f)) reveals that the discrepancy in the values of the temperature in the grids with the number of cells 1535641, 1651206 and 1981447 are 2.1%, 2.9% and 2.9% respectively when compared with that in the grid with the number of cells 1486055. In the TACCT (frame (g)), there is a discrepancy of 2.0%, 2.9% and 2.9% between the values of temperature in grids with the number of cells 1609513, 1730639 and 2076767 respectively and that in the grid with the number of cells 1557545. For the TATCT (frame (h)), the difference in comparing the values of temperature in the grids with the number of cells 1658638, 2515756 and 3018907 with that in the grid with the number of cells 1255502 are 1.9%, 2.8% and 2.8% respectively.

The results of the velocity for the grid resolution test are shown in Figure 4.8. For the PT, frame (a)), the discrepancy in the values of the velocity obtained in the grids with the number of cells 476554, 512420 and 614904 are 3.4%, 4.6% and 4.6% respectively with that in the grid with the number of cells 461178. In the TPT (frame (b)), there is a variation of 3.4%, 6.6% and 6.6% in comparing the values of the velocity in the grids with the number of cells 944154, 1015216 and 1218259 respectively with that in the grid with the number of cells 913594. For the TECT (frame (c)), the difference in comparing the values of the velocity in the grids with the number of cells 1159966, 1247298 and 1496758 with that in the grid with the number of cells 1122468 are 3.1%, 5.1% and 5.1% respectively. The TCCT (frame (d)) indicates a variation of 3.6%, 6.5% and 6.5% in comparing the values of velocity in the grids with the number of cells 1254681, 1349142 and 1618970 respectively with that in the grid with the number of cells 1214178. In the TTCT (frame (e)), there is a discrepancy of 3.5%, 5.1% and 5.1% between the values of velocity in the grids with the number of

cells 1277931, 1374099 and 1648919 respectively and that in the grid with the number of cells 1236639.

Furthermore, Figure 4.8 indicates that in the TAECT (frame (f)), there is a variation of 2.5%, 5.7% and 5.7% in comparing the values of velocity in the grids with the number of cells 1535641, 1651206 and 1981447 respectively with that in the grid with the number of cell 1486055. For the TACCT (frame (g)), there is a variation of 2.6%, 5.4% and 5.4% in comparing the values of velocity in the grids with the number of cells 1609513, 1730639 and 2076767 respectively with that in the grid with the number of cell 1557545. The TATCT (frame (h)) shows a discrepancy of 2.9%, 5.8% and 5.8% in comparing the values of velocity in the grids with the number of cells 1658638, 2515756 and 3018907 respectively with that in the grid with the number of cell 1255502.

The above analysis for both the temperature and velocity shows that any of the grids with the number of cells 512420 and 614904 can be adopted for the PT; any of the grids with the number of cells 1015216 and 1218259 can be adopted for the TPT while any of the grids with the number of cells 1247298 and 1496758 can be adopted for the TECT. For the TCCT, any of the grids with the number of cells 1349142 and 1618970 is appropriate; any of the grids with the number of cells 1374099 and 1648919 is fit for the TTCT while any of the grids with the number of cells 1651206 and 1981447 is suitable for the TAECT. The TACCT can adopt any of the grids with the number of cells 1730639 and 2076767 while any of the grids with the number of cells 2515756 and 3018907 is suitable for the TATCT. However, considering accuracy of the solution and simulation time for convergence to be reached, the grids with the number of cells 512420, 1015216, 1247298, 1349142, 1374099, 1651206, 1730639 and 2515756 are adopted

for the domains PT, TPT, TECT, TCCT, TTCT, TAECT, TACCT and TATCT respectively.

4.4 Computational Results and Discussions

In this section, the flow fields, contour plots, Nusselt number, friction factor and thermal performance of the tubes induced individually with the different types of twisted tapes are discussed. A Reynolds number $Re = 1820$ is selected for giving an overview for the flow field, velocity contour, temperature profile and pressure distribution. Where results at axial locations are presented, an axial location $0.866m$ has been considered because this location is near the exit of the domains. Also, in a domain the flows across its cross-sections which have the same cut are the same as the flows are approaching the end of the domain [79]. A sectional view of this location on a TPT is displayed in Figure 4.6.

4.4.1 Flow field

In order to track the path which the particles of the flow follow, streamlines are drawn in the domain at a particular location to describe the nature of the fluid flow. As has been mentioned above, an axial location of $0.866m$ is selected as a particular location for all the domains.

Figure 4.9 shows the streamline patterns for the various designs at the same axial location of $0.866m$. As a result of absence of a twisted tape in the PT (frame a), the concentration of the streamlines around its wall is weak. The twisted tape insert in the TPT (frame b) generates swirls and therefore make the distribution of the streamlines in the domain to be uniform. In the TECT (frame c), however, the streamlines have more concentration inside the cut. This is because of the additional mixing that

is created by the cut. Due to the periphery of the circular cut in the TCCT (frame d) having an equal distance from the centre of the cut, the streamlines inside the cut are spread but not concentrated. The edges of the triangular cuts in the TTCT (frame e) increases which improves the fluid mixing and makes the streamlines in the TTCT to concentrate at the centre of the cut.

The presence of alternate axis in TAECT (frame f) alters the streamline pattern while the cut in the TAECT (frame f) makes the streamlines to concentrate at the centre of the cross-section. The alternate axis in the TAECT creates dome-shaped streamlines around the wall of the domain. In the TACCT (frame g), the alternate-axis also generates dome-shaped streamlines in the wall of the domain but the streamlines in the cut are not as dense as that in the TAECT (frame f). This is due to the fact that the better fluid mixing occurs in the latter case. The intensity of the streamline in the TATCT (frame h) is higher than that in the TAECT (frame f). In particular, the edge of the triangular cut in the TATCT gives a better mixing of the fluid than that in the circular cut in TACCT.

4.4.2 Velocity contour

With the aim of understanding the detailed flow physics and phenomena throughout the length of the domain the velocity vectors along with the magnitude of the streamwise velocity of the flow at a randomly selected axial location are presented in Figure 4.10 for all the pipe models undertaken. The randomly selected locations considered for each of the induced tubes has either a cut or an alternate axis or neither.

In the PT (Figure 4.10 (A)), the velocity profile is almost the same at all locations and the maximum velocity occurs at the centre implying that the

flow is fully developed and parabolic at these locations. However, when the tube is induced with a plain twisted tape (Figure 4.10 (B)), the velocity near the wall at all the locations (frames a - e) increases by about 6.17% of that in the PT. This is due to the swirl generated by the twisted tape as also seen in the previous figure.

The cut at the location $0.637m$ (frame d) in the TECT (Figure 4.10 (C)) increases the swirl and makes the magnitude of the velocity in the region to be about 2.01%, 1.98% and 2.01% higher than that in the upstream regions, e.g. in $0.5m$ (frame a), $0.516m$ (frame b) and $0.6m$ (frame c) respectively. In the further downstream region, that is at the location of $0.7m$ (frame e), the peak velocity magnitude is about 2.11% less than that in the previous region (frame d). It is interesting to note that the trends in the variations in the values of the velocities for the TECT (Figure 4.10 (C)) are similar to those in the TCCT (Figure 4.10 (D)) and TTCT (Figure 4.10 (E)).

As a result of the alternate axis in the TAECT (Figure 4.10 (F)), TACCT (Figure 4.10 (G)) and TATCT (Figure 4.10 (H)), their maximum velocity magnitude ($0.153 m/s$ in TAECT, $0.156 m/s$ in TACCT, $0.158 m/s$ in TATCT) is about 2.13%, 3.89% and 3.11% higher than that in the TECT (Figure 4.10 (C)), TCCT (Figure 4.10 (D)) and TTCT (Figure 4.10 (E)) respectively. Moreover, due to the presence of the cuts at the location $0.516m$ (frame b of dome F-H), the velocities are shown to be 2.88% higher than that at the location of $0.5m$ (frame a). However, in the downstream region (frame c) in each of the TAECT, TACCT and TATCT, the alternate axis on the tape creates an additional churning to the fluid. Consequently, the velocities in these regions (frames c) are different from those in their upstream regions. Due to the presence of alternate axis at the location $0.6m$ (frame c), its velocity is higher than that at the location $0.673m$ (frame d) which has a

cut. Also, the velocity at the location $0.7m$ (frame e), which has no cut, is less than in the location $0.673m$ (frame d). Specifically, the velocity at $0.7m$ (frame e) is 3.78% and 2.31% lower than those at the location $0.6m$ (frame c) and $0.673m$ (frame d) respectively.

4.4.3 Temperature profile

By reporting the results in the form of contours, the variations in the temperature at different locations in the domains are discussed in this section.

Figure 4.11 depicts the contours of the temperature in the various domains at their different locations already mentioned in the previous section. The contours of temperature at these locations are approximately the same for the PT (Figure 4.11 (A)). The development of the flow at these points which results in the thermal boundary layer being the same may be responsible for this occurrence. In Figure 4.11 (B), the temperature in the TPT is 2.01% higher than that in the PT and this increase in the temperature is attributed to the inclusion of the plain twisted tape inserts which caused an increased disturbance to the boundary layer as a result of the increased mixing imparted on the fluid.

Due to the presence of cuts in the TECT (Figure 4.11 (C)), TCCT (Figure 4.11 (D)) and TTCT (Figure 4.11 (E)), an additional mixing occurs in the fluid flow which again causes further disturbance to the flow field. As a result, higher temperature is shown in the TECT, TCCT and TTCT [122]. Further in the TECT (Figure 4.11 (C)), the temperature at the axial location $0.673m$ (frame d) is found to be about 2% to 3% higher than that at its upstream axial locations $0.5m$ (frame a), $0.516m$ (frame b) and $0.6m$ (frame c). Again, this is caused by the section of the cut present at this

axial location ($0.673m$). However due to the absence of the cut in the downstream region (frame e), the temperature drops and is found to be about 2.14% lower than that at the location $0.673m$ (frame d). Note that the temperature increase also applies to the TCCT (Figure 4.11 (D)), and TTCT (Figure 4.11 (E)).

In the next three cases, TAECT (Figure 4.11 (F)), TACCT (Figure 4.11 (G)) and TATCT (Figure 4.11 (H)), the temperature at the location of $0.516m$ (frame b) shows about 1.91% rise over that in the upstream location (frame a) because of the presence of the cuts. The temperature rise continues and it is 2.89% higher at the location $0.6m$ (frame c) than that in the previous frame, which is mainly caused by the creation of thermal energy from an extra disturbance exerted on the fluid flow by the alternate axes [123]. However, due to the presence of a cut (but not alternate -axis) at location $0.673m$ (frame d), and the absence of the cut and alternate axes in $0.7m$ (frame e), the temperature is reduced from $0.6m$ (frame c) towards the downstream region $0.7m$ (frame e) with an overall temperature drop of about 3.89%.

4.4.4 Pressure distribution

The domains considered in this work have different designs and therefore the pressure in them will not be the same. In addition, it is important to consider the pressure at different locations in the tube designs. In this section, this pressure variation is discussed by examining the contours of the pressure at different locations.

The pressure contours at different axial locations in the domains are presented in Figure 4.12. These locations have already been mentioned in the previous sections. It is seen in the PT (Figure 4.12 (A)) that the pressure

in it decreases along the downstream of the flow. The pressure at $x = 0.5m$ (frame a) decreased by 3.88% and 2.41% at locations $x = 0.51m$ (frame b), $x = 0.6m$ (frame c) respectively. The pressure at $x = 0.6m$ (frame c) suffers a reduction of 25.68% and 38.55% at $x = 0.673m$ (frame d) and $x = 0.7m$ (frame e) respectively. The decrease in pressure is caused by the viscous effect generated by the surface of the tube when the fluid comes in contact with the tube [124]. In Figure 4.12 (B), the twisted tape in the TPT caused disturbance to the fluid the pressure which results in additional dissipation of pressure of the fluid. Thus, the pressure in the TPT is higher than that in the PT.

In each of the TECT (Figure 4.12 (C)), TCCT (Figure 4.12 (D)) and TTCT (Figure 4.12 (E)), the pressure at $x = 0.5m$ (frame a) decreases by approximately 5.25%, 26.19%, 51.73% and 65.33% at $x = 0.516m$ (frame b), $x = 0.6m$ (frame c), $x = 0.673m$ (frame d) and $x = 0.7m$ (frame e) respectively. Also, the dissipation of additional pressure due to the presence of cuts on the tapes at $x = 0.673m$ (frame d, C-E) make the regions to have a pressure that is 9.02%, 7.69% and 11.12% respectively higher than that in its corresponding location in the domain TPT (Figure 4.12 (B)). In addition, these results indicate that the dissipation of additional pressure due to the presence of cuts on the tapes is most impactful in the TTCT (with triangular cut) than in the TECT (with elliptical cut) and TCCT (with circular cut).

For the remaining three domains, TAECT (Figure 4.12 (F)), TACCT (Figure 4.12 (G)) and TATCT (Figure 4.12 (H)), the pressure at the location $0.516m$ is 7.41% over those in the upstream (frame a) because of the presence of cuts at the location $0.516m$ (frame b). The pressure reduction continues and the pressure at the location $0.673m$ (frame d) is reduced by 54.18%, 50.11% and 52.21% respectively of those at location $x = 0.6m$ (frame c).

Also, the additional pressure created by the alternate axes at location $x = 0.6m$ (frame c) makes the pressure at the location to be 6.07% higher than at location $x = 0.516m$ (frame b). It should be mentioned that the pressure at $x = 0.6m$ (frame c) for TAECT, TACCT and TATCT are 58.82%, 62.52% and 72.86% respectively higher than those in TECT, TCCT and TTCT respectively. This proves the effect of the cuts and the alternate axes at the location.

4.4.5 Heat transfer assessment

For the laminar flow under consideration, the heat transfer is presented in terms of the dimensionless quantity known as Nusselt number. The expression for the average Nusselt number (Nu) is calculated [125] by

$$Nu = \frac{1}{L} \int_0^L \frac{D}{k} h(x) dx \quad (4.1)$$

where L = length of the tube

$h(x)$ = heat transfer coefficient at a point (x) along the tube

D = inner diameter of the tube

k = thermal conductivity of fluid

The heat transfer coefficient $h(x)$ is given as

$$h(x) = \frac{q''}{T_w(x) - T_m(x)} \quad (4.2)$$

The term $T_m(x)$ is determined as

$$T_m(x) = T_{m,i} + \frac{q'' \pi D x}{\dot{m} C_p} \quad (4.3)$$

where q'' is the heat flux, $T_w(x)$ is the wall temperature of the tube at a position (x) along the tube, $T_m(x)$ is the mean temperature of the fluid at a position (x) along the tube, $T_{m,i}$ is the mean temperature of the fluid at the inlet of the tube, \dot{m} is the mass flow rate of the fluid, and C_p is the specific heat capacity of the fluid.

It is important to see how the simulated results match experimental results and correlations. According to Stoiber et al. [126], the quality of the validation results depends on various factors such as quality of the grid, boundary conditions and the computational model of the fluid. Therefore, it is important to validate the computational results obtained.

The validation of Nusselt number of the plain tube (PT) with the experimental data obtained by Wongcharee and Eiamsa-ard [121], as shown in Figure 4.13, gives a deviation of 2.06%. The Nusselt number results of the tube induced with a plain twisted tape insert were also validated with their experimental results as well as with a correlation derived by Hong and Bergles [37]. The correlation of Hong and Bergles is given as

$$Nu = 5.17 \left[1 + 5.484 \times 10^{-3} Pr^{0.7} \left(\frac{Re}{y} \right)^{1.25} \right]^{0.5} \quad (4.4)$$

Figure 4.14 shows the validation results of the Nusselt number between the numerical result of the TPT and the Wongcharee and Eiamsa-ard experiment [121] and Hong and Bergles correlation [37]. The numerical result is in very good agreement with the experimental data of Wongcharee and Eiamsa-ard with a deviation of 2.55%, while its agreement with the Hong and Bergles correlation is excellent and falls within a deviation of 0.66%. The above observations therefore indicate that the simulated results are in very good agreement with the experimental and correlated data.

The effect of the various twisted tape on the heat transfer for the laminar flow is presented in Figure 4.15. It can generally be observed that the Nusselt number increases as the Reynolds number increases. This arises as a result of the momentum that overcomes the viscous force of the fluid as the Reynolds number increases and in effect diminishes the shear between the fluid and the tube wall [2]. It is also evident in Figure 4.15 that the Nusselt number in the TPT is higher than that in the PT. This, according to Gou et al. [79], is caused by the decrease in the flow cross-sectional area and an increase in the velocity of the induced tubes, already depicted in Figure 4.10 (B - H), which makes the fluid inside them to swirl with a higher velocity. This resulted in increase of the heat transfer coefficient of the induced tube.

It is also evident in Figure 4.15 that the Nusselt number in the TECT, TCCT and TTCT are 7.25% to 17.08%, 5.28% to 11.97% and 8.78% to 21.60% respectively higher than that in the TPT. The reason behind this is that once a cut is made on the surface of the twisted tape, the cut creates additional swirls in the tube and therefore more disturbance is imparted to the flow by the tapes [79], the result of which is the augmentation of the Nusselt number in the induced tubes.

Another observation in Figure 4.15 is the higher Nusselt number in the tubes which have tapes with combined cuts and alternate axes (TAECT, TACCT and TATCT) than in their corresponding tubes which have only cuts on the tapes (TECT, TCCT and TTCT). The reason behind this is that the alternate points of the alternate axes of the TAECT, TACCT and TATCT provide additional mixing and better fluid disturbance over those of the TECT, TCCT and TTCT with cuts alone. For the present investigation, the Nusselt number in the TAECT, TACCT and TATCT are 74.54% to 84.78%, 75.10% to 84.92% and 75.33% to 84.67% higher than those in the TECT,

TCCT and TTCT respectively. It is therefore evident that the tube induced with an alternate-axis triangular cut twisted tape (TATCT) produced the highest Nusselt number. The ranking of the different domains at $Re = 2000$ for the heat transfer is presented in Table 4.2.

4.4.6 Friction factor

The pressure drop that occurs in the flow is illustrated the Darcy friction factor which is given [125] as

$$f = \frac{2D \cdot \Delta P}{u_m^2 \cdot L \cdot \rho} \quad (4.5)$$

where f is the friction factor, ΔP is the pressure drop, u_m is the mean velocity of fluid and ρ is the density of fluid.

In order to examine the degree to which the numerical results for the friction factor match experimental results and correlations, validation was carried out on the simulated results of the friction factor. The friction factor of the plain tube (PT) was validated with the experimental results of Wongcharee and Eiamsa-ard [121] and the result, shown in Figure 4.16, indicates that the friction factor for the simulated result and the experimental result has a maximum discrepancy of 8.9%.

The friction factor of the tube induced with plain twisted tape insert (TPT) were validated with the experimental results of Wongcharee and Eiamsa-ard [121] and the correlation of Donevski and Kulesza [127]. The Donevski and Kulesza correlation is given as:

$$f = \left(\frac{15.625}{Re} \right) \left[1 + \left(\frac{0.85}{y^2} \right) \right]^{1/2} \left[\frac{\pi + 2 - \frac{2\delta}{D}}{\pi - \frac{4\delta}{D}} \right]^2 \left[\frac{\pi}{\pi - \frac{4\delta}{D}} \right] \quad (4.6)$$

As depicted in Figure 4.17, the friction factor for the simulated result and the experimental result has a maximum discrepancy of 3.06%. The simulated results agreed with the Donevski and Kulesza correlation with a deviation of 0.70%.

The above observations indicate that the simulated results are in very good agreement with the experimental and correlation results. The small deviations shown in the comparison are possibly as a result of different conditions under which each result was obtained.

The variation of the friction factor with Reynolds number for the tubes with different types of twisted tape inserts is illustrated in Figure 4.18. It is observed that as any of the twisted tape is placed inside the tube, the falling trend of the friction factor becomes sharper in comparison with the plain tube (TPT). This is due to the blockage which the tapes impart on the flow and thereby diminishing the momentum of the flow. It is also observed that the friction factor of the TPT is 6.38 to 21.41 times that of the PT and that at a lower Reynolds number the friction factors are higher. This, according to Holman [2], is because at lower Reynolds number the momentum of the flow is lower and therefore the flow suffers a higher resistance.

The friction factor of the TECT, TCCT and TTCT are 6.75 to 13.65 times, 6.67 to 13.35 times and 6.92 to 14.01 times respectively that of the PT. The increase in the friction factor over the TPT is caused by the presence of cuts on them which generates supplementary pressure as shown in Figure 4.12. The friction factor of the TAECT, TACCT and TATCT are 9.80 to 19.77 times, 9.75 to 19.58 times and 10.13 to 20.30 times respectively that of the PT. The translation of this result is that the friction factor in the TAECT, TACCT and TATCT are higher than those in the TECT, TCCT and TTCT

respectively. The supplementary mixing supplied by the alternate points of the TAECT, TACCT and TATCT (which are absent in the TECT, TCCT and TTCT) is responsible for this, as shown in Figure 4.10.

The friction factor of TECT is 1.05 - 1.10 times that of the TPT. The friction factor of the TCCT is lower compared with the TECT while those of the TCCT and TTCT are 1.04 - 1.07 and 1.08 - 1.12 respectively times that of the TPT. For the TAECT, TACCT and TATCT, their friction factor is 1.54 - 1.59, 1.52 - 1.57 and 1.58 - 1.63 respectively times that of the TPT. The ranking of the different domains at $Re = 2000$ for the friction factor is presented in Table 4.2.

4.4.7 Thermal performance factor

To evaluate the practical use of the twisted tape, a thermal performance factor, also known as heat transfer enhancement index, is used. It is an indication of the potential of a twisted tape for practical applications in enhancement of heat transfer [12, 16]. It compares the thermal performance of the induced tube and the plain tube by considering the same pumping power consumption for tubes with or without a tape insert. It is obtained by simultaneously considering the effect of heat transfer promotion and the rise of pressure drop. It is mathematically given [12, 16] as

$$\eta = \frac{Nu}{Nu_p} \left(\frac{f}{f_p} \right)^{-1/3} \quad (4.7)$$

where Nu and Nu_p are the Nusselt numbers of the induced tube and plain tube respectively while f and f_p are the friction factor of the induced tube and plain tube respectively.

The thermal performance factor for the TPT, TECT, TCCT, TTCT, TAECT, TACCT and TATCT are compared in Figure 4.19. The performance factor increases as the Reynolds number increases, owing to considerable consequence of the augmentation of heat transfer provided by the twisted tapes. An indication of achievement of heat transfer enhancement is proved since the thermal performance factors are all above unity [16].

As can be seen in the Figure 4.19, the thermal performance factor of the TPT is lower than the other tube designs. This is a consequence of the Nusselt number that is lower in the TPT than in the other tube designs considered in Figure 4.19. The thermal performance factor of the TECT, TCCT and TTCT is 3.84 to 15.92%, 2.9 to 12.48% and 4.53 to 1.69% respectively higher than that in the TPT. As explained in §4.4.5 above, this improvement in the thermal performance factor is sequel to the promotion of the Nusselt number caused by the cuts on the tapes. It is also observed that the performance factor in the TAECT, TACCT and TATCT is 63.08 to 97.47%, 61.30 to 89.54% and 64.69 to 103.23% respectively higher than that of the TPT. From the energy point of view, this is an indication of the benefit of the alternate axes of the TAECT, TACCT and TATCT. For the entire range investigated, the maximum thermal performance factor of 2.03 is found with the use of TATCT at $Re = 2000$. The ranking of the different domains at $Re = 2000$ for the thermal performance factor is presented in Table 4.2.

4.5 Correlations for the heat transfer and fluid flow

Correlations were developed for the TAECT, TACCT and TATCT in order to predict their Nusselt number and friction factor for the laminar flow. Furthermore, the correlation is important in revealing the degree of

matching of the simulated results and the predicted results. It should be mentioned that a non-linear regression analysis was applied for the correlation. The correlations take account of the effects of Reynolds number (Re), Prandtl number (Pr), perimeter of cut on twisted tape (p), width of twisted tape (w) and twist ratio of twisted tape (y). The correlations developed for the Nusselt number and the friction factor as given by Equations (4.8) and (4.9) respectively are

$$Nu = -16.532 + Re^{0.646} \left(\frac{Pr}{y}\right)^{-1.098} \left(\frac{w}{p}\right)^{-0.182} \quad (4.8)$$

$$f = \frac{207.283}{Re} + y^{-0.949} \left(\frac{w}{p}\right)^{-0.129} \quad (4.9)$$

Comparisons were made between the simulated results and the predicted results of the Nusselt number as demonstrated in Figure 4.20. It reveals that the simulated Nusselt number and the predicted Nusselt number agree within a discrepancy of 4.07%. For the friction factor, as indicated in Figure 4.21, the simulated friction factor and the predicted friction factor has a discrepancy of 1.09%. These values of discrepancies make the agreement between the simulated and the predicted results to be reasonable. Comparing the results of the correlations with those presented in the literature review in Chapter 2 gives an indication that the numerical results obtained in the present Chapter are reliable.

4.6 Conclusion

The thermo-hydraulic behaviour of laminar flow of water inside tubes of various designs under uniform wall heat flux conditions was determined by

numerical simulation. The Reynolds numbers considered for the laminar flow range between 830 and 2000. The objective is to know which of the tube designs give the best performance in terms of the heat transfer and thermal performance index under the laminar flow. The various tube designs considered are the plain tube, tube with plain twisted tape, tube with elliptical cut twisted tape, tube with circular cut twisted tape, tube with triangular cut twisted tape, tube with alternate-axis elliptical cut twisted tape, tube with alternate-axis circular cut twisted tape and tube with alternate-axis triangular cut twisted tape. It was discovered that the geometry of the cut on the twisted tape inserts has effects on the performance of the tube designs.

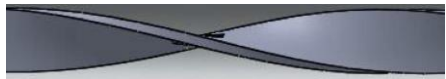
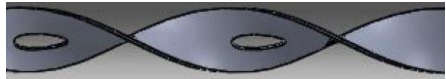
The tube with alternate-axis triangular cut twisted tape has the highest temperature gradient and a temperature distribution that is superior to other tube designs. As a result of the improved swirl and superior temperature distribution of the tube with alternate-axis triangular cut twisted tape over the other tube designs, it produces the best performance. Its Nusselt number and friction factor are 90.73% to 124.57% and 58.8% to 63.52% respectively higher than those in the tube with plain twisted tape while its thermal performance factor is 64.69% to 103.23% higher than that in the tube with plain twisted tape.

In addition, correlations were developed and comparisons were made between the results of the correlation and the numerical results. The numerical results are in good agreement with the experimental results as well as with the established correlations. There is a discrepancy of 4.07% between the Nusselt number of the predicted and numerical results. In the case of the friction factor, the discrepancy is 1.09%.

Table 4.1: Number of cells for grid resolution study for the laminar flow

Domain	Number of cells			
PT	461178	476554	512420	614904
TPT	913594	944154	1015216	1218259
TECT	1122468	1159966	1247298	1496758
TCCT	1214178	1254681	1349142	1618970
TTCT	1236639	1277931	1374099	1648919
TAECT	1486055	1535641	1651206	1981447
TACCT	1557545	1609513	1730639	2076767
TATCT	1255502	1658638	2515756	3018907

Table 4.2: Thermo-hydraulic values of different induced tubes for the laminar flow at $Re = 2000$

Induced tube	Nu	f	η	Tape geometry
TPT	30.86	0.298	3.07	
TECT	33.10	0.327	3.24	
TCCT	32.49	0.320	3.21	
TTCT	33.57	0.336	3.26	
TAECT	57.77	0.475	5.00	
TACCT	56.97	0.470	4.95	
TATCT	58.86	0.487	5.05	

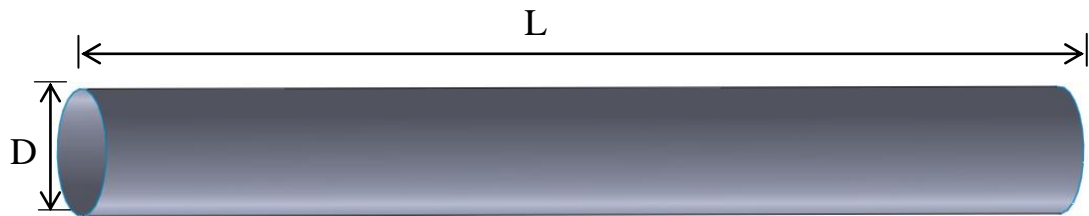


Figure 4.1: Tube.

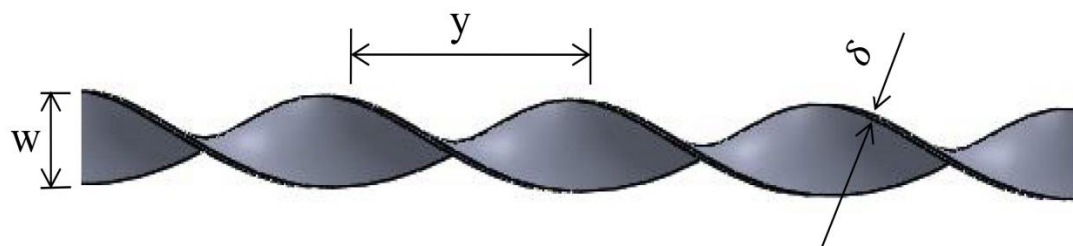


Figure 4.2: Twisted tape.

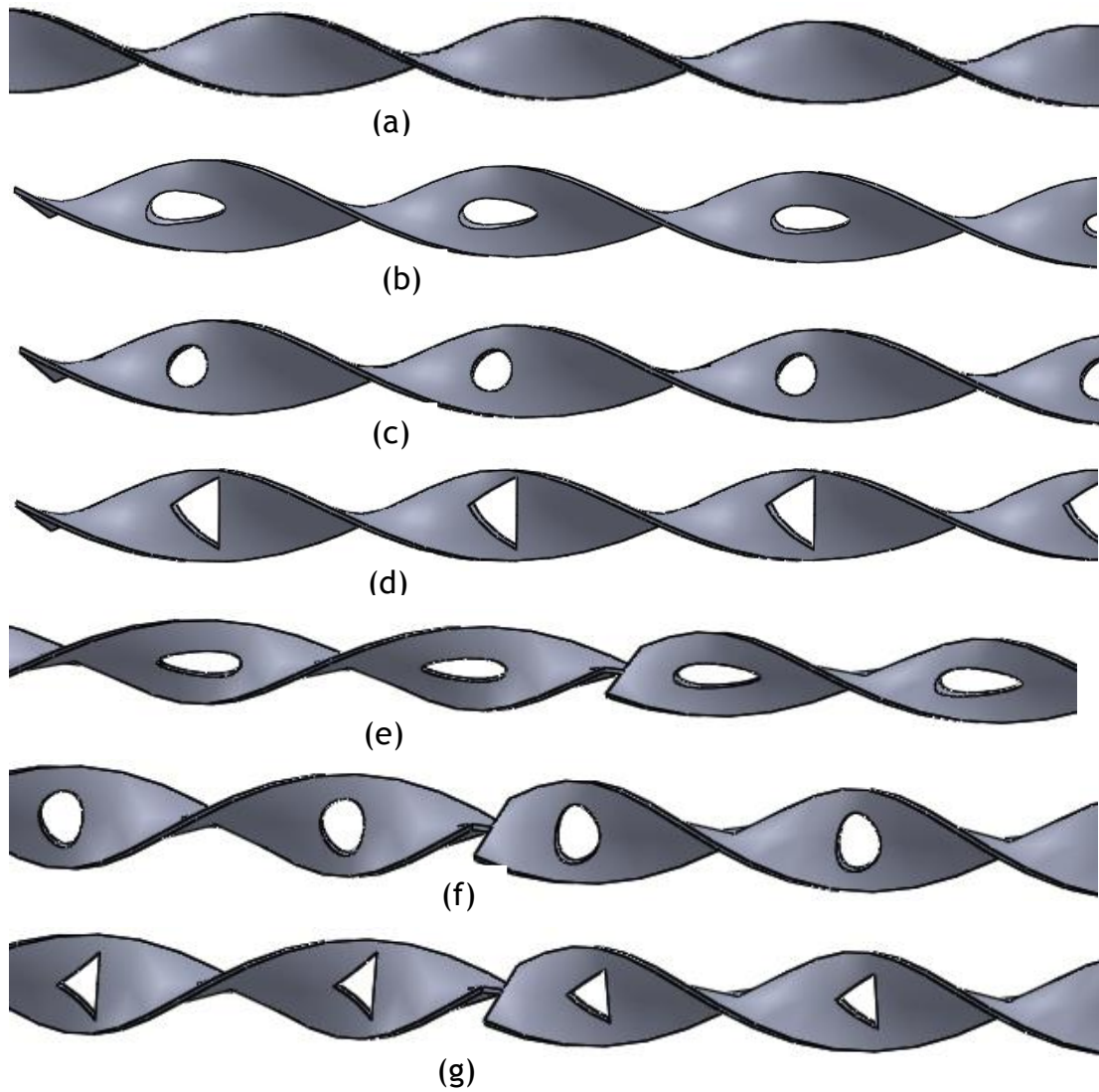


Figure 4.3: Different types of twisted tape insert used for the domains: (a) PTT, (b) ECT, (c) CCT, (d) TCT, (e) AECT, (f) ACCT (g) ATCT.

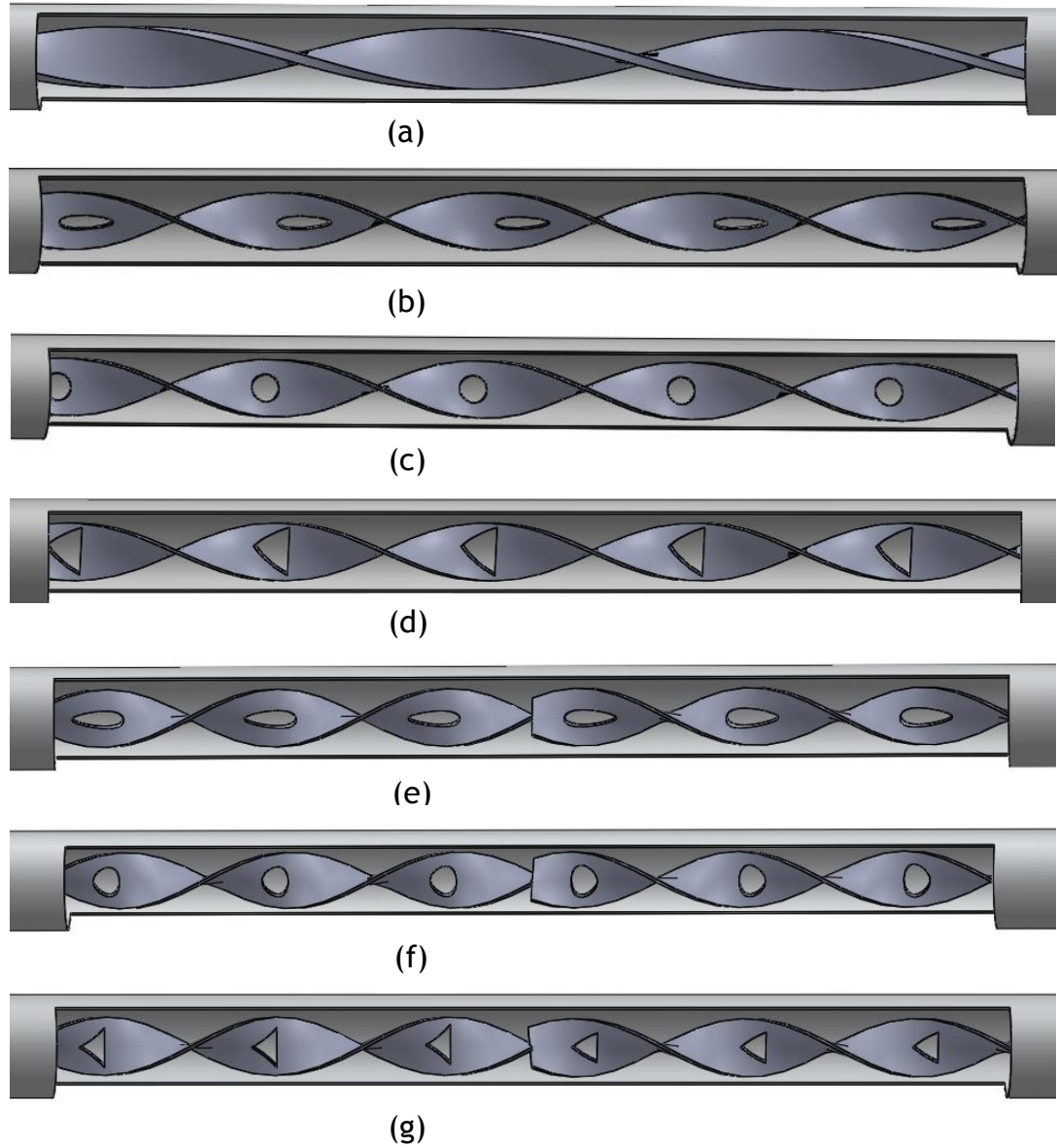


Figure 4.4: Computational domains with twisted tape inserts for (a) TPT, (b) TECT, (c) TCCT, (d) TTCT, (e) TAECT, (f) TACCT and (g) TATCT.

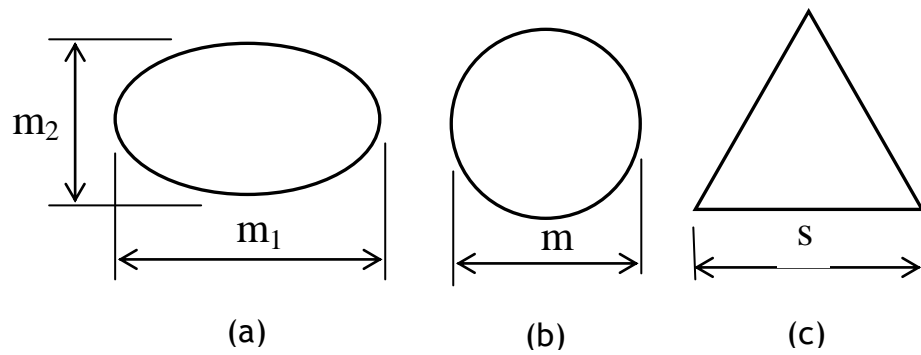


Figure 4.5: Geometries of the cuts on the tapes for (a) elliptical cut, (b) circular cut and (c) triangular cut.

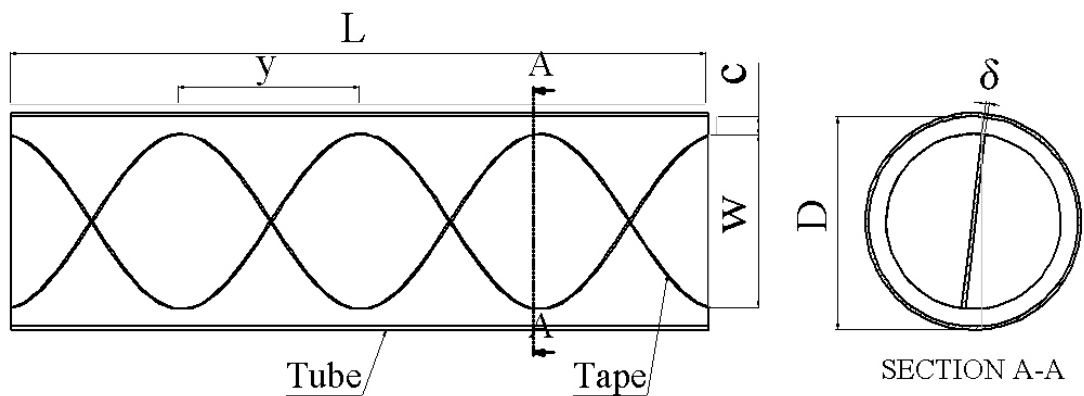


Figure 4.6: Sectional view of a computational domain for the tube induced with a plain twisted tape.

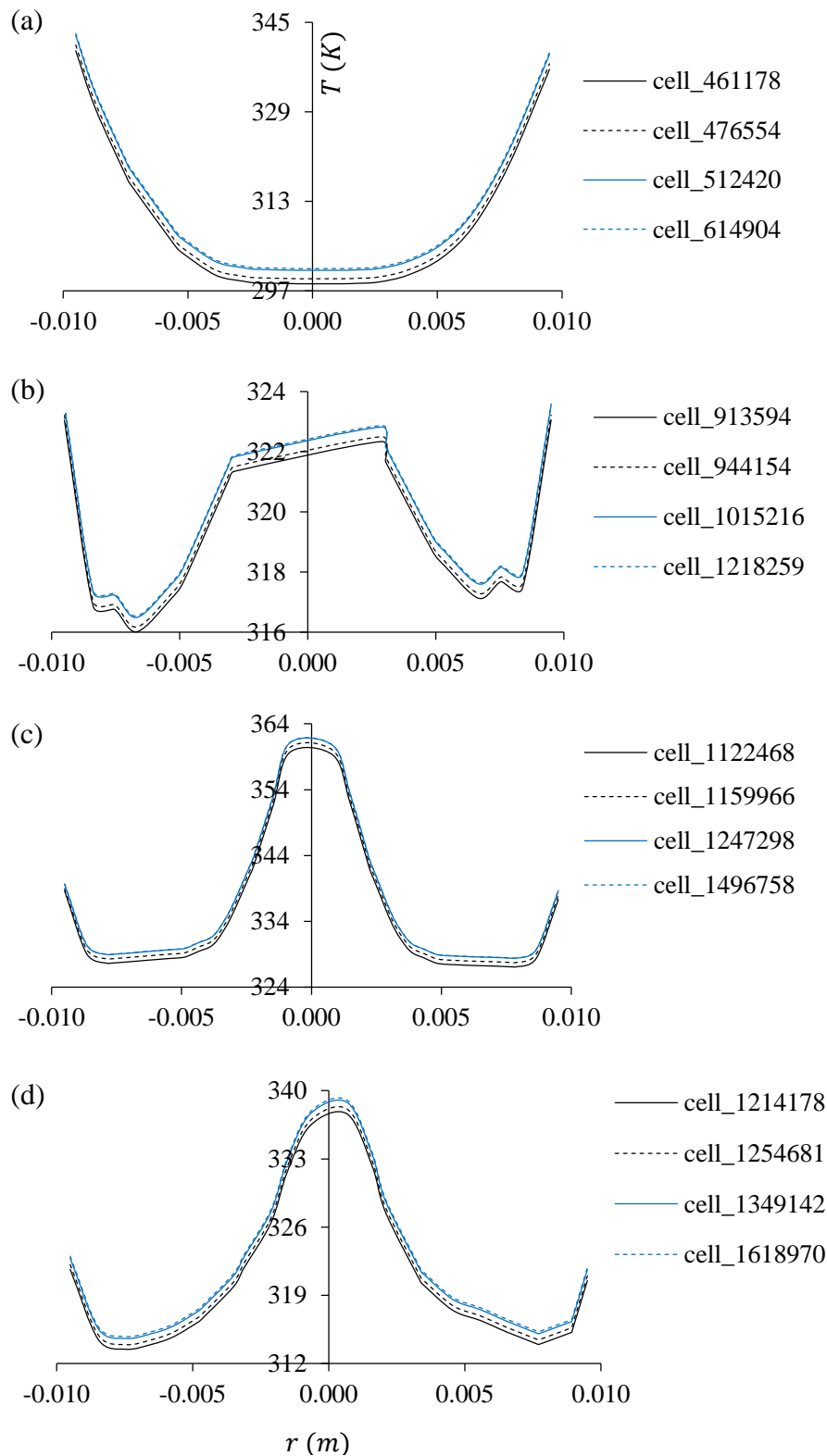


Figure 4.7: Temperature across the cross-section at the exit of (a) PT, (b) TPT, (c) TECT, (d) TCCT, (e) TTCT, (f) TAECT, (g) TACCT and (h) TATCT for $Re = 1820$ with different grids.

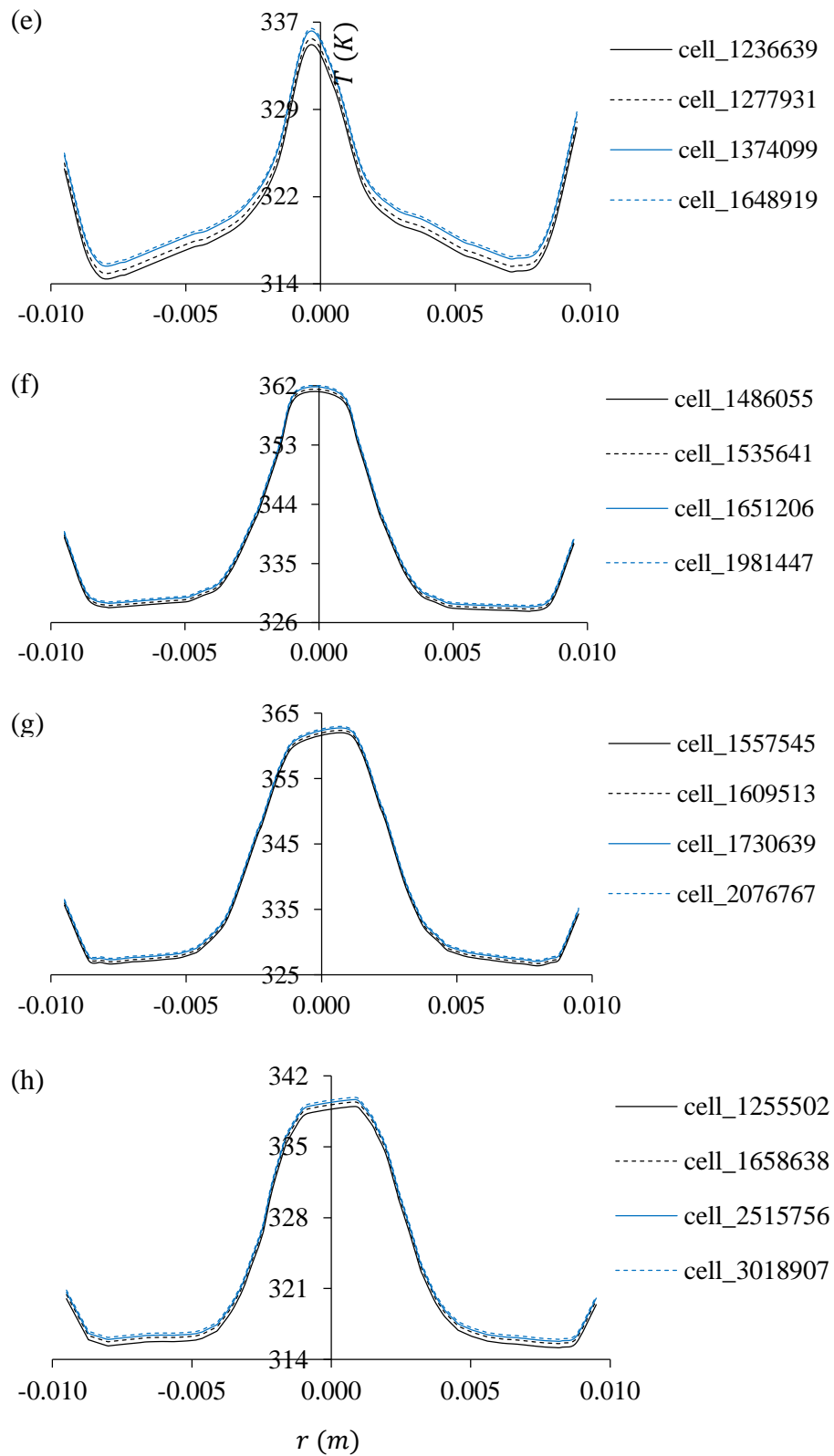


Figure 4.7 caption continued.

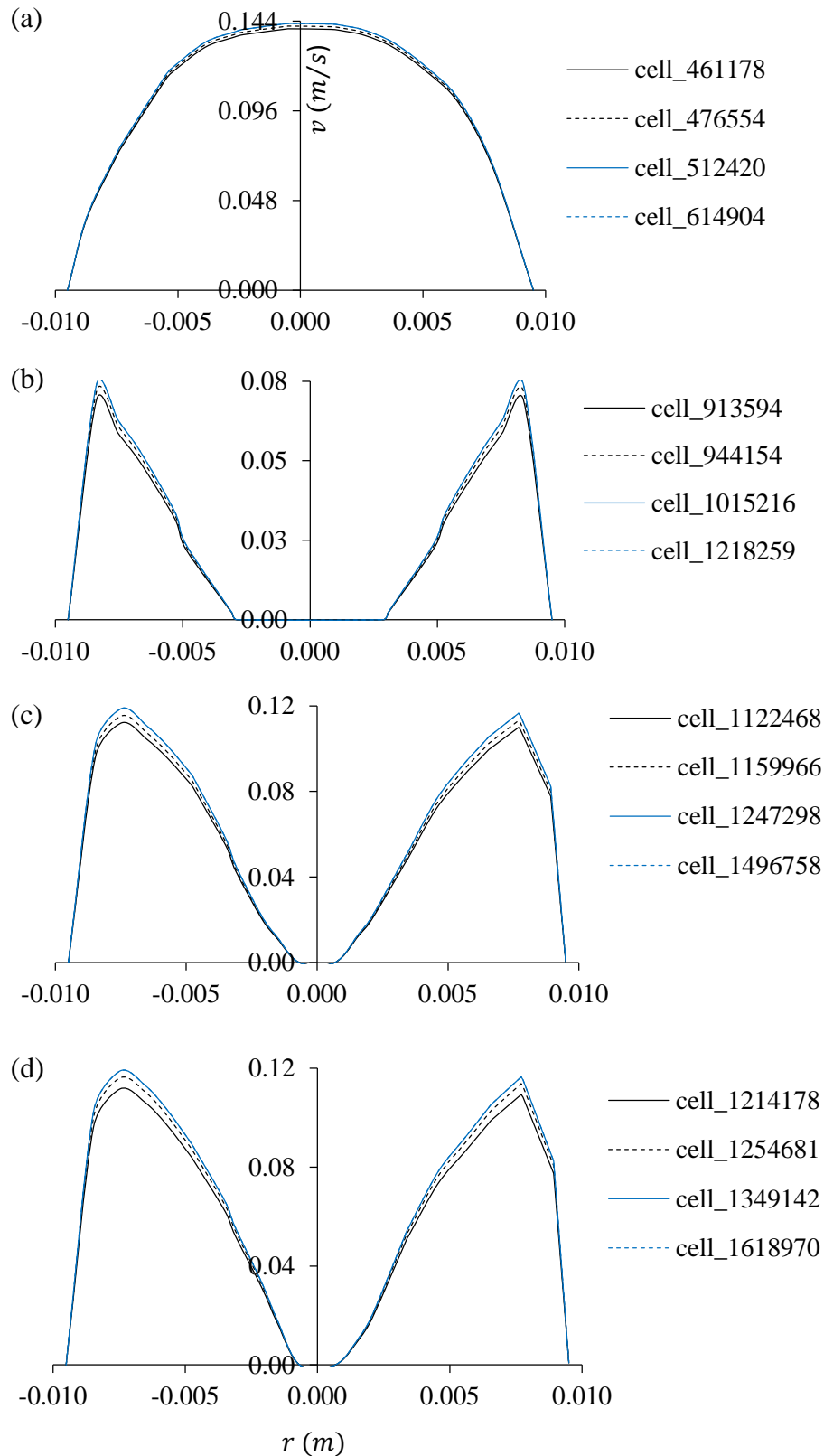


Figure 4.8: Velocity across the cross-section at the exit of (a) PT, (b) TPT, (c) TECT, (d) TCCT, (e) TTCT, (f) TAECT, (g) TACCT and (h) TATCT for $Re = 1820$ with different grids.

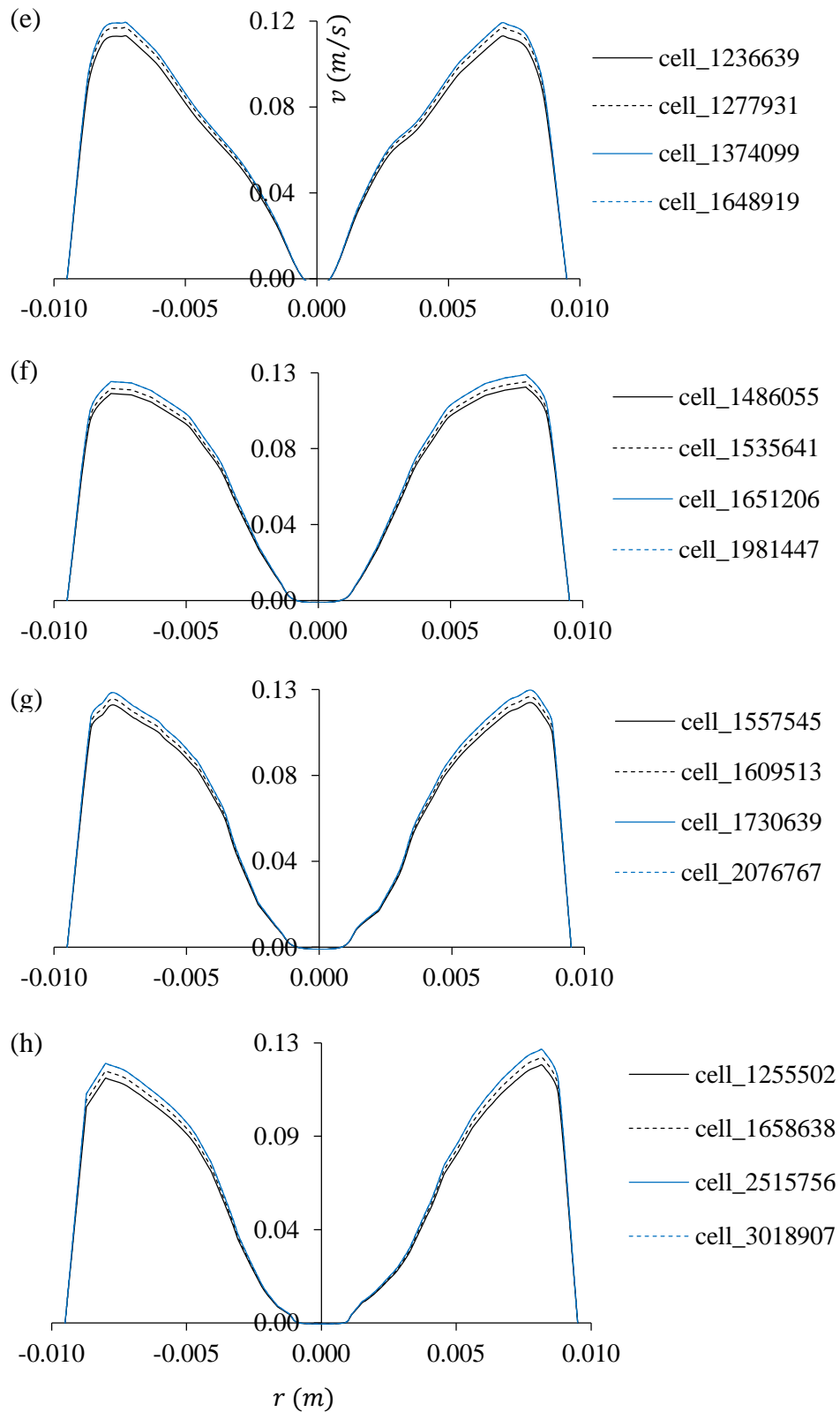


Figure 4.8 caption continued.

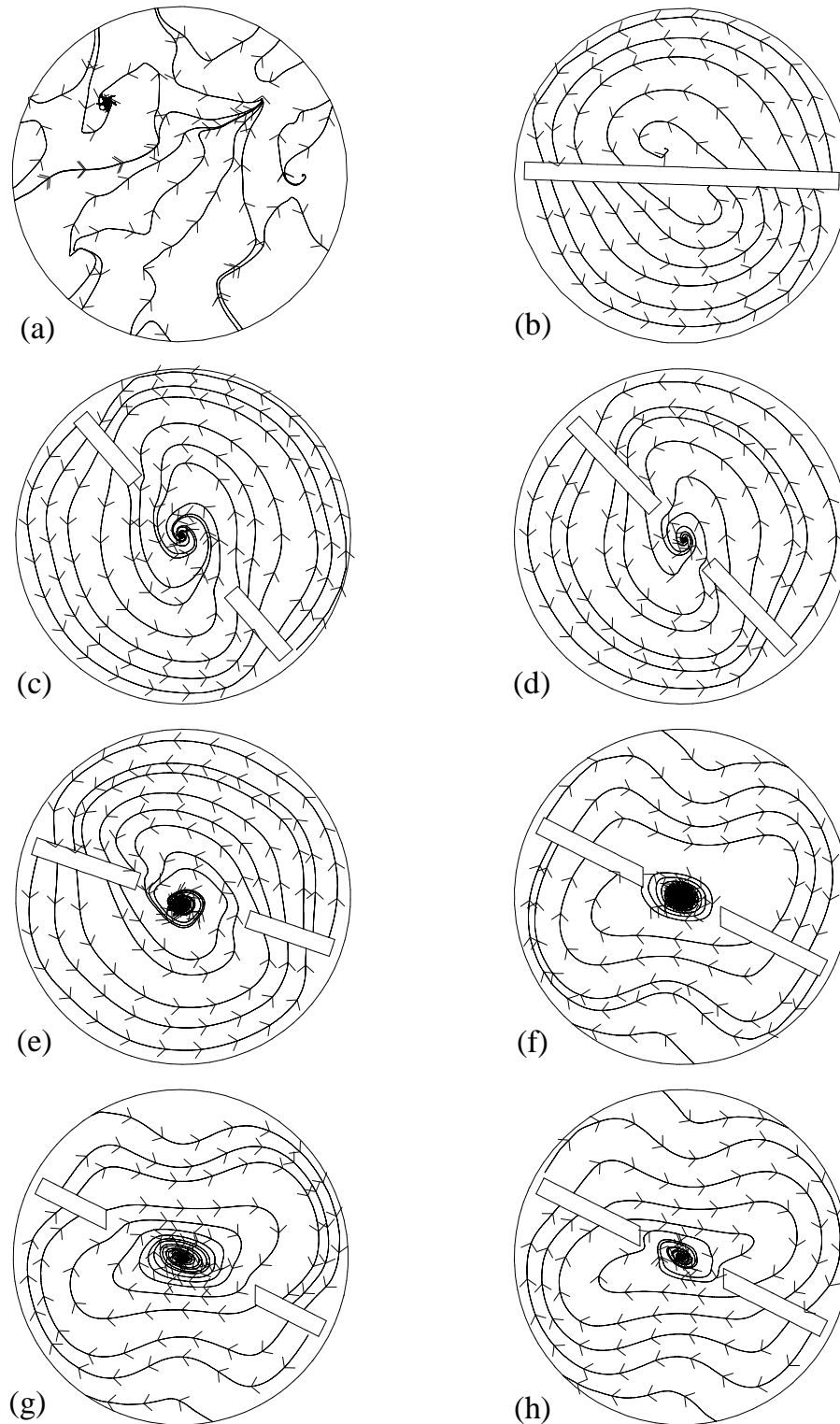


Figure 4.9: Streamlines across the domain cross-section at axial location $0.866m$ of (a) PT, (b) TPT, (c) TECT, (d) TCCT, (e) TTCT, (f) TAECT, (g) TACCT and (h) TATCT for $Re=1820$.

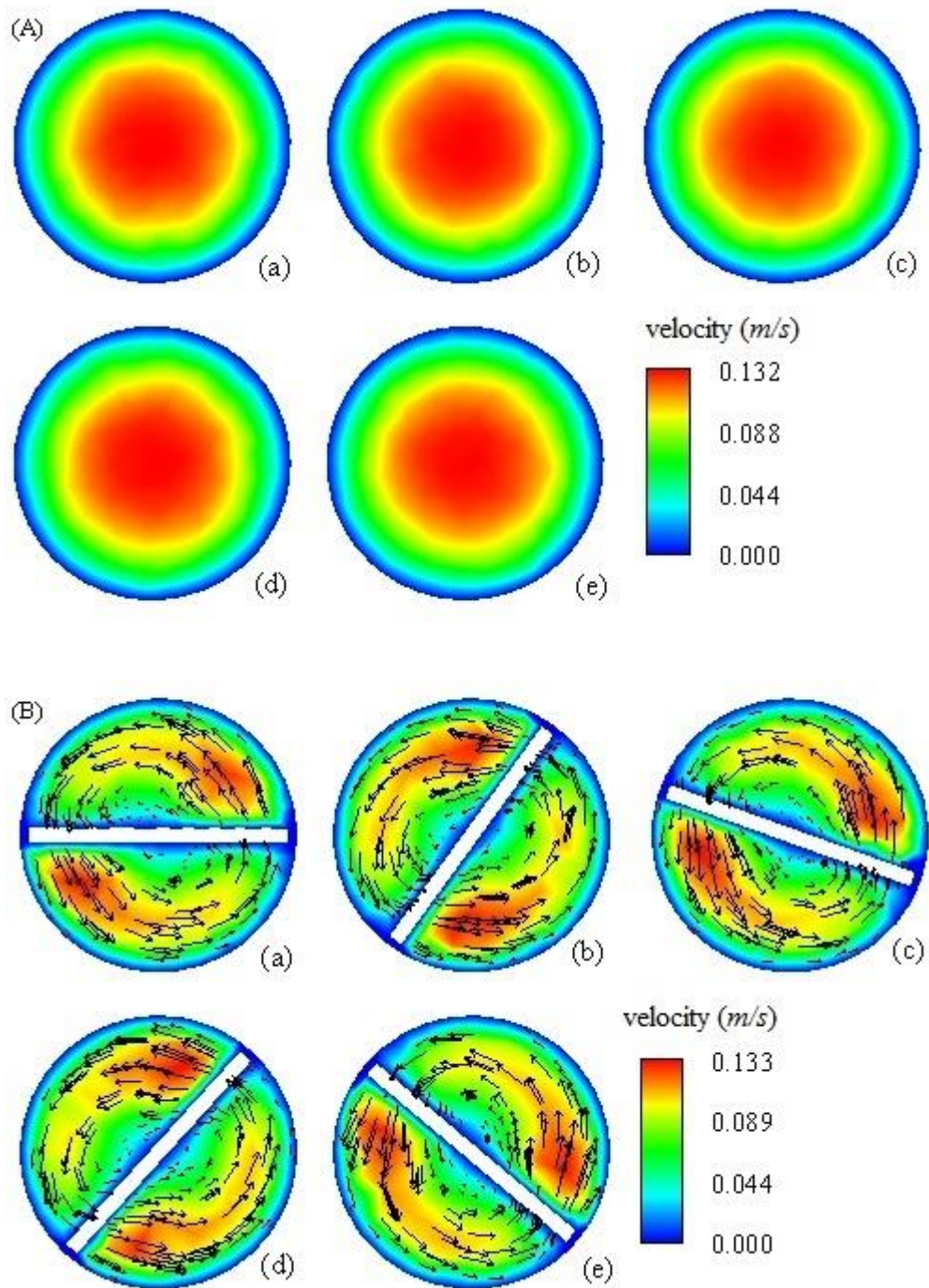


Figure 4.10: Vector plot appended on contour of velocity for PT (A), TPT (B), TECT (C), TCCT (D), TTCT (E), TAECT (F), TACCT (G) and TATCT (H) for $Re=1820$ at axial location (a) 0.5m, (b) 0.516m, (c) 0.6m, (d) 0.673m and (e) 0.7m.

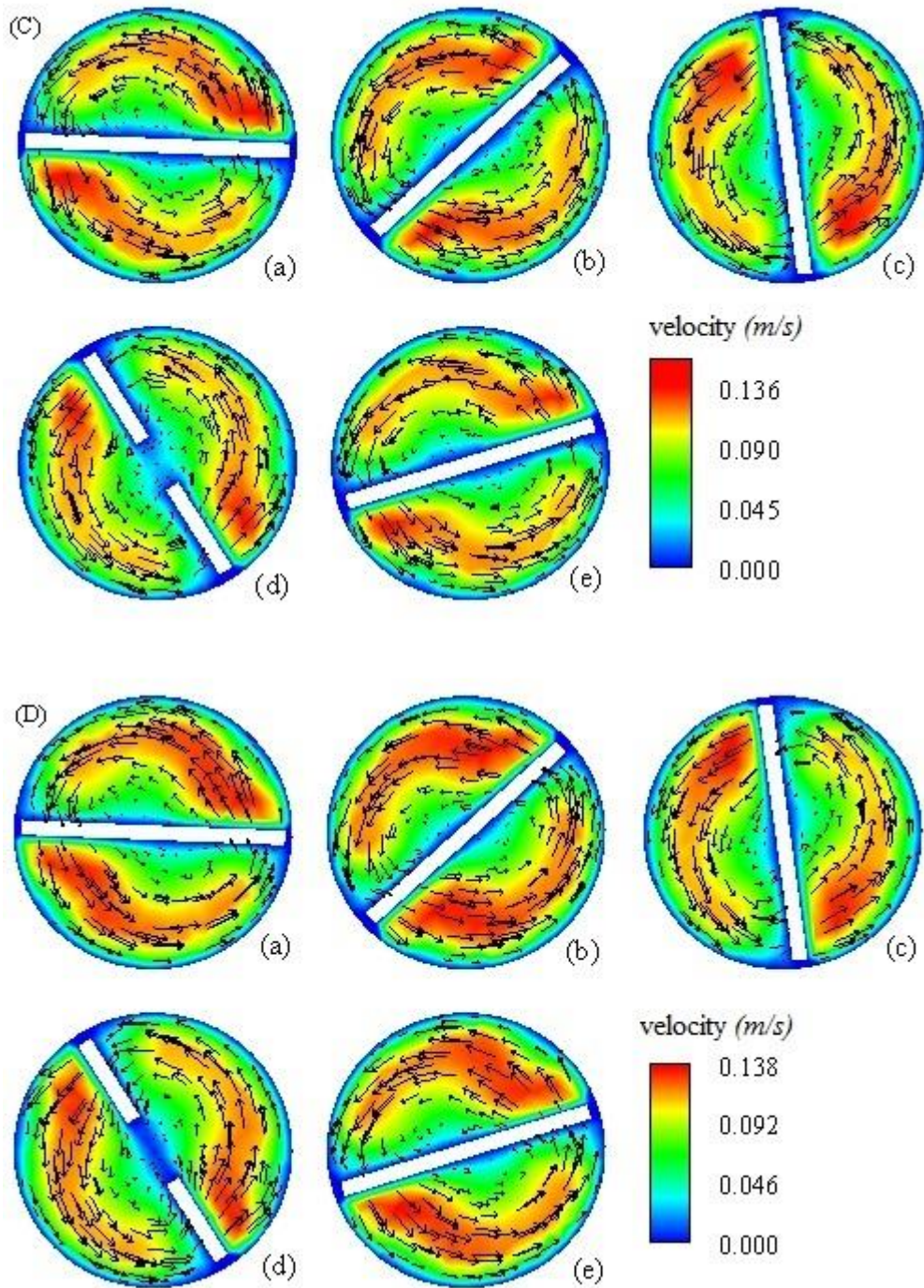


Figure 4.10 Caption continued.

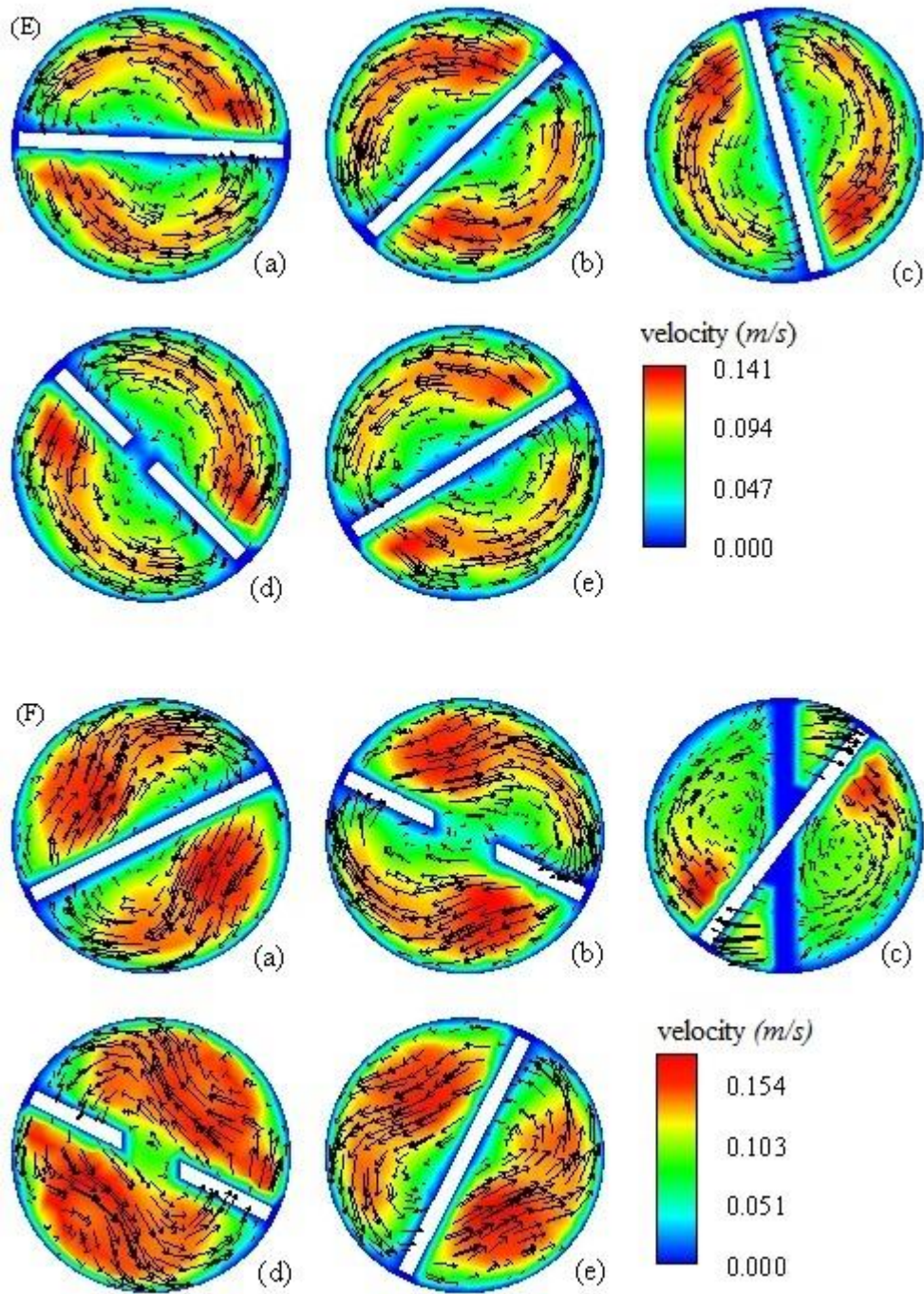


Figure 4.10 Caption continued.

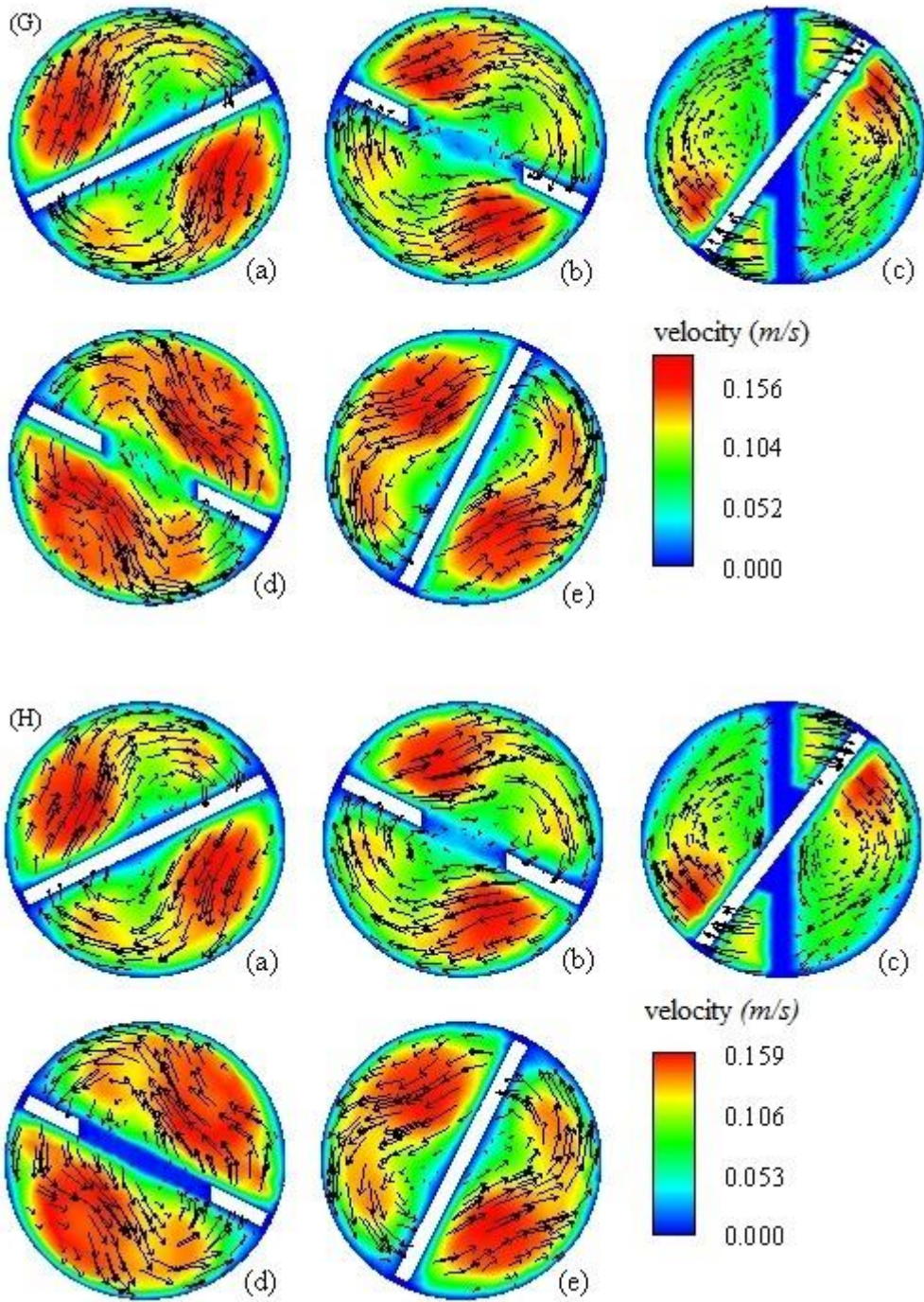


Figure 4.10 Caption continued.

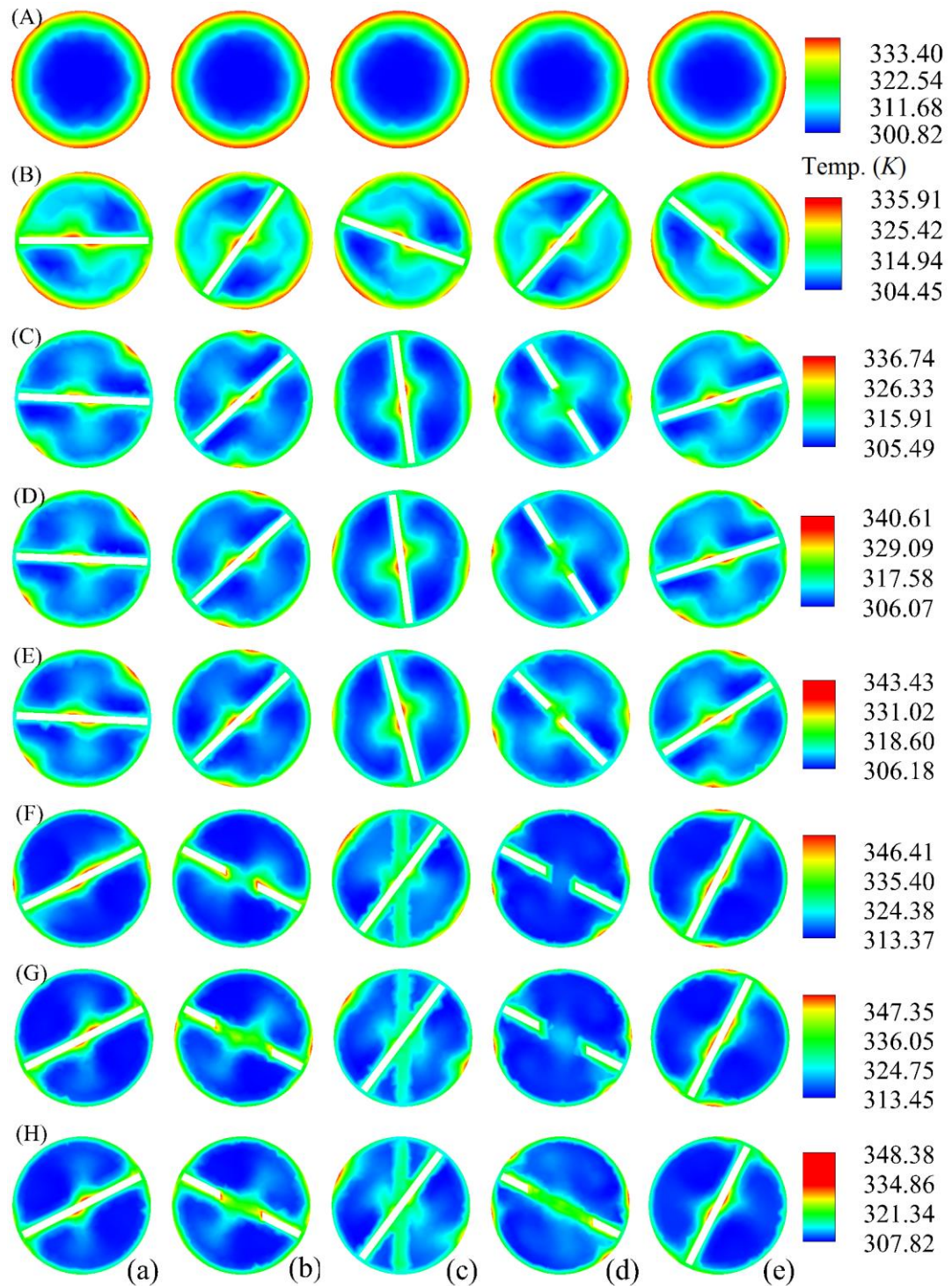


Figure 4.11: Contour plots of temperature for PT (A), TPT (B), TECT (C), TCCT (D), TTCT (E), TAECT (F), TACCT (G) and TATCT (H) for $Re=1820$ at axial location (a) 0.5m, (b) 0.516m, (c) 0.6m, (d) 0.673m and (e) 0.7m.

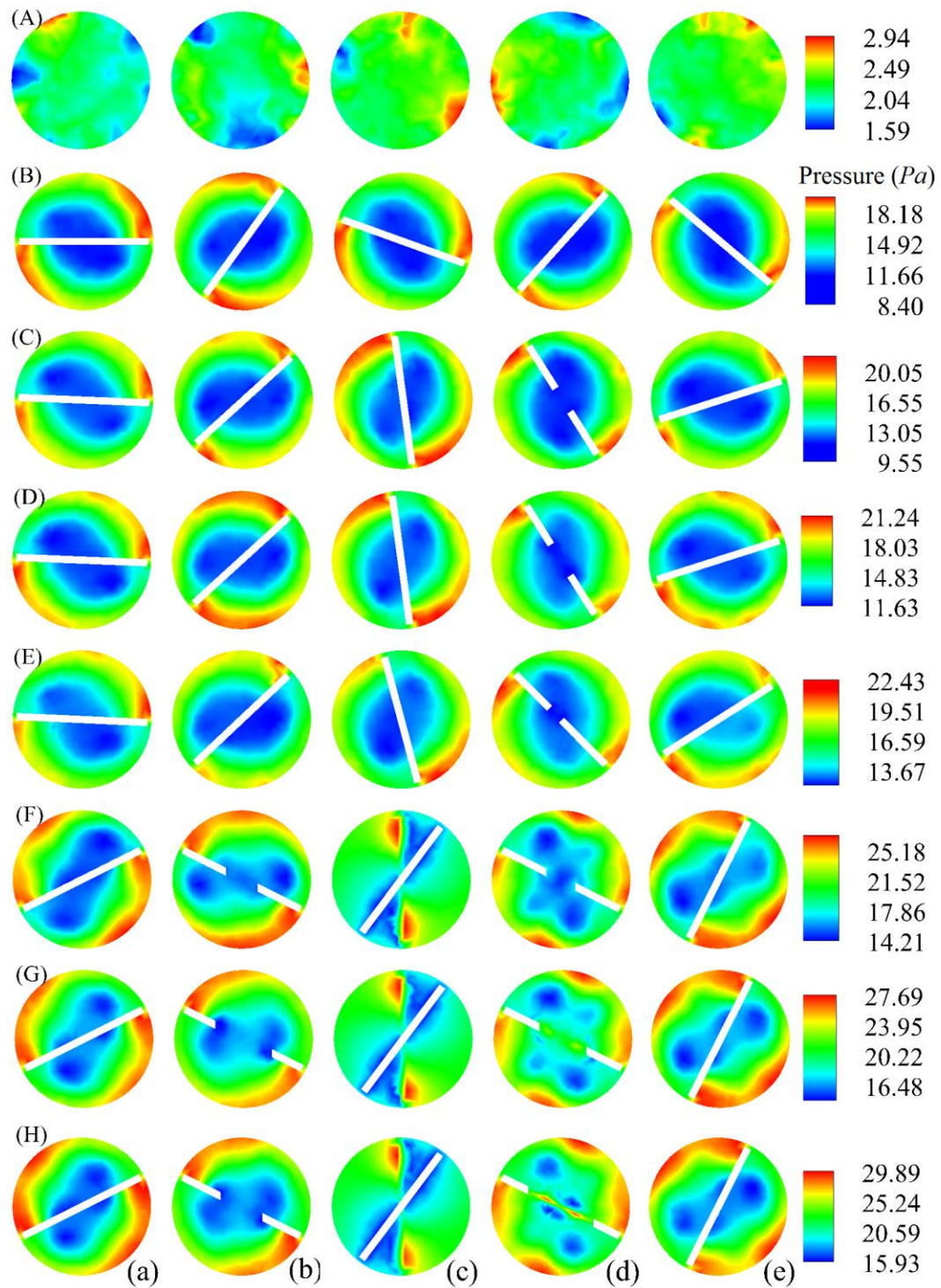


Figure 4.12: Contour plots of pressure for PT (A), TPT (B), TECT (C), TCCT (D), TTCT (E), TAECT (F), TACCT (G) and TATCT (H) for $Re=1820$ at axial location (a) $0.5m$, (b) $0.516m$, (c) $0.6m$, (d) $0.673m$ and (e) $0.7m$.

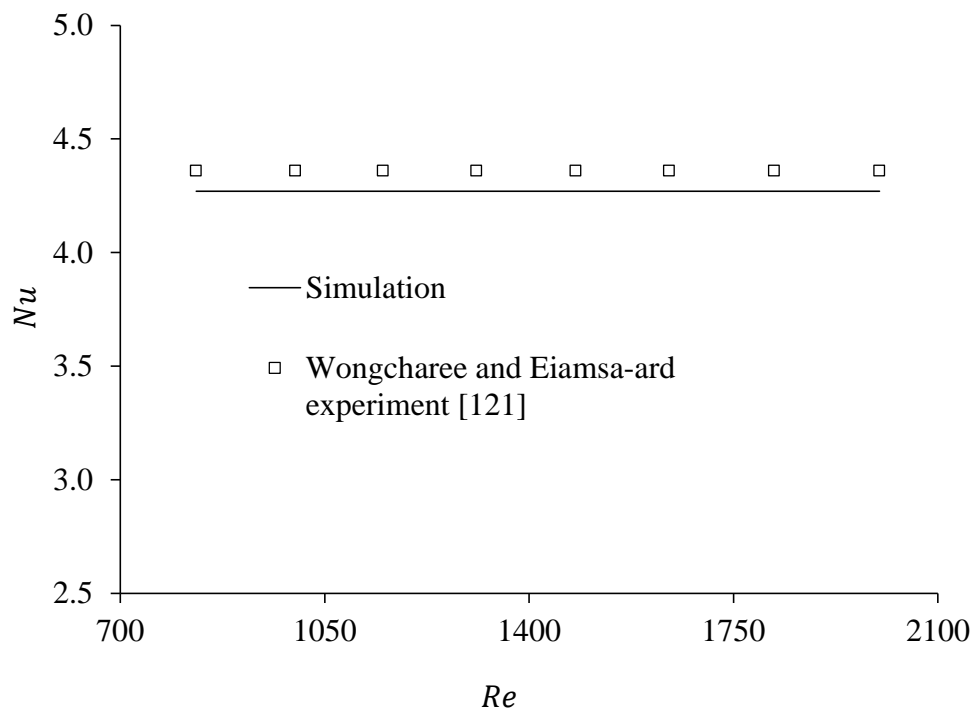


Figure 4.13: Validation of Nusselt number of the plain tube.

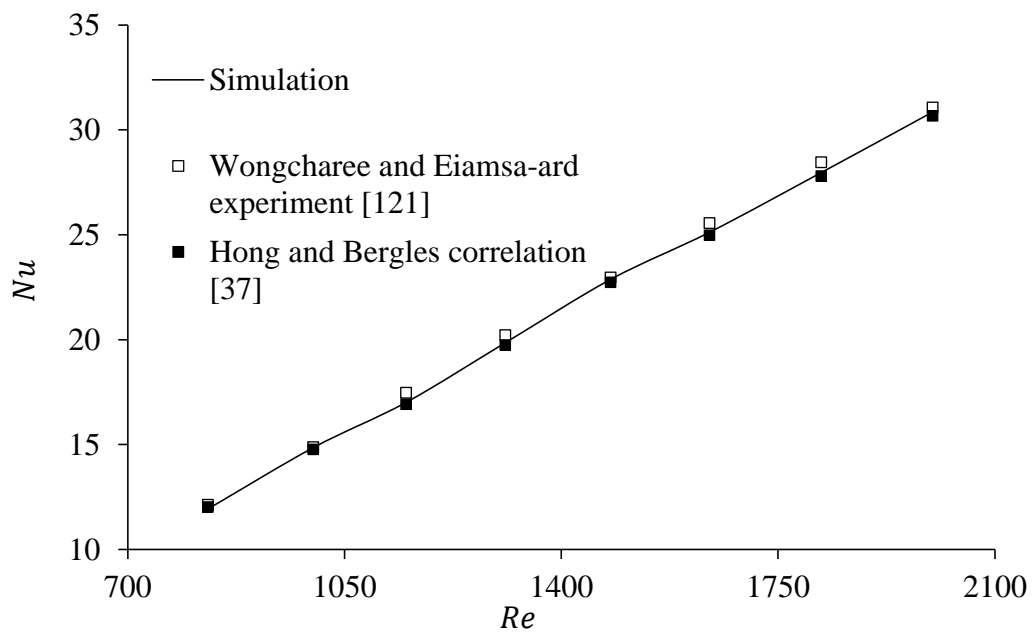


Figure 4.14: Validation of Nusselt number of the tube induced with plain twisted tape insert.

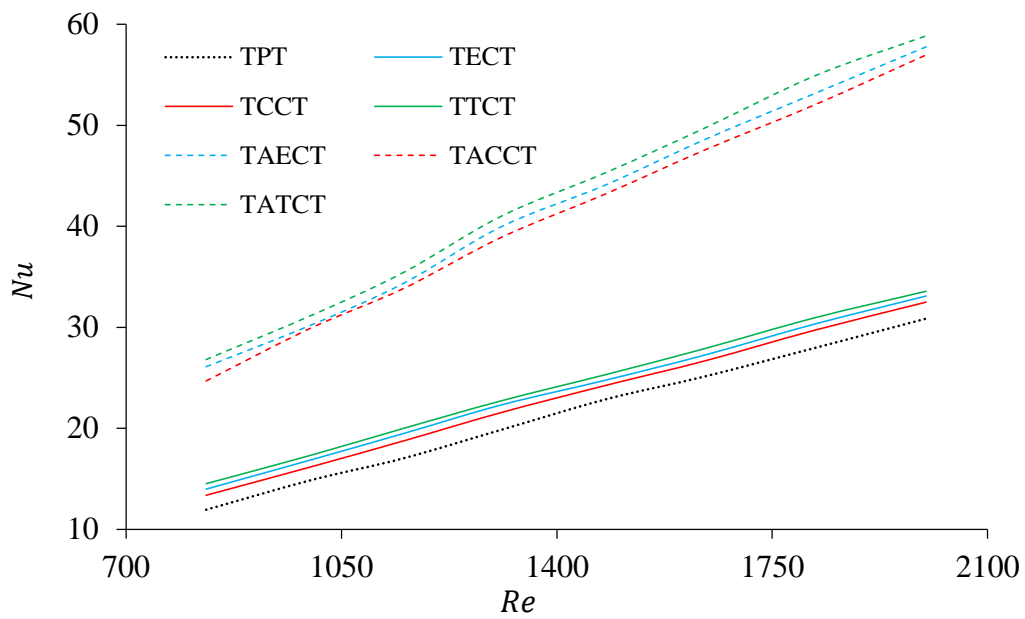


Figure 4.15: Effect of different twisted tape on Nusselt number with Reynolds number.

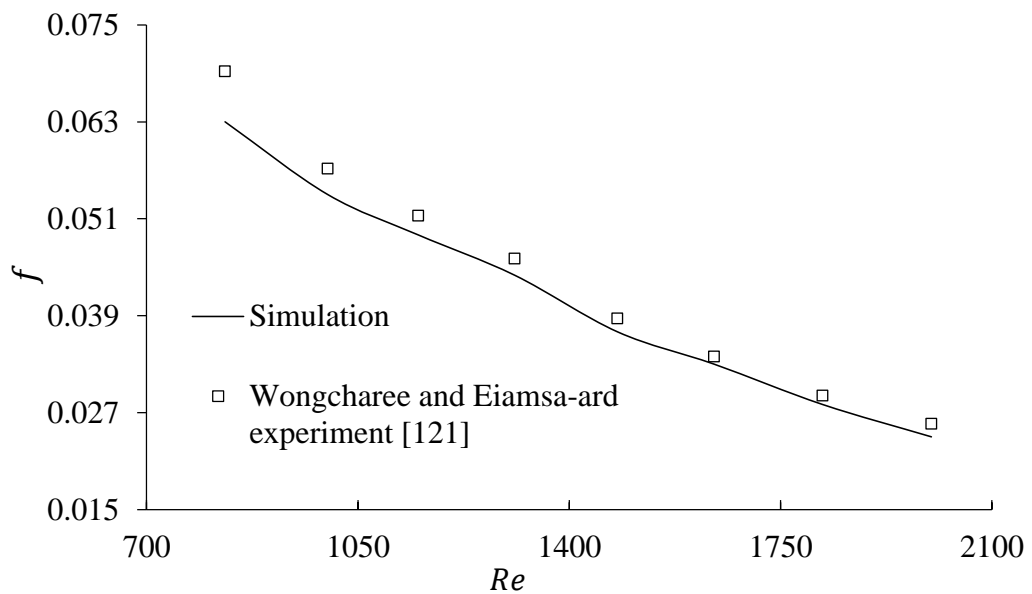


Figure 4.16: Validation of friction factor of the plain tube.

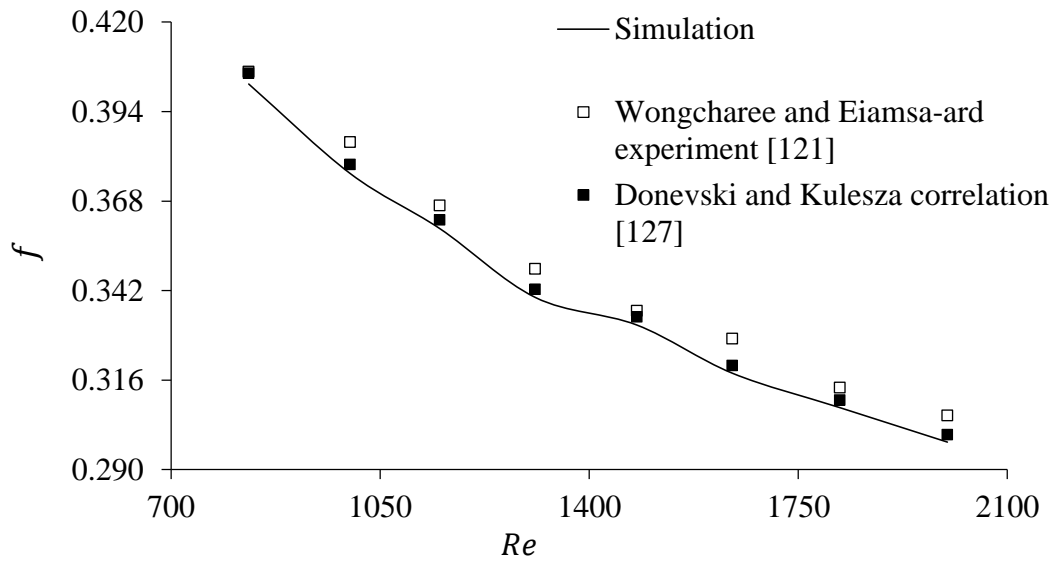


Figure 4.17: Validation of friction factor of the tube induced with plain twisted tape insert.

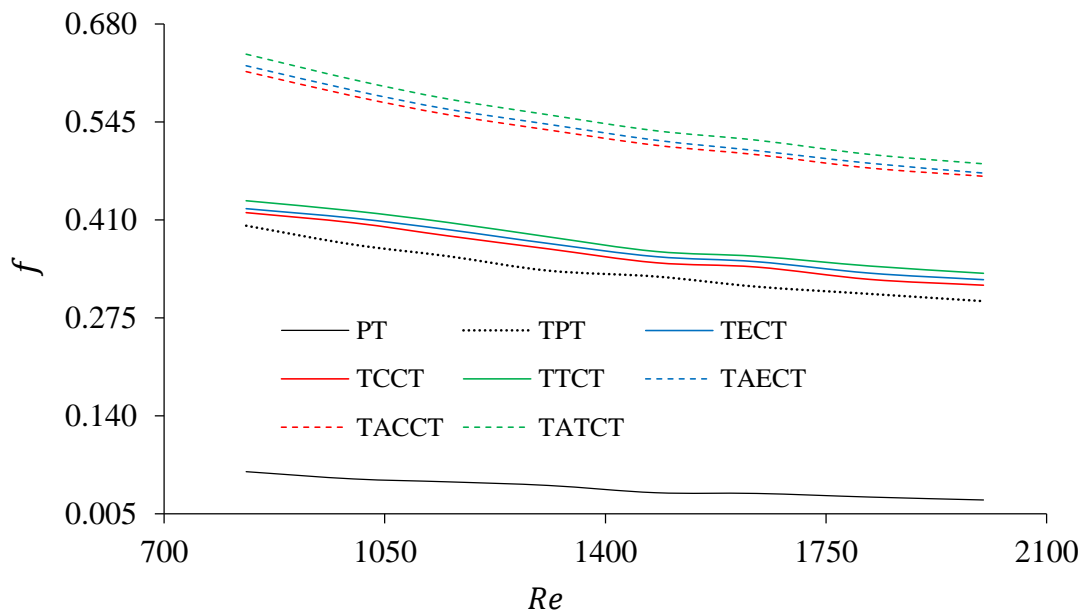


Figure 4.18: Effect of different twisted tape on friction factor with Reynolds number.

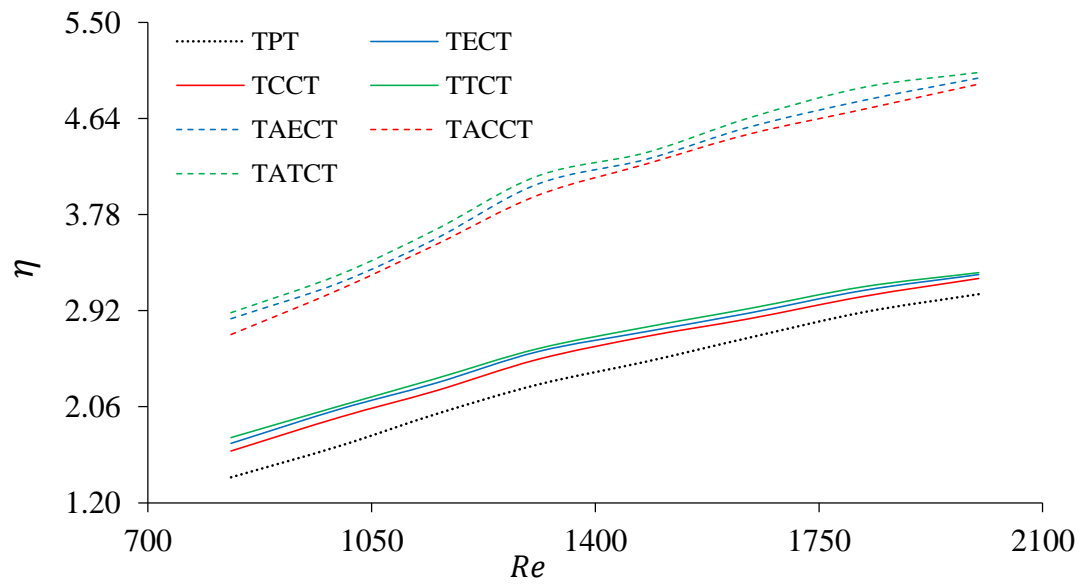


Figure 4.19: Effect of different twisted tape on thermal performance factor with Reynolds number.

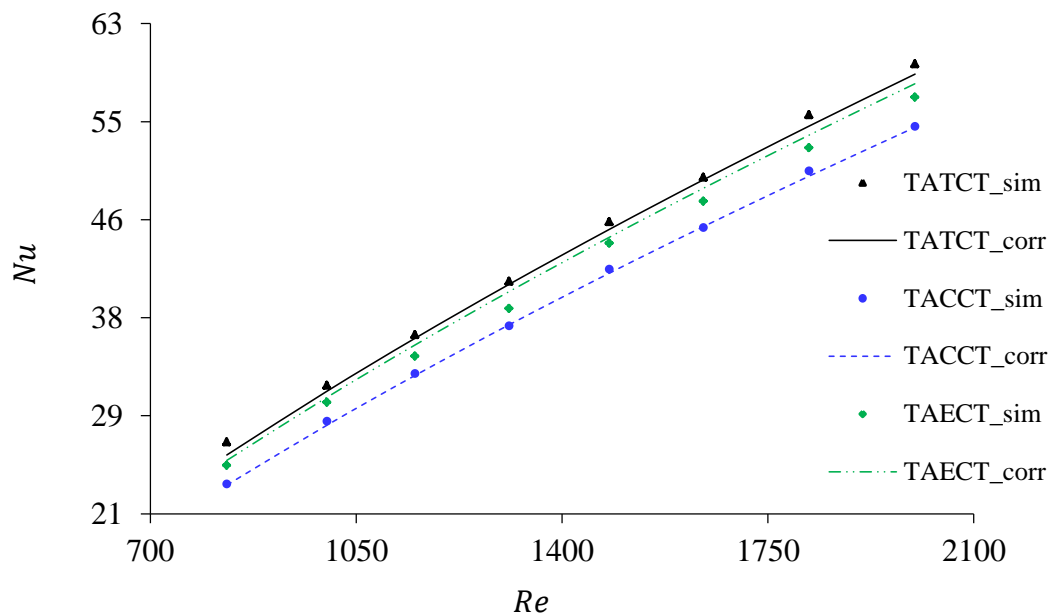


Figure 4.20: Comparison between simulated and predicted results for Nusselt number of laminar flow.

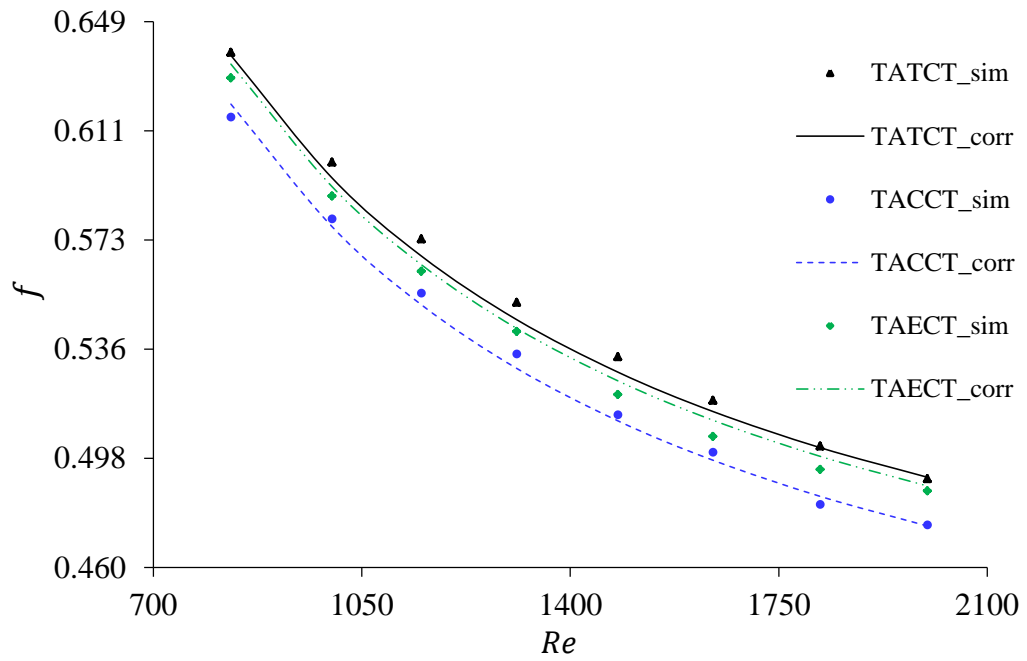


Figure 4.21: Comparison between simulated and predicted results for friction factor of laminar flow.

Chapter 5

NUMERICAL SIMULATION OF TURBULENT HEAT TRANSFER AND FLUID FLOW IN DIFFERENT TUBE DESIGNS

5.1 Introduction

Numerical investigations of thermo-hydraulic characteristics of turbulent flow have been carried out over the years. These investigations have found useful applications in enhancement of heat transfer by means of tube insert technology.

In industrial environment, turbulent flows are applied in diffuser flow in centrifugal pumps and in transonic flow in an axial compressor rotor [128]. The flow conditions in many industrial equipment (such as gas scrubbers, dynamic scraped surface heat exchangers, etc.), machines (for instance, gas turbines and internal combustion engines), external flow over all kind of transportation systems (such as cars, airplanes, ships and submarines), and a jet exhausting from a nozzle into a quiescent fluid are another useful practical applications of turbulent flows. Other applications include the medical field of cardiology in which a stethoscope is used to detect heart sounds and bruits, which are due to turbulent blood flow [128-130].

As mentioned in Chapter 2, numerous experimental and numerical studies have been conducted on this tube insert technology and have led to the incorporation of different cuts on the tape inserts with the view to

obtaining a better performance. Despite these numerous studies, no aspect of them has reported on tape inserts having cuts of different geometrical shape but equal area and their performance under turbulent flow conditions.

In this Chapter, the thermo-hydraulic characteristics of turbulent flow of water inside different tubes with different twisted tape inserts is numerically investigated with the aim of ascertaining which of the tube designs gives the best performance. Aside from the geometrical shape of the cuts on the tape inserts, the effects which the variations in the tape width, tape pitch and area of the cuts are having on the thermo-hydraulic characteristics are considered. Turbulent flow with Reynolds number between 5000 and 20000 is considered and the RNG $\kappa - \varepsilon$ model is employed. Correlations are developed and comparisons are made between the numerical and predicted results.

5.2 Computational Domains

The various geometries used for the simulation of the turbulent flow are the same as those used for the laminar flow in §4.2 of Chapter 4 and are shown in Figure 4.1 and Figure 4.4. They are plain tube (PT), tube with plain twisted tape (TPT), tube with elliptical cut twisted tape (TECT), tube with circular cut twisted tape (TCCT), tube with triangular cut twisted tape (TTCT), tube with alternate-axis elliptical cut twisted tape (TAECT), tube with alternate-axis circular cut twisted tape (TACCT) and tube with alternate-axis triangular cut twisted tape (TATCT). These domains were created in GAMBIT [120].

The three different geometrical shapes (ellipse, circle and triangle) chosen as the cuts on the modified tapes are as described in §4.2 and Figure 4.5 of

Chapter 4. Also, as it has been explained in §4.2 and Figure 4.6 of Chapter 4, the tape pitch (y), the tape width (w), twist ratio (y/w) and clearance (c) in the domains are $54mm$, $18mm$, 3 and $0.5mm$ respectively.

5.3 Grid Generation

In order to confirm accuracy of the numerical solutions, grid independence tests were conducted for the domains. Six grids with different number of cells were used for each domain as given in Table 5.1. In carrying out the grid resolution study, temperature, velocity and turbulent kinetic energy across the cross-section at the exit of each of the domain for Reynolds number of 20000 were extracted. The results for the temperature, velocity and turbulent kinetic energy are shown in Figure 5.1, Figure 5.2 and Figure 5.3 respectively.

Temperature

Figure 5.1 shows the results of the temperature for the grid resolution test. For the PT (frame (a)), there is a variation of 3.2% in comparing the values of the temperature in the grids with number of cells 461178 and 476554 but the variation in the grid with number of cells 512420 is almost 0% of those in the grids with number of cells 614904, 717388 and 768630. In the TPT (frame (b)), there is a variation of 3.6% in comparing the values of the temperature in the grids with number of cells 913594 and 944154. Comparison of the values in the grid with number of cells 944154 with those in the grids with number of cells 1015216, 1218259, 1421302 and 1522824 indicate a variation of 0%. The TECT (frame (c)) shows a discrepancy of 4.6% between the values of the temperature in the grids with number of cells 1122468 and 1159966 but there is a near 0% variation

in comparing the values in the grid with number of cells 1247298 with those in the grids with number of cells 1496758, 1746217 and 1870947.

For the TCCT, frame (d)), the discrepancy in the values of the temperature between the grids with number of cells 1214178 and 1254681 is 3.8% while it is 0% between the values in the grid with number of cells 1349142 and those of the grids with number of cells 1618970, 1888799 and 2023713. In the TTCT (frame (e)), there is a discrepancy of 3.6% between the values of the temperature in the grids with number of cells 1236639 and 1277931. Comparing the values in the grid with number of cells 1277931 with those in the grids with number of cells 1374099, 1648919, 1923739 and 2061149 yields a variation of almost 0%. For the TAECT (frame (f)), the difference in comparing the values of the temperature in the grids with number of cells 1486055 and 1535641 is 7.1% but the difference in comparing the values in the grid with number of cells 1535641 with those in the grids with number of cells 1651206, 1981447, 2311688 and 2476809 is very close to 0%.

In the TACCT (frame (g)), there is a variation of 3.7% in comparing the values of the temperature in the grids with number of cells 1557545 and 1609513. Comparison of the values of temperature in the grid with number of cells 1609513 with those in the grids with number of cells 1730639, 2076767, 2422895 and 2595959 show a variation of 0.1%. The TATCT (frame (h)) indicates a discrepancy of 3.8% between the value of the temperature in the grid with number of cells 1255502 and 1658638 but comparing the values in the grid with number of cells 1658638 with those in the grids with number of cells 2515756, 3018907, 3522058 and 3773634 reveals a variation of 0.1%.

Velocity and turbulent kinetic energy

The same trend in the results of the temperature for the grid resolution test presented above is observed in the results of the velocity shown in Figure 5.2. This is also the case for the turbulent kinetic energy demonstrated in Figure 5.3.

From the above, it can be seen that any of the grids with number of cells 512420, 614904, 717388 and 768630 can be adopted for the PT; any of the grids with number of cells 1015216, 1218259, 1421302 and 1522824 can be adopted for the TPT while any of the grids with number of cells 1247298, 1496758, 1746217 and 1870947 can be adopted for the TECT. For the TCCT, any of the grids with number of cells 1349142, 1618970, 1888799 and 2023713 is appropriate; any of the grids with number of cells 1374099, 1648919, 1923739 and 2061149 is fit for the TTCT while any of the grids with number of cells 1651206, 1981447, 2311688 and 2476809 is suitable for the TAECT. The TACCT can adopt any of the grids with number of cells 1730639, 2076767, 2422895 and 2595959 while any of the grids with number of cells 2515756, 3018907, 3522058 and 3773634 is suitable for the TATCT. By giving consideration to solution precision and convergent time, the grids with number of cells 512420, 1015216, 1247298, 1349142, 1374099, 1651206, 1730639 and 2515756 were therefore adopted for the domains PT, TPT, TECT, TCCT, TTCT, TAECT, TACCT and TATCT respectively.

Explanation on the boundary conditions have been given in §3.5 of Chapter 3 and will not be repeated in this chapter.

5.4 Validation with Experimental Works

The Nusselt number obtained with the standard $\kappa - \varepsilon$ and RNG $\kappa - \varepsilon$ turbulence models for the plain tube (PT) and the tube induced with a plain twisted tape insert (TPT) were validated with experimental results and established correlations. The objective is to ascertain the model which gives results that are closer to the experimental data and hence to know which of the models to be selected to perform other numerical simulations. Nusselt number for the PT were validated with the experimental results of Seemawute and Eiamsa-ard [131] and the correlation of Gnielinski [132]. While for the TPT, the validations were carried out with the experimental results of Seemawute and Eiamsa-ard [131], and the correlations of Kidd [133] and Drizius et al. [134].

The Gnielinski correlation [132] is given as

$$Nu = \frac{\left(\frac{f}{8}\right)(Re - 1000)Pr}{1 + 12.7\left(\frac{f}{8}\right)^{1/2}(Pr^{2/3} - 1)} \quad (5.1)$$

For the plain tube, the friction factor f is obtained from the Petukhov correlation [135]:

$$f = (0.790 \ln Re - 1.64)^{-2} \quad (5.2)$$

Both equations (5.2) and (5.3) are valid for

$$3000 \lesssim Re \lesssim 5 \times 10^6, \quad (L/D) \gtrsim 10, \quad 0.5 \lesssim Pr \lesssim 2000 \quad (5.3)$$

The Kidd correlation is defined as

$$Nu = 0.024 Re^{0.8} Pr^{0.4} \left[\frac{y}{y-1} \right]^{1.1} \left[\frac{T_b}{T_w} \right]^{0.7} \quad (5.4)$$

$$[1 + (D/L)^{0.55}] \times \left[\frac{\pi + 2 - 2\delta/D}{\pi - \frac{4\delta}{D}} \right]^{0.2} \left[\frac{\pi}{\pi - \frac{4\delta}{D}} \right]^{0.8}$$

The correlation of Drizius et al. [134] is expressed as:

$$Nu = 0.025 Re^{0.84} Pr^{0.43} \left[\frac{1}{0.5 + 8 \left(\frac{y}{\pi} \right)^2} \right]^{0.11} \left[\frac{\mu_b}{\mu_w} \right]^{0.06} \quad (5.5)$$

$$\times \left[\frac{\pi + 2 - 2\delta/D}{\pi - \frac{4\delta}{D}} \right]^{0.16} \left[\frac{\pi}{\pi - \frac{4\delta}{D}} \right]^{0.84}$$

For the PT, the validation results as shown in Figure 5.4 reveal that the Nusselt number of the standard $\kappa - \varepsilon$ model is in agreement with the Seemawute and Eiamsa-ard experimental results with a maximum deviation of 8.74%. This numerical result yields a maximum deviation of 7.67% when compared with the Gnielinski correlation. For the RNG $\kappa - \varepsilon$ model, the Nusselt number agree with the experimental results with a maximum deviation of 4.12% but it is in agreement with the Gnielinski correlation with a maximum deviation of 6.25%.

For the TPT, results are shown in Figure 5.5. It is seen that the Nusselt numbers for the standard $\kappa - \varepsilon$ model agree with the experimental data with a maximum deviation of 8.33%. Its agreement with the Kidd correlation has a maximum deviation of 10.03%. A maximum deviation of 7.16% is observed in its agreement with the Drizius et al. correlation. For the RNG $\kappa - \varepsilon$ model, the Nusselt number has a maximum deviation of 3.89% when compared with the experimental data. Its agreement with the

Kidd correlation gives a maximum deviation of 8.54%. It agrees with the Drizius et al. correlation with a maximum deviation of 9.11%.

From the above comparisons, it is seen that on the overall the RNG $\kappa - \varepsilon$ model has an improved performance over the standard $\kappa - \varepsilon$ model and it is more accurate and reliable than the standard $\kappa - \varepsilon$ model. It is therefore selected for other numerical simulations of turbulence flow in the work.

5.5 Results and Discussions

The flow fields, contour plots and heat transfer characteristics of the tubes induced individually with the different types of twisted tapes are discussed in this section. An axial location $0.866m$ is considered for the results that are presented at the cross-sections of the domains. This is because this location is near the exit of the domains and further explanation on this has been given in §4.4. In addition, the nature of the fluid flow along the entire length is looked into.

5.5.1 Flow field

The nature of the fluid flow at a location of $0.866m$ is considered in this section. This is done by drawing streamlines in the flow to track the path followed by the particle of the fluid. The patterns of the streamlines for the various designs at the axial location $0.866m$ are shown in Figure 5.6. In the PT (frame a), the concentration of the streamlines around the wall is weak as a result of absence of twisted tape in it. With the addition of plain twisted tape to the tube (frame b), there is a uniform distribution of the streamlines. This is because the twisted tape insert generates swirls. However, in TECT (frame c) the streamlines have more concentration inside the cut. This arises as a result of additional disturbance and mixing created by the cut. This pattern is not the same in TCCT (frame d) in which the

streamlines inside the cut is widely dispersed due to the periphery of the circular cut having equal distance from the centre of the cut. The streamlines in the TTCT (frame e) concentrates at the centre of the cut as a result of the triangular cuts in the TTCT that increases the disturbance in the flow more than the increase impacted by the circular cuts in the TCCT (frame d).

The cut in the TAECT (frame f) makes the streamlines to concentrate at the centre of the cross-section while the alternate-axis creates additional disturbance to the flow and therefore generates dome-shaped streamlines in the vicinity of the wall of the domain. In the case of the TACCT (frame g), the alternate-axis generates dome-shaped streamlines in the wall of the domain but unlike in the elliptical cut (frame f) the concentration of the cut is further away from the centre of cut. For the TATCT (frame h), the edge of the triangular cut gives better fluid mixing than that of the circular cut (frame g) and therefore its streamline is more concentrated at the immediate centre of the triangular cut (frame h) than at the immediate centre of the circular cut.

The nature of the fluid flow along the entire length of the domain is also considered in order to track the path followed by the fluid. This is done by placing the streamlines in the flow. The direction which a massless fluid element will travel in at any point in time is known as the streamlines [136]. The streamlines through the domains are displayed in Figure 5.7. The geometry of the tape in each of the induced domains is appended on their right side. The PT (frame a) exhibits an axial flow while the other domains (frames b to g) which are induced with twisted tapes generate a swirling flow and an axial flow near the wall of the tubes. In the domains with alternate axis (frames f to h), the fluid which comes in contact with the alternate points is interrupted and therefore promote mixing of the fluid.

In addition, the fluid delivered from different sides of the tape are engaged in collision and eventually led to the separation of the fluid.

5.5.2 Velocity contour

This section is presented with the aim of having an insight into the physics of the flow along the domain. The velocity vectors are appended to the magnitude of the streamwise velocity of the flow and the results for $Re = 20000$ at different axial locations randomly selected along the length of each of the models are depicted in Figure 5.8.

The domain PT (Figure 5.8 (A)) is not induced with tape and its maximum velocity occurs at the centre indicating that the flow is fully developed at these locations. It is seen that the velocity is almost the same at all locations. When the tube is induced with plain twisted tape (Figure 5.8 (B)), the near wall velocity increases due to the fact that the tape generates swirl and make it to have higher velocity of about 7.8% over those in the PT. As a result of the cuts in the TECT (Figure 5.8 (C)), additional swirl is generated in the flow and this manifests in the value of the velocity magnitude at the location 0.637m (frame d). At this location, the magnitude of the velocity is 2.26%, 2.12% and 2.06% higher than those in the upstream regions in 0.5m (frame a), 0.516m (frame b) and 0.6m (frame c) respectively. In the further downstream region (frame e) in which there is no cut on the tape, the velocity is 2.28% less than that in the upstream region (frame d). The same explanations apply to the domains TCCT (Figure 5.8 (D)) and TTCT (Figure 5.8 (E)) as the changes in the values of the velocity at their various locations are approximately the same as those in the TECT.

The velocity in TAECT (Figure 5.8 (F)), TACCT (Figure 5.8 (G)) and TATCT (Figure 5.8 (H)) are 2.93%, 4.68% and 3.44% higher than those in TECT (Figure 5.8 (C)), TCCT (Figure 5.8 (D)) and TTCT (Figure 5.8 (E))

respectively. This is caused by the alternate axis in TAECT, TACCT and TATCT. As a result of the cut at the location $0.516m$ (frame b, F-G), the velocity is about 3.62% higher than those in their upstream regions (frames a). The velocity in the further downstream region at location $x = 0.6m$ (frame c, F-G) is higher than that at the upstream region (frame b) because of the alternate axis in the region (frame c). The alternate axis that is not present at the location $x = 0.673m$ (frame d) make its velocity to be less than that at $x = 0.6m$. However, the velocity at $x = 0.6m$ (frame c) is higher than that at $x = 0.7m$ (frame e). Quantitatively, the velocity at $x = 0.7m$ (frame e) is 4.41% and 2.97% lower than those in $x = 0.6m$ (frame c) and $x = 0.673m$ (frame d) respectively.

5.5.3 Temperature contours

In this section, the variation in the temperature is the domain in examined. The results are reported in the form of contours at different axial locations for $Re = 20000$ and are shown in Figure 5.9. In the PT (Figure 5.9 (A)) the contours at these locations are approximately the same. This is possibly due to the fact that the flow is developed at these locations. As a result of the inclusion of plain twisted tape in the plain tube (Figure 5.9 (B)) which causes the fluid to undergo mixing, the temperature distributions at the locations improve over that of the PT.

Due to the impact of cuts, the temperature at the location $0.673m$ (frame d) of TECT (Figure 5.9 (C)) is about 2.71%, 2.70% and 2.53% higher than those at axial locations $0.5m$ (frame a), $0.516m$ (frame b) and $0.6m$ (frame c) respectively. However, from the location $0.673m$ (frame d) to $0.7m$ (frame e), there is a drop in temperature of about 2.01% due to absence of cut in the region. This pattern of temperature distribution in the TECT is also applicable to the TCCT (Figure 5.9 (D)), and TTCT (Figure 5.9 (E)).

The tubes induced with tapes with alternate axis (Figure 5.9 (F) to (H)) indicate that the alternate axis have effect on the temperature distribution in the domain. At the location $0.516m$ (frame b), the temperature is 2.11% over those in the upstream (frame a) because of the presence of the cuts (frame b). The presence of the alternate axis (frame c) causes an additional disturbance in the flow and this results in the creation of thermal energy [123] which eventually made the temperature at this location to be 3.17% higher than those of the immediate upstream (frame b). Beyond these locations (frame d), the temperature in the region reduces by 1.80% and reduces by 2.59% in the downstream region (frame e) by the reason of the absence of cut on the tape.

5.5.4 Pressure contour

As the fluid flows through the tube there will be a pressure drop. Also, the pressure that will be required to drive the fluid in the induced tubes will be higher than that required in the plain tube. Therefore, this section discusses the pressure distribution at different axial locations of the tube designs.

The pressure contours at different axial locations in the domains are presented in Figure 5.10. In the domain PT (Figure 5.10 (A)), the pressure decreases along the flow downstream. The pressure at $x = 0.5m$ (frame a) decreases by 2.5%, 19.74%, 34.62% and 40.21% at points $x = 0.51m$ (frame b), $x = 0.6m$ (frame c), $x = 0.673m$ (frame d) and $x = 0.7m$ (frame e) respectively. Comparing these variations shows that there is a large difference in the value of pressure between the locations $x = 0.6m$ (frame c) and $x = 0.673m$ (frame d). This confirms the observation of Liao and Xin [16] that, in some situations, as the flow in a tube reaches a particular point, it experiences an unexpected degree of change in pressure. For all

the induced tubes (Figure 5.10 (B) - (H)), the pressure at the locations corresponding to the locations in the PT increases as a result of additional dissipation of pressure of the fluid caused by the disturbance due to the presence of the tape inserts.

The cut at the location $x = 0.673m$ (frame d) on the TECT (Figure 5.10 (C)) results in an increase in pressure of about 12.39% above its corresponding location in the TPT (Figure 5.10 (B)). This arises because of the additional dissipation of pressure of the fluid caused by the cut on the tape [137]. For the TCCT (Figure 5.10 (D)) and TTCT (Figure 5.10 (E)), their pressure at $x = 0.673m$ (frame d) are 10.26% and 14.74% respectively higher than that in the corresponding location in the TPT.

At the location $x = 0.6m$ (frame c) of the TAECT (Figure 5.10 (F)), TACCT (Figure 5.10 (G)) and TATCT (Figure 5.10 (H)), the alternate axis causes an extra dissipation of pressure to be exerted on the fluid [137]. Comparatively, the pressure at this location for TAECT, TACCT and TATCT are 12.17%, 14.62% and 14.11% respectively higher than those in TECT, TCCT and TTCT. By the reason of the absence of cut in the upstream regions (frames a to c) as well as in the further downstream region (frame e) of the domain, the pressure in these regions are lower than those in the regions in which there are cuts (frame d).

5.5.5 Turbulent kinetic energy

The intensity of turbulence in the domain is measured by means of turbulence kinetic energy. The effect of the various domains on the turbulent kinetic energy at different locations in the domain is presented in Figure 5.11. In the PT (Figure 5.11(A)), the maximum turbulent kinetic energy (TKE) occurs at the wall of the tube. The reason of this is that the

velocity is minimum at the wall and consequently the turbulent kinetic energy at the wall will be maximum [138]. When the tube is induced with plain twisted tape, Figure 5.11(B), the swirl flow of the tape makes the turbulent kinetic energy to be maximum near the tape wall. This is in agreement with the work of Eiamsa-ard et al. [86]. Also, there is 27.73% increase in the magnitude of the turbulent kinetic energy in the TPT compared to that in the PT in all its corresponding locations. This increase arises because of the boundary layer which become more turbulent due to the presence of the tape [138].

As a result of the cuts on the TECT (Figure 5.11 (C)), TECT (Figure 5.11 (D)) and TECT (Figure 5.11 (E)) which increase the boundary layer disturbance in the domains the magnitude of the turbulent kinetic energy changed from that in the TPT. The effect is more pronounced in the TTCT than in the TECT and TCCT, indicating the boundary layer disturbance in the triangular cut in the TTCT is more than in the TECT and TCCT. In the TECT (Figure 5.11 (C)), there is a cut on the tape at a location $0.637m$ (frame d) on the domain the magnitude of the turbulent kinetic energy in this region to be 18.9%, 21.19% and 33.31% respectively higher than those in the upstream regions (frames a to c). In the further downstream region (frame e), the turbulent kinetic energy is 29.28% less than that in the previous region (frame d) in which there are no cuts. It is interesting to observe that the same explanations is applicable to the TCCT (Figure 5.11 (D)) and TTCT (Figure 5.11 (E)) as the changes in the values of their turbulent kinetic energy at their various locations (frames a to e) are approximately the same as those in the TECT. The turbulent kinetic energy in TAECT (Figure 5.11 (F)), TACCT (Figure 5.11 (G)) and TATCT (Figure 5.11 (H)) is 11.92%, 13.25% and 17.07% respectively higher than those in TECT (Figure 5.11 (C)), TCCT (Figure 5.11 (D)) and TTCT (Figure 5.11 (E)). This is caused by the

alternate axis in TAECT, TACCT and TATCT which make the boundary layer to be more turbulent. The turbulent kinetic energy at the location $0.516m$ (frame b) in the TAECT, TACCT and TATCT are higher than those in their upstream regions (frames a).

In the TAECT (Figure 5.11 (F)) the turbulent kinetic energy at the location $0.516m$ (frame b) is 8.68% over those in the upstream (frame a) because of the presence of the cuts at the location $0.516m$ (frame b). The presence of the alternate axis (frame c) make the turbulent kinetic energy to be 10.11% higher than those of the upstream (frame b). The turbulent kinetic energy in the frame (c) reduces by 5.24% in the frame (d) and owing to the absence of cut on the tape in the downstream region (frame e) the turbulent kinetic energy reduces by 8.66% in this region. In both the TACCT (Figure 5.11 (G)) and TATCT (Figure 5.11 (H)), the turbulent kinetic energy at the location $0.516m$ (frame b) is 9.38% over those in the upstream (frame a). The turbulent kinetic energy in (frame c) is 7.2% higher than those of the upstream (frame b) while the turbulent kinetic energy in the frame (c) reduces by 4.04% and 6.21% in the frame (d) and frame (e) respectively.

The above presentations indicate that of the all the domains considered, the TATCT has the highest turbulent kinetic energy. If turbulent kinetic energy increases, the boundary layer becomes more disturbed and this produces more momentum [138]. Then it can be argued that of all the domains considered, TATCT gives the highest momentum to the fluid.

5.5.6 Heat transfer

The heat transfer is presented in terms of the Nusselt. The expressions for the average Nusselt number (Nu), heat transfer coefficient (h) and mean

temperature (T_m) of the fluid is given in Equations (4.1), (4.2) and (4.3) respectively of Chapter 4.

The effect of the various twisted tape on heat transfer rates for the turbulent flow is presented in Figure 5.12. It can be observed that as the Reynolds number increases, the Nusselt number also increases. According to Wongcharee [123], this is due to increase in turbulent intensity as the Reynolds number increases resulting in more destruction of the boundary layer. As illustrated in Figure 5.12, the Nusselt number of the induced tubes is higher than those of the PT. The increase in the velocity and decrease in the flow cross-sectional area of the induced tubes, as demonstrated in Figure 5.8 (B - H), make the fluid inside them to swirl with a higher velocity and consequently cause the heat transfer coefficient of the induced tube to be higher than that of the plain tube. This observation of the increase in the Nusselt number is supported by the reports of Eiamsa-ard et al. [86].

It is observed that the improvement in the Nusselt number of the induced tubes over that of the plain tube decreases as the Reynolds number increases. The Nusselt number of TPT is 26.9 to 52.7% higher than that of the PT. The Nusselt number of TECT, TCCT, TTCT, TAECT, TACCT and TATCT is 9.1 to 20.0%, 6.9 to 8.3%, 11.0 to 25.6%, 60.8 to 109.4%, 57.6 to 101.2% and 63.6 to 118.4% respectively higher than that of the TPT. The Nusselt number of the TAECT, TACCT and TATCT is 47.3 to 74.5%, 47.3 to 74.5% and 47.3 to 85.6% higher than those in the TECT, TCCT and TTCT respectively. This means that the alternate axis contribute to the heat transfer promotion due to better fluid mixing near a tube wall caused by the alternate points. The heat transfer of the different induced tubes at $Re = 20000$ is quantitatively presented in Table 5.4.

5.5.7 Friction factor

The Darcy friction factor is given in Equation (4.5). The results of the friction factor of the plain tube (PT) were validated with the experimental results of Seemawute and Eiamsa-ard [131] as well with Blasius correlation [139] and Petukhov correlation [135]. The Petukhov correlation is given in equation (5.2) above.

The Blasius correlation [139] is expressed as

$$f = 0.316 Re^{-0.25} \quad (5.6)$$

The results of the validation are shown in Figure 5.13. The numerical results predicts well the Blasius correlation and Petukhov correlation up to around Reynolds number $Re = 13200$. Beyond this value of Reynolds number, the numerical results over-predict the correlations. The conditions under which the correlations were developed are responsible for the over-prediction. The Seemawute and Eiamsa-ard experimental data are over-predicted by the simulated results. This may arise from the assumptions and conditions imposed on the experiment. The simulated friction factors for the PT match the experimental results with discrepancy of 18.08%. They matched the Blasius correlation with a discrepancy of 15.84% but agree with the Petukhov correlation with a deviation of 13.55%.

The results of the experiment of Seemawute and Eiamsa-ard [131], correlation of Gambill and Bundy [140] and correlation of Manglik and Bergles [21] were used for the validation of the friction factor of the tube induced with plain twisted tape insert (TPT) as shown in Figure 5.14. The correlation of Gambill and Bundy is given as

$$\begin{aligned}
f = & 0.046 Re^{-0.2} \left[\frac{\pi + 2 - \frac{2\delta}{D}}{\pi - \frac{4\delta}{D}} \right]^{1.8} \left[\frac{\pi}{\pi - \frac{4\delta}{D}} \right]^{1.2} \\
& + \frac{0.0525}{y^{1.31}} \left[\frac{2000}{Re} \right]^{0.81} \left[\frac{\pi + 2 - \frac{2\delta}{D}}{\pi - \frac{4\delta}{D}} \right]^{0.38} \left[\frac{\pi}{\pi - \frac{4\delta}{D}} \right]^{2.62}
\end{aligned} \tag{5.7}$$

Manglik and Bergles [21] expressed the friction factor correlation as

$$\begin{aligned}
f = & 0.316 Re^{-0.25} \left[\frac{\pi}{\pi - \frac{4\delta}{D}} \right]^{1.75} \times \left[\frac{\pi + 2 - \frac{2\delta}{D}}{\pi - \frac{4\delta}{D}} \right]^{1.25} \\
& \times \left[1 + \frac{2.752}{y^{1.29}} \right]
\end{aligned} \tag{5.8}$$

The experimental results predict the simulated results of the PTP better than the other correlations.

The simulation results predict the experimental data well. The Manglik and Bergles correlation is predicted well from around $Re = 10300$ to $Re = 20000$ but there is over-prediction between around $Re = 5000$ to $Re = 10300$. The simulation results fairly predict the experimental data and the Gambill and Bundy correlation from around $Re = 5000$ up to $Re = 8000$ after which over-prediction occurs. The conditions and approximations under which the correlations and the experiments were generated may account for the over-predictions. The simulated results match the experimental results with a deviation of 6.4% but match the Gambill and Bundy correlation with a deviation 19.61%. A deviation of 13.35% is observed in its agreement with the Manglik and Bergles correlation.

Figure 5.15 illustrates the variation of the friction factor with Reynolds number for the tubes with different types of twisted tape inserts. The

value of the friction factor is higher at lower Reynolds number. This is because as the Reynolds number increases the momentum overcomes the viscous force of the fluid and consequently lowers the shear between the fluid and the tube wall [2]. The induced tubes have high friction factor over the plain tube. This is attributed to the flow blockage and swirl flow due to tape insert. Thus, the friction factor of TPT is up to 4.15 times that of the PT. The additional dissipation of pressure of the fluid caused by the fluid disturbance due to the presence of cuts on the tapes results in an increase in pressure. Consequently, the friction factor of TECT, TCCT, TTCT, TAECT, TACCT and TATCT is 9.1 to 12.2%, 6.5 to 10.0%, 11.4 to 16.4%, 151.7 to 205.1%, 145.8 to 197.9% and 160.5 to 215.8% respectively higher than that of the TPT. The friction factor obtained in the tubes with alternate axis is higher than those without alternate axes. The explanation given to this is that more effective fluid disturbance and extra mixing are provided at the alternate points of the alternate axis. The friction factor of the different induced tubes at $Re = 20000$ is quantitatively presented in Table 5.4.

5.5.8 Thermal performance factor

Thermal performance factor is used to appraise the potential of a twisted tape for practical applications in enhancement of heat transfer [12, 16]. Its mathematical expression is given in Equation (4.7).

The variation of the thermal performance factor for the different tube designs are compared in Figure 5.16. It depicts that the performance factor decreases as the Reynolds number increases. This is caused by a larger drop in pressure at higher Reynolds number. However, the thermal performance factors are above unity and therefore the trade-off between the heat transfer and pressure drop yields a promising heat transfer enhancement.

As demonstrated in the Figure 5.16, the thermal performance factor of TPT is lower than the other tube designs. The thermal performance factor of TECT, TCCT and TTCT are up to 1.25, 1.23 and 1.27 times respectively that of TPT. For the TAECT, TACCT and TATCT, their thermal performance factors are up to 1.38, 1.32 and 1.43 times respectively that of the TPT. This shows the profitable impact of the alternate axis over the tapes with cuts only. For the entire range investigated, the maximum thermal performance factor of 1.42 is found with the use of TATCT and $Re = 5000$. The thermal performance factor of the different induced tubes at $Re = 20000$ is quantitatively presented in Table 5.4.

5.6 Comparison of the quantity of material and thermal performance of the different domains

In the previous sections, different tapes have been used to produce different domains and their thermal performances have been numerically investigated. In this section, the cost implication of using the different domains to obtain the different thermal performances is examined. The objective is to ascertain if it is financially beneficial using the domain (TATCT) that gives the best performance.

The production of the various domains TPT, TECT, TCCT, TTCT, TAECT, TACCT and TATCT shall require the use of material of volume $1.15 \times 10^{-4}m^3$, $1.14 \times 10^{-4}m^3$, $1.14 \times 10^{-4}m^3$, $1.14 \times 10^{-4}m^3$, $1.14 \times 10^{-4}m^3$,

$1.14 \times 10^{-4}m^3$ and $1.14 \times 10^{-4}m^3$ respectively. The details are given in Table 5.2. The material used is copper and its cost is directly proportional to its quantity [141].

Figure 5.17 compares the quantity of the material and the thermal performance of the different domains. It is seen that the domain TPT uses material of volume $1.15 \times 10^{-4}m^3$ while each of the other domains uses material of volume $1.14 \times 10^{-4}m^3$, meaning that each of them uses less amount of material than the TPT. Also, of all the domains, TATCT has the highest thermal performance factor of 1.238. It can be therefore reasoned that the domain TATCT is beneficial in terms of both the thermal performance and the cost.

5.7 Investigations of the Effects of Variations in the Tape Geometry of TATCT

Having discovered in the results presented above in §5.5 that the tube with alternate-axis triangular cut twisted tape (that is, the domain TATCT) produced the best result in terms of thermal performance, more research was conducted on the TATCT by varying the geometry of its tape (that is, alternate-axis triangular cut twisted tape, ATCT). The tape geometry is varied by changing its width (w), pitch (y) and perimeter (p) of the cut (corresponding to area of the cut). The aim is to ascertain the effect of the change in each of these variables on the heat transfer, fluid flow and thermal performance. The variations in the geometry of the tape are shown in Figure 5.18. The value of the length of a side of the triangular (s) in Figure 4.5 (c) for each of the tapes (a), (b), (c), (f) and (g) in Figure 5.18 is $11.42mm$; but for the tapes (d) and (e), the values of s are $9mm$ and $6mm$ respectively.

Figure 5.18 (a) is the initial tape (ATCT) with $w = 18mm$, $y = 54mm$ and $p = 34.26mm$. In Figure 5.18 (b) and (c), only the tape width (w) is changed

to 15mm and 13mm respectively but the tape pitch (y) and the perimeter (p) of the cut (corresponding to area of the cut) remain the same. In Figure 5.18 (d) and (e), only the perimeter (p) of the cut on the tape is altered to 27mm and 18mm respectively but the tape width (w) and the tape pitch (y) remain the same. Figure 5.18 (f) and (g) show the alteration of the pitch (y) to 36mm and 72mm respectively while maintaining the tape width (w) and the perimeter (p) of the cut on the tape. The space ratio (sr), as defined in §4.2 of Chapter 4 and provided in Table 5.3, for the domains with the tape width $w = 18mm$, 15mm and 13mm are $sr = 0.052$, 0.21 and 0.31 respectively.

5.8 Grid Generation for the Variations in the Tape Geometries of TATCT

Grid independence tests were conducted on the domains of TATCT with the variations in the geometry of its tape. A description of the various geometries of the alternate-axis triangular cut twisted tape (ATCT) used for the various domains of the TATCT is given in Table 5.3. In conducting the grid independence test, three grids with different number of cells were used for each of the six domains as presented in Table 5.5. Temperature, velocity and turbulent kinetic energy across the cross-section at the exit of the domains were extracted and the results are shown in Figure 5.19, Figure 5.20 and Figure 5.21 respectively. It should be noted that Figure 5.19(a), Figure 5.20(a) and Figure 5.21(a) are for the TATCT and have been included in order to compare them with the results obtained in the variations made to the tape geometry of the TATCT.

Temperature

The results of the temperature for the grid independence are shown in Figure 5.19. It has been discussed in §5.3 that the TATCT (Figure 5.19 (a)) become grid independent with the number of cells 2515756. The TATCT_{w1} (frame b) indicates a discrepancy of 2.1% between the value of temperature in the grids with the number of cells 1714567 and 2449381 but comparing the values in the grids with the number of cells 2449381 and 3184196 reveals a variation of 0%. In the TATCT_{w2} (frame c), there is a variation of 1.9% in comparing the values of temperature in the grids with the number of cells 1683592 and 2405132. Comparison of the values in the grids with the number of cells 2405132 and 316671 show a variation of 0%.

For the TATCT_{a1} (frame d), the difference in comparing the values of temperature in the grids with the number of cells 1766015 and 2522878 is 2.3% but the difference in comparing the values in the grids with the number of cells 2522878 and 3279741 is 0%. In the TATCT_{a2} (frame e), there is a discrepancy of 2.2% between the values in the grids with the number of cells 1770542 and 2529346. Comparing the values in the grids with the number of cells 2529346 and 3288150 has a variation of almost 0%.

Velocity and turbulent kinetic energy

The grid independence results for the velocity and turbulent kinetic energy demonstrated Figure 5.20 and Figure 5.21 respectively. As discussed in §5.3, the results for both the velocity (Figure 5.20(a)) and the turbulent kinetic energy (Figure 5.21(a)) indicate that the TATCT become grid independent with the number of cells 2515756.

The grid independence results for the velocity and turbulent kinetic energy follows the same pattern of the results of the grid independence for

temperature discussed above. Thus, it is clear that either of the grids with the number of cells 2499381 and 3184196 can be adopted for the TATCT_{w1}; either of the grids with the number of cells 2405132 and 3126671 can be adopted for the TATCT_{w2} while either of the grids with the number of cells 2522878 and 3279741 can be adopted for the TATCT_{a1}. For the TATCT_{a2}, the grids with the number of cells 2529346 or 3288150 is appropriate; either of the grids with the number of cells 2503249 and 3254223 is fit for the TATCT_{y1} while the grids with the number of cells 2515756 or 3270483 is suitable for the TATCT_{y2}.

5.9 Results for the Variations in the Tape Geometries of TATCT

The computational results for the variations in the tape geometries of the TATCT are presented below.

5.9.1 Effect on the flow field

In this section, the path followed by the flow in the tube designs with variations in their tape geometry is tracked by drawing streamlines in the flow. The streamline patterns for the various designs for $Re = 20000$ at the same axial location 0.866m are demonstrated in Figure 5.22 while the streamlines through the length of the domains are shown in Figure 5.23.

The TATCT_{w1} (frame b) with space ratio of 0.21 has a weaker swirl than TATCT (frame a) with space ratio of 0.052. Therefore, the streamline in the TATCT_{w1} (frame b) is not as concentrated at the centre of the cut as in the TATCT. The space ratio of 0.31 in TATCT_{w2} (frame c) is greater than that in

TATCT_{w1} (frame b). In effect, the streamline in the space between the tape and the wall in TATCT_{w2} has less concentration than that in TATCT_{w1}.

The size of the cut of $27mm$ in TATCT_{a1} (frame d) is smaller than what is obtained in TATCT (frame a). This lowers the fluid disturbance in the TATCT_{a1} (frame d) and make the concentration of the streamline at the centre of TATCT (frame a) to be more than that in the TATCT_{w1}. The cut size of $18mm$ in TATCT_{a2} (frame e) is less than that in TATCT_{a1} (frame d) and therefore the disturbance in TATCT_{a2} (frame e) is less than that in TATCT_{a1} (frame d). Hence, the concentration of streamline in TATCT_{a2} (frame d) is less than in TATCT_{a1} (frame d).

The TATCT_{y1} (frame f) with tape pitch of $36mm$ has a stronger swirl than TATCT (frame a) of pitch $54mm$ and therefore the streamline of TATCT_{y1} (frame f) is of more concentration than that in TATCT (frame a). The tape pitch of $72mm$ in TATCT_{y2} (frame g) is greater than that of $54mm$ in TATCT (frame a). This makes the streamlines to be more concentrated in TATCT_{y2} than in TATCT. The streamlines through the length of the domains are displayed in Figure 5.23.

5.9.2 Effect on velocity vector

To demonstrate the differences in the velocity vector in the tubes with variations in the tape geometries, explanations on vector plots at the same location of $x = 0.866m$ is presented in this section.

The velocity vectors for the various designs at the same location $0.866m$ are depicted in Figure 5.24. The velocity vectors for the variations in width $w = 18mm$, $w = 15mm$ and $w = 13mm$ are shown in frames (a), (b) and (c) respectively. It is seen that when $w = 15mm$ (frame b), the velocity near

the wall is smaller than when $w = 18\text{mm}$ (frame a), which means a weaker disturbance and fluid mixing. A further reduction of the width of the tape to $w = 13\text{mm}$ (frame c) weakens the swirls in the area. The velocity vectors for the variations in size of the cut on the tape $p = 34.26\text{mm}$, $p = 27\text{mm}$ and $p = 18\text{mm}$ are shown in frames (a), (d) and (e) respectively. From these, it can be seen that the swirl in the tube with tape cut $p = 34.26\text{mm}$ (frame a) is stronger than that in the tape with cut $p = 27\text{mm}$ (frame d) while the swirl in the tube with tape cut $p = 27\text{mm}$ (frame d) is stronger than that in the tape with cut $p = 18\text{mm}$ (frame e). This means that as the size of the cut reduces the swirls near the wall diminishes. The velocity vectors for the variations in tape pitch $y = 54\text{mm}$, $y = 36\text{mm}$ and $y = 72\text{mm}$ are shown in frames (a), (f) and (g) respectively. It is seen that the swirl in the tube with the smallest tape pitch $y = 36\text{mm}$ (frame f) is the strongest but the swirl in the tube with the largest tape pitch $y = 72\text{mm}$ (frame g) is the weakest.

5.9.3 Effects on the heat transfer

It is necessary to ascertain the response of the heat transfer to the variations in the tape width, size of the cut on the tape and the tape pitch. This will reveal if the variations in these parameters are advantageous to the system.

The effects of the variations in the geometries of the tape on the heat transfer rate are studied numerically and the results are presented in Figure 5.25. In the Figure 5.25(a), the effects of the variations in the width $w = 18\text{mm}$, (TATCT), 15mm (TATCT_{w1}) and 13mm (TATCT_{w2}) and hence the space ratio $sr = 0.052$, 0.21 and 0.31 respectively on the heat transfer rate is presented. It is discovered that the heat transfer rates decrease with

increasing space ratio and that the smaller the space ratio, the better the heat transfer enhancement. This is because the domain with the largest free space ($TATCT_{w2}$) between the tube wall and edge of the tape generates the weakest swirl flow, as demonstrated in Figure 5.24 (frame c), which in turn weakens the disturbance of the boundary layer [79] while the domain with the smallest space ratio ($TATCT$) creates the strongest swirl, as displayed in Figure 5.24 (frame a), and this generates fluctuation of energy between the tape and tube wall, leading to an effective transfer of heat across the layers of the fluids. The results in Figure 5.25(a) show that the Nusselt number with tape geometry with $w = 15mm$ ($TATCT_{w1}$) and $13mm$ ($TATCT_{w2}$) are up to 6.1% and 8.9% respectively lower than that with $w = 18mm$ ($TATCT$).

The effects of the variations in the perimeter of the cuts on the tape (and hence the area of the cut) on the heat transfer enhancement with $p = 34.26mm$ ($TATCT$), $27mm$ ($TATCT_{a1}$) and $18mm$ ($TATCT_{a2}$) are given in Figure 5.25(b). It is observed that the heat transfer decreases with the decrease in the size of the cut. The reason behind this is that once a cut is made on the surface of the twisted tape, the cut generates additional swirls and thus improves fluid mixing [79]. When the perimeter of cut is small, this additional effect has little impact on the heat transfer. The tape with smallest perimeter of cut ($TATCT_{a2}$), impacts lowest disturbance to the flow between the wall tube and edge of the tapes (Figure 5.24 (frame e)) and correspondingly lowers the Nusselt number. As shown in Figure 5.25(b), the heat transfer rate in term of Nusselt number for the tape with $p = 27mm$ ($TATCT_{a1}$) and $18mm$ ($TATCT_{a2}$) are respectively up to 2.6% and 7.9% lower than that for the tape with $p = 34.26mm$ ($TATCT$).

The heat transfer in term of Nusselt number in the tubes induced with tape at various pitches $y = 36\text{mm}$ (TATCT), 54mm (TATCT_{y1}) and 72mm (TATCT_{y2}) are demonstrated in Figure 5.25(c). The results reveal that the Nusselt number increases when the pitch decreases from 54mm to 36mm but decreases when the pitch increases from 54mm to 72mm . The increase in the heat transfer rate at small pitch is attributed to longer flowing path which makes the fluid to have a long time for heat exchange. As depicted in Figure 5.24 (frames a, f and g), a higher intensity of swirl is enjoyed by the fluid as a result of the reduction in the tape pitch. The results in Figure 5.25(c) indicates that the twisted tape with $y = 36\text{mm}$ (TATCT_{y1}) enhances the heat transfer rate up to 2.1% over that of the tape with $y = 54\text{mm}$ (TATCT). On the contrary, the twisted tape with $y = 72\text{mm}$ (TATCT_{y2}) suffers a reduction in heat transfer rate of up to 3.4% of the tape with $y = 54\text{mm}$. The results for the Nusselt number for all the cases for the variations (w , p and y) in the tape geometries are given in Figure 5.26. It is seen in the Figure 5.26 that the tape with the least pitch (TATCT_{y1}) provides the highest heat transfer enhancement.

5.9.4 Effects on friction factor

In this section, there is a discussion on the impact of the variation in the tape geometry on the friction factor in the domain and it is demonstrated in Figure 5.27. It can be seen in Figure 5.27(a) that the friction factor decreases with the reduction of the tape width from $w = 18\text{mm}$ (TATCT), to 15mm (TATCT_{w1}) and then to 13mm (TATCT_{w2}). The value of the friction factor decreases by up to 5.9% when $w = 18\text{mm}$ (TATCT) as compared with that when $w = 15\text{mm}$ (TATCT_{w1}) but decreases by up to 8.6% when $w = 13\text{mm}$ (TATCT_{w2}). The variation of the friction factor with the variation in the perimeter (p) of the cut is presented in Figure 5.27(b). It is seen that

the friction factor decreases as the perimeter of the cut decreases. This is because the tape with large perimeter of cut has a less blocking area [81]. Also, the additional dissipation of pressure of the fluid caused by the fluid disturbance due to the presence of cuts on the tapes resulted in an increase of interaction of the pressure force around a velocity boundary layer [81]. The friction factors of the tape with $p = 27mm$ (TATCT_{a1}) and $18mm$ (TATCT_{a2}) are found to be lower than that of the tape with $p = 34.26mm$ (TATCT) by up to 2.3% and 7.5% respectively.

The friction factor in the tubes with variation in the pitch of its tape is shown in Figure 5.27(c). As with the results presented for the Nusselt number, the friction factor is increased with the pitch decreasing from $y = 54mm$ (TATCT) to $36mm$ (TATCT_{y1}) but decreases when the pitch is increased from $54mm$ to $72mm$ (TATCT_{y2}). The friction factors obtained with the tape with $y = 36mm$ and $72mm$ are up to 2.2% higher and 3.2% lower respectively than that obtained in the tape with $y = 54mm$. As seen in Figure 5.28 which demonstrates the results for the friction factor for all the cases for the variations in the tape geometries, the tape with the least width (TATCT_{w2}) has the least pressure drop.

5.9.5 Effects on the thermal performance factor

The implications of the variations in the geometries of the tape on the thermal performance factor are investigated and the results are presented in Figure 5.29. The thermal performance factor (η) as it is affected by variations in the tape width is shown in Figure 5.29(a). The thermal performances got from the tape with $w = 15mm$ (TATCT_{w1}) and $13mm$ (TATCT_{w2}) are 1.4% and 3.3% respectively lower than that of the tape with $w = 18mm$. Thus, the tapes with largest width $w = 18mm$ (TATCT) offers

highest thermal performance factor. Even though the increase in the tape width yields an increase in friction factor (§5.9.4), yet a higher thermal performance is obtained as a result of a reasonable increase in heat transfer rate. The applications of the various tape geometries for the enhancement of heat transfer are found to be promising since the thermal performance factors determined under these conditions power are all above unity.

Effect of the perimeter of the cut on the thermal performance factor is given in Figure 5.29(b). The thermal performance increases as the perimeter (p) of the cut increases. The thermal performance factor obtained with the tape with $p = 27mm$ (TATCT_{a1}) and $18mm$ (TATCT_{a2}) are 1.1% and 3.1% respectively lower than that with $p = 34.26mm$ (TATCT). The response of thermal performance factor to a variation in the pitch of the tape is presented in Figure 5.29(c). It is indicated by the results that the tapes with smallest pitch ($y = 36mm$) produces the highest thermal performance factor whereas the smallest thermal performance factor is obtained from the tape with the largest pitch ($y = 72mm$). From the result, it can be inferred that the thermal performance factors associated with the tape with $y = 36mm$ (TATCT_{y1}) is enhanced up to 1.1% over that of the tape with $y =$ and $54mm$ (TATCT) but the tape with $y = 72mm$ (TATCT_{y2}) has its thermal performance factor diminished by 1.3% compared with that of the tape with $y = 54mm$. The results displayed in Figure 5.30 is an indication that of all the cases considered for the variations in the tape geometry, the highest thermal performance factor is obtained in the tape with the least pitch (TATCT_{y1}).

5.10 Implication of Various Tape Geometries on Production Cost and Thermal Performance

It has been established in §5.9.5 that the applications of the various tape geometries for the enhancement of heat transfer are promising. In this section, the cost implication of the various tape geometries in enhancing the heat transfer is looked into.

As provided in Table 5.6, the quantity of copper material for production of the various domains TATCT, TATCT_{w1}, TATCT_{w2}, TATCT_{a1}, TATCT_{a2}, TATCT_{y1} and TATCT_{y2} are $1.14 \times 10^{-4}m^3$, $1.11 \times 10^{-4}m^3$, $1.09 \times 10^{-4}m^3$, $1.14 \times 10^{-4}m^3$, $1.14 \times 10^{-4}m^3$, $1.13 \times 10^{-4}m^3$ and $1.14 \times 10^{-4}m^3$ respectively. Since the cost of the material is directly proportional to its quantity [141], then the quantity of the material for the domain and the cost of production of the domain can be used interchangeably.

The implication of the various tape geometries on the production cost of their domains and the thermal performance of the domains are discussed in Figure 5.31. Choosing the domain with the highest thermal performance (TATCT_{y1}) gives a thermal performance of 1.1% over that of TATCT and saves 0.5% of the material (and hence the production cost) of the TATCT. The domain with the least quantity of material (TATCT_{w2}) has its thermal performance 3.3% less than that of TATCT but saves the material by 4.3% of the TATCT. The domain that uses the highest quantity of material (TATCT_{a2}) has a thermal performance that is 3.1% lower than that of TATCT and uses a quantity of material of 0.54% above that of TATCT.

From the Figure 5.31, it is seen that comparing the ratio of the production cost of the TATCT_{w1}, TATCT_{w2}, TATCT_{a1}, TATCT_{a2}, TATCT_{y1} and TATCT_{y2} with

that of TATCT and also comparing the ratio of their thermal performance factor over that of TATCT indicate that the quantity of the material used for the TATCT_{y1} is much close to those of the TATCT_{w1} and TATCT_{w2}. It is also seen that the thermal performance factor of TATCT_{y1} is much better than those of TATCT_{w1} and TATCT_{w2}. Therefore, the domain TATCT_{y1} is considered the best among the modifications made to the tapes.

5.11 Correlations for the Heat Transfer and Fluid Flow

It is important to develop appropriate correlations in order to predict the heat transfer and flow characteristics in the tubes. The correlations show how the pairs of the simulated results and predicted results are related and this will be useful in relevant applications. In this study, non-linear regression analysis was used to develop the correlations that predict the Nusselt number and friction factor for the TAECT, TACCT and TATCT. Since the tubes are induced with full-length twisted tapes and the flow in the induced tubes is not developed, the effect of entrance length on the correlation is negligible. The correlation for the Nusselt number, Equation (5.9), is a function of Reynolds number (Re), Prandtl number (Pr), perimeter of cut on twisted tape (p), width of twisted tape (w) and twist ratio of twisted tape (y). The correlation of the friction factor, Equation (5.10), is also a function of those of the Nusselt number except Pr .

$$Nu = 116.961 + Re^{1.323} Pr^{-2.938} \left(\frac{p}{w}\right)^{0.296} y^{-2.645} \quad (5.9)$$

$$f = 20.294 Re^{-0.522} \left(\frac{p}{w}\right)^{0.151} \left(\frac{y}{y-1}\right)^{1.462} \quad (5.10)$$

The validity of these correlations is demonstrated in Figure 5.32 and Figure 5.33 in which comparisons are made between the numerical results and the predicted results. For the Nusselt number, the predicted results agree with the numerical results within deviation 2.52% respectively. In the case of the friction factor, the predicted and the numerical results are in agreement within deviation of 4.23%. Judging by the results of the correlations of the other researchers presented in the literature review, it can be asserted that the numerical results obtained in the present Chapter are reliable.

5.12 Conclusion

Numerical analysis was carried out to study the heat transfer, friction factor and thermal performance factor of water inside different tubes induced with different twisted tapes. The purpose is to ascertain which of the tube design gives the best performance when compared with the plain tube. The different tube designs considered are the plain tube (PT), tube with plain twisted tape (TPT), tube with elliptical cut twisted tape (TECT), tube with circular cut twisted tape (TCCT), tube with triangular cut twisted tape (TTCT), tube with alternate-axis elliptical cut twisted tape (TAECT), tube with alternate-axis circular cut twisted tape (TACCT) and tube with alternate-axis triangular cut twisted tape (TATCT). The tubes were under uniform wall heat flux conditions and turbulent flow were considered in the Reynolds number range between 5000 and 20000. RNG $\kappa - \varepsilon$ turbulence model was selected for the simulation.

As a result of improved tangential contacts and swirls, the TATCT provides temperature distribution, velocity and pressure that are superior to the other tube designs and therefore produces the best performance among all the other tube designs considered. Its Nusselt number is 63.66% to 118.4%

higher than that in the TPT and its friction factor is 160.5% to 215.8% higher than that in the TPT. The thermal performance factor of the TATCT is 37.35% to 43.89% higher than that in the TPT.

The influence which the variations in the tape width, the tape pitch and the size of cut on the tape have on the thermo-hydraulic characteristics is also considered. It was discovered that increasing the tape width is favourable to the flow system as this augments the heat transfer and thermal performance factor of the system. Also, increasing the size of the cuts on the tape is advantageous to the system. On the contrary, the Nusselt number, friction factor and thermal performance factor were found to decrease as the tape pitch increases. The ratio of the production cost of the domains with various tape geometries ($TATCT_{w1}$, $TATCT_{w2}$, $TATCT_{a1}$, $TATCT_{a2}$, $TATCT_{y1}$ and $TATCT_{y2}$) over that of TATCT and the ratio of their performance over that of TATCT indicates that $TATCT_{y1}$ uses materials that closely match that of $TATCT_{w1}$ and $TATCT_{w2}$ and its performance is much better than those of $TATCT_{w1}$ and $TATCT_{w2}$. The domain whose alternate-axis triangular cut twisted tape has the least pitch (that is, $TATCT_{y1}$) is considered the best among the modification made to the geometry of the tape of the TATCT.

Table 5.1: Cells for grid resolution study for the turbulent flow.

Domain	Cell					
PT	461178	476554	512420	614904	717388	768630
TPT	913594	944154	1015216	1218259	1421302	1522824
TECT	1122468	1159966	1247298	1496758	1746217	1870947
TCCT	1214178	1254681	1349142	1618970	1888799	2023713
TTCT	1236639	1277931	1374099	1648919	1923739	2061149
TAECT	1486055	1535641	1651206	1981447	2311688	2476809
TACCT	1557545	1609513	1730639	2076767	2422895	2595959
TATCT	1255502	1658638	2515756	3018907	3522058	3773634

Table 5.2: Amount of material for different domains.

Tape	Width of tape ($\times 10^{-3}$ <i>m</i>)	Total vol. of tape ($\times 10^{-5}$ m^3)	No. of cut on tape	Vol. of cut ($\times 10^{-7}$ m^3)	Net vol. of Tape ($\times 10^{-5}$ m^3)	Domain	Vol. of domain ($\times 10^{-4}$ m^3)
PT	18	1.8	0	0	1.80	TPT	1.146
ECT	18	1.8	15	8.48	1.72	TECT	1.137
CCT	18	1.8	15	8.48	1.72	TCCT	1.137
TCT	18	1.8	15	8.48	1.72	TTCT	1.137
AECT	18	1.8	15	8.48	1.72	TAECT	1.137
ACCT	18	1.8	15	8.48	1.72	TACCT	1.137
ATCT	18	1.8	15	8.48	1.72	TATCT	1.137

Table 5.3: Description of the various geometries of the alternate-axis triangular cut twisted tape (ATCT) used for the domain TATCT.

Tape	Geometry			
	w (mm)	p (mm)	y (mm)	sr
ATCT _{w1}	15	34.26	54	0.21
ATCT _{w2}	13	34.26	54	0.31
ATCT _{a1}	18	27.00	54	0.052
ATCT _{a2}	18	18.00	54	0.052
ATCT _{y1}	18	34.26	36	0.052
ATCT _{y2}	18	34.26	72	0.052

Table 5.4: Thermo-hydraulic values of different induced tubes for the turbulent flow at $Re = 20000$.

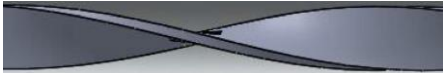
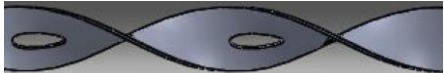
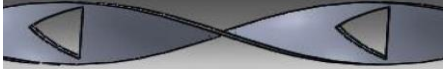
Induced tube	Nu	f	η	Tape geometry
TPT	185.81	0.0871	0.83	
TECT	202.76	0.0978	1.04	
TCCT	198.8	0.0959	1.03	
TTCT	206.35	0.1014	1.05	
TAECT	298.81	0.2193	1.11	
TACCT	292.98	0.2141	1.07	
TATCT	304.11	0.227	1.14	

Table 5.5: Cells for grid resolution study for various domains of TATCT for the turbulent flow.

Domain	Cell		
TATCT _{w1}	1714567	2449381	3184196
TATCT _{w2}	1683592	2405132	3126671
TATCT _{a1}	1766015	2522878	3279741
TATCT _{a2}	1770542	2529346	3288150
TATCT _{y1}	1752274	2503249	3254223
TATCT _{y2}	1761029	2515756	3270483

Table 5.6: Amount of material for various geometries of the alternate-axis triangular cut twisted tape (ATCT) used for the TATCT.

Tape	Width of tape ($\times 10^{-3}$ m)	Total vol. of tape ($\times 10^{-5}$ m^3)	Vol. of cut ($\times 10^{-7}$ m^3)	Net vol. of Tape ($\times 10^{-5}$ m^3)	Domain	Vol. of domain ($\times 10^{-4}$ m^3)
ATCT	18	1.8	8.48	1.72	TATCT	1.137
ATCT _{w1}	15	1.5	8.48	1.42	TATCT _{w1}	1.107
ATCT _{w2}	13	1.3	8.48	1.22	TATCT _{w2}	1.087
ATCT _{a1}	18	1.8	5.26	1.75	TATCT _{a1}	1.140
ATCT _{a2}	18	1.8	2.34	1.78	TATCT _{a2}	1.143
ATCT _{y1}	18	1.8	14.13	1.66	TATCT _{y1}	1.131
ATCT _{y2}	18	1.8	8.48	1.72	TATCT _{y2}	1.137

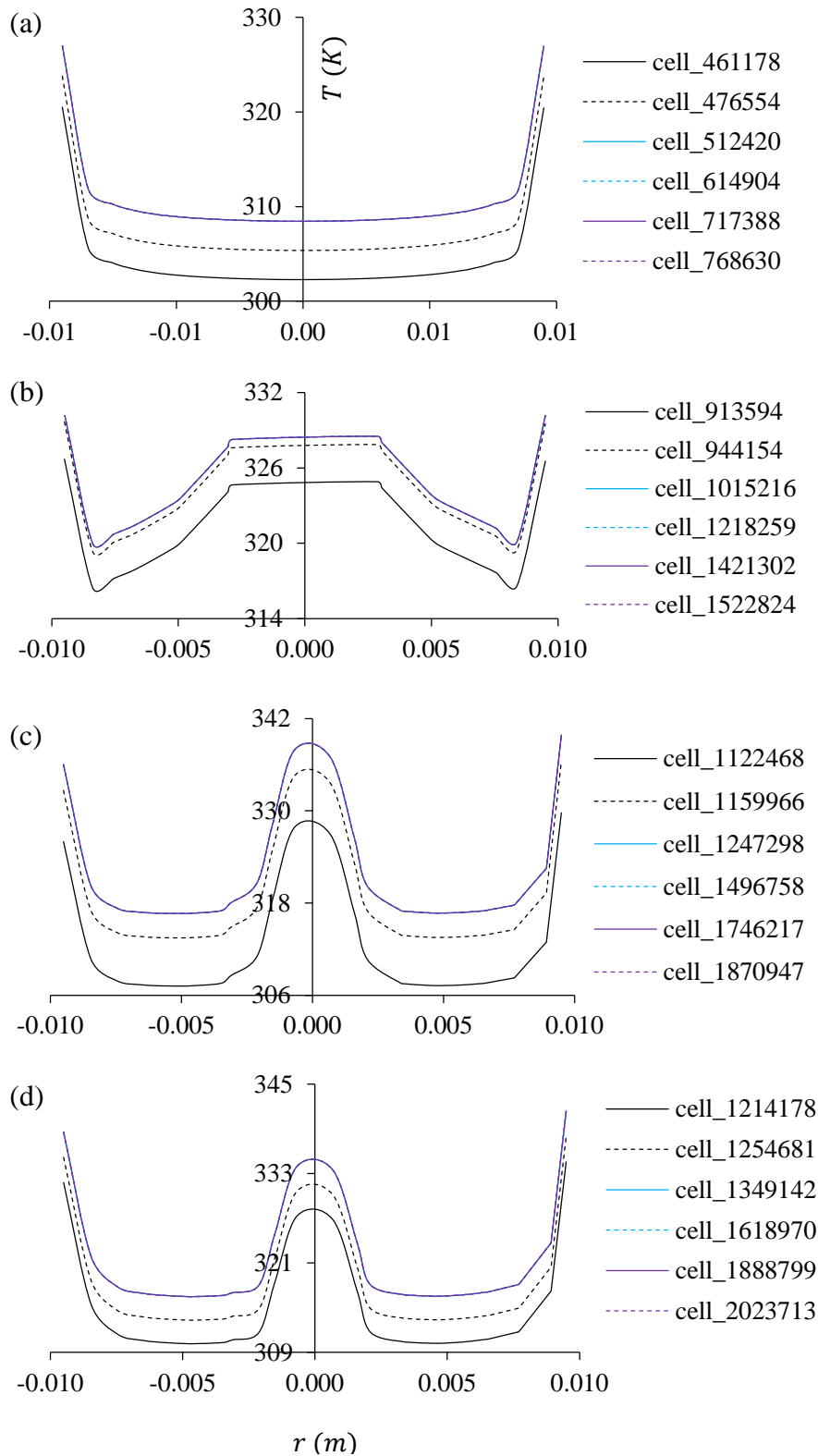


Figure 5.1: Temperature across the cross-section at the exit of (a) PT, (b) TPT, (c) TECT, (d) TCCT, (e) TTCT, (f) TAECT, (g) TACCT and (h) TATCT for $Re=20000$ for different grids.

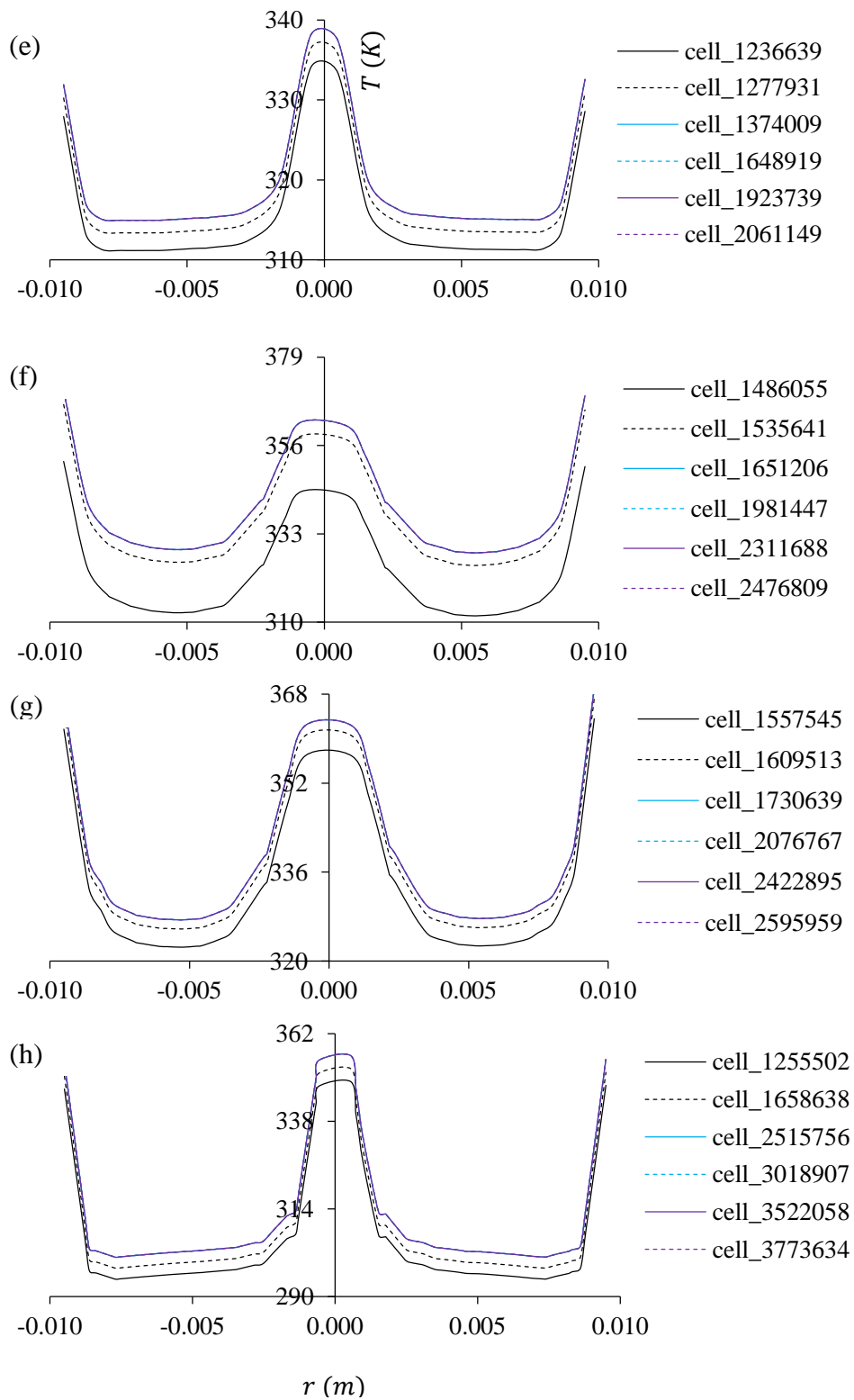


Figure 5.1 caption continued.

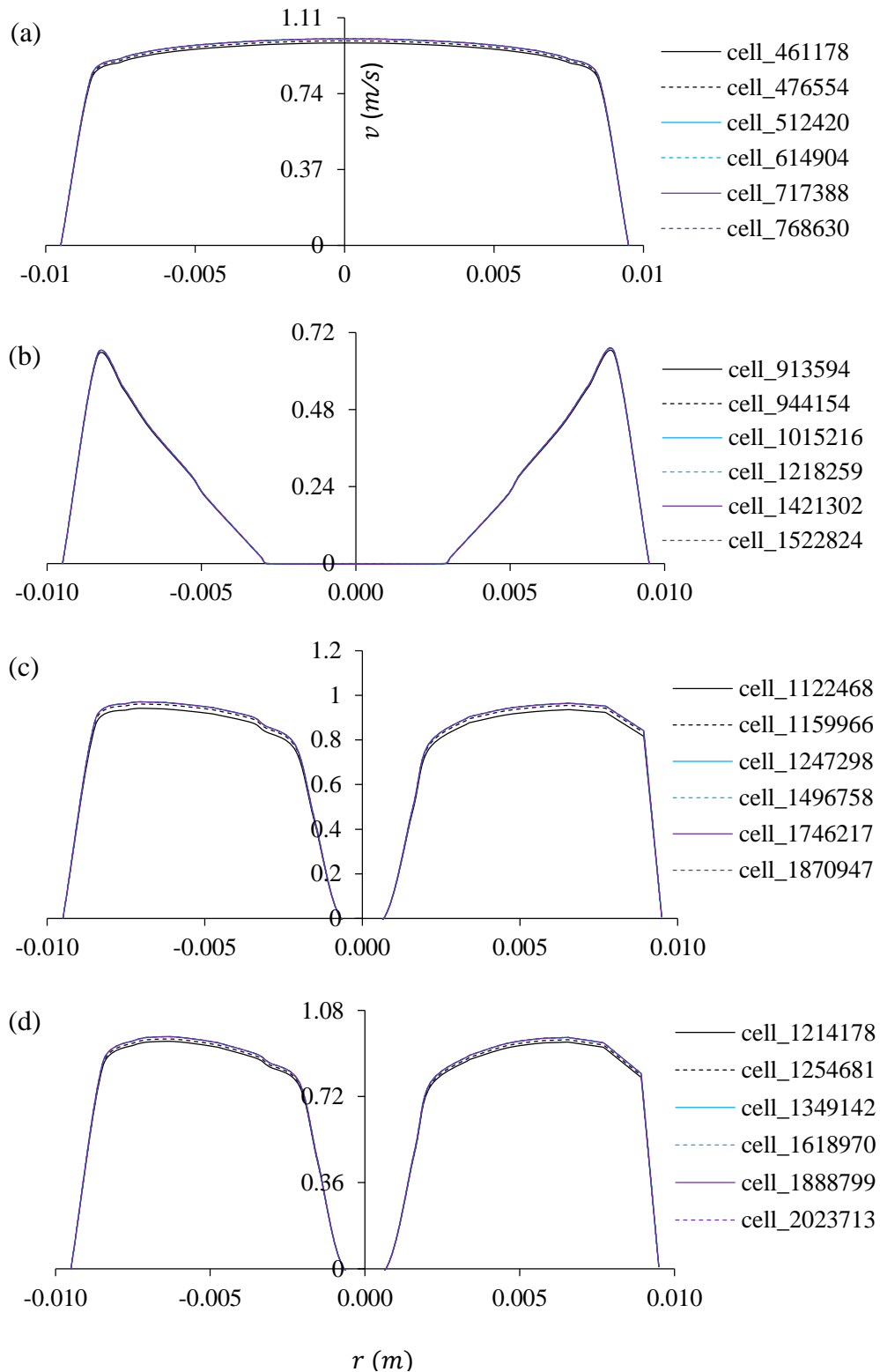


Figure 5.2: Velocity across the cross-section at the exit of (a) PT, (b) TPT, (c) TECT, (d) TCCT, (e) TTCT, (f) TAECT, (g) TACCT and (h) TATCT for $Re=20000$ for different grids.

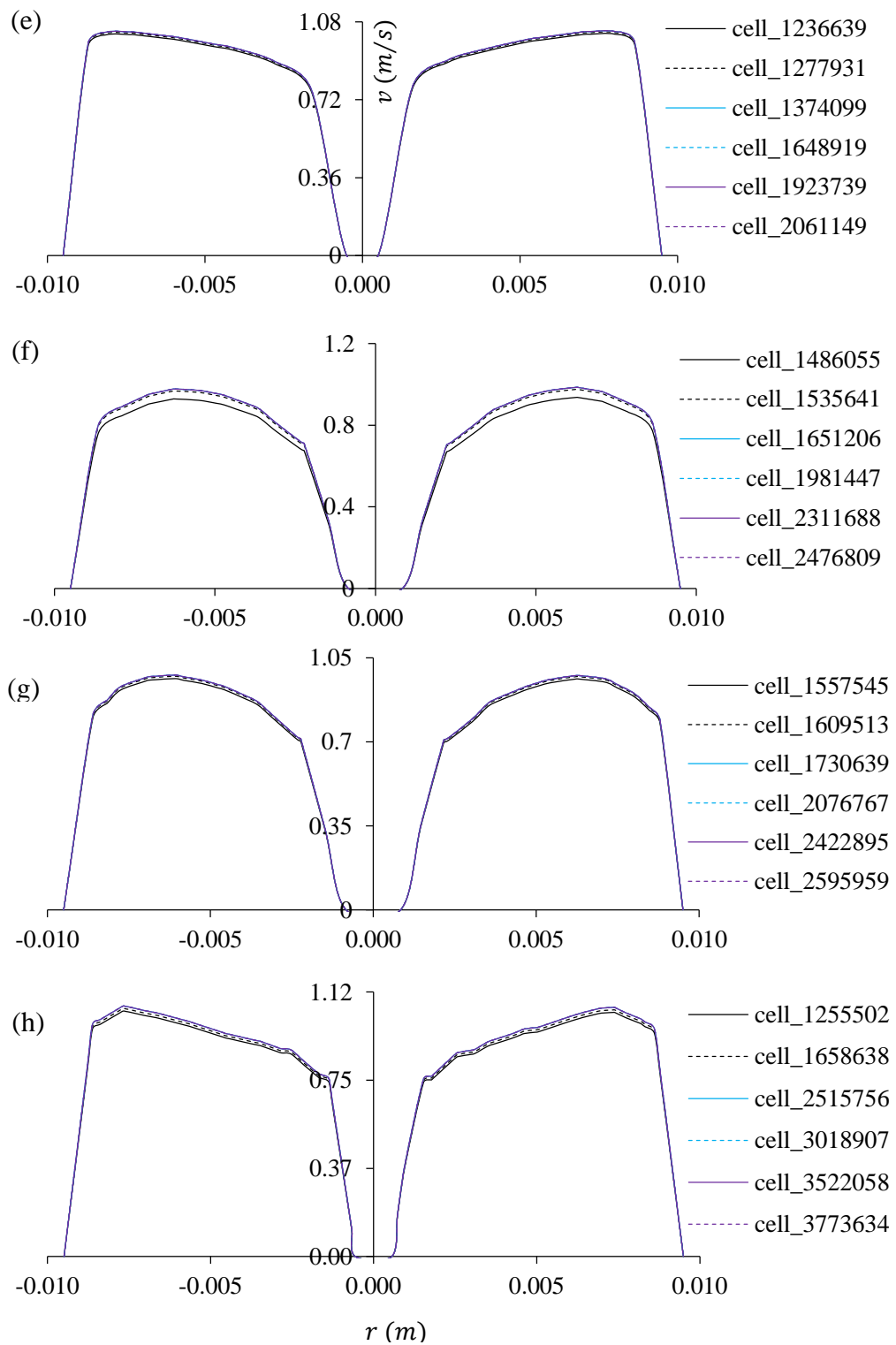


Figure 5.2 caption continued.

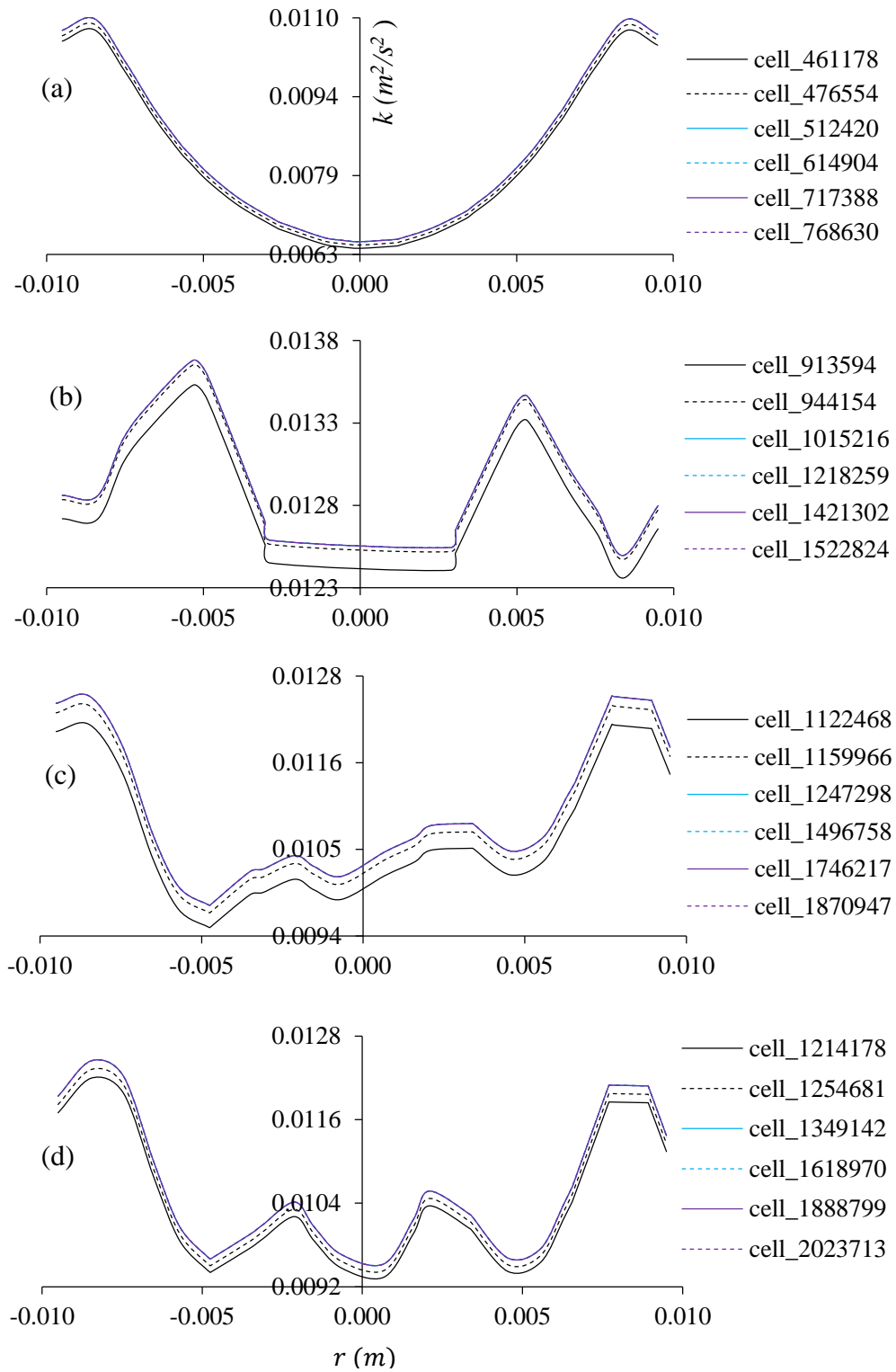


Figure 5.3: Turbulent kinetic energy across the cross-section at the exit of (a) PT, (b) TPT, (c) TECT, (d) TCCT, (e) TTCT, (f) TAECT, (g) TACCT and (h) TATCT for $Re=20000$ for different grids.

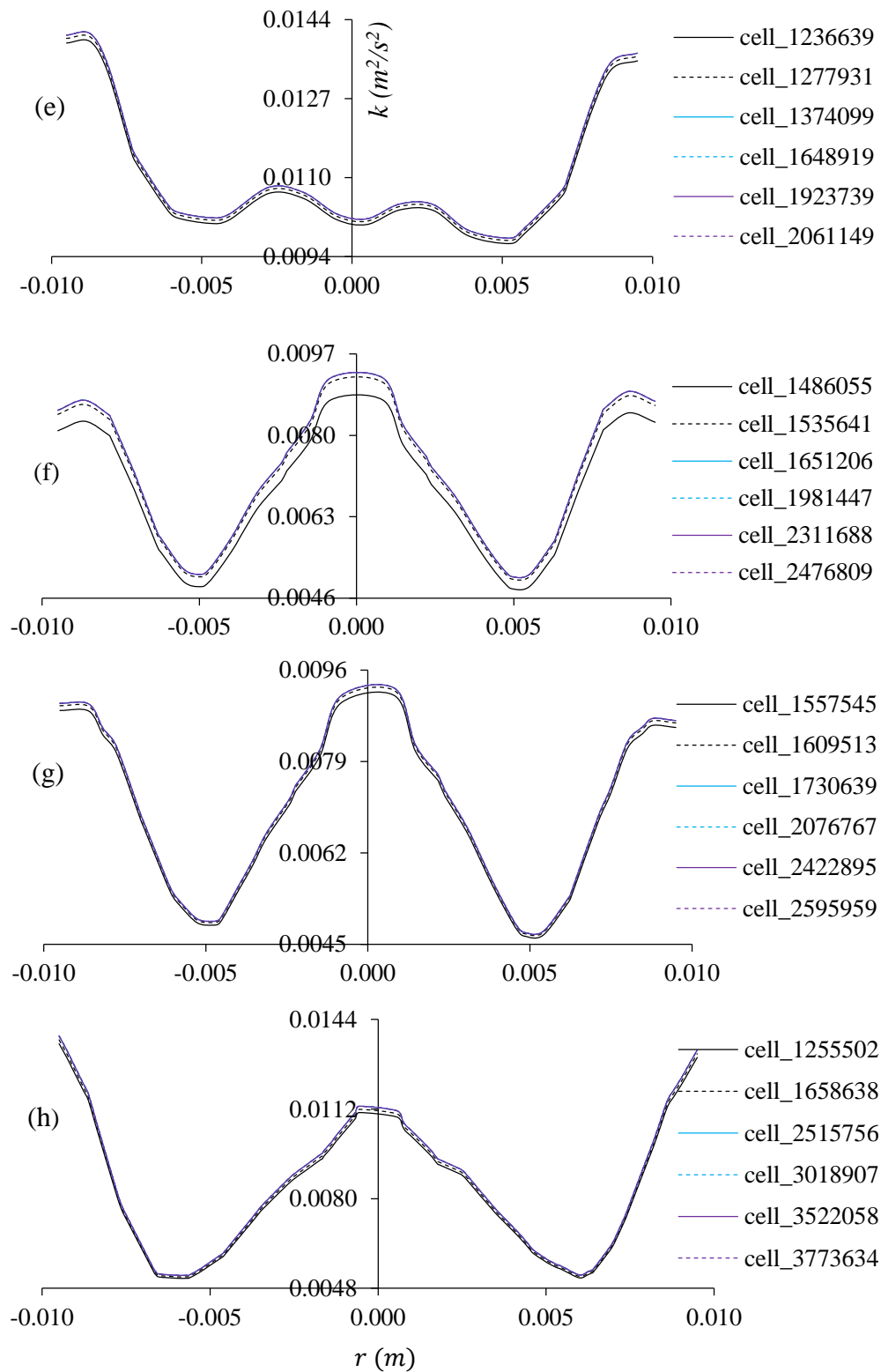


Figure 5.3 caption continued.

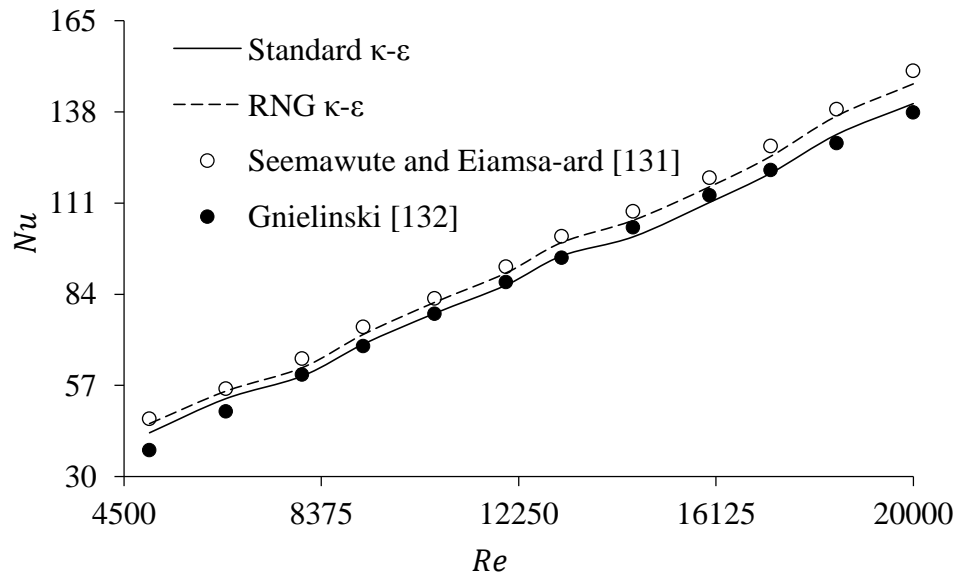


Figure 5.4: Validation with experimental works for PT.

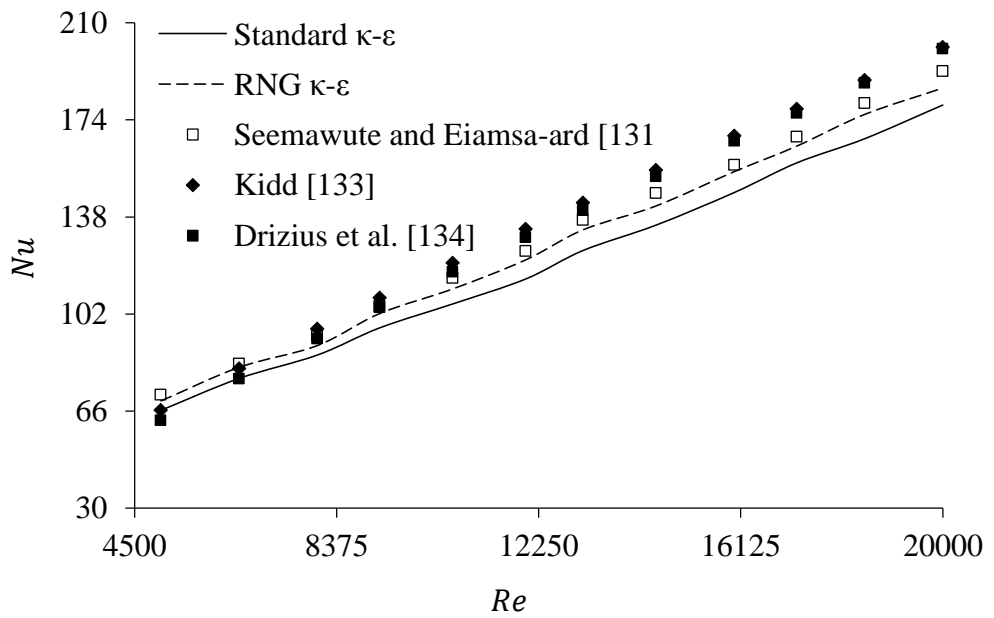


Figure 5.5: Validation with experimental works for TPT.

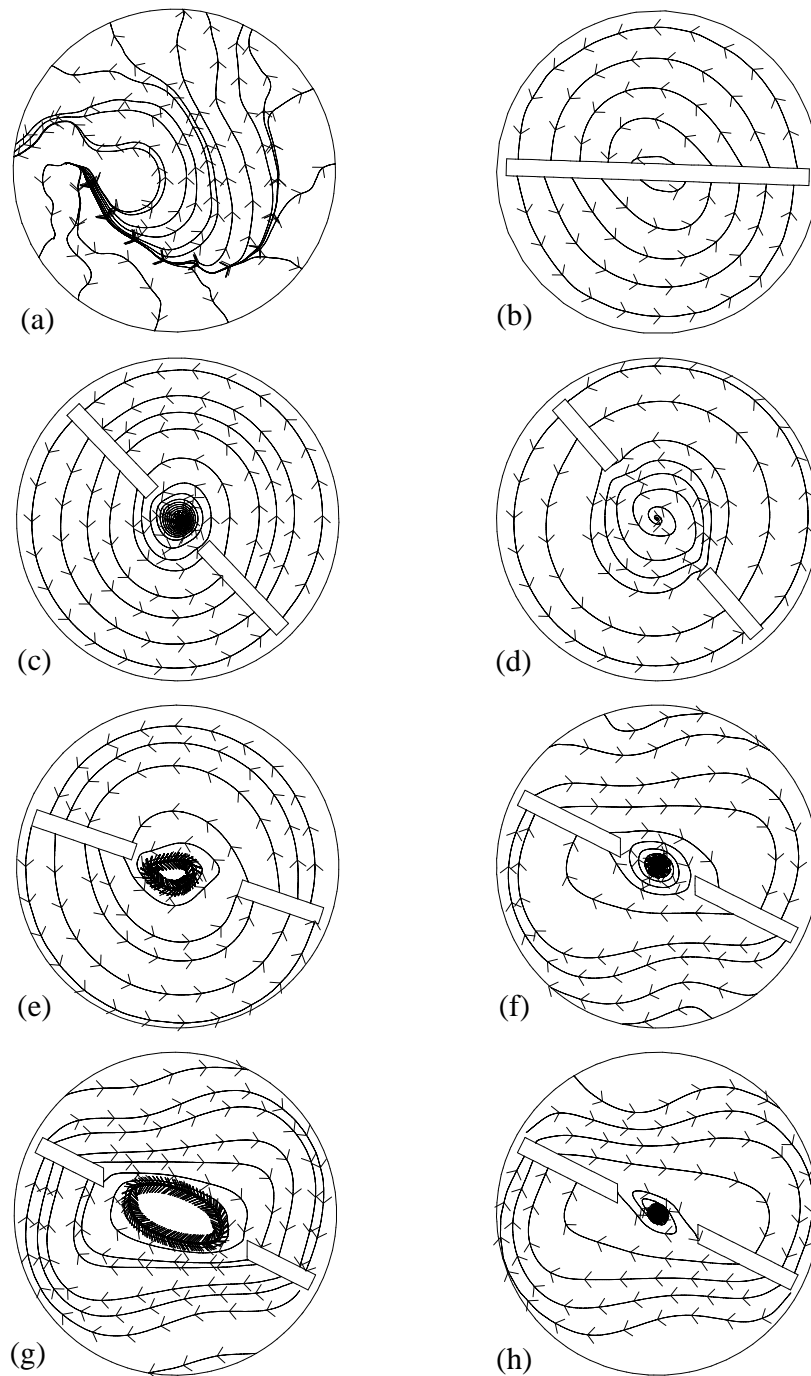


Figure 5.6: Streamlines across the domain cross-section at axial location $0.866m$ of (a) PT, (b) TPT, (c) TECT, (d) TCCT, (e) TTCT, (f) TAECT, (g) TACCT and (h) TATCT for $Re=20000$.

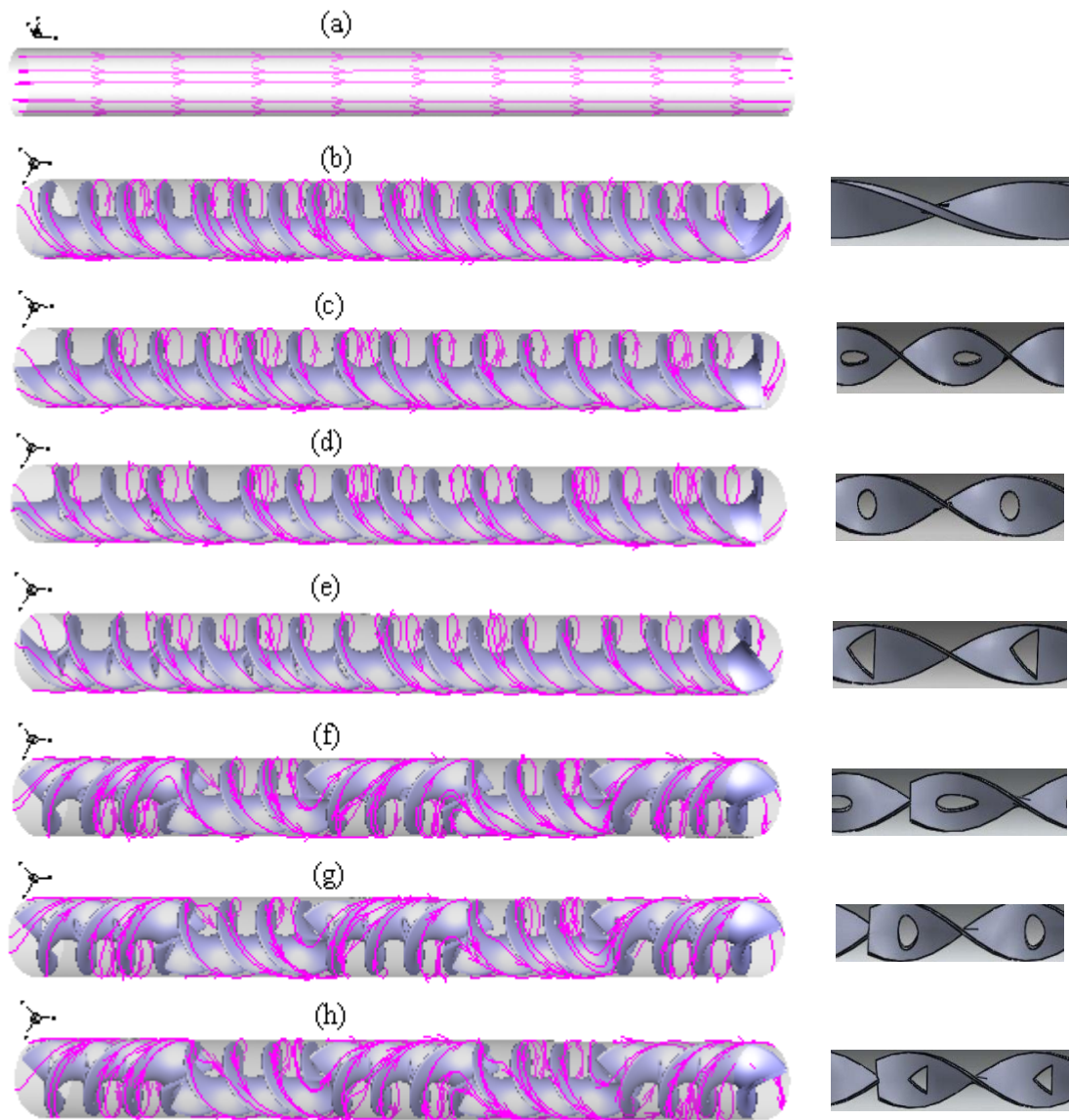


Figure 5.7: Streamlines for turbulent flow inside the domains of (a) PT, (b) TPT, (c) TECT, (d) TCCT, (e) TTCT, (f) TAECT, (g) TACCT and (h) TATCT.

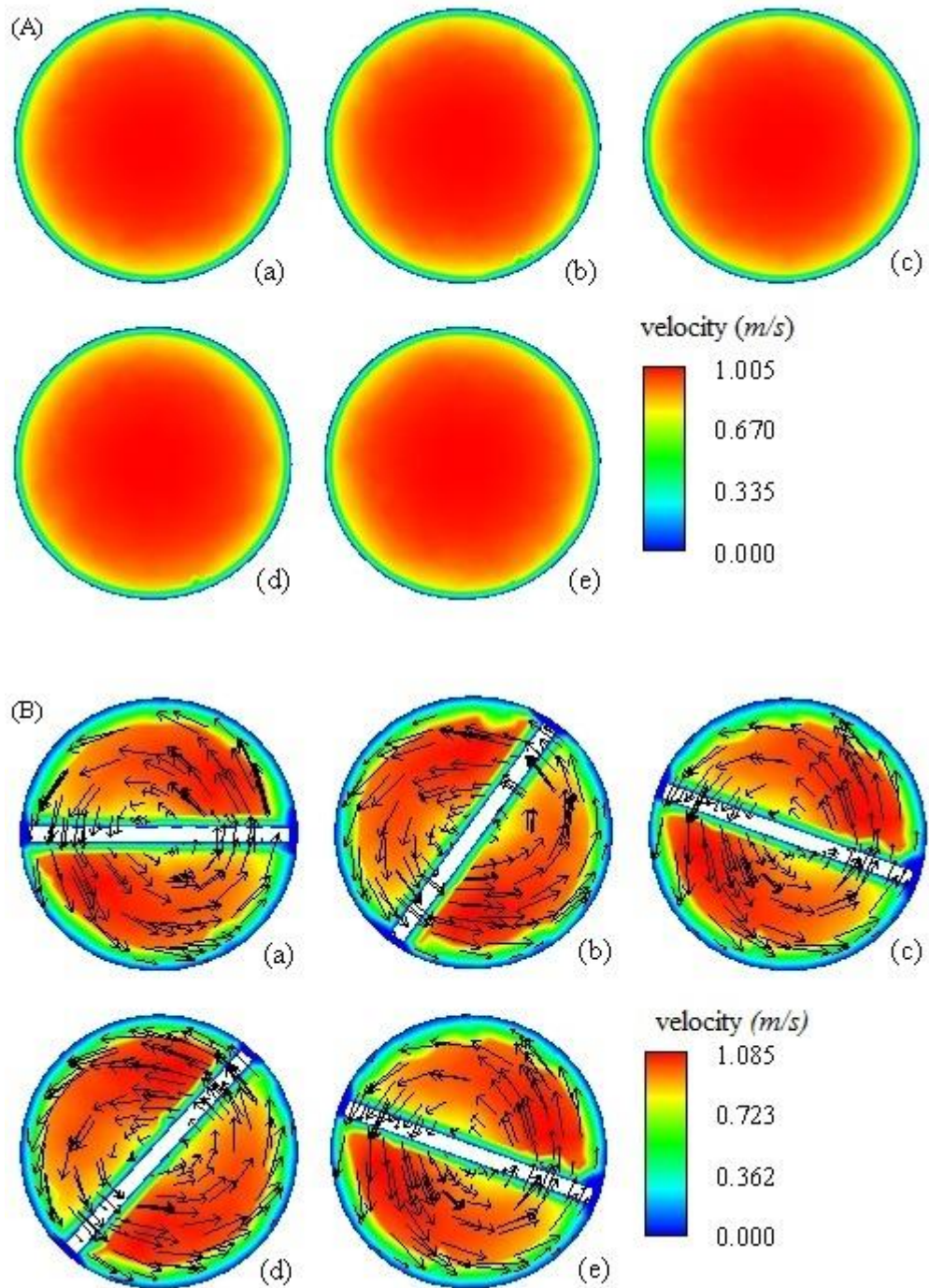


Figure 5.8: Vector plot appended on velocity contour of velocity for PT (A), TPT (B), TECT (C), TCCT (D), TTCT (E), TAECT (F), TACCT (G) and TATCT (H) for $Re=20000$ at axial location (a) $0.5m$, (b) $0.516m$, (c) $0.6m$, (d) $0.673m$ and (e) $0.7m$.

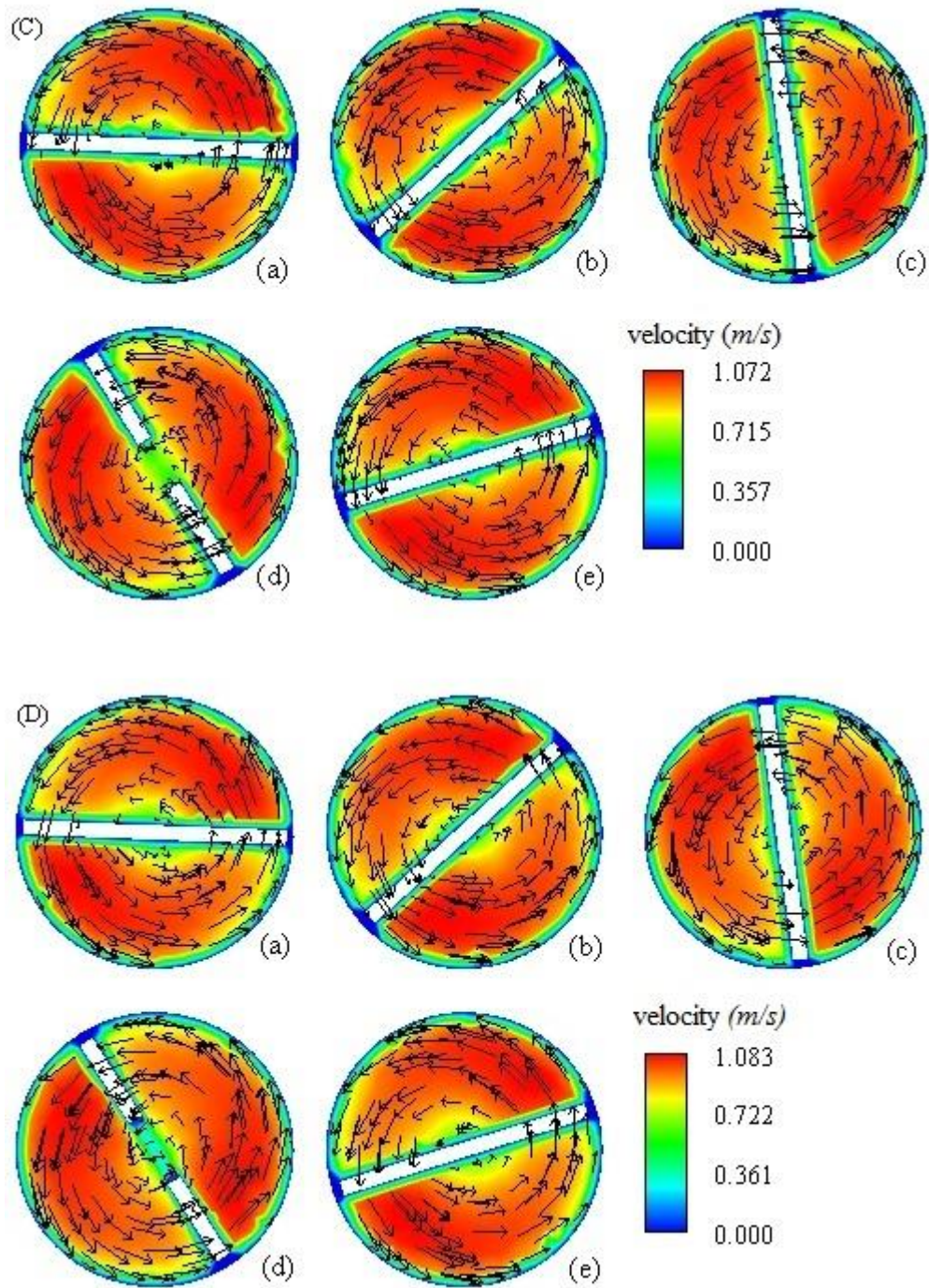


Figure 5.8 Caption continued.

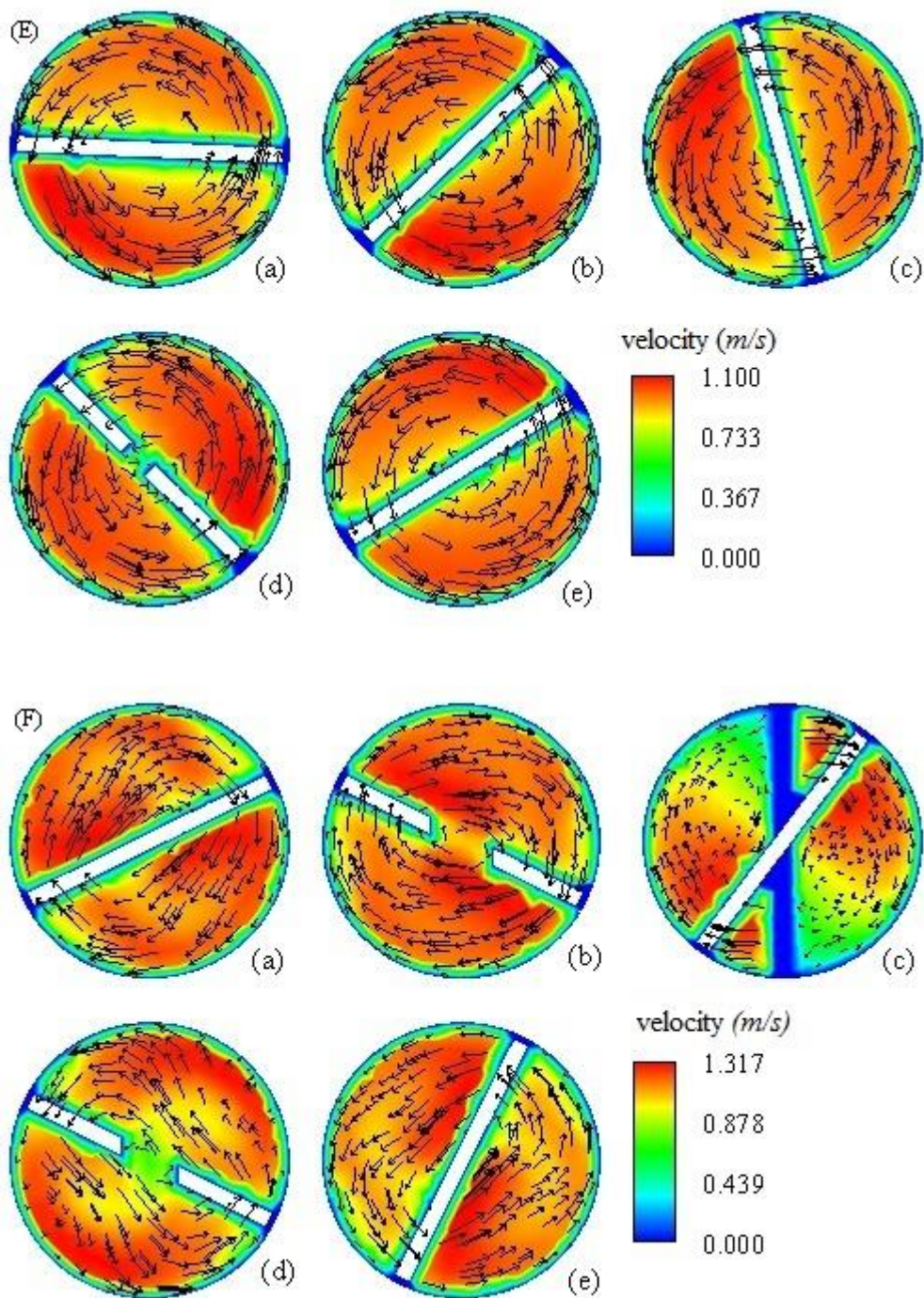


Figure 5.8 Caption continued.

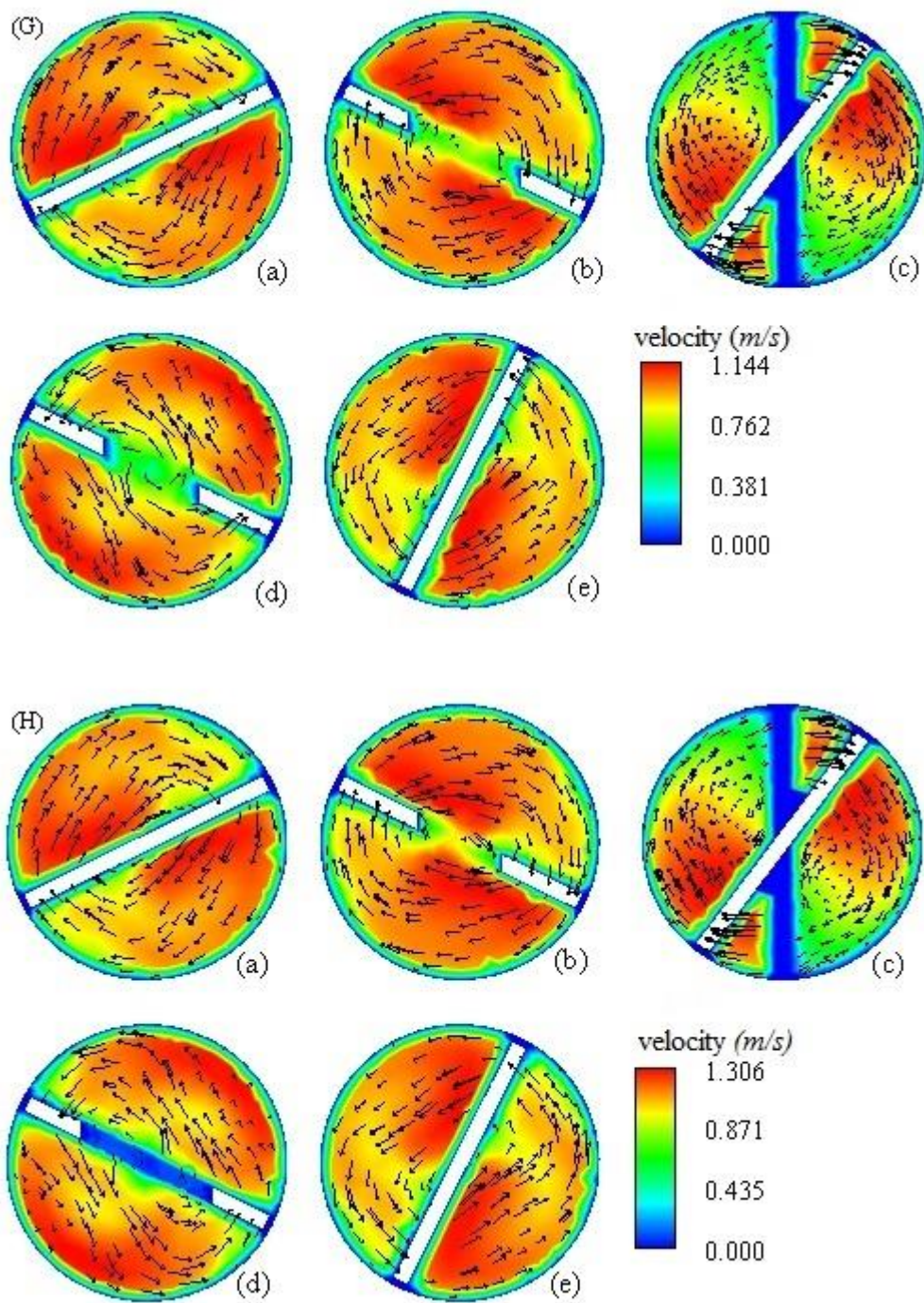


Figure 5.8 Caption continued.

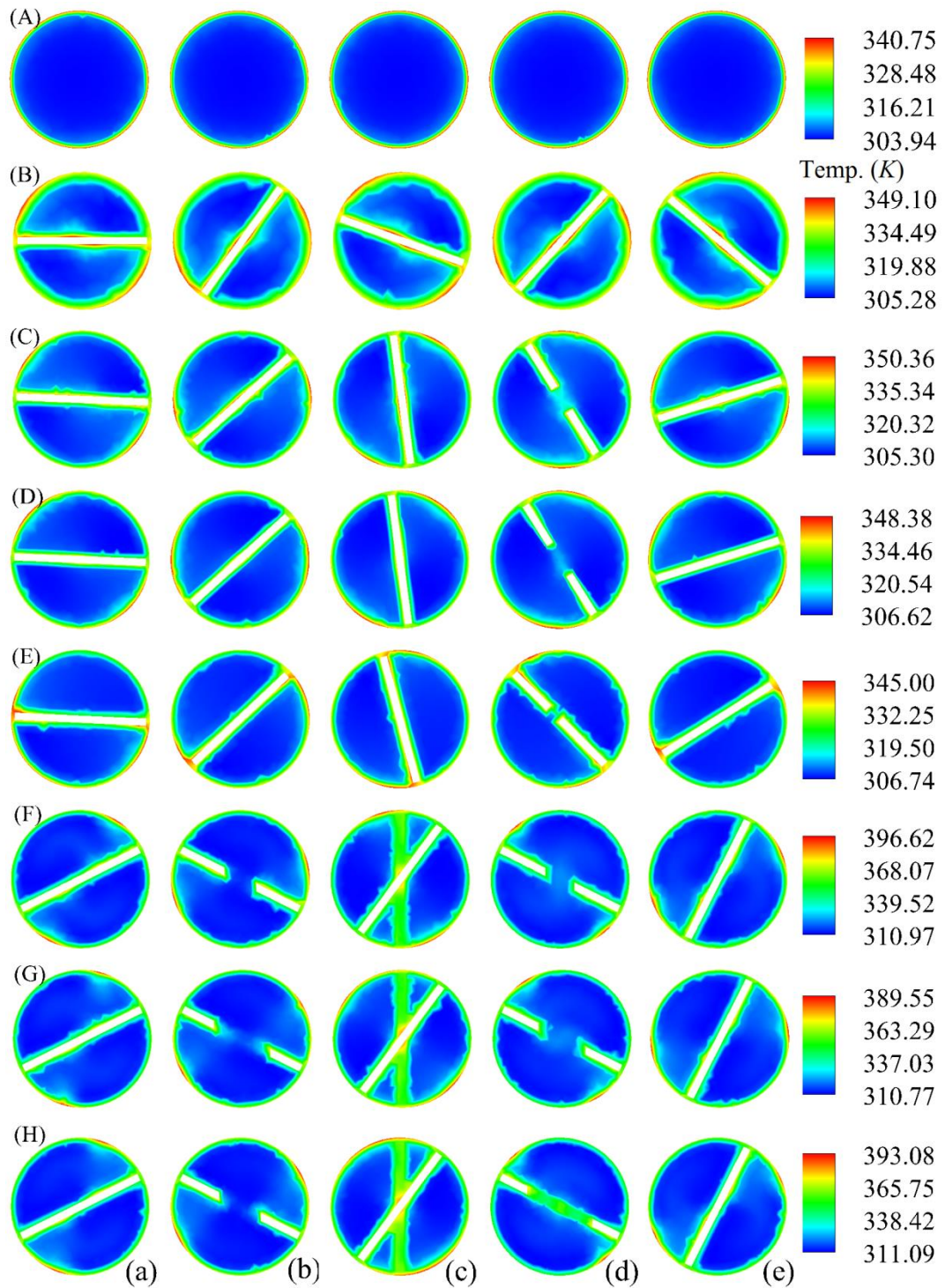


Figure 5.9: Contour plots of temperature for PT (A), TPT (B), TECT (C), TCCT (D), TTCT (E), TAECT (F), TACCT (G) and TATCT (H) for $Re=20000$ at axial location (a) 0.5m, (b) 0.516m, (c) 0.6m, (d) 0.673m and (e) 0.7m.

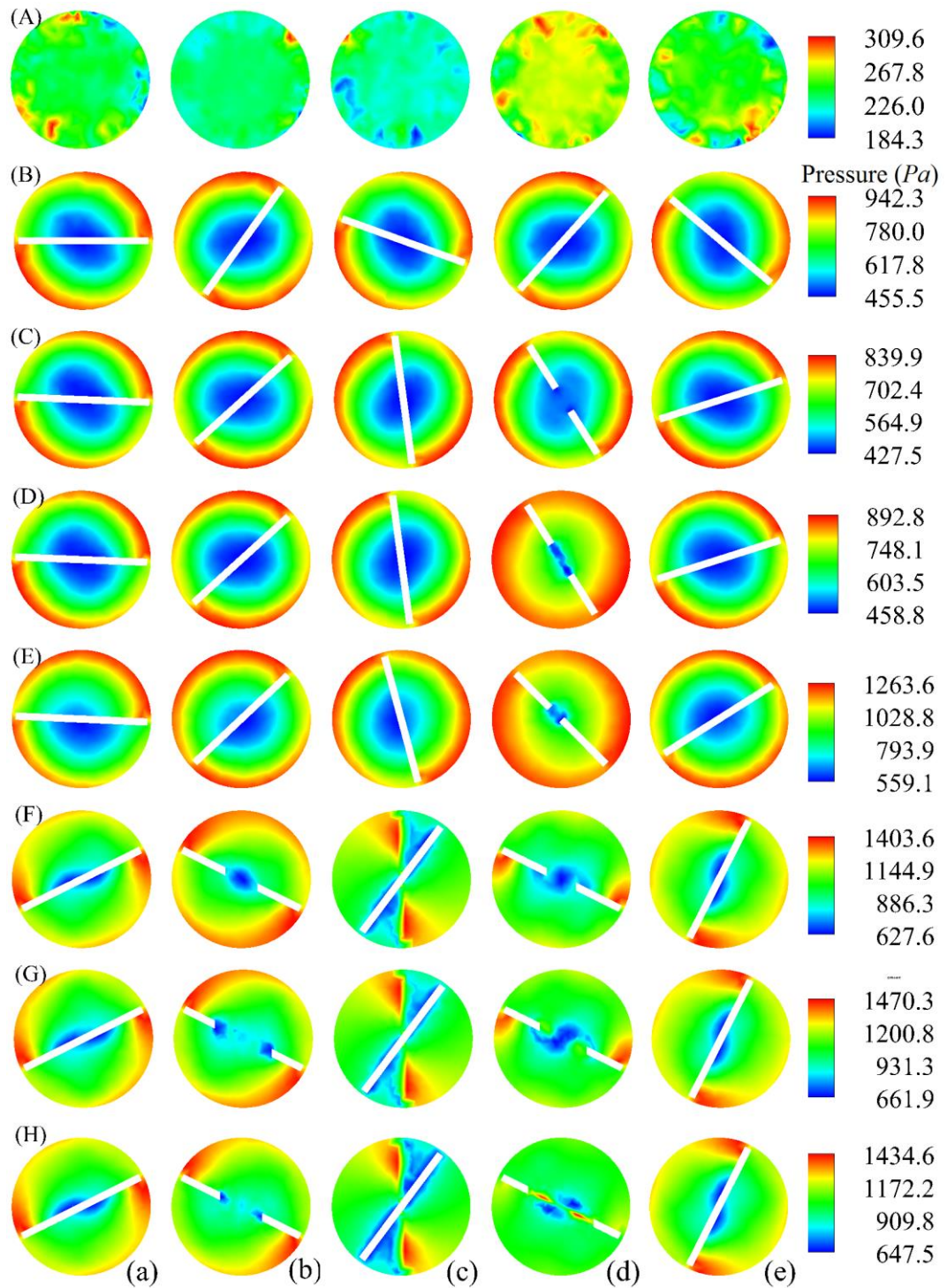


Figure 5.10: Contour plots of pressure for PT (A), TPT (B), TECT (C), TCCT (D), TTCT (E), TAECT (F), TACCT (G) and TATCT (H) for $Re=20000$ at axial location (a) $0.5m$, (b) $0.516m$, (c) $0.6m$, (d) $0.673m$ and (e) $0.7m$.

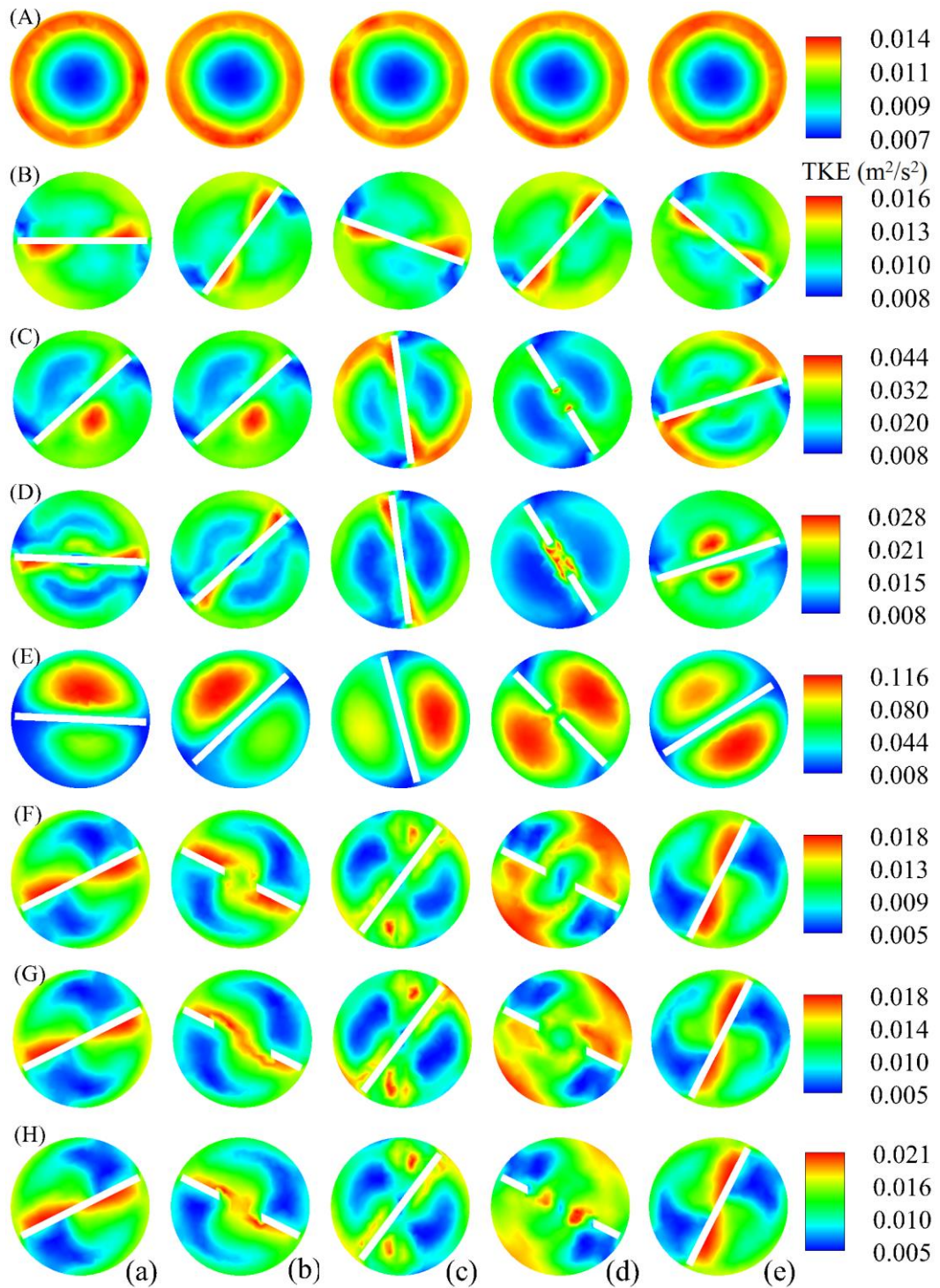


Figure 5.11: Contour plots of turbulent kinetic energy for PT (A), TPT (B), TECT (C), TCCT (D), TTCT (E), TAECT (F), TACCT (G) and TATCT (H) for $Re=20000$ at axial location (a) 0.5m, (b) 0.516m, (c) 0.6m, (d) 0.673m and (e) 0.7m.

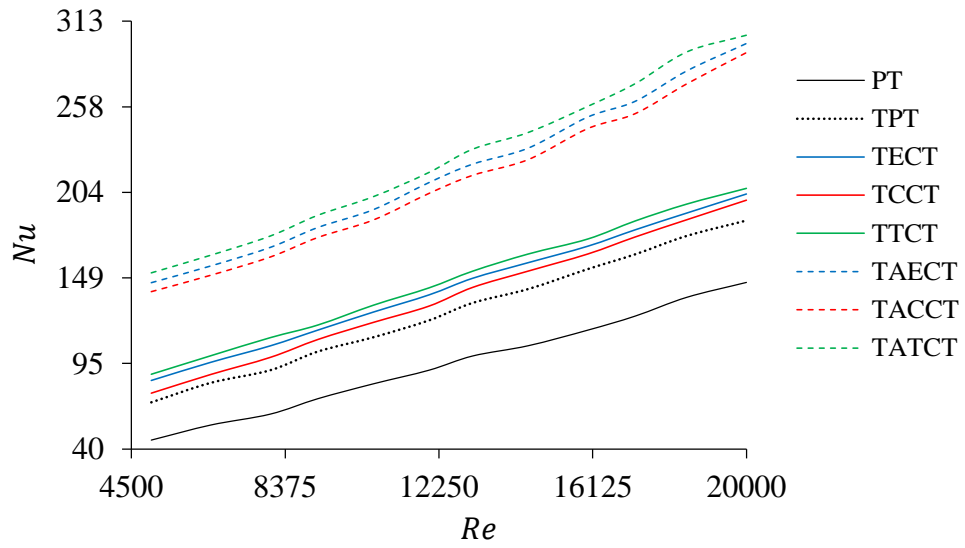


Figure 5.12: Effect of different twisted tape on Nusselt number vs. Reynolds number.

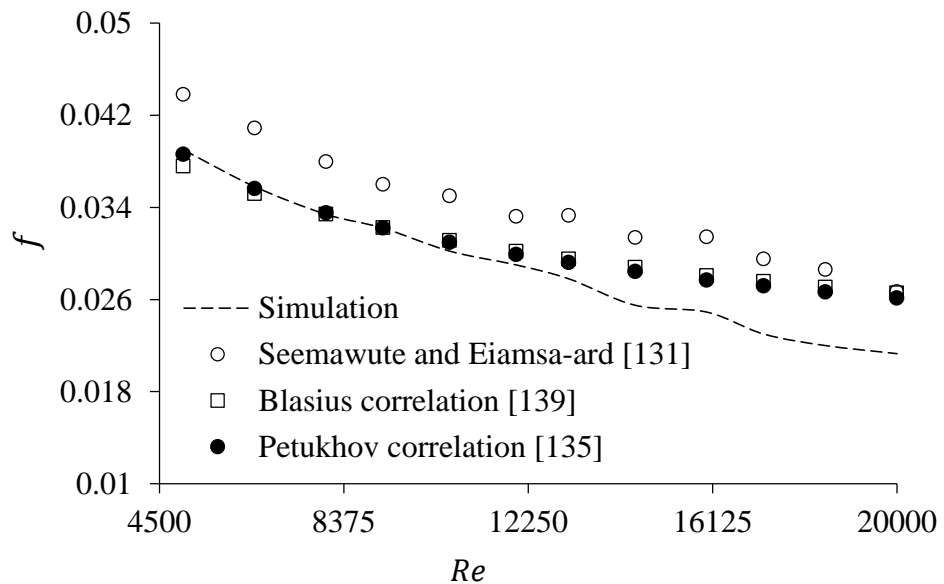


Figure 5.13: Validation of friction factor of plain tube.

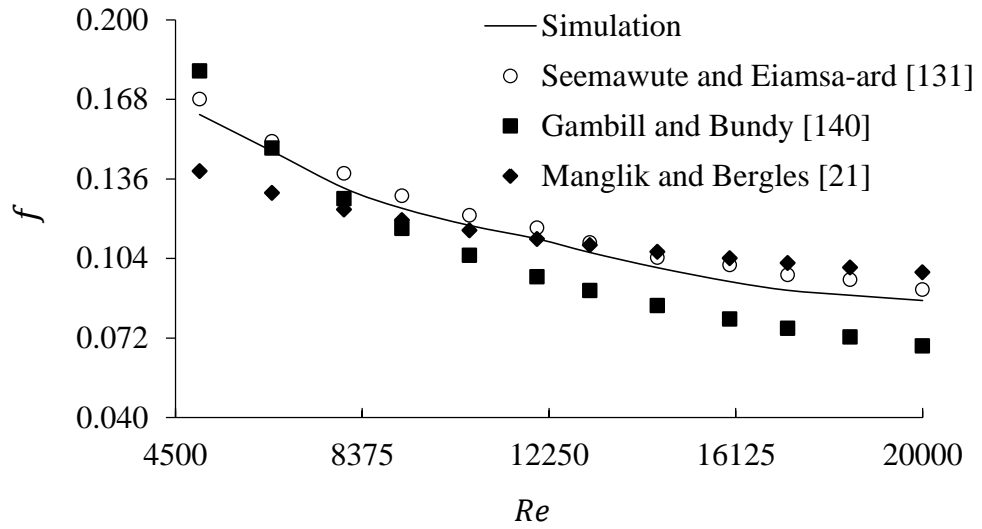


Figure 5.14: Validation of friction factor of tube induced with plain twisted tape insert.

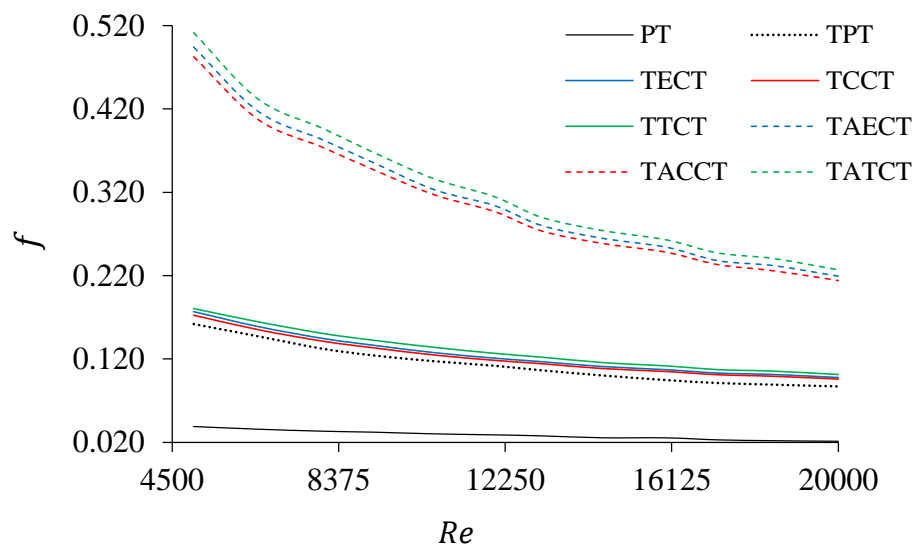


Figure 5.15: Effect of different twisted tape on friction factor vs. Reynolds number.

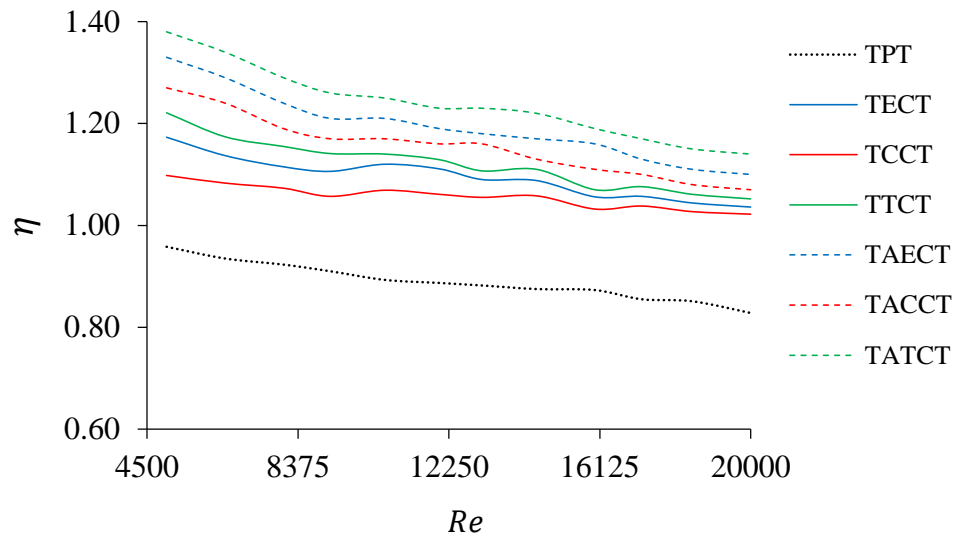


Figure 5.16: Effect of different twisted tape on thermal performance factor vs. Reynolds number.

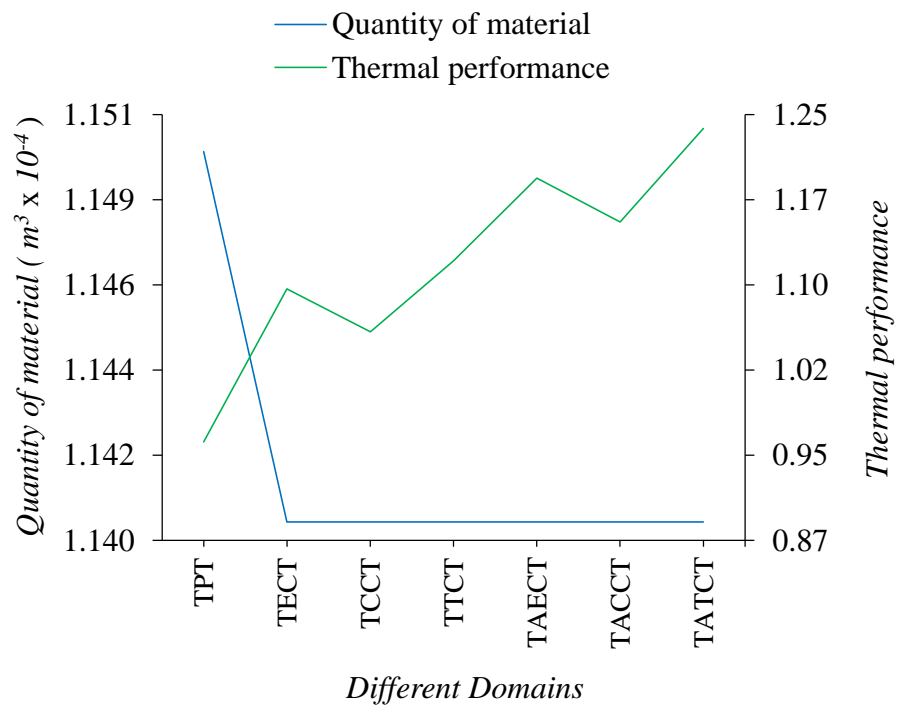


Figure 5.17: Comparison of the quantity of material and the thermal performance of the different domains.

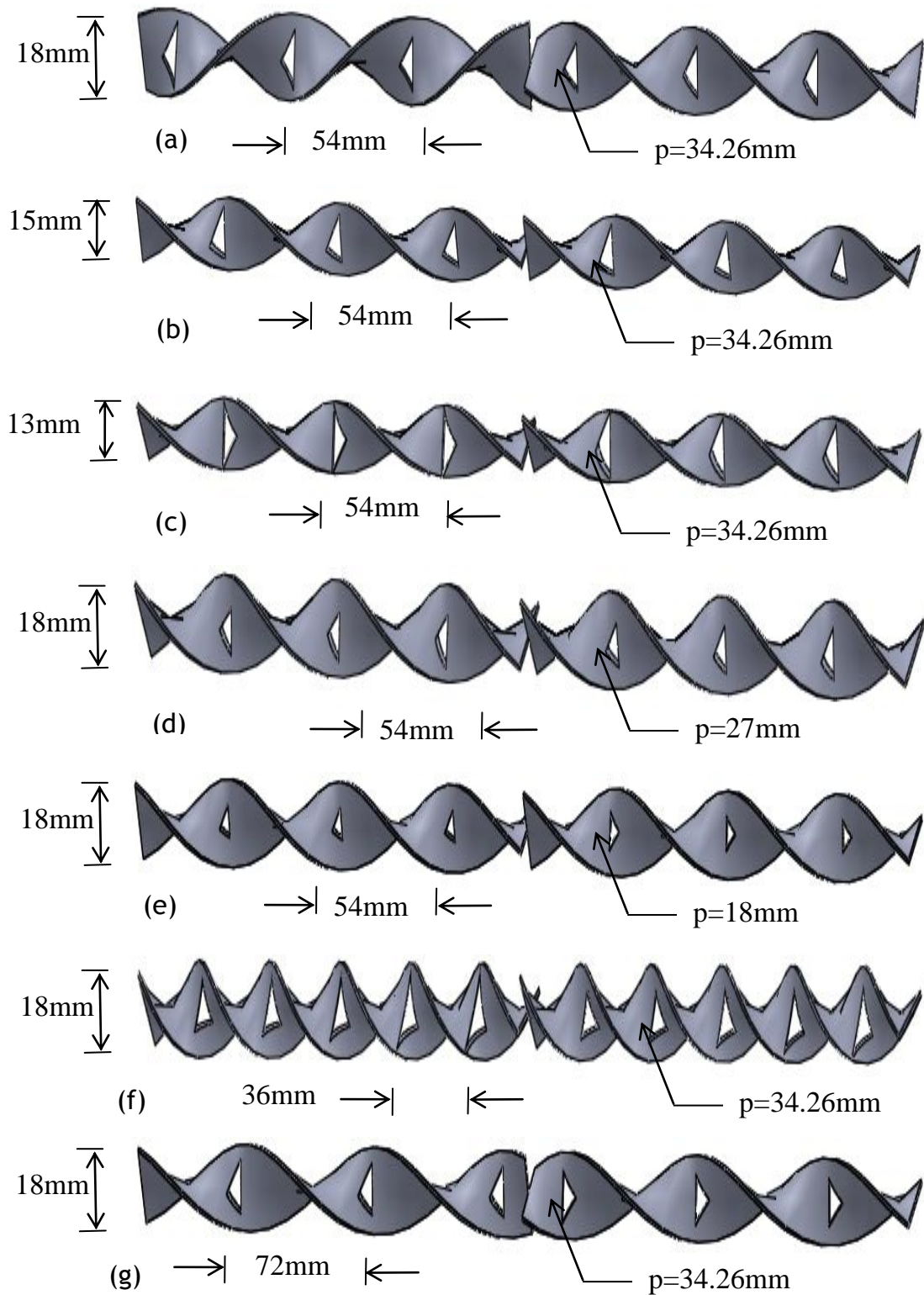


Figure 5.18: Geometries of the alternate-axis triangular cut twisted tape of (a) TATCT, (b) TATCT_{w1}, (c) TATCT_{w2}, (d) TATCT_{a1}, (e) TATCT_{a2}, (f) TATCT_{y1} and (g) TATCT_{y2}.

(Note: p = perimeter of the cut.)

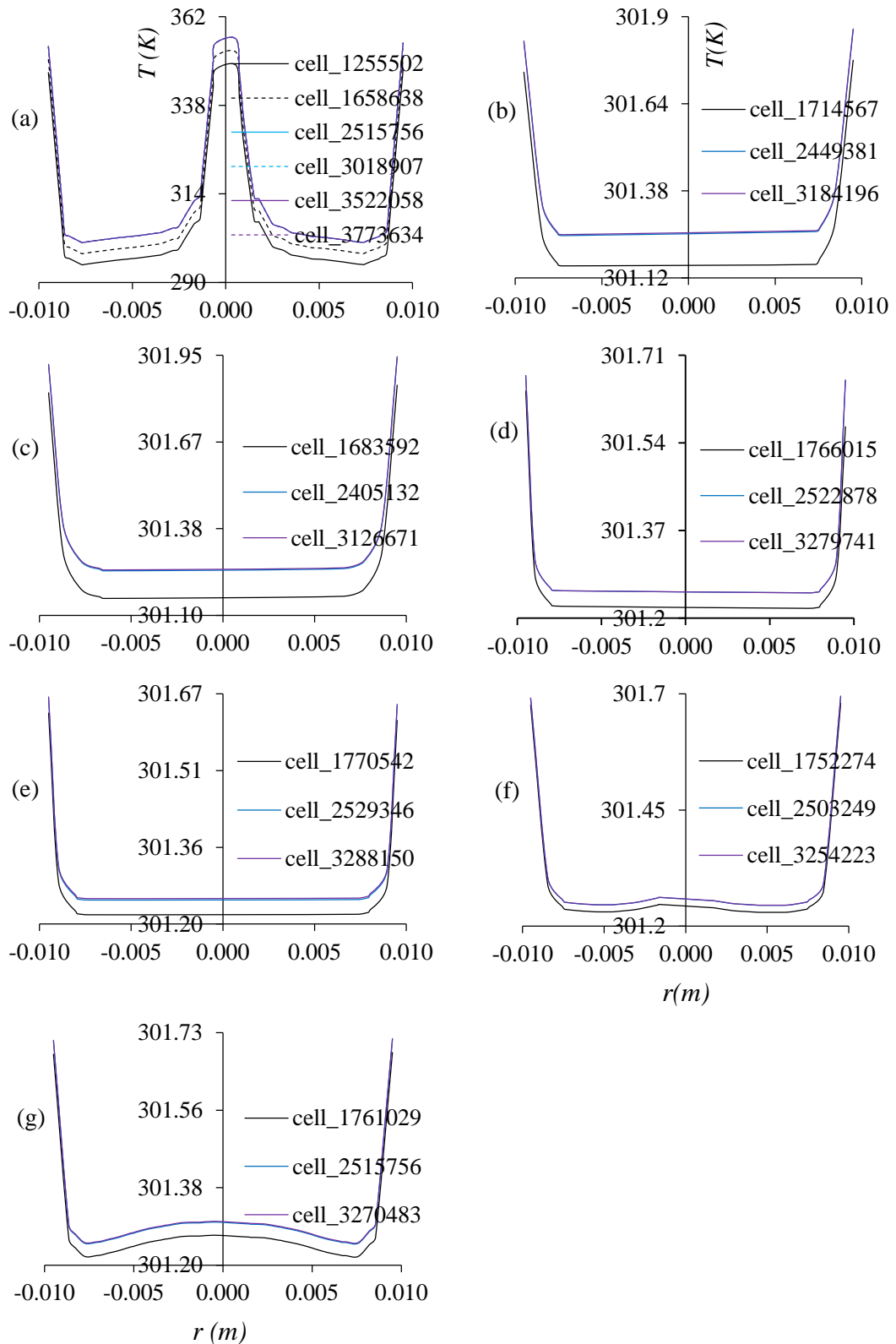


Figure 5.19: Temperature across the cross-section at the exit of (a) TATCT, (b) TATCT_{w1}, (c) TATCT_{w2}, (d) TATCT_{a1}, (e) TATCT_{a2}, (f) TATCT_{y1} and (g) TATCT_{y2} for $Re=20000$ for different grids.

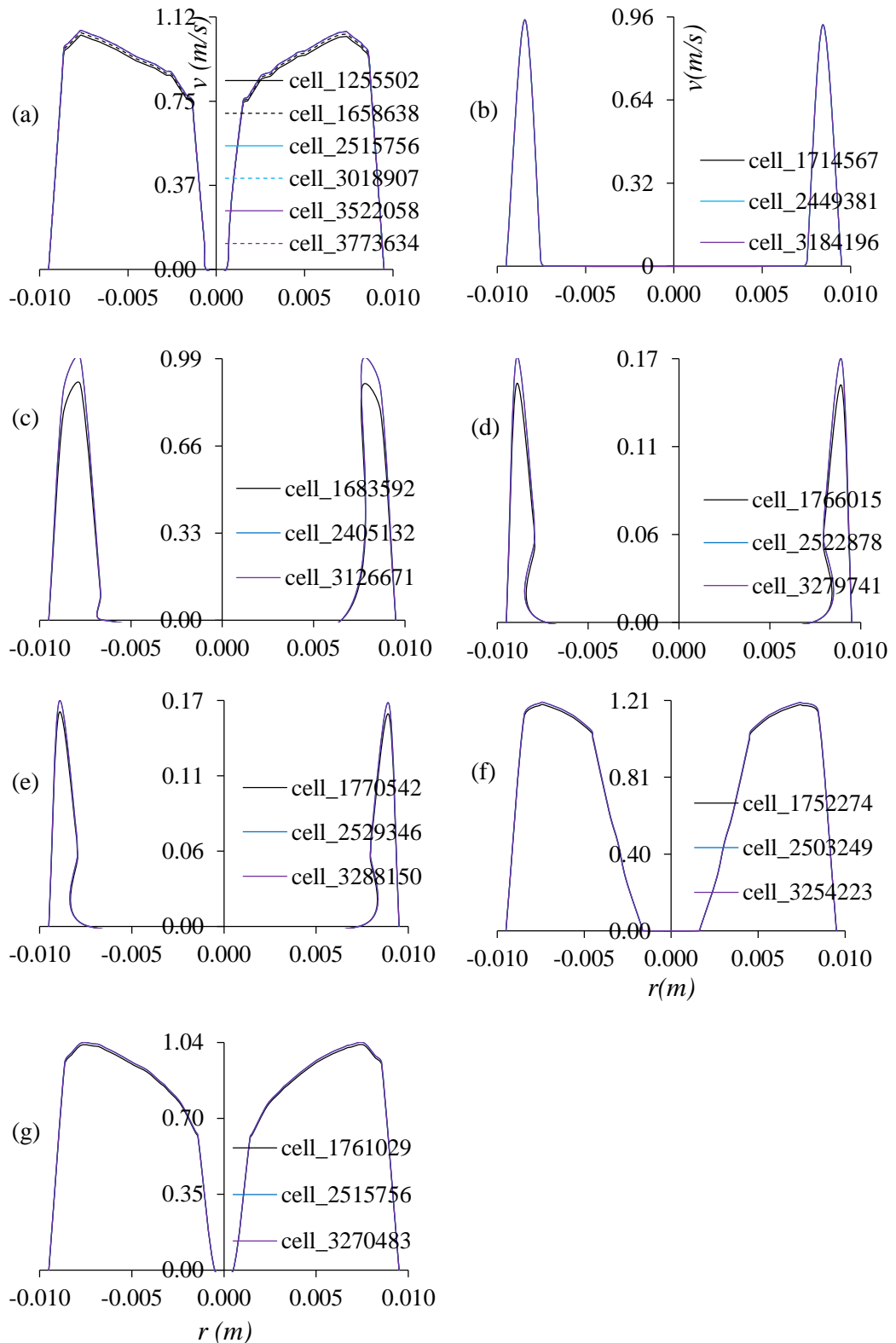


Figure 5.20: Velocity across the cross-section at the exit of (a) TATCT, (b) TATCT_{w1}, (c) TATCT_{w2}, (d) TATCT_{a1}, (e) TATCT_{a2}, (f) TATCT_{y1} and (g) TATCT_{y2} for $Re=20000$ for different grids

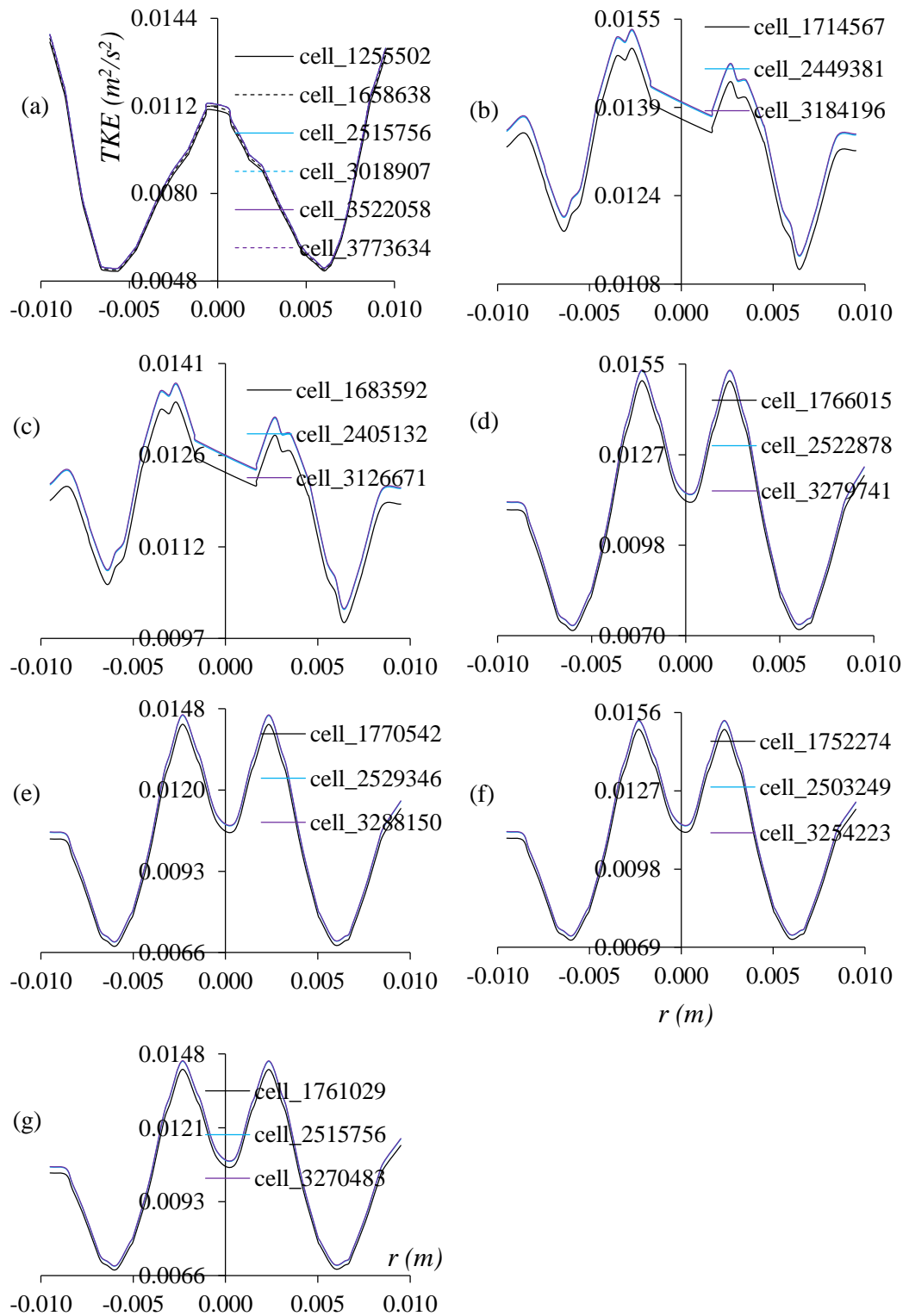


Figure 5.21: Turbulent kinetic energy (TKE) across the cross-section at the exit of (a) TATCT, (b) TATCT_{w1}, (c) TATCT_{w2}, (d) TATCT_{a1}, (e) TATCT_{a2}, (f) TATCT_{y1} and (g) TATCT_{y2} for $Re=20000$ for different grids.

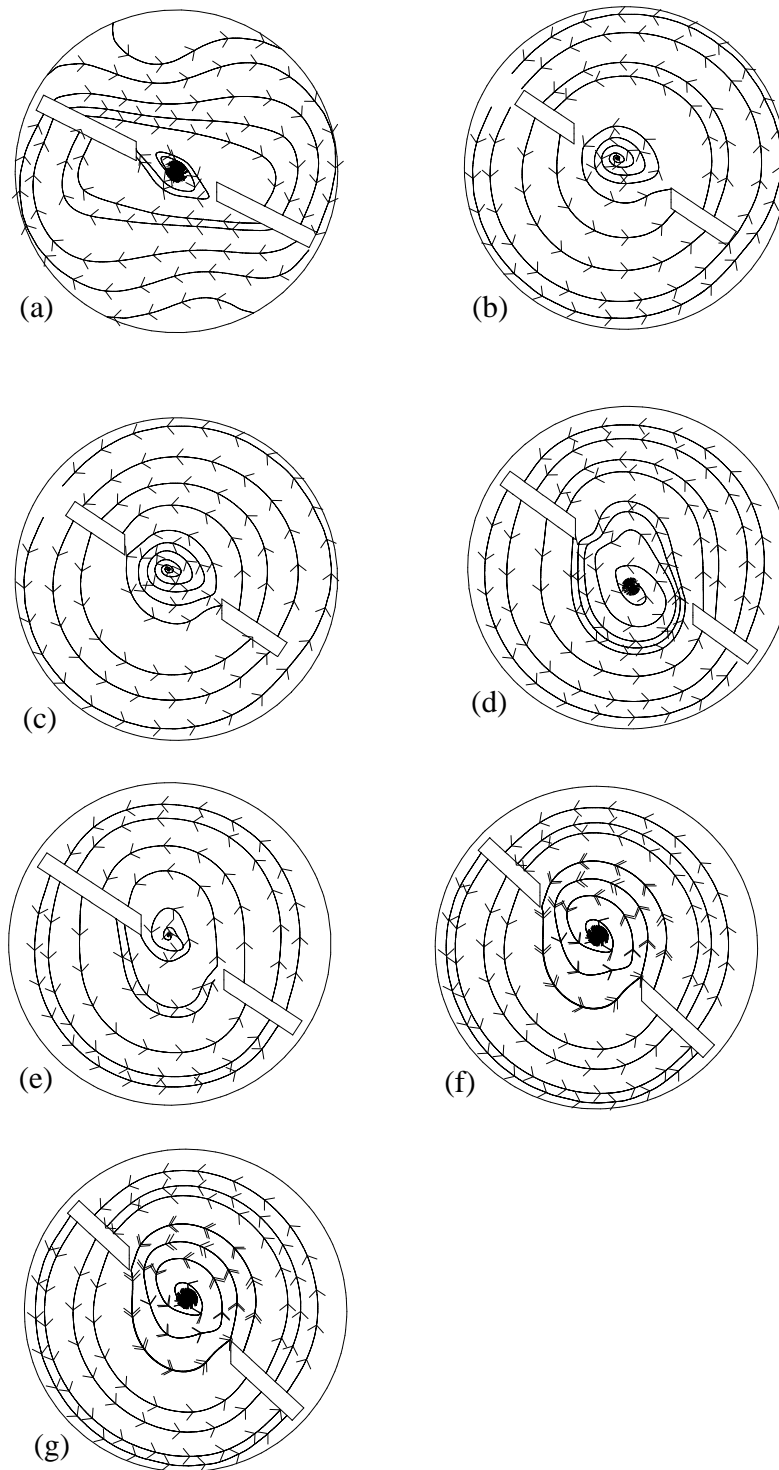


Figure 5.22: Streamlines across the cross-section at axial location $0.866m$ of (a) TATCT, (b) TATCT_{w1}, (c) TATCT_{w2}, (d) TATCT_{a1}, (e) TATCT_{a2}, (f) TATCT_{y1} and (g) TATCT_{y2} for $Re=20000$.

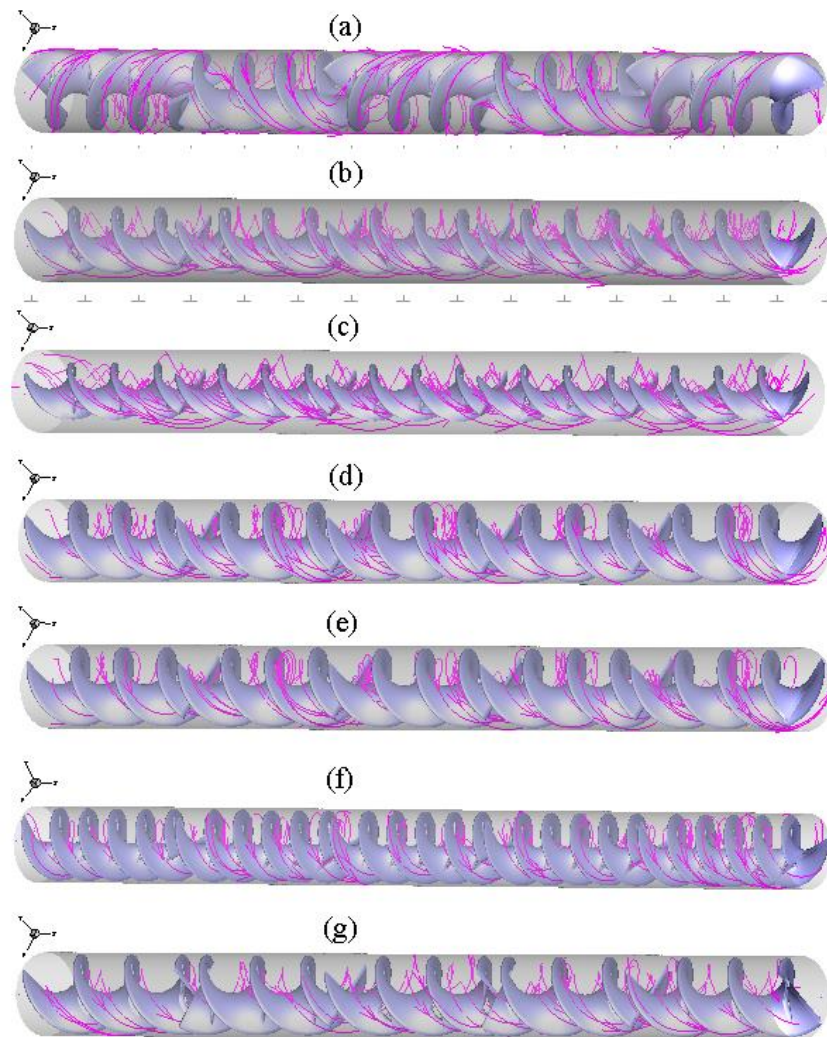


Figure 5.23: Streamlines for turbulent flow inside the domains of (a) TATCT, (b) TATCT_{w1}, (c) TATCT_{w2}, (d) TATCT_{a1}, (e) TATCT_{a2}, (f) TATCT_{y1} and (g) TATCT_{y2}.

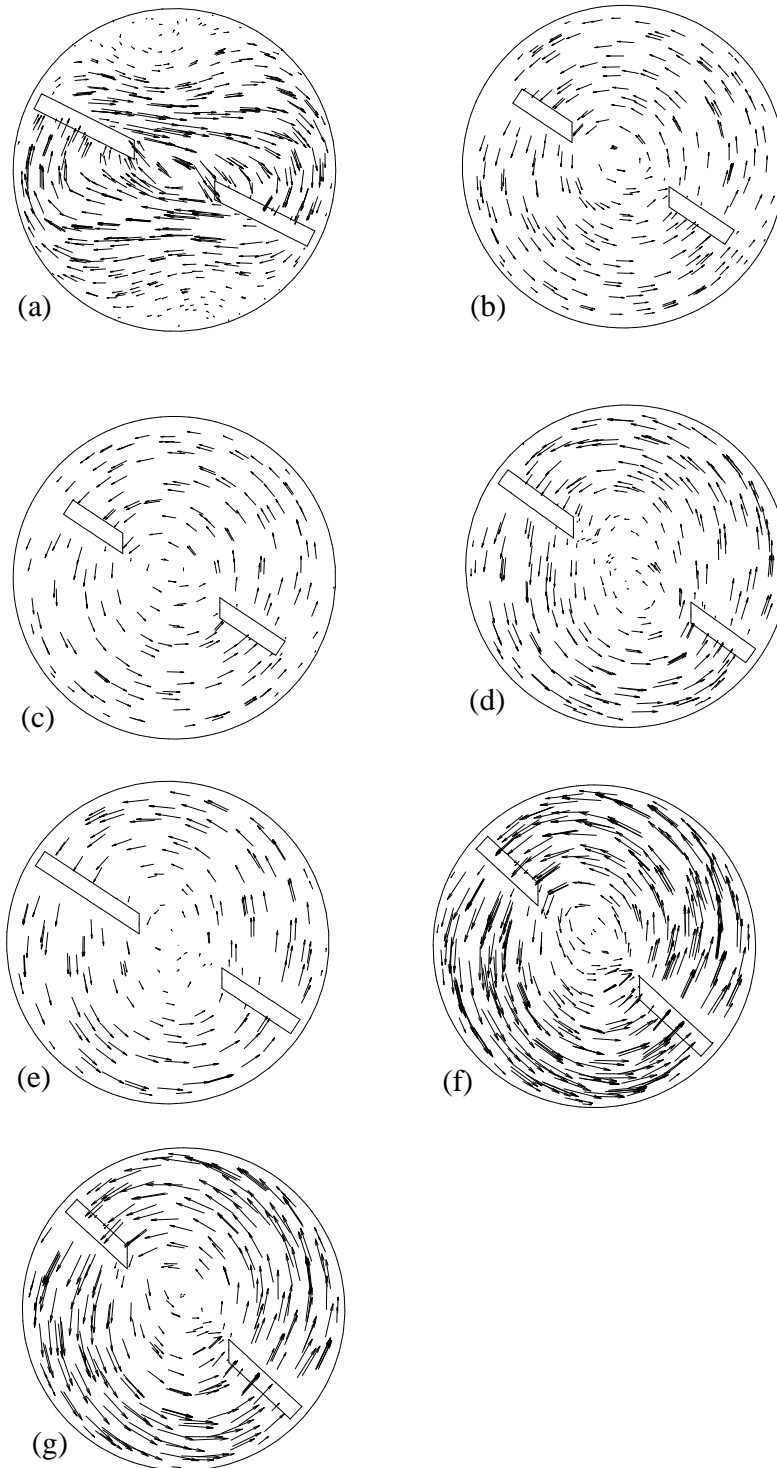


Figure 5.24: Velocity vector plots for turbulent flow inside the domains of (a) TATCT, (b) $TATCT_{w1}$, (c) $TATCT_{w2}$, (d) $TATCT_{a1}$, (e) $TATCT_{a2}$, (f) $TATCT_{y1}$ and (g) $TATCT_{y2}$.

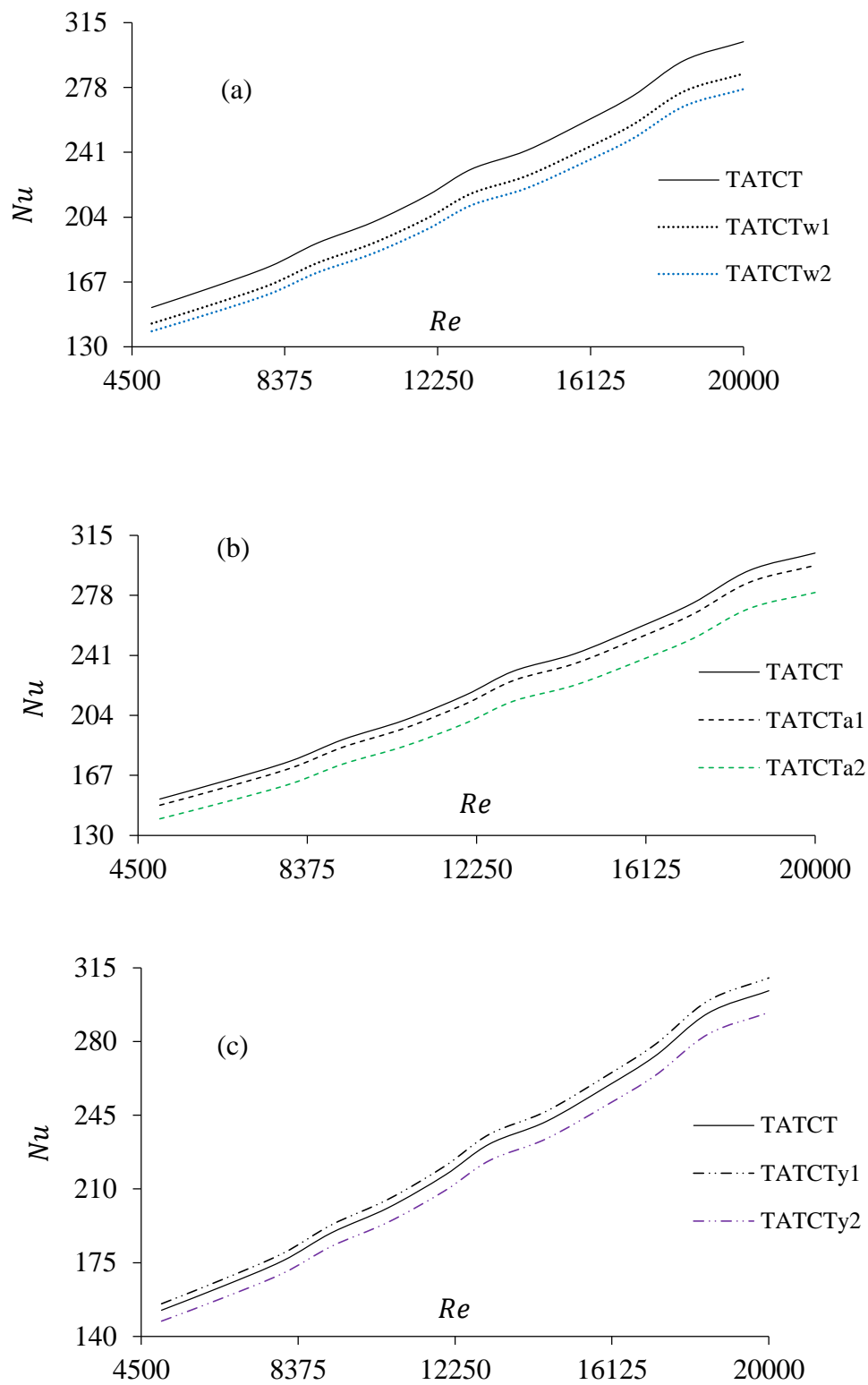


Figure 5.25: Effect of variations in (a) tape width, (b) area of cut on tape and (c) tape pitch of TATCT on Nusselt number vs. Reynolds number.

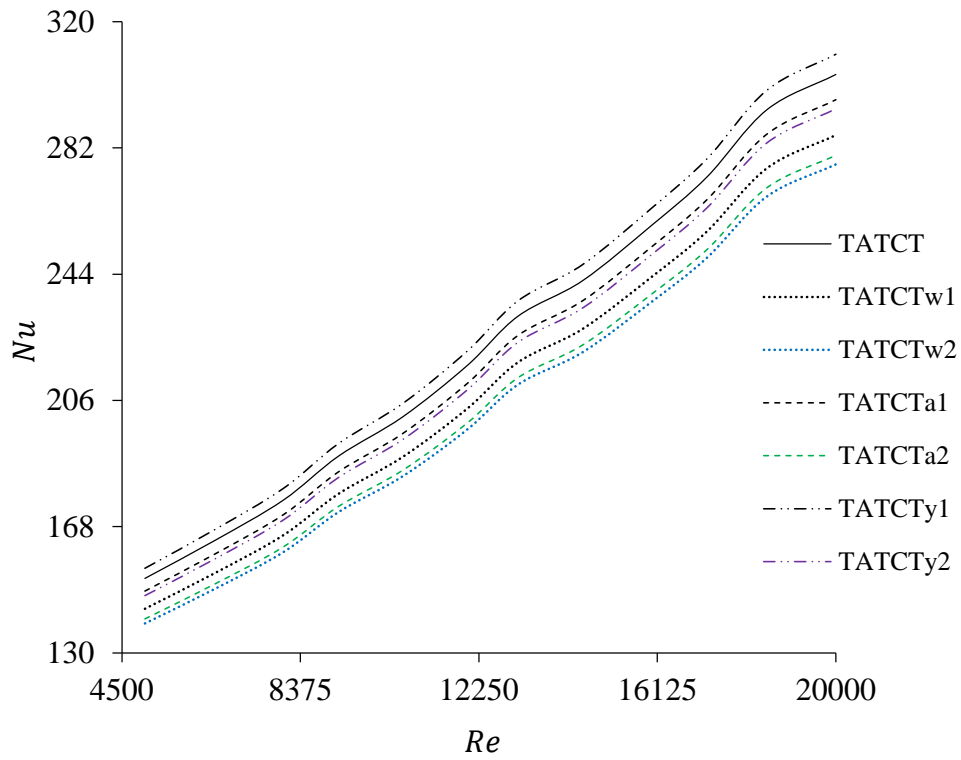


Figure 5.26: Effect of variations in tape geometries of TATCT on Nusselt number vs. Reynolds number.

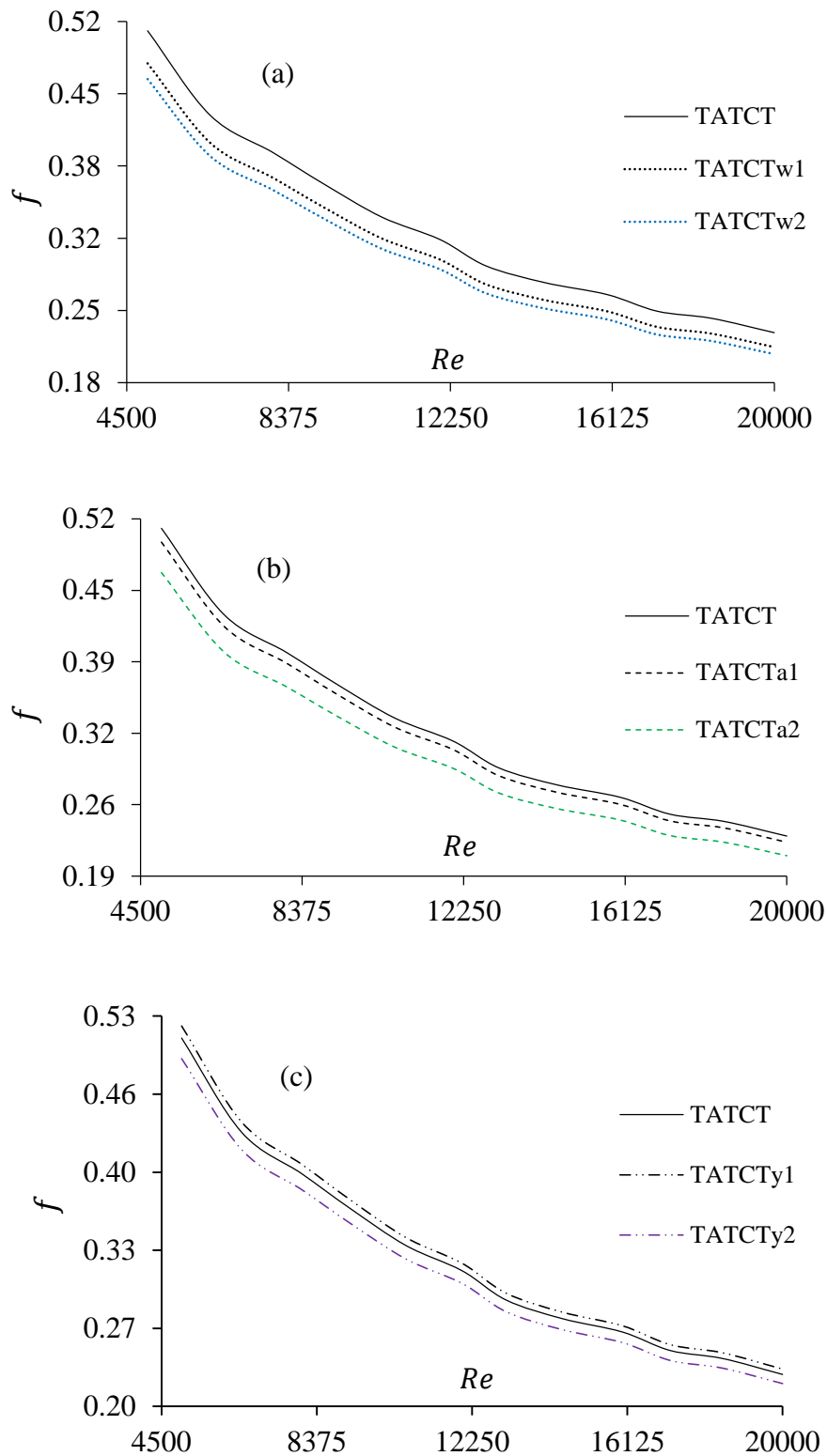


Figure 5.27: Effect of variations in (a) width of tape, (b) area of cut on tape and (c) pitch of tape of TATCT on friction factor vs. Reynolds number.

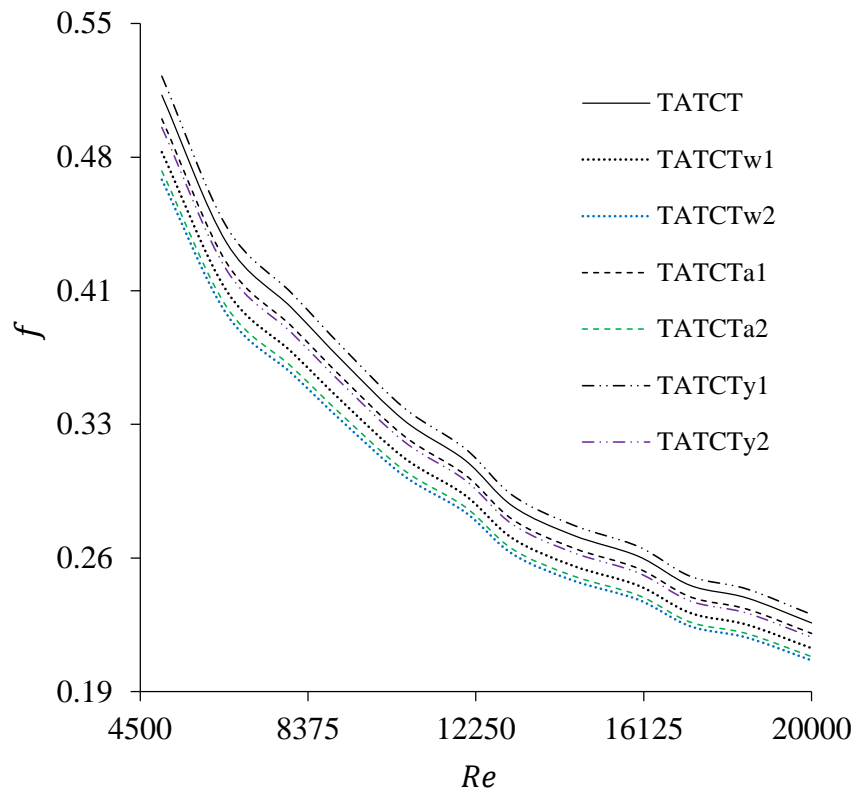


Figure 5.28: Effect of variations in tape geometries of TATCT on friction factor vs. Reynolds number.

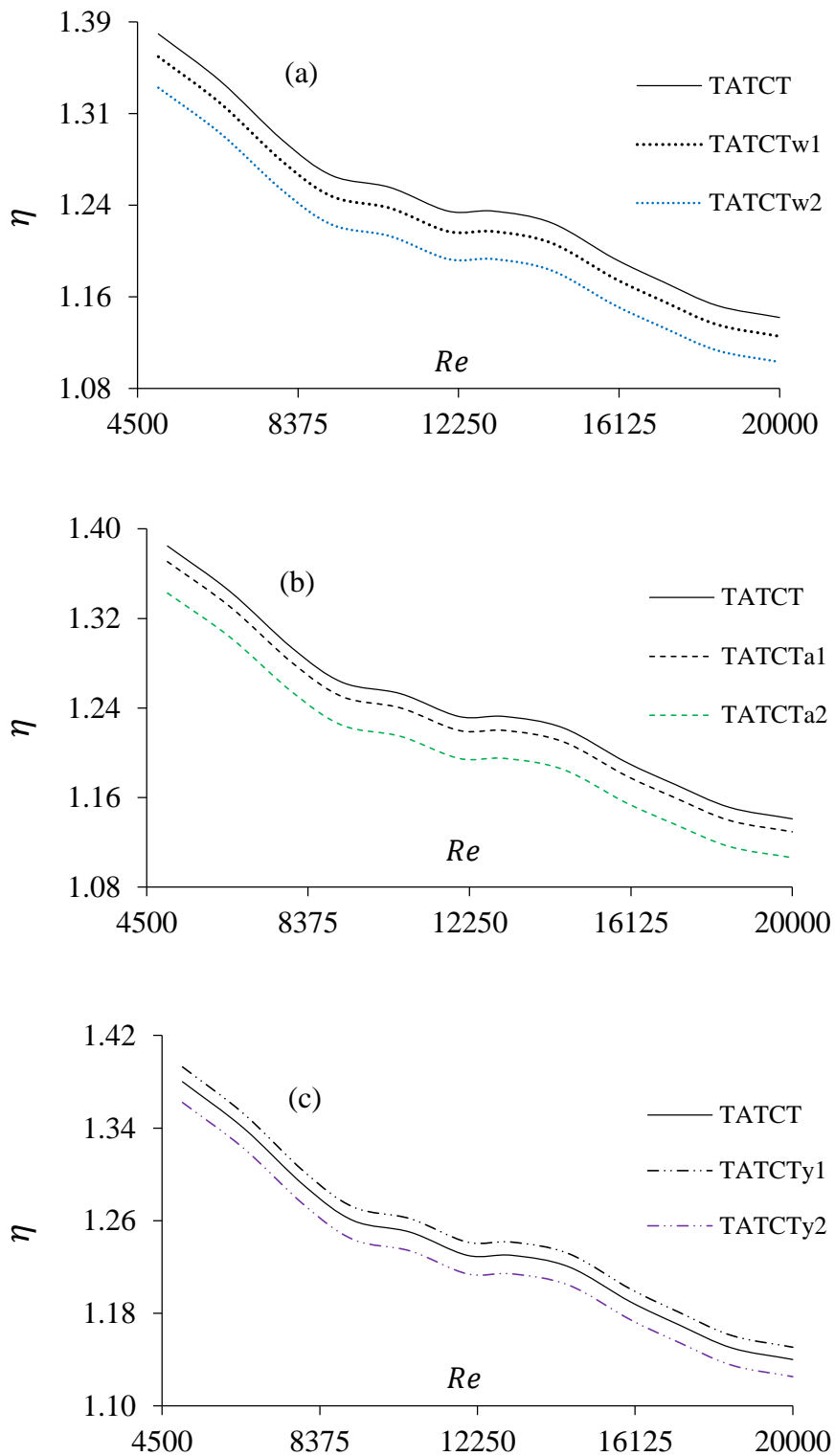


Figure 5.29: Effect of variations in (a) width of tape, (b) area of cut on tape and (c) pitch of tape of TATCT on thermal performance factor vs. Reynolds number.

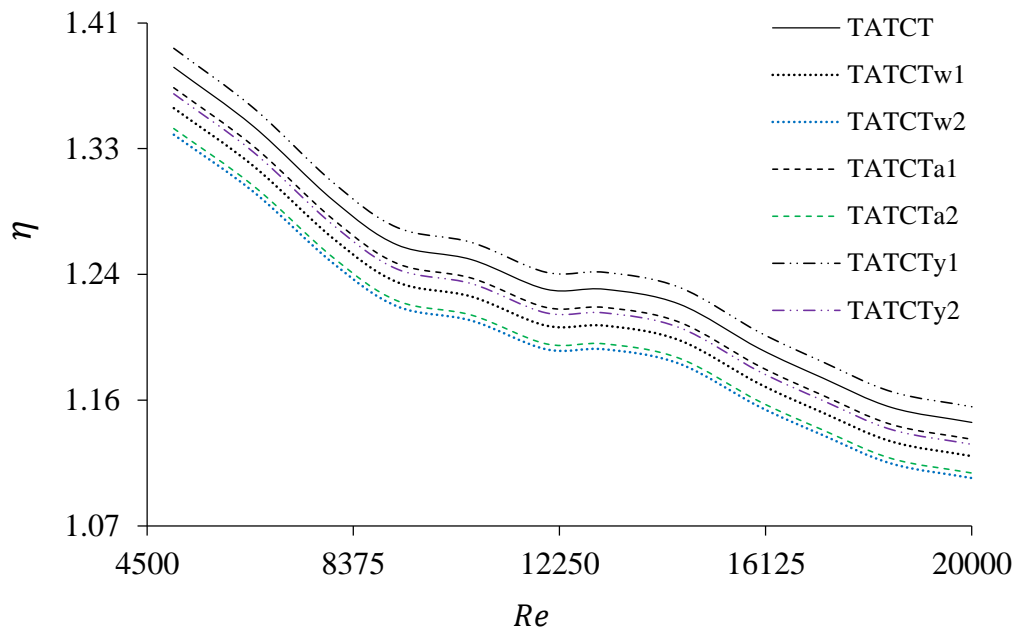


Figure 5.30: Effect of variations in tape geometries of TATCT on thermal performance factor vs. Reynolds number.

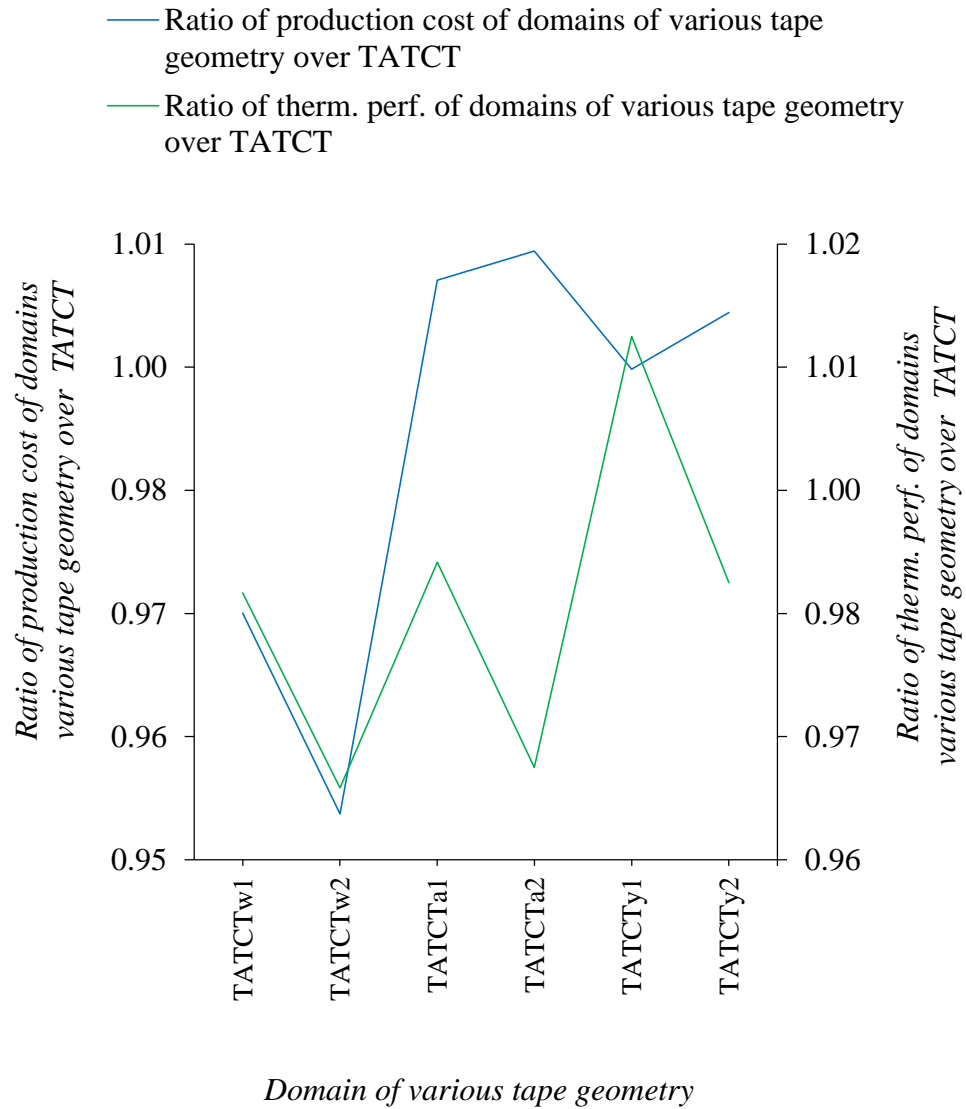


Figure 5.31: Implication of the various tape geometries on its production cost and the thermal performance.

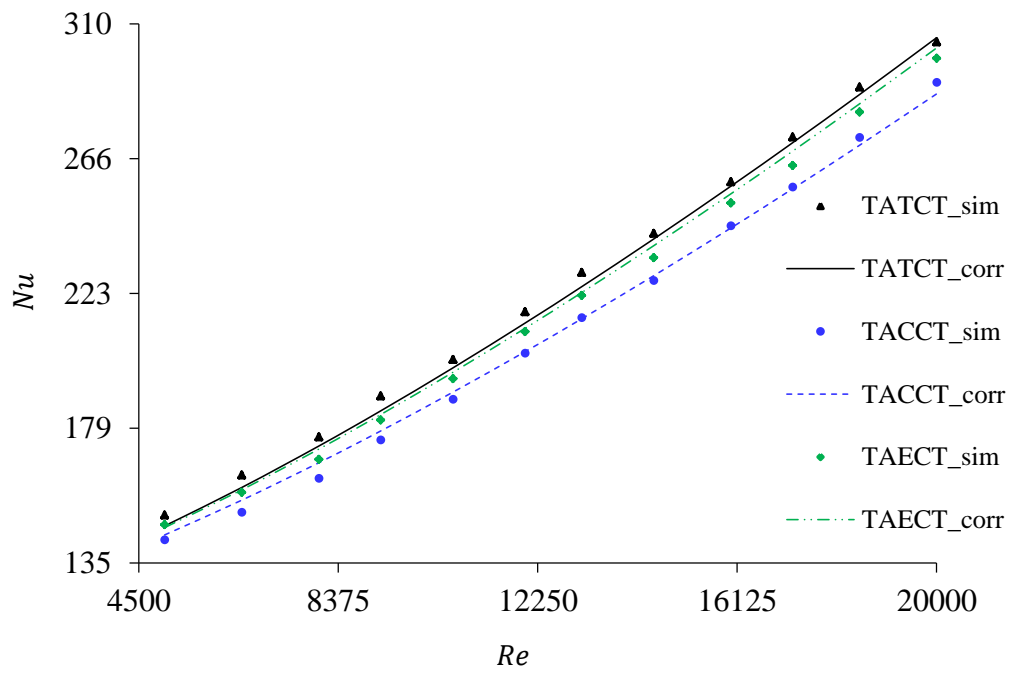


Figure 5.32: Comparison between numerical and predicted results for Nusselt number.

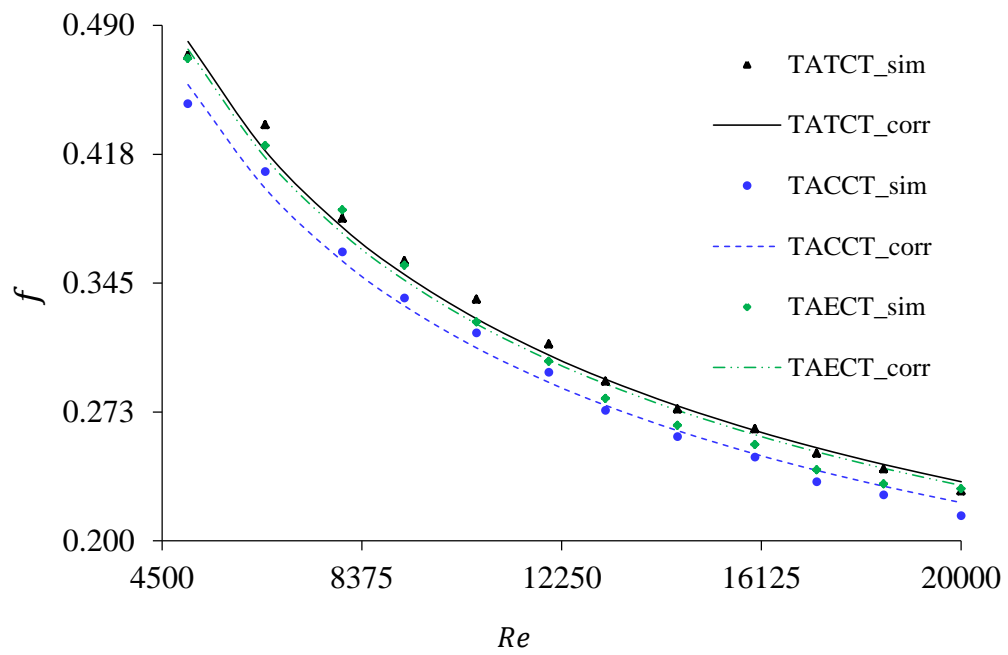


Figure 5.33: Comparison between numerical and predicted results for friction factor of turbulent flow.

Chapter 6

NUMERICAL STUDY OF THERMAL-HYDRAULIC CHARACTERISTICS IN THE TRANSITION REGIME IN AN INDUCED TUBE

6.1 Introduction

Reynolds identified a transitional flow, which is the motion of a fluid changing from laminar to turbulent flow [23]. It has been established that disturbances are responsible for initiation of transitional flow and that many researchers have reached the conclusion that the value of the flow rate at which laminar flow can no longer be maintained can vary significantly [24-26].

In practical applications, transitional flow plays important roles in hypersonic flows for applications encompassing reentry vehicles, scramjets, tactical and ballistic missiles, and interceptor missiles with divert jets [142]. In the design and application of engineering systems such as aerospace, heating and cooling, chemical processing, biomedical, automotive, power generation and others, it is important to predict fluid behaviour in the transition regime as many heat transfer equipment operates in transition regime. The transition regime, despite its importance, still remains a range in which the values available for heat transfer and friction factor in transition regime are considered as being unclearly expressed.

In this Chapter, numerical investigation on heat transfer and fluid flow in transition regime are carried out on the tube induced with an alternate-axis triangular cut twisted tape (TATCT). As it has been provided in the results of the investigation carried out on the laminar and turbulent flows (Chapter 4 and Chapter 5 respectively), TATCT (that is, the tube with alternate-axis triangular cut twisted tape) produced the best result out of all the seven different induced tubes considered. Therefore, TATCT is selected as a case study for the transitional flow in this Chapter. The Reynolds number considered for the transitional flow is between 2150 and 4650 and the transitional variant of the SST $\kappa - \omega$ model is employed. The details of transition model is presented in §3.4 of Chapter 3 where it has been mentioned that the transitional variant of the SST $\kappa - \omega$ model is appropriate for the simulation because transitional flow is not fully turbulent. Moreover, correlations were developed to predict the Nusselt number and friction factor of the transitional flow.

6.2 Flow Model

The model geometry used for the simulation of the transitional flow is shown Figure 4.4 (g) in §4.2 of Chapter 4; the tape in the domain is shown in Figure 4.3 (g). The detail of the cuts on the tape is described in Figure 4.5 (c) in §4.2 of Chapter 4. The tape pitch (y), the tape width (w), twist ratio (y/w) and clearance (c) in the domains as has been explained in Figure 4.6 of Chapter 4 are $54mm$, $18mm$, $3mm$ and $0.5mm$ respectively.

6.3 Grid independence Test

In order to confirm the accuracy of the numerical solutions grid independence tests were conducted. Four different Grids named as Grid 1,

Grid 2, Grid 3 and Grid 4 having cells 1255502, 1658638, 2515756 and 3018907 respectively are used. In carrying out the grid resolution study, data of temperature and velocity each for Reynolds numbers 2300 and 4650 at different axial locations ($x = 0.117m$, $0.866m$ and $1.0m$) using SST $\kappa - \omega$ were extracted.

The results, as shown in Figure 6.1 (a) - (c) and Figure 6.2 (a) - (c), indicate that at each of the axial locations for $Re = 2300$ and $Re = 4650$ respectively, Grid 1 (1255502) and Grid 2 (1658638) produce a less satisfactory result since the difference in the value of the temperature in each of them and that in Grid 3 (2515756) is noticeable, though small. It is evident that the difference in the value of the temperature between Grid 3 (2515756) and Grid 4 (3018907) is negligible and can therefore be concluded that they produce a more satisfactory result. The same trend is observed in values of the velocity in each of the four Grids as demonstrated in Figure 6.1 (d) - (f) and Figure 6.2 (d) - (f).

From the foregoing, it is clear that either of Grid 3 and Grid 4 can be used for the simulation. Considering convergence time as well as accuracy of solution, Grid 3 (cell 2515756) is selected.

6.4 Comparison of Different Models

Different RANS based turbulent models were used to run the simulations for $Re = 2300$ and 4650 and their results compared at different axial locations ($x = 0.117m$, $0.866m$ and $1.0m$). The aim of the comparison of the results is to select the best model from among them. The selected best model is then used to run the remaining simulations. The three models which were used are RNG $\kappa - \varepsilon$, Shear Stress Transport (SST) $\kappa - \omega$ and standard $\kappa - \omega$. These models have been explained in §3.3.2, §3.4.1 and §3.4.2 respectively

in Chapter 3. The equations associated with these models are given in Equations (3.22) to (3.23) of Chapter 3.

Data of temperature and velocity for different Reynolds number at the different axial locations ($x = 0.117m$, $0.866m$ and $1.0m$) were extracted for each of the three models and the results are presented for $Re = 2300$ and $Re = 4650$ in Figure 6.3 and Figure 6.4 respectively.

Figure 6.3(a) - (c) show the data of the temperature for $Re = 2300$. The difference between the value of the temperature in the standard $\kappa - \omega$ model and that in the SST $\kappa - \omega$ model is negligible. The difference between the values of the temperature in the RNG $\kappa - \varepsilon$ model and the standard $\kappa - \omega$ model and SST $\kappa - \omega$ model are 2.1% and 2.3% respectively. For the velocity shown in Figure 6.3(d) - (f), the difference between the value of the velocity in the standard $\kappa - \omega$ model and that in the SST $\kappa - \omega$ model is negligible but the difference between the values of the velocity in the RNG $\kappa - \varepsilon$ and either of the standard $\kappa - \omega$ or SST $\kappa - \omega$ are 4.7% and 2.3% respectively. The data of the temperature and velocity for $Re = 4650$, shown in Figure 6.4, have similar pattern to those of $Re = 4650$ discussed above. From this analysis it is seen that the SST $\kappa - \omega$ model produces a satisfactory result for both the temperature and velocity whereas the standard $\kappa - \omega$ produces a satisfactory result for only the temperature. Therefore, the SST $\kappa - \omega$ model is selected to run the simulations for the transitional flow. Since transitional flow is not fully turbulent, the transitional variant of the SST $\kappa - \omega$ is applied for the simulation.

6.5 Computational Results and Discussions

This section examines the contour plots and heat transfer characteristics in the domain. In situations where the results at axial location are considered,

an axial location of $0.866m$ is chosen. The reason for the choice of this location has been given in §4.4.

6.5.1 Temperature contours

The variation in the temperature in the TATCT under transitional flow is x-rayed in this section. This is done by illustrating the contours of temperature across a cross-section of the domain at axial location $x = 0.866m$ for various Reynolds numbers between 2150 and 4650.

As demonstrated in Figure 6.5, when $Re = 2150$ (frame a) the maximum temperature at the cross-section is $324.24K$, but at $Re = 2300$ (frame b), the maximum temperature at the cross-section increased to $326.26K$. An increase of the Reynolds number to $Re = 4400$ (frame c) yields a maximum temperature of $329.12K$ and at $Re = 4650$ (frame d) the maximum temperature at cross-section is $332.57K$. It is observed that the maximum temperature increases as the Reynolds number increases. The reason for this is that as the Reynolds number increases the momentum overcomes the viscous force of the fluid and leads to conversion of energy from the momentum to heat energy which is an offshoot of an increase in temperature of heat energy [2, 123]. Another important observation is that the maximum temperature occurs at the wall of the tube.

6.5.2 Velocity contour

In this section, the velocity of the flow at various Reynolds number is presented in form of contour. The contours of velocity across a cross-section of TATCT at axial location $x = 0.866m$ are shown in Figure 6.6. A maximum velocity of $0.141m/s$ is obtained at the cross-section when $Re = 2150$ (frame a) but this elevates to $0.148m/s$ when $Re = 2300$ (frame

b). At $Re = 4400$ (frame c) and $Re = 4650$ (frame d), the maximum velocity at the cross-section becomes 0.270m/s and 0.285m/s respectively. As the Reynolds number at the axial location increases, its velocity increases. This is due to the force of movement of the fluid which prevails over the viscous force of the fluid with the increase in Reynolds number. Furthermore, it is seen from Figure 6.6 that the maximum velocity occurs around the wall. This is due to the twisted tape insert which induces swirl around the wall and therefore increases the agitation of the fluid around the wall.

6.5.3 Turbulent kinetic energy

Figure 6.7 shows the contour plots of turbulent kinetic energy across the cross-section of the TATCT at an axial location of 0.866m for different Reynolds numbers. The value of the turbulent kinetic energy increases towards the wall of the domain and has its lowest value at around the core. The reason for this, according to Lang and Lombargo [138], is because of the velocity which is minimum at the wall. The turbulent kinetic energy for both $Re = 2150$ (frame a) and $Re = 2300$ (frame b) are approximately the same and the turbulent kinetic energy at both Reynolds number are the least. However, there is a significant increase in the turbulent kinetic energy when $Re = 4400$ (frame c) and $Re = 4650$ (frame d). The rise in the turbulent kinetic energy is due to higher velocity that accompanies higher Reynolds number.

The turbulent kinetic energy across the cross-section of the domain at axial locations 0.117m , 0.866m and 1.0m for different Reynolds numbers are plotted in Figure 6.8. It is confirmed in Figure 6.8 that the turbulent kinetic energy increases towards the wall of the domain and that at Reynolds number above 2300 there is a significant increase in the turbulent kinetic

energy. Also, it is seen in Figure 6.8 that there is a difference in the turbulent kinetic energy across the cross-section at axial locations of $0.117m$ and $0.866m$ but the turbulent kinetic energy at axial locations $0.866m$ and $1.0m$ are approximately the same.

6.5.4 Turbulent intensity

The turbulence intensity, also often referred to as turbulence level, is the ratio of the root-mean-square of the turbulent velocity fluctuations and the mean velocity [143]. The contour plots of turbulent intensity across the cross-section of the TATCT at an axial location $0.866m$ are illustrated in Figure 6.9. The value of the turbulent intensity increases towards the wall of the domain. The turbulent intensity for $Re = 2150$ (frame a) and $Re = 2300$ (frame b) are the least and they are approximately the same. There is a remarkable increase in the turbulent intensity as can be observed in both $Re = 4400$ (frame c) and $Re = 4650$ (frame d).

Figure 6.10 presents turbulent intensity for different Reynolds numbers at different axial locations. From Figure 6.10, it can be inferred that the turbulent intensity at axial location $0.866m$ differs from that at location $0.117m$ but the same as that at location $1.0m$. The turbulent intensity decreases from the wall of the domain where the velocity is maximum and then increased before decreasing towards the core of the domain. The factor that accounts for this is the presence of the cut in the domain which causes the velocity of the fluid around the cut to be higher than that in the core of the domain.

6.5.5 Heat transfer

Since predictions in the flow in transition regime is unreliable little design information is available on heat transfer in the regime. It is the objective of this section to make addition to the existing information on flow in the transition regime. In this section, a report is given on the role of different tape inserts in determining the Reynolds number at which transition begins and ends in the induced tubes. Apart from the tube with alternate-axis circular cut twisted tape (TACCT), the results of the tube with alternate-axis elliptical cut twisted tape (TAECT) and the tube with alternate-axis circular cut twisted tape (TACCT) for the laminar flow and turbulent flow discussed in Chapter 4 and Chapter 5 respectively are included so as to compare the the role of different tape inserts. The laminar flow is in the range $830 \leq Re \leq 2000$ while for the turbulent flow it is $5000 \leq Re \leq 20000$. A measure of the heat transfer for the flow in the domain is given by Nusselt numbers. The average Nusselt number (Nu) is expressed in Equation (4.5).

The Nusselt number for the laminar, transition and turbulent regimes for the three different tube designs at various Reynolds numbers is graphically represented in Figure 6.11. Within the transition region, there is an increase in Nusselt number as the Reynolds number increases. These are also the cases of the laminar flow and turbulent flow discussed in Chapter 4 and Chapter 5 respectively. This is due to increase in destruction of the boundary layer as the Reynolds number increases.

As illustrated in Figure 6.11, in all the tube designs transition from laminar to turbulent flow is smooth but not sudden. Garcia et al. [48] has explained that the smooth transition is as a result of the mechanism of swirl flow which occurs as a result of the tape inserts and consequently augment the

disturbance imparted on the fluid. The Reynolds numbers indicating the beginning and end of the transition are marked with vertical lines in Figure 6.11. For the TATCT, transition occurs at a Reynolds number of 2300 and ends at 4400. For the TACCT, transition occurs at Reynolds number of 2780 and ends at 4610 but for the TAECT, it occurs at Reynolds number of 2550 and ends at 4500. This means that transition occurs earlier in the TATCT than in the TAECT but it occurs earlier in the TAECT than in the TACCT. For the case under investigation, these observations indicate transition to turbulent flow occurs earliest and ends earliest in TATCT.

It is seen in Figure 6.11 that the values of the Nusselt number in the transition regime in the tube designs are in descending order of TATCT, TAECT and TACCT. The Nusselt number in the TATCT is 19.29% to 45.58% higher than that in the TACCT and the Nusselt number in the TATCT is 3.59% to 28.34% higher than that in the TAECT. The enhancement in heat transfer produced in the tubes in the transition regime is directly proportional to the Nusselt number [2, 25], meaning that the heat transfer enhancement in the TATCT is higher than that in the TAECT and the heat transfer enhancement in the TAECT is higher than that in the TACCT. Since the transition occurs first in the TATCT, then in the TAECT and finally in TACCT, it can be inferred that the higher the Nusselt number, the higher the heat transfer enhancement and the earlier the transition to turbulent flow will occur.

6.5.6 Friction factor

Since flows in transition regime are uncertain, it is important to investigate the friction factor characteristics in the regime. As with the Nusselt number discussed above, the Reynolds number at which transition occurs and ends with respect to the friction factor are also considered for the

TATCT, TAECT and TACCT. The friction factor is expressed mathematically in Equation (4.5).

Figure 6.12 shows the variation of friction factor with Reynolds number for laminar ($830 \leq Re \leq 2000$), transition ($2150 \leq Re \leq 4650$) and turbulent flow ($5000 \leq Re \leq 20000$). It should be noted that the results for the friction factor for the laminar flow and turbulent flow have been discussed in Chapter 4 and Chapter 5 respectively. The friction factor for the TATCT reduces from when $Re = 2150$ up to $Re = 2300$ from where the friction factor starts to increase up to when $Re = 4400$ and then begins to decrease up to when $Re = 20000$. For the TACCT, the friction factor reduces from when $Re = 2150$ up to $Re = 2780$ from where the friction factor starts to increase up to when $Re = 4650$ and then decrease up to when $Re = 20000$. The friction factor for the TAECT reduces from when $Re = 2150$ up to $Re = 2550$ from where the friction factor starts to increase up to when $Re = 4500$ and then begins to decrease up to when $Re = 20000$.

It is demonstrated in Figure 6.12 that there is a vertical line (representing Reynolds number) drawn through each of the two kinks in each of the TATCT, TAECT and TACCT. The values of the Reynolds numbers at the intersection of the vertical line and the kink represent the start or end of the transition. Going by this, in Figure 6.12, the transition occurs first in the TATCT at $Re = 2300$ followed by TAECT at $Re = 2550$ and then in TACCT at $Re = 2780$. The end of the transition also follows the same order of occurrence as the transition ends first in the TATCT at $Re = 4400$ followed by TAECT at $Re = 4550$ and then in TACCT at $Re = 4610$.

In addition, as it is indicated by the kinks in Figure 6.12, the commencement and end of the transition in the induced tubes do not occur in a gradual way. Garcia et al. [144] found that the start and end of the transition in

induced tubes do not occur in a gradual way. Mayer and Oliver [23] disagreed with this and concluded that the commencement and end of the transition in the induced tubes occur in a gradual way. Although these sets of authors worked on different induced tubes, the difference in the outcomes of their research corroborate the observation of other authors that flow in transition regime is uncertain.

As shown in Figure 6.12, within the transition region the friction factor increases as the Reynolds number increases but in the laminar and turbulent regimes the friction factor decreases as the Reynolds number increases. In the work of Tam and Ghajar [145], the reason adduced in support of the friction factor increase in the transition regime as the Reynolds number increases is that a large amount of pressure is expended in carrying fluid in transition regime. Garcia et al. [49] in their research stated this as a reason why fluid flow in transition regime is unstable and uncertain.

It is also evident in Figure 6.12 that in all the regimes the values of the friction factor in the TATCT is higher than that those in the TAECT and TACCT. The friction factor in the TATCT is 0.84% to 3.32% higher than that in the TAECT and the Nusselt number in the TATCT is 2.16% to 4.55% higher than that in the TACCT.

From the foregoing paragraphs, it is observed that TATCT has the highest friction factor and transition occurs in it before it occurs in the TAECT and TACCT. It also informs that TACCT has the least friction factor and that transition occurs in it after it has occurred in the TATCT and TAECT. Therefore, it can be inferred that the higher the friction factor the earlier the transition to turbulent flow will occur.

6.5.7 Correlation for the transitional flow

For the purpose of knowing how closely the simulated results and predicted results are, correlations were developed for the heat transfer and friction factor of the transitional flow in the TAECT, TACCT and TATCT. The correlations, developed by non-linear regression analysis, are functions of Reynolds number (Re), Prandtl number (Pr), twist ratio of twisted tape (y), perimeter of cut on twisted tape (p), and width of twisted tape (w). The correlation for the Nusselt number and the friction factor are given in Equations (6.1) and

(6.2) respectively.

$$Nu = 0.254 Re^{1.074} Pr^{0.619} \left(\frac{0.052}{y^{0.957}} \right) \left(\frac{p}{w} \right)^{0.294} \quad (6.1)$$

$$f = 2.854 Re^{0.0019} \left(\frac{w}{p-w} \right)^{-0.037} (y-1)^{-2.619} \quad (6.2)$$

In addition to the development of the predicted equation, comparison is made between the simulated and the predicted results of the Nusselt number and demonstrated in Figure 6.13. The predicted results agree with the simulated results with a deviation of 4.43%. The simulated and the predicted friction factor are also compared and the result of the validity of the correlation in predicting the simulated results is portrayed in Figure 6.14. The correlations for the friction factors are valid for the regions where transition begin and end. That is,

TATCT: $2300 \leq Re \leq 4400$

TAECT: $2550 \leq Re \leq 4500$

TACCT: $2780 \leq Re \leq 4610$

There is a discrepancy of 1.97% between the predicted and the simulated results of the friction factor.

6.6 Conclusion

By employing finite volume approach to solve the governing partial differential equation, heat transfer and fluid flow in transition regime were numerically carried out on induced tubes. Reynolds number between 2150 and 4650 were considered and the tubes were under uniform wall heat flux condition. The transitional variant of the Shear-Stress Transport (SST) $\kappa - \omega$ model was selected to run the simulations.

The Nusselt number and friction factor for laminar, transition and turbulent regimes for different tube designs (TAECT, TACCT and TATCT) were obtained. It is revealed that within the transition region, as the Reynolds number increases both the Nusselt number and the friction factor increase. It was observed in all the tube designs that transition from laminar to turbulent flow is smooth for the Nusselt number but this is not the case for the friction factor. Also, it was deduced the higher the Nusselt number and the friction factor, the earlier the transition to turbulent flow will occur and the earlier the transition will end. Transition occurs earlier in TATCT than in TAECT but it occurs earlier in TAECT than in TACCT. For TATCT, transition occurs at a Reynolds number of 2300 and ends at 4400; for TACCT, transition occurs at Reynolds number of 2780 and ends at 4610 but for TAECT, it occurs at Reynolds number of 2550 and ends at 4500.

Correlations were developed for the Nusselt number and friction factor of the transitional flow and comparison was made between the simulated and

the results predicted by the correlations. The predicted and simulated results agree within a deviation of 4.43%. For the friction factor, the predicted and the simulated results are in agreement within 1.97%. These indicate that the predicted and the simulated results for both the Nusselt number and friction factor are in good agreement.

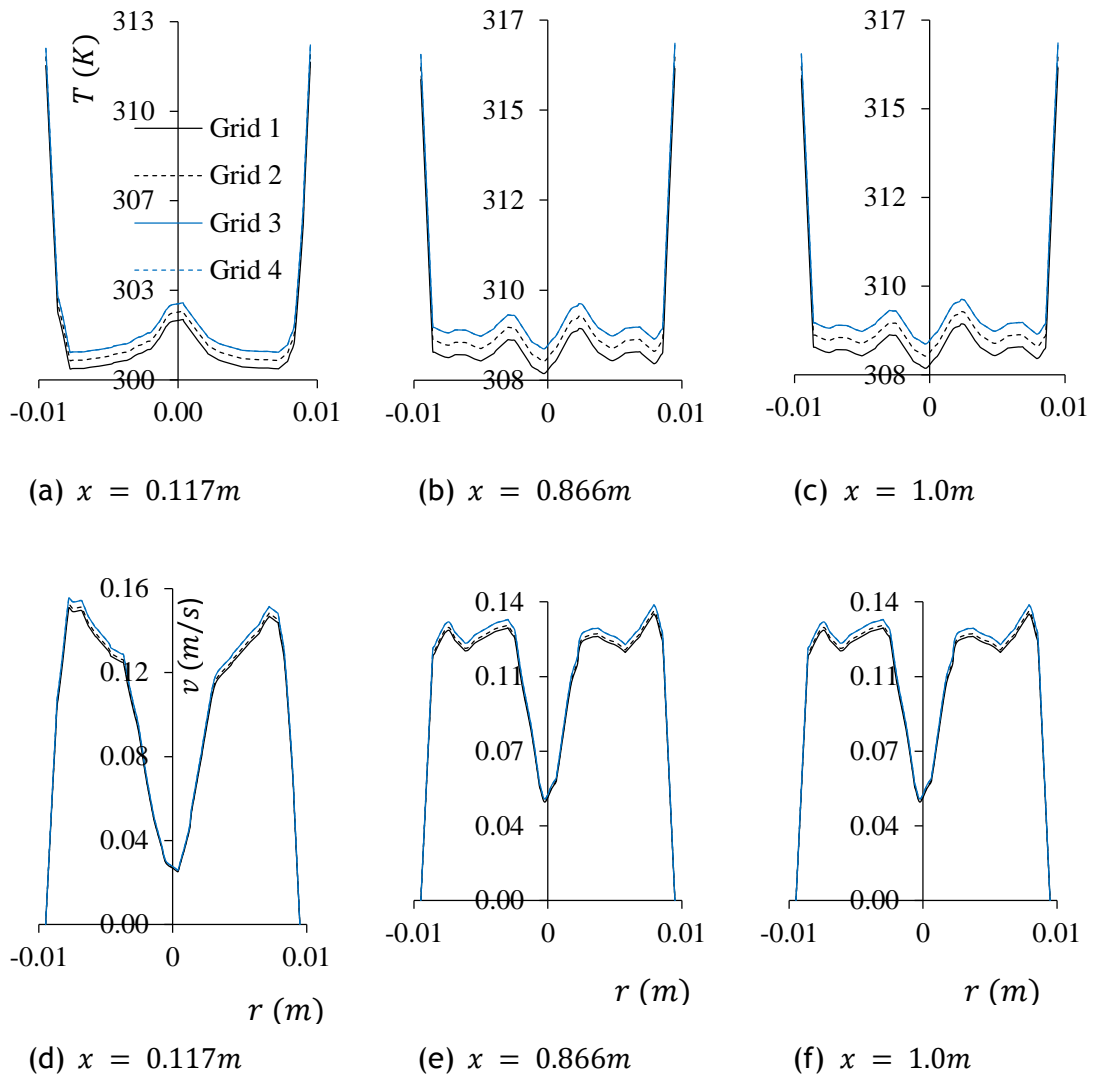


Figure 6.1: Grid resolution study for the SST $\kappa - \omega$ of TATCT showing the results of temperature and velocity at different locations for $Re = 2300$.

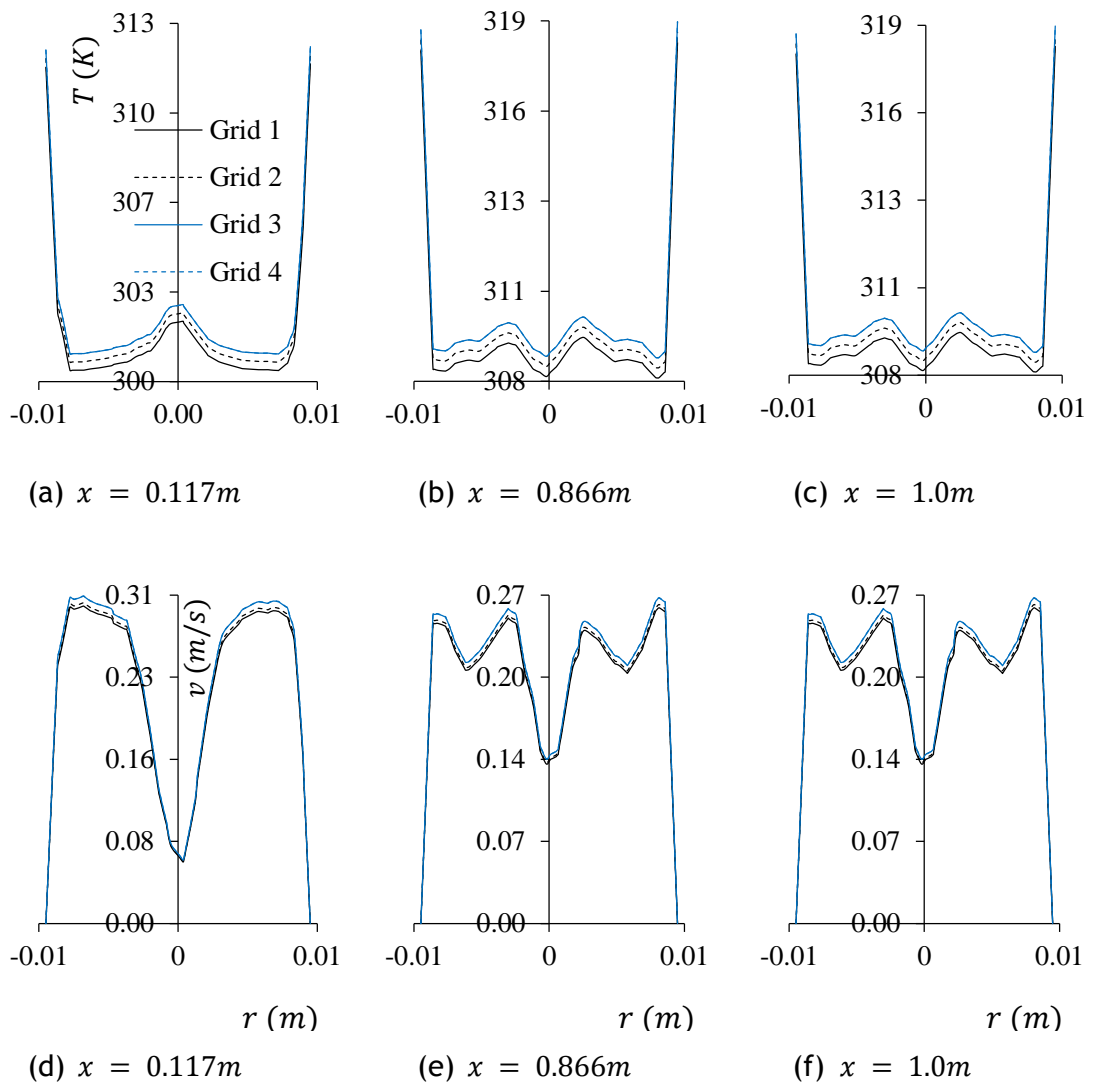


Figure 6.2: Grid resolution study for the SST $\kappa - \omega$ of TATCT showing the results of temperature and velocity at different locations for $Re = 4650$.

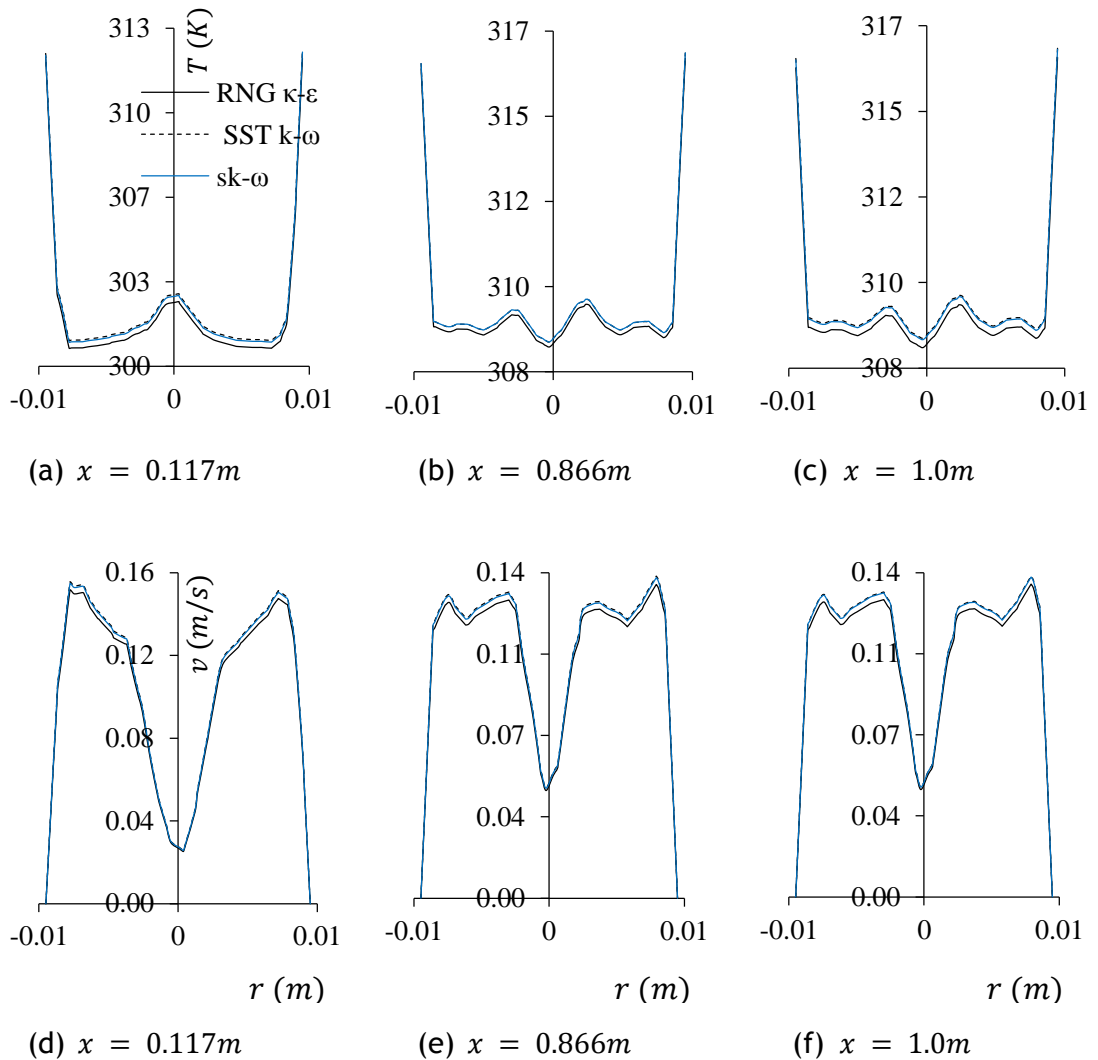


Figure 6.3: Comparison of various models with Grid 3 of TATCT showing the results of temperature and velocity at different locations for $Re = 2300$.

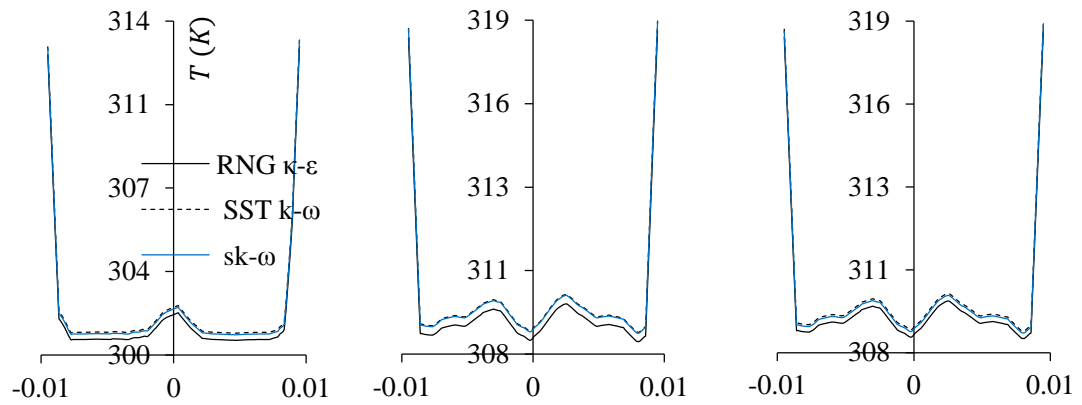
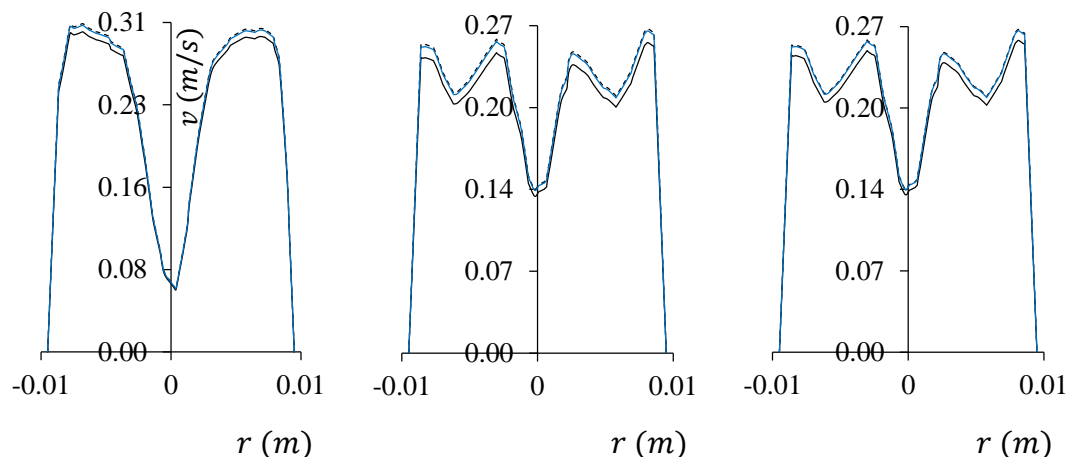
(a) $x = 0.117m$ (b) $x = 0.866m$ (c) $x = 1.0m$ (d) $x = 0.117m$ (e) $x = 0.866m$ (f) $x = 1.0m$

Figure 6.4: Comparison of various models with Grid 3 of TATCT showing the results of temperature and velocity at different locations for $Re = 4650$.

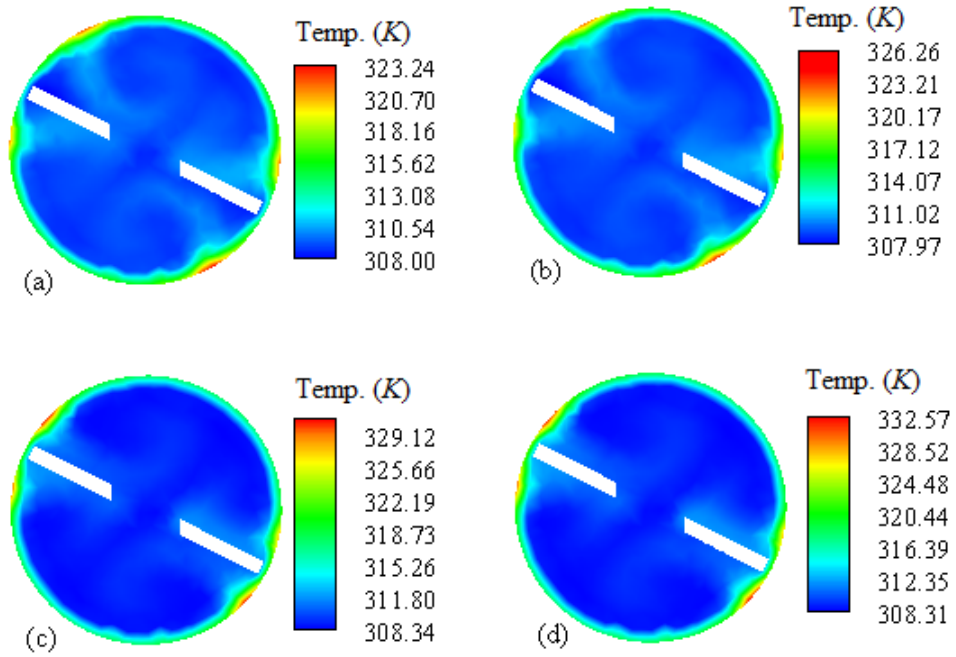


Figure 6.5: Contour plots of temperature across the TATCT cross-section at axial location $0.866m$ for (a) $Re=2150$, (b) $Re=2300$, (c) $Re=4400$ and (d) $Re=4650$.

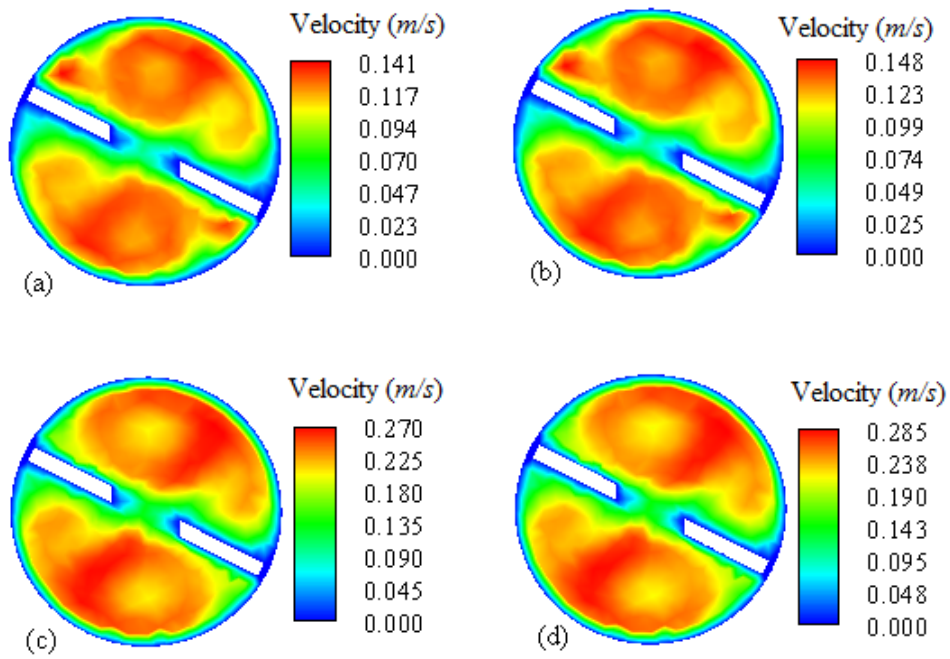


Figure 6.6: Contour plots of velocity across the TATCT cross-section at axial location $0.866m$ for (a) $Re=2150$, (b) $Re=2300$, (c) $Re=4400$ and (d) $Re=4650$.

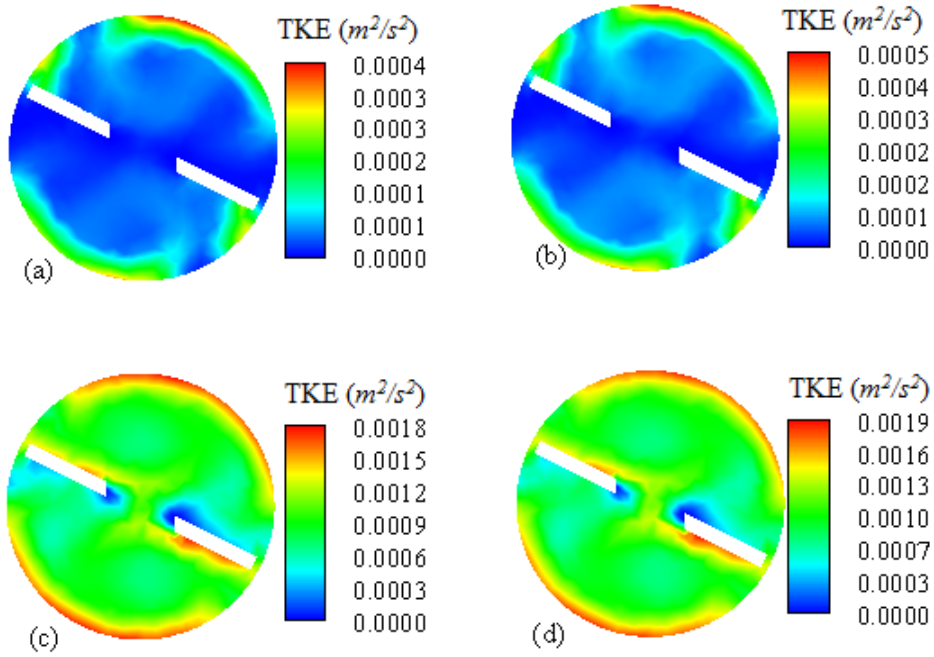


Figure 6.7: Contour plots of the turbulent kinetic energy (TKE) across the TATCT cross-section at axial location $0.866m$ for (a) $Re=2150$, (b) $Re=2300$, (c) $Re=4400$ and (d) $Re=4650$.

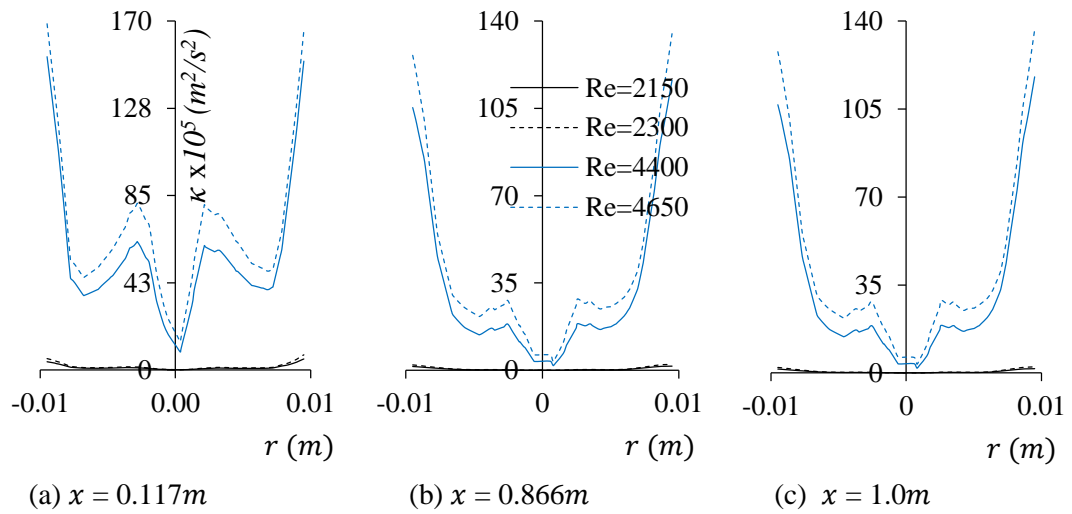


Figure 6.8: Turbulent kinetic energy across the TATCT cross-section for different Reynolds number at different axial locations.

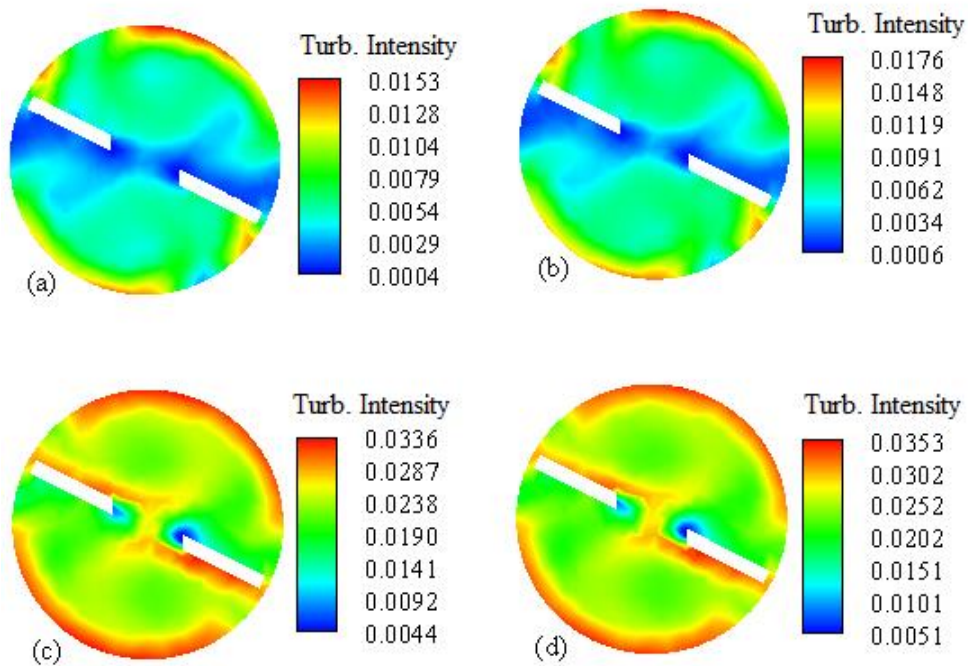


Figure 6.9: Contour plots of turbulent intensity across the TATCT cross-section at axial location $0.866m$ for (a) $Re=2150$, (b) $Re=2300$, (c) $Re=4400$ and (d) $Re=4650$.

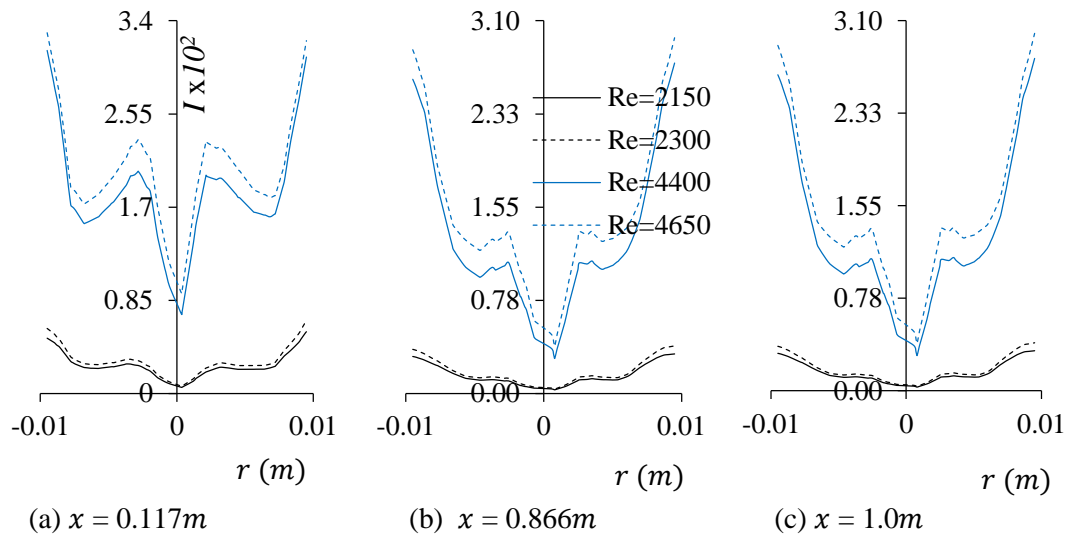


Figure 6.10: Turbulent intensity across the TATCT cross-section for different Reynolds number at different axial locations.

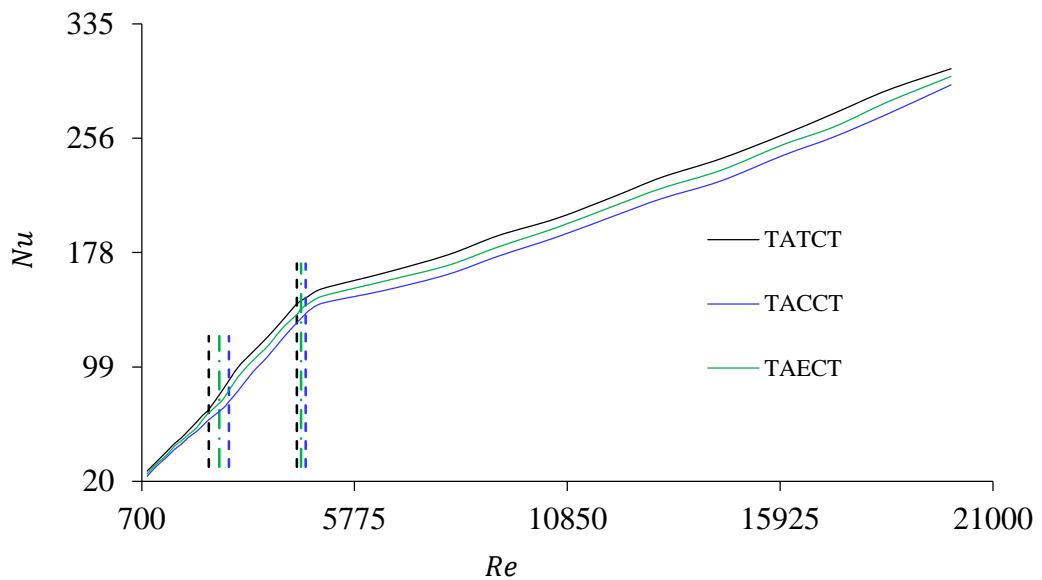


Figure 6.11: Nusselt number vs Reynolds number for TATCT, TACCT and TAECT showing laminar, transition and turbulent regimes.

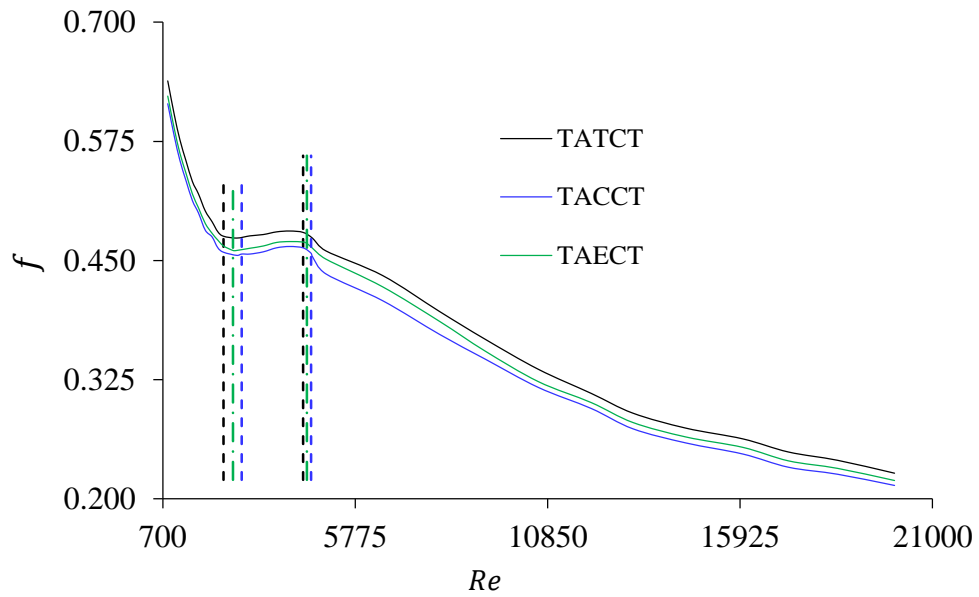


Figure 6.12: Friction factor vs Reynolds number for TATCT, TACCT and TAECT showing laminar, transition and turbulent regimes.

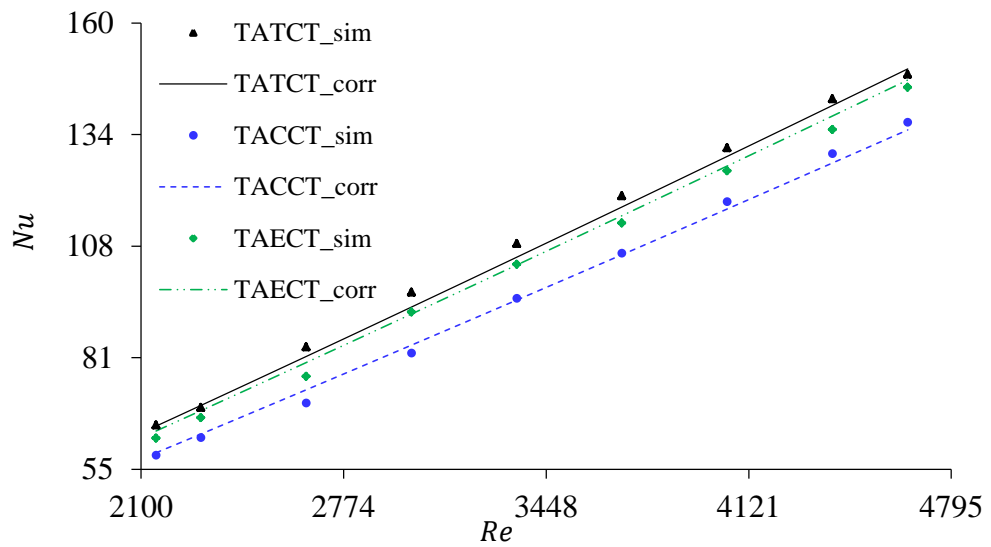


Figure 6.13: Comparison between simulated and predicted results for Nusselt number of transitional flow.

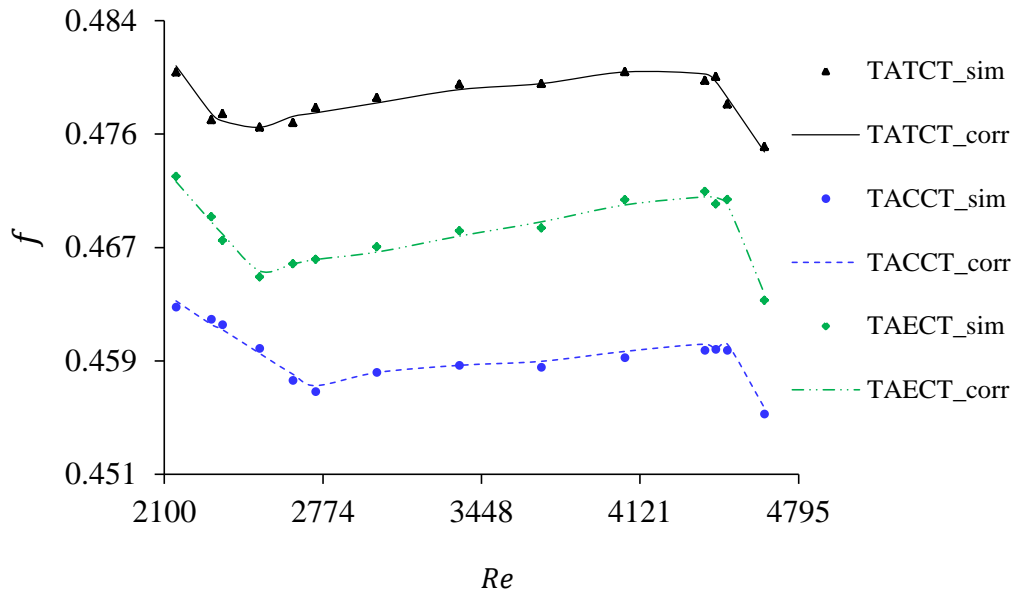


Figure 6.14: Comparison between simulated and predicted results for friction factor of transitional flow.

Chapter 7

INVESTIGATION OF MIXED CONVECTION HEAT TRANSFER IN A FLOW THROUGH AN INDUCED TUBE

7.1 Introduction

A numerical study of heat transfer in a combined forced and free convection for laminar, transitional and turbulent flows of water through an induced tube is reported in this Chapter. The transitional variant of the SST $\kappa - \omega$ model is employed for the transitional flow while the RNG $\kappa - \varepsilon$ model is employed for the turbulent flow. The induced tube is subjected to uniform heat flux at its wall and its inclination angle is varied from 15° to 90° with respect to the horizontal position. The Grashof number (Gr) is 3.37×10^5 .

In practical applications, mixed convection is seen as very-high-power-output devices where the forced convection is not enough to dissipate all of the heat necessary and these have been applied in nuclear reactor technology and cooling of computer systems and other electronic equipment [146, 147]. The practical application of mixed convection has also played a significant role in meeting the demand of industries for faster and denser circuit technologies and packages [148].

It has been stated in the results of the investigation carried out in the previous Chapters that of all the domains considered for the investigation,

the tube with alternate-axis triangular cut twisted tape (TATCT) produced the best thermal performance in terms of heat transfer enhancement. Also, the survey of literature has revealed that the aspect of mixed convection on induced tube for laminar, transition and turbulent flows has virtually been neglected in spite of its importance in practical applications. Hence, the present Chapter examines the effects of buoyancy on the thermo-hydraulic characteristics of water flow through a tube induced with an alternate-axis triangular cut twisted tape (TATCT). In addition, the distribution of velocity and temperature in the domain are taken into consideration.

7.2 Model Geometry

The geometry which was described by Figure 4.4 (g) in §4.2 of Chapter 4 is used for the simulation of the mixed convection in this Chapter. However, for the mixed convection, the model is inclined at an angle (θ) to the horizontal to initiate buoyancy to the flow. The model, shown in Figure 7.1, is sliced so that the tape inside the tube can be seen.

7.3 Grid Sensitivity Analysis

Analyses on the grid independence were carried out on different grids for the TATCT to know the grid which gives acceptable numerical accuracy. The grids combination used for the grid independence of the TATCT for the forced convection of the laminar, transitional and turbulent flows in the previous Chapters are applied to the mixed convection in the present Chapter. The analysis of the grid independence was carried out on the domain at an inclination angle of 60° . For the laminar flow of the mixed convection, four different grids with number of cells 1255502, 1658638,

2515756 and 3018907 are used. Temperature and velocity across the cross-section at the exit of the domain for Reynolds number of 1820 are extracted and displayed in Figure 7.2. Interestingly, the results obtained are the same as those for the TATCT in the forced convection in the previous study (§4.3 of Chapter 4). Therefore, as in the previous study, the grid with 2515756 cells is adopted to obtain a good numerical solution and save time for the computation.

Six different grids with number of cells 1255502, 1658638, 2515756, 3018907, 3522058 and 3773634 were used for the turbulent mixed convection flow. Temperature, velocity and turbulent kinetic energy across the cross-section at the exit of the domain for Reynolds number of 20000 are extracted and presented in Figure 7.3. The results obtained are in the same agreement with those for the TATCT in the forced convection in §5.3 of Chapter 5. Consequently, the grid with 2515756 cells is adopted.

For the numerical solutions of the transitional flow of the mixed convection, grid independence tests were conducted on four different grids with number of cells 1255502, 1658638, 2515756 and 3018907. In doing this, data of temperature and velocity for Reynolds number 2300 at the exit of the domain were extracted, and the results are shown in Figure 7.4. It is observed that the results obtained are similar to those for the TATCT in the forced convection in §6.3 of Chapter 6. As a result of this, the grid with 2515756 cells is adopted for simulation.

7.4 Computational Results and Discussions

The effects of the buoyant force on the heat transfer and fluid flow in the induced tube as well as the distributions of velocity and temperature in the domain are discussed in this section. To achieve these objectives, four

different orientations ($\theta = 15^\circ, 30^\circ, 60^\circ$ and 90°) with Grashof number $Gr = 3.37 \times 10^5$ and Prandtl number $Pr = 5.83$ are considered for water.

7.4.1 Turbulent kinetic energy

In this section, the turbulent kinetic energy of the mixed convection flow through the tube is compared with that of the forced convection. The turbulent kinetic energy of a turbulent flow for $Re = 20000$ at different inclination angles are considered for the mixed convection. The results are presented in Figure 7.5.

It can be seen in Figure 7.5 that in all the induced tubes, the turbulent kinetic energy grows gradually up to the end of the tube. The values of the turbulent kinetic energy in the mixed convection flow with tube inclination angles of 15° (frame b) show a little departure from the forced convection values (frame a). This means that there is a low buoyancy influence from the tube when the inclination is 15° . Comparison between the contours plots for the mixed convection flow at angles 30° (frame c), 60° (frame d) and 90° (frame e) with that of the forced convection (frame a) shows that as the inclination angle increases, the magnitude of the turbulent kinetic energy of the mixed convection increases. The maximum turbulent kinetic energy in the tube with forced convection is approximately 8%, 14%, 22% and 26% less than those in the tube with the mixed convection at inclination angles of $15^\circ, 30^\circ, 60^\circ$ and 90° respectively. The turbulent kinetic energy in the vicinity of the cuts on the tape is higher than those in the region that is not in close proximity to the cuts. This is due to the disturbances which the cuts impart on the flow as discussed in the previous Chapters.

7.4.2 Surface temperature

The effects of inclination angles on the surface temperature of the tube at four different orientations are presented in this section. The distribution of the surface temperature for the laminar flow along the dimensionless tube length for different Reynolds numbers and inclination angles are portrayed in Figure 7.6 and are compared with the results of the horizontal tube under forced convection. Reynolds number $Re = 830$, 1150 and 1640 are presented for the laminar flow. It is seen that there is a gradual increase in the surface temperature from the inlet of the tube to the outlet. It is also evident that keeping the Reynolds number constant but increasing the inclination angle of the tube, the surface temperature along the length of the tube increases as the inclination angle changes from $\theta = 15^\circ$ to $\theta = 90^\circ$.

The effect of the buoyancy forces on the inclined tube make the surface temperature of the tube under forced convection to be less than that of the inclined tube. Referring to $Re = 1150$, the surface temperature of the tube with buoyancy-influenced flow at inclination angles of 15° , 30° , 60° and 90° are approximately 6%, 6.1%, 6.2% and 6.5% respectively higher than that of the tube under forced convection. The explanation for this is that when heat is transferred in the tube the density of the fluid are not the same at all locations in the tube. As a result, the body forces acting due to the change in the density of the fluid caused the hotter fluid to move upward along the surface while the colder fluid, because of its higher density, moves downward through the core of the tube. Comparing the surface temperature for $Re = 830$ (Figure 7.6(a)), $Re = 1150$ (Figure 7.6(b)) and $Re = 1640$ (Figure 7.6(c)) indicates that for each of the inclination angles, the surface temperatures for higher Reynolds number are lower than those for the lower Reynolds number. This is because the higher the

Reynolds number, the more the domination of the forced convection on the heat transfer process [149, 150].

The distribution of the surface temperature for the transitional flow (Figure 7.7) has the same trend as that of the laminar flow. The surface temperature increases gradually from the inlet of the tube to the outlet. Moreover, at each of the Reynolds numbers ($Re = 2150, 3000$ and 3700), the surface temperature along the length of the tube increases as the inclination angle increases from $\theta = 15^\circ$ to $\theta = 90^\circ$. Also, the surface temperature of the tube under forced convection is less than that of the inclined tube. For example, for $Re = 3700$ (Figure 7.7(c)) the surface temperature due to buoyant force at inclination angles of $15^\circ, 30^\circ, 60^\circ$ and 90° are approximately 6.7%, 6.1%, 6.2% and 6.3% respectively higher than that of the tube that is not influenced by buoyant force.

For the turbulent flow, Reynolds numbers $Re = 5000, 16000$ and 20000 are presented in Figure 7.8. The surface temperature of the tube under the influence of buoyant force is greater than that under forced convection. The surface temperature along the length of the tube increases as the inclination angle increases from $\theta = 15^\circ$ to $\theta = 90^\circ$. The surface temperature for $Re = 16000$ under the influence of buoyancy at inclination angles of $15^\circ, 30^\circ, 60^\circ$ and 90° are approximately 6.1%, 6.3%, 6% and 6.2% respectively higher than that of the tube under forced convection. However, the distribution of the surface temperature shows a trend different from those in the laminar and transitional flows. As can be seen in Figure 7.8, the surface temperature along the length of the tube increases gradually from the inlet until it reaches a point where it decreases a little, particularly for $Re = 16000$ (Figure 7.8(b)), and then increases. This different trend that is exhibited by the turbulent flow is similar to those that were observed by Hsu and Smith [151] and Watts and Chou [152].

7.4.3 Temperature inside the domain

This section examines the temperature inside the induced tube under combined forced and natural convection. The aim is to investigate the effect of the buoyant force at different inclination angles on the temperature inside the induced tube. The results obtained for the laminar flow (Figure 7.9), transitional flow (Figure 7.10) and turbulent flow (Figure 7.11), reveal the temperature gradually increases along the tube. Due to the buoyancy effect, which causes a density difference in the fluid, the temperature in the tubes under combined mixed convection (frames b, c, d and e) are higher than that in the tube under forced convection (frame a). The temperature inside the tube under combined convection increases as the inclination angle increases.

For the laminar, transitional and turbulent flows considered, the temperature of the tube under forced convection is slightly higher than that in the tube inclined at 15° under the mixed convection. In addition, the temperature in the tube under mixed convection increased slightly as the inclination angle increases from 15° to 60° but increases noticeably as the inclination angle is increased from 60° to 90° .

7.4.4 Outlet velocity and outlet temperature

The effects of the different inclination angles ($\theta = 15^\circ, 30^\circ, 60^\circ$ and 90°) and different Reynolds numbers on the outlet velocity and outlet temperature of the tube are discussed in this section and demonstrated in Figure 7.12. For the laminar flow (Figure 7.12(a)), the velocity increases as the Reynolds number increases. In addition, the velocity is reduced as the inclination angle is increased from 15° to 90° due to a drawback to the flow moving toward the end of the tube. There seems to be a sudden drop at an

inclination angle of about 23° . Therefore, the velocity drop is divided into two portions: from 15° to 23° and 23° to 90° . The highest velocity drop is about 7% and it occurs at $Re = 830$ for $23^\circ \leq \theta \leq 90^\circ$.

In the transitional flow (Figure 7.12(b)), the increase in Reynolds number yields an increase in velocity but the velocity for $Re = 2150$ and $Re = 3000$ are approximately the same for $15^\circ \leq \theta \leq 90^\circ$. Moreover, for all the Reynolds numbers the velocity decreases as the inclination angle increases. The velocity drop is gradual for the inclination angle $15^\circ \leq \theta \leq 27^\circ$ but between an inclination angle of 27° and 90° , the drop in the velocity is sudden with the highest velocity drop of about 8% occurring at $Re = 3000$. For the turbulent flow (Figure 7.12(c)), the velocity increases as the Reynolds number reduces and the increase is not so significant at lower Reynolds number. There is a sudden drop in the velocity at an inclination angle of about 23° and the highest velocity drop of 9% occurs at $Re = 20000$ for the inclination angle between 23° and 90° .

Figure 7.13 depicts the effects of the inclination angle at different Reynolds numbers on the normalised outlet temperature of the tube for the laminar (Figure 7.13(a)), transitional (Figure 7.13(b)) and turbulent flows (Figure 7.13(c)). The results show that the outlet temperature decreases when the Reynolds number increases. In addition, the normalised temperature increases slightly as the inclination angle increases. However, the increase in the normalised temperature in the transitional flow is more pronounced when the inclination angle is greater than 23° .

7.4.1 Heat transfer

In order to investigate the effect of buoyancy on the heat transfer, the result of Nusselt number at different tube orientations ($\theta = 15^\circ, 30^\circ, 60^\circ$

and 90°) for different Reynolds numbers are obtained and compared with the Nusselt number of the forced convection already obtained in the previous Chapters. The results, as shown demonstrated in Figure 7.14, indicate that for the laminar, transitional and turbulent flows, the Nusselt number in the inclined tubes are higher than those in the tube under forced convection.

In each of the inclined tubes, the maximum enhancement in the Nusselt number is obtained at an inclination of 90° . For the laminar flow, shown in Figure 7.14(a), the Nusselt number in the tubes with inclination angles 15° , 30° , 60° and 90° are 3.8 to 5.8%, 5.1 to 7.0%, 4.8 to 7.45% and 6.4 to 8.9% respectively higher than that in the tube under forced convection. The Nusselt number in the tubes with inclination angles 15° , 30° , 60° and 90° for the transitional flow Figure 7.14(b), are 4.0 to 6.1%, 4.6 to 7.4%, 5.3 to 8.7% and 6.3 to 10.1% respectively higher than that in the tube under forced convection. For the turbulent flow (Figure 7.14(c)), the Nusselt number in the tubes with inclination angles 15° , 30° , 60° and 90° are 3.3 to 3.9%, 3.5 to 4.4%, 4.0 to 4.9% and 5.5 to 6.4% respectively higher than that in the tube under forced convection.

The results in the foregoing paragraph indicate that the Nusselt number in the inclined tubes are higher than those in the tube under forced convection and that in each of the inclined tubes, the maximum enhancement in the Nusselt number is obtained at an inclination of 90° . The heat transfer enhancement resulted from the combined forced and natural convections which yields three different mechanisms. These mechanisms, as provided by Maughan and Incropera [153] and Wickern [154], are the external force from the forced convection, and the parallel and normal components of the buoyant force from the natural convection. Each of the three mechanisms plays an important role in determining the

heat transfer. The external force from the forced convection reduces the thermal resistance, and consequently results in an increase in heat transfer. The parallel component of the buoyant force is in the same direction to the main flow in the tube and thus leads to a decrease in thermal resistance and an increase in the heat transfer. The normal component of the buoyant force disturbs the boundary layer and consequently increases the heat transfer.

7.4.2 Friction factor

In the design of heat transfer equipment, it is necessary to consider the pressure drop in the system. In this section, the pressure drop is presented in the form of friction factor. The effects of buoyancy on the friction factor are examined by comparing the results of the friction factor of the forced convection with the friction factor of the mixed convection at different inclination angles and Reynolds number. The results are demonstrated in Figure 7.15 for laminar, transitional and turbulent flows.

As seen in the Figure 7.15, the friction factor for the mixed convection increases as the inclination angle increases from 15° to 90° . It is also observed that the friction factor for the mixed convection is higher than that of the forced convection. The factor responsible for this is the buoyant force due to the natural convection acting on the flow in addition to the forces due the forced convection that is also acting on the flow.

Quantitatively, the friction factor for the laminar flow (Figure 7.15 (a)) in the tubes with inclination angles 15° , 30° , 60° and 90° are 4.3%, 5.6%, 6.2% and 9.2% respectively higher than in than the tube under forced convection. The friction factor in the tubes with inclination angles 15° , 30° , 60° and 90° for the transitional flow (Figure 7.15 (b)) are 6.6%,

8.4%, 9.8% and 10.8% respectively higher than that in the tube under forced convection. The friction factor for the forced convection has been discussed in detail in §6.5.6 of Chapter 6. For the turbulent flow (Figure 7.15 (c)), the friction factor in the tubes with inclination angles 15° , 30° , 60° and 90° are up to 10.7%, 13.7%, 15.3% and 18% respectively higher than that in the tube under forced convection. This show that the maximum enhancement in the friction factor in each of the inclined tubes is obtained at an inclination of 90° .

7.5 Conclusion

Investigation was numerically performed to study the effects of inclination angles on the heat transfer and flow characteristics of laminar, transitional and turbulent mixed convection in inclined tubes induced with an alternate-axis triangular cut twisted tape. Water is the working fluid and the wall of the tube is subjected to uniform heat flux. The solutions are obtained with Prandtl number $Pr = 5.83$, Grashorf number $Gr = 3.37 \times 10^5$ and inclination angles $15^\circ \leq \theta \leq 90^\circ$. The laminar, transitional and turbulent flows are in the Reynolds number range $830 \leq Re \leq 2000$, $830 \leq Re \leq 2000$ and $830 \leq Re \leq 2000$ respectively.

As a result of the effect of buoyancy forces on the inclined tube the temperature inside the tube under forced convection is less than that of the inclined tube. As a result of the forced convection that has more dominion at higher Reynolds number, the surface temperatures for higher Reynolds number are lower than those for the lower Reynolds number. It is observed that keeping the Reynolds number constant but increasing the inclination angle of the tube, the surface temperature along the length of the tube increases as the inclination angle changes from $\theta = 15^\circ$ to $\theta =$

90°. However, at $Re = 16000$ for turbulent flow, a different trend is exhibited.

The results indicate that for the laminar, transitional and turbulent flows, both the Nusselt number and the friction factor obtained in the tubes under mixed convection are higher than those in the tube under forced convection. Also, the Nusselt number and the friction factor for the mixed convection increases as the inclination angle increases from 15° to 90°. For the inclination angles considered, the maximum enhancement in the Nusselt number and friction factor are obtained at an inclination of 90° while the minimum enhancement in the Nusselt number and friction factor are obtained at an inclination angle of 15°. At the inclination angle of 90°, the induced tubes under mixed convection provide a maximum enhancement in the Nusselt number of up to 8.9%, 10.1% and 6.4% for the laminar, transitional and turbulent flows respectively over that in the induced tube under forced convection. For the friction, a maximum enhancement up to 9.2%, 10.8% and 18% for the laminar, transitional and turbulent flows respectively over that in the forced convection are obtained in the mixed convection.

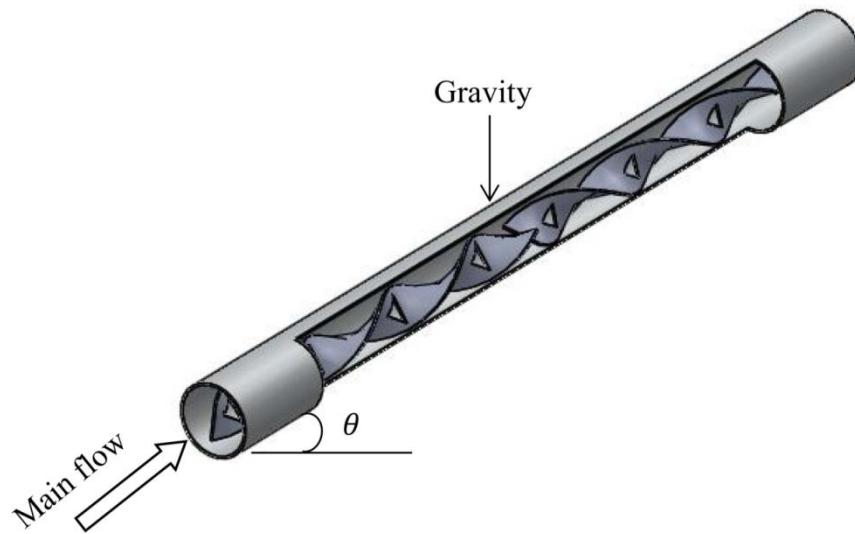


Figure 7.1: Model geometry of TATCT inclined at an angle.

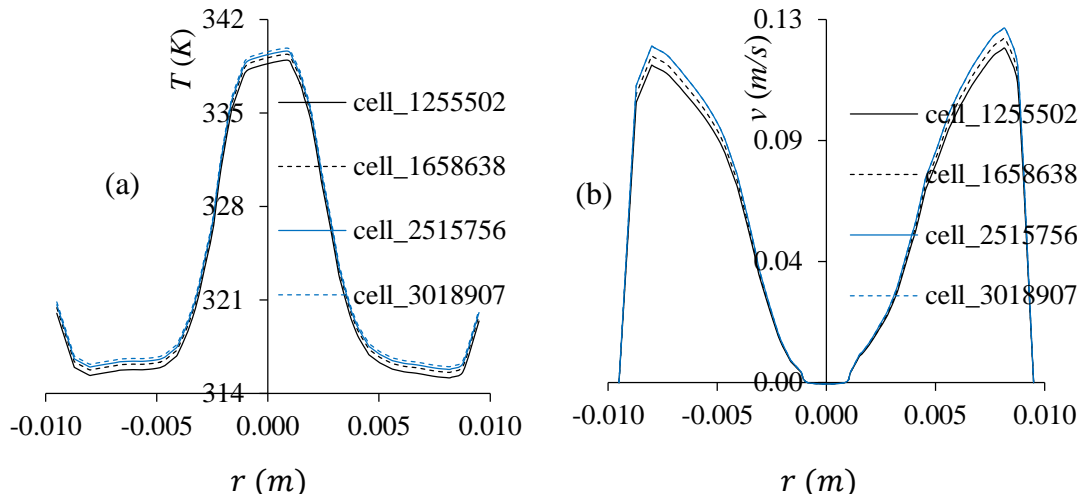


Figure 7.2: Grid independence test of laminar flow of mixed convection for (a) temperature and (b) velocity across the cross-section at the exit of TATCT inclined at 60° .

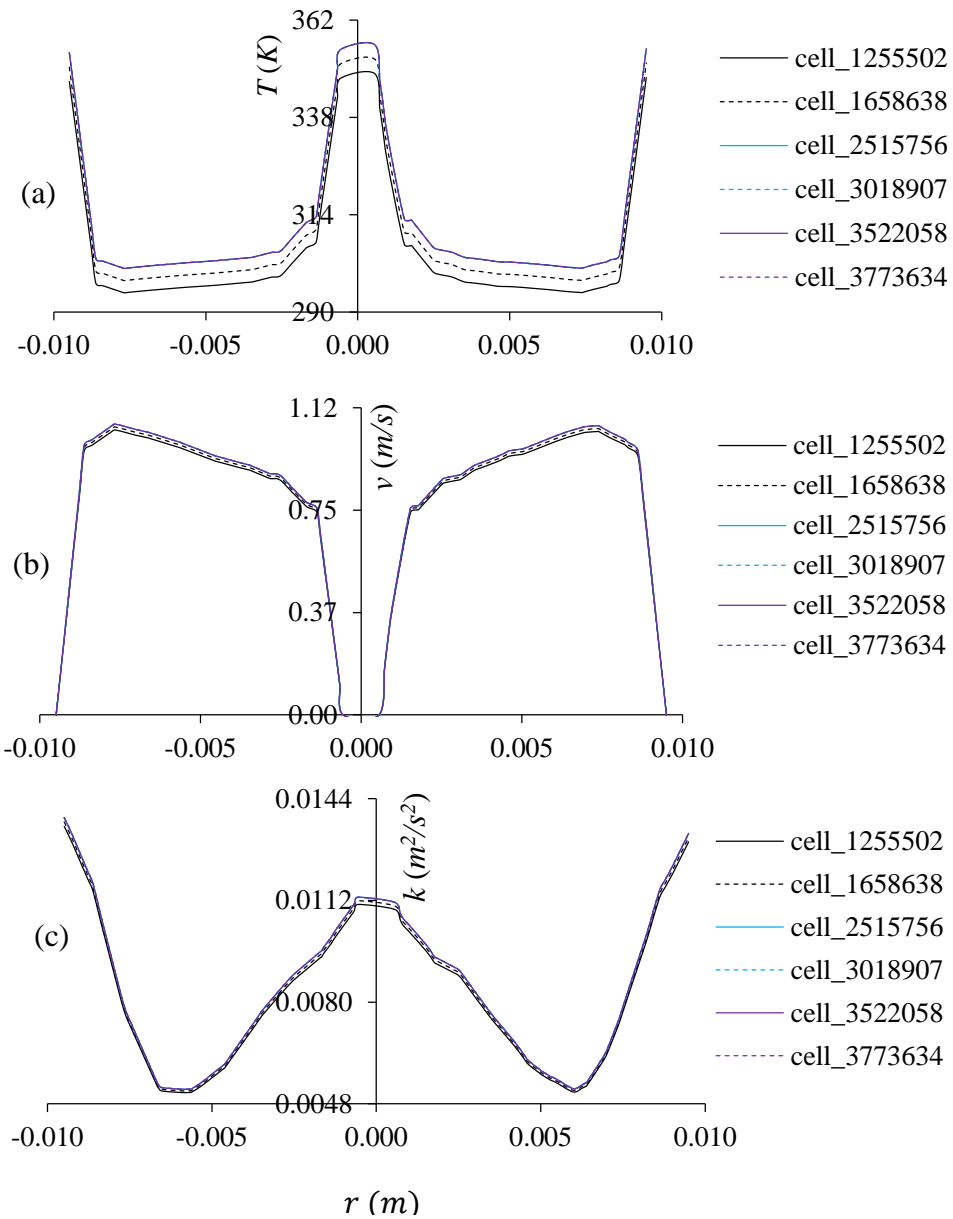


Figure 7.3: Grid independence test of turbulent flow of mixed convection for (a) temperature, (b) velocity and (c) turbulent kinetic energy across the cross-section at the exit of TATCT inclined at 60° .

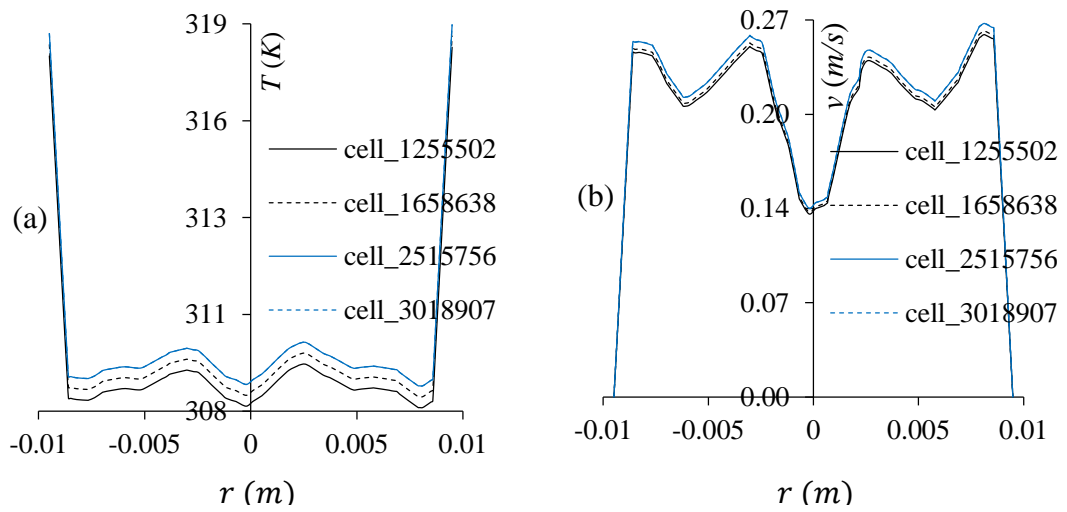


Figure 7.4: Grid independence test of transitional flow of mixed convection for (a) temperature and (b) velocity across the cross-section at the exit of TATCT inclined at 60° .

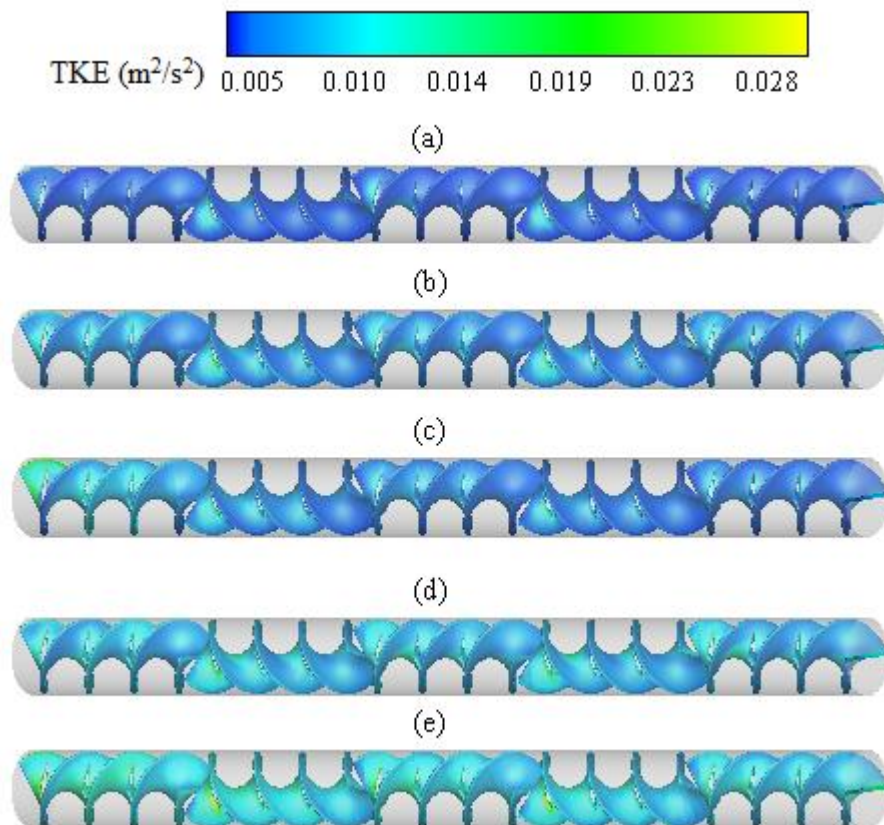


Figure 7.5: Turbulent kinetic energy for turbulent flow ($Re = 20000$) inside the TATCT for (a) forced convection, and mixed convection at inclination angle of (b) 15° , (c) 30° , (d) 60° , (e) 90° .

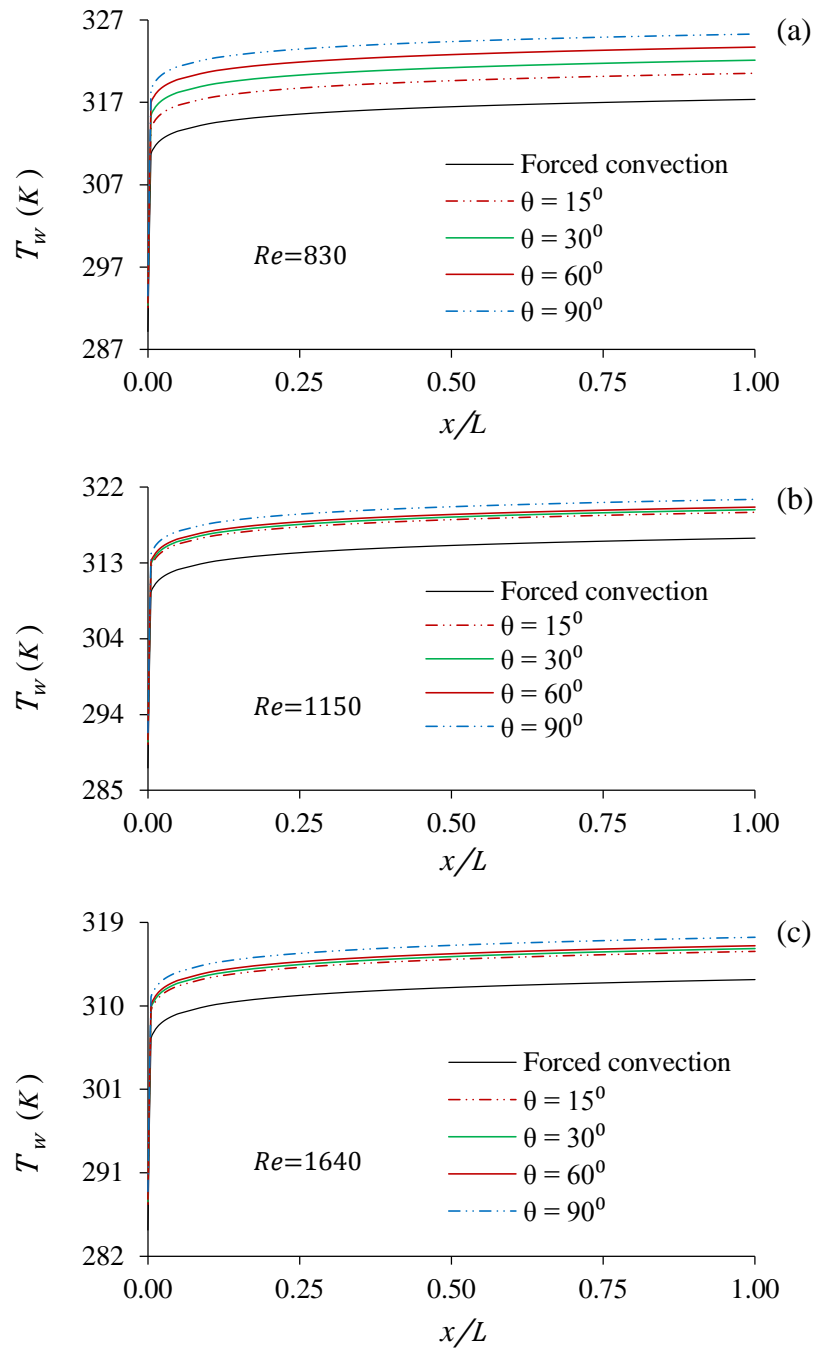


Figure 7.6: Surface temperature variation with dimensionless length for various Reynolds numbers of laminar flow.

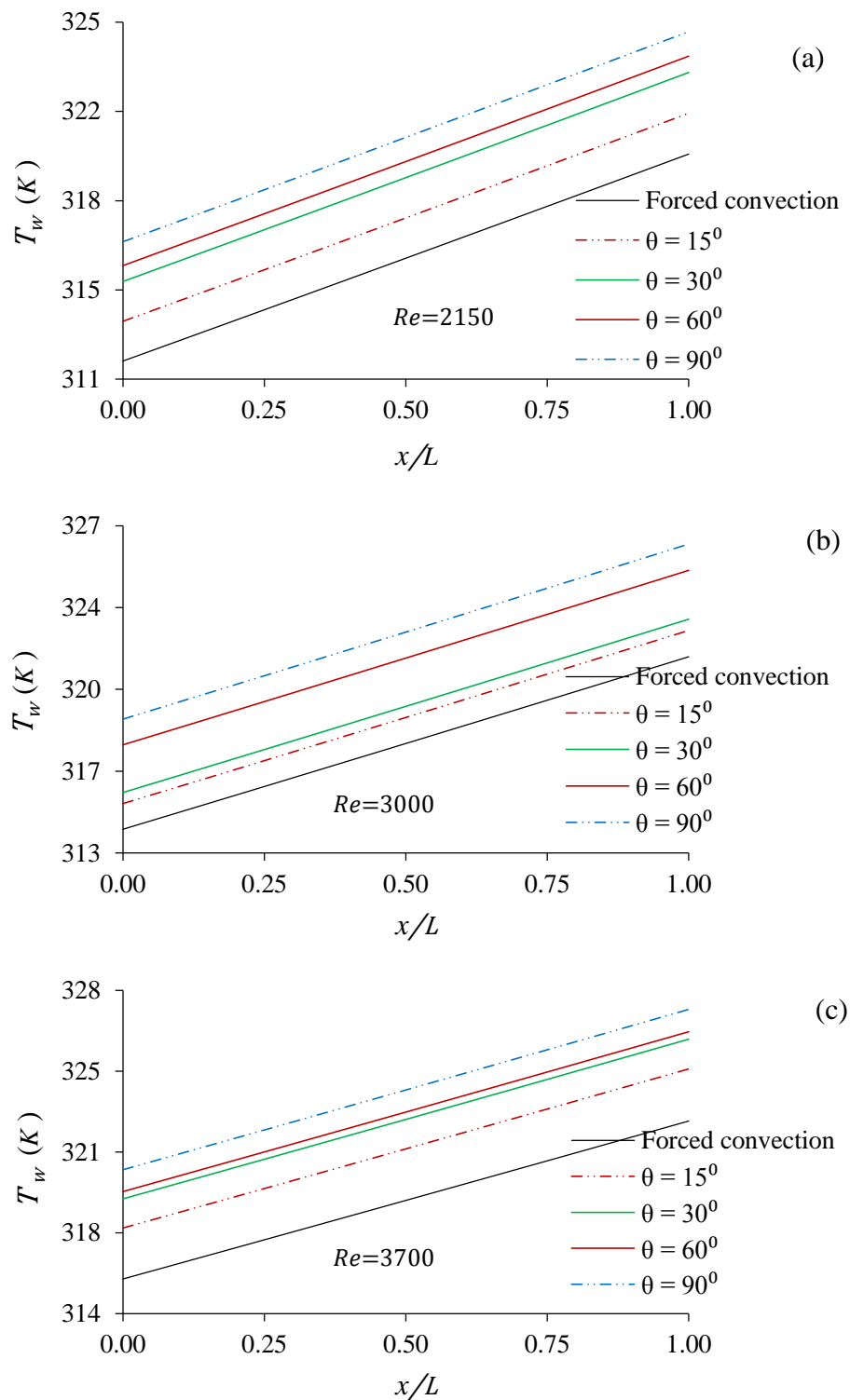


Figure 7.7: Surface temperature variation with dimensionless length for various Reynolds numbers of transitional flow.

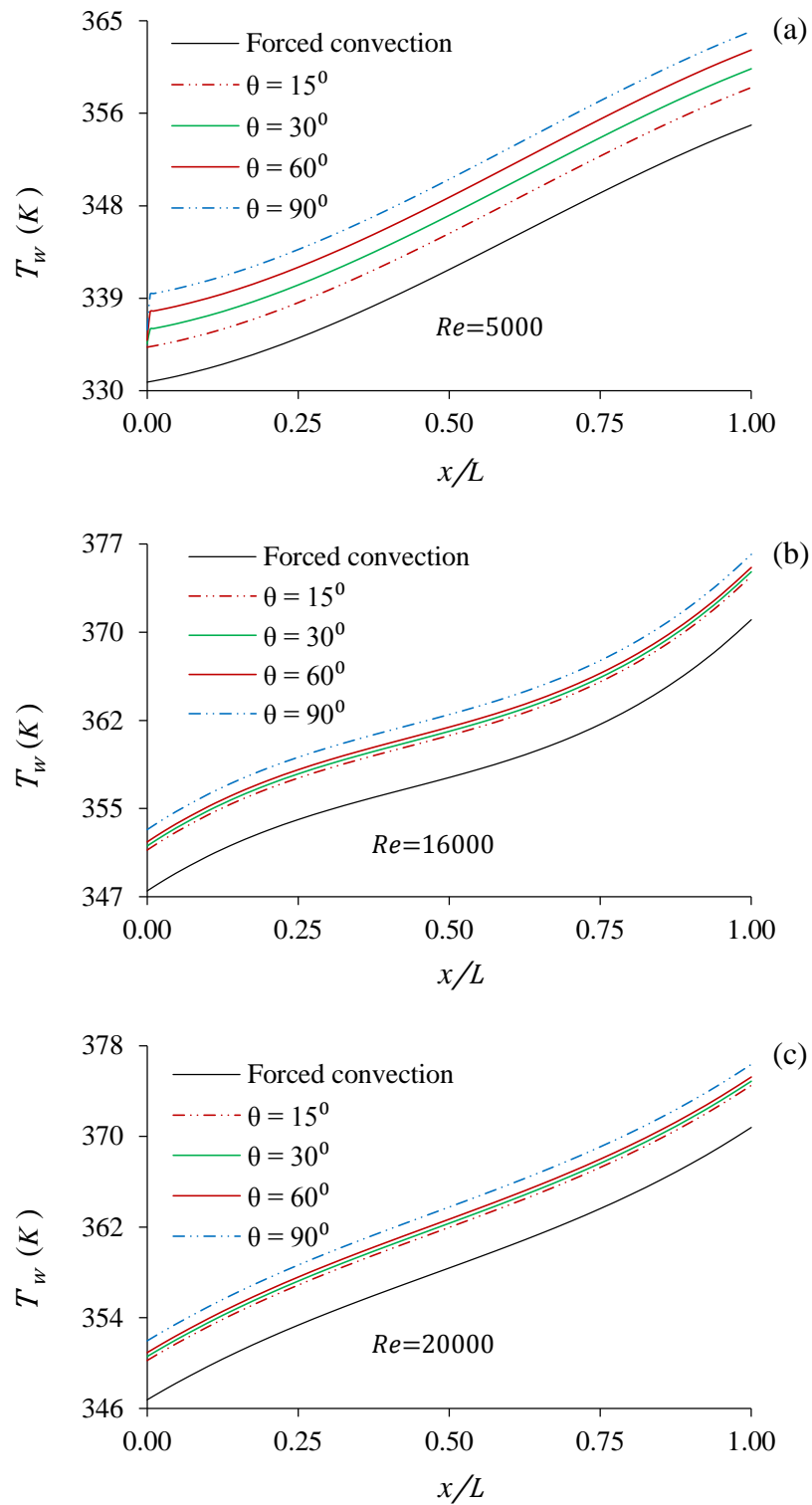


Figure 7.8: Surface temperature variation with dimensionless length for various Reynolds numbers of turbulent flow.

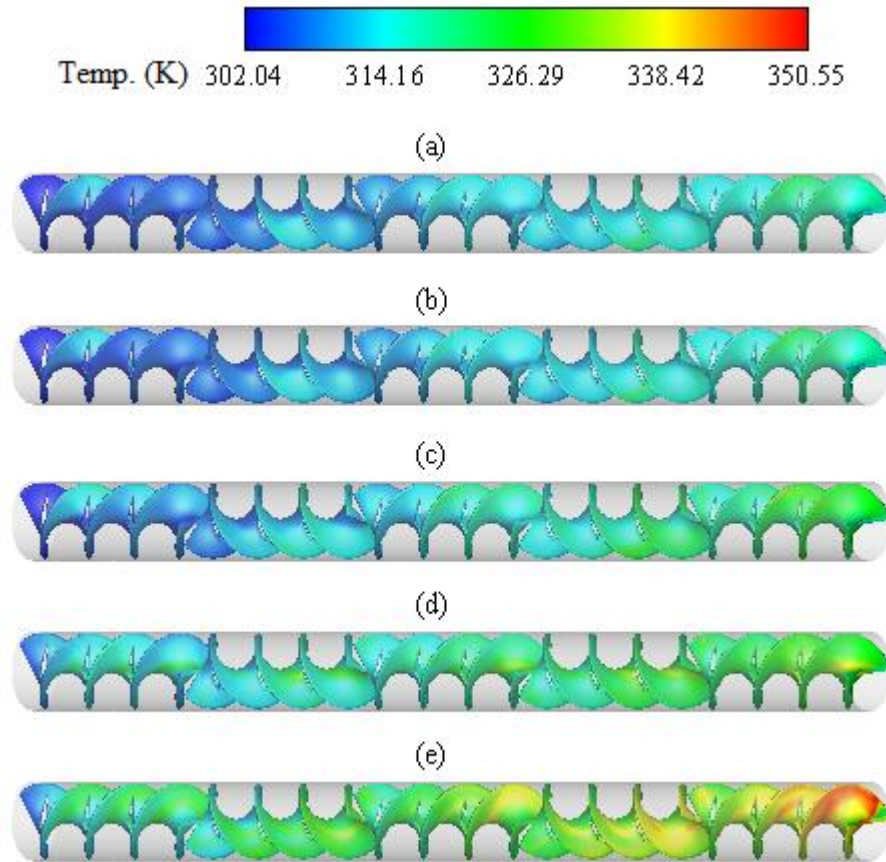


Figure 7.9: Contour plots of temperature for laminar flow ($Re = 1820$) inside through TATCT for (a) forced convection, and mixed convection at inclination angle of (b) 15°, (c) 30°, (d) 60°, (e) 90°.

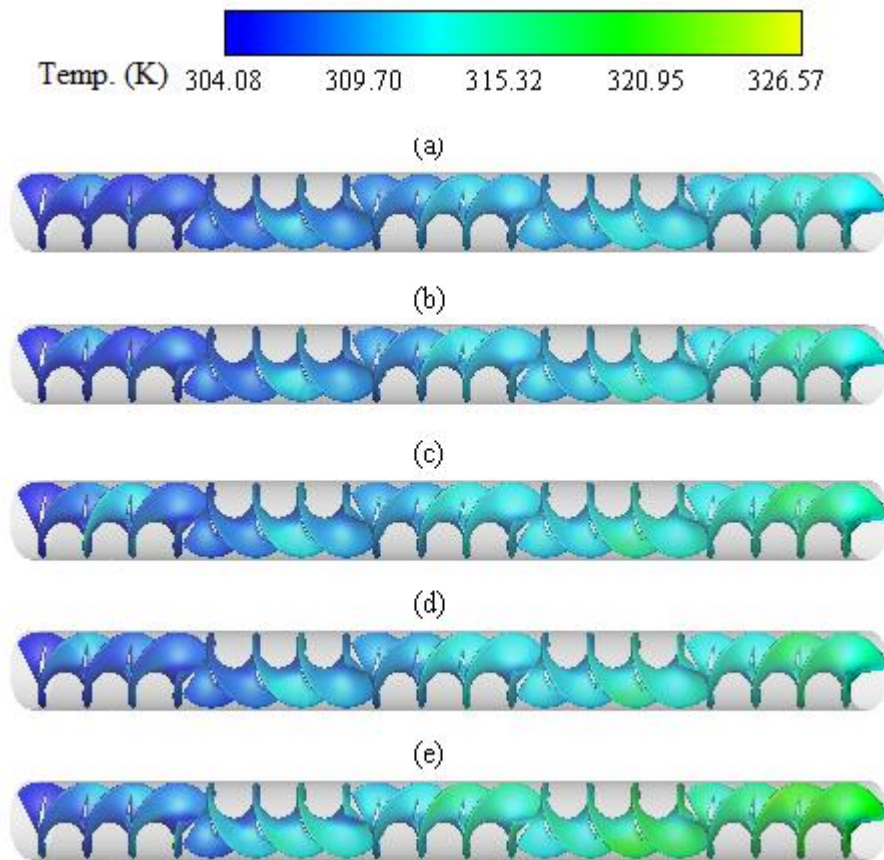


Figure 7.10: Contour plots of temperature for transitional flow ($Re = 2150$) inside through TATCT for (a) forced convection, and mixed convection at inclination angle of (b) 15° , (c) 30° , (d) 60° , (e) 90° .

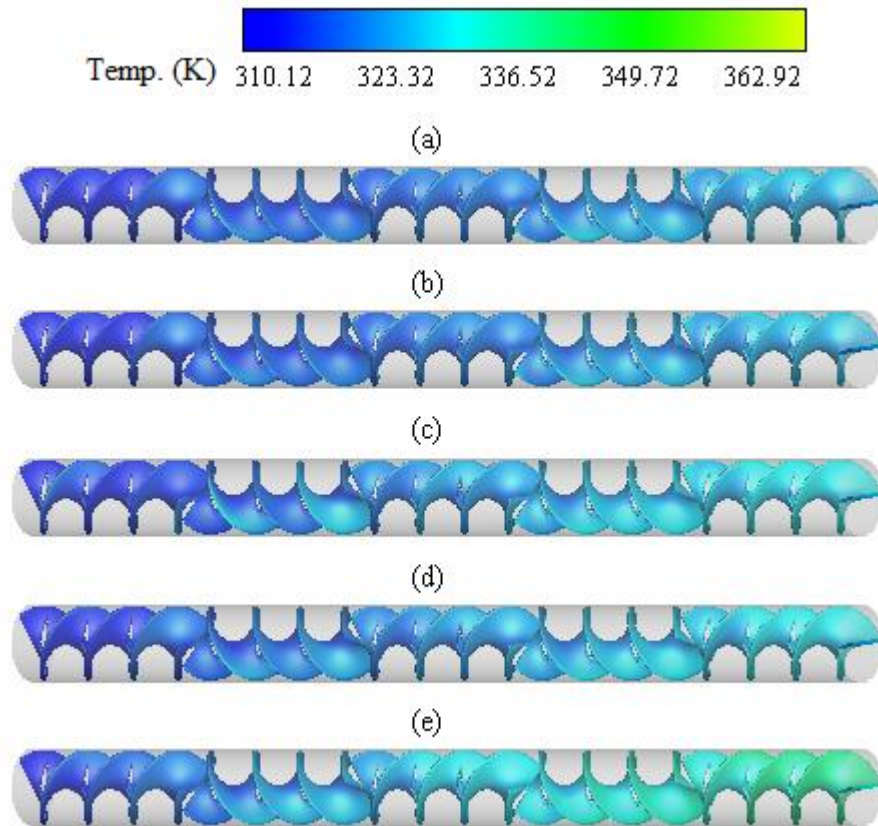


Figure 7.11: Contour plots of temperature for turbulent flow ($Re = 20000$) inside through TATCT for (a) forced convection, and mixed convection at inclination angle of (b) 15°, (c) 30°, (d) 60°, (e) 90°.

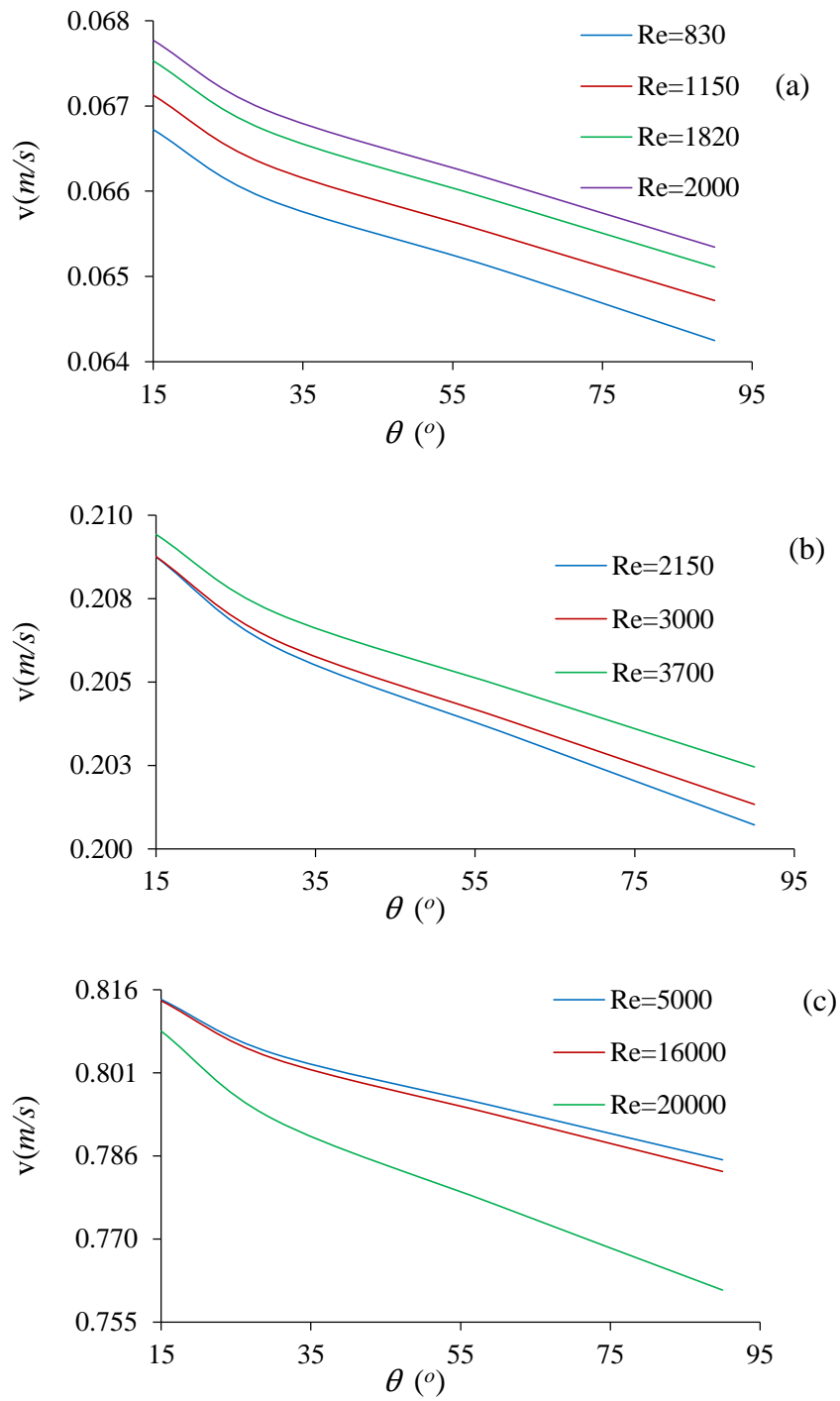


Figure 7.12: Average outlet velocity at various inclinations for various Reynolds numbers of (a) laminar flow, (b) transitional flow and (c) turbulent flow.

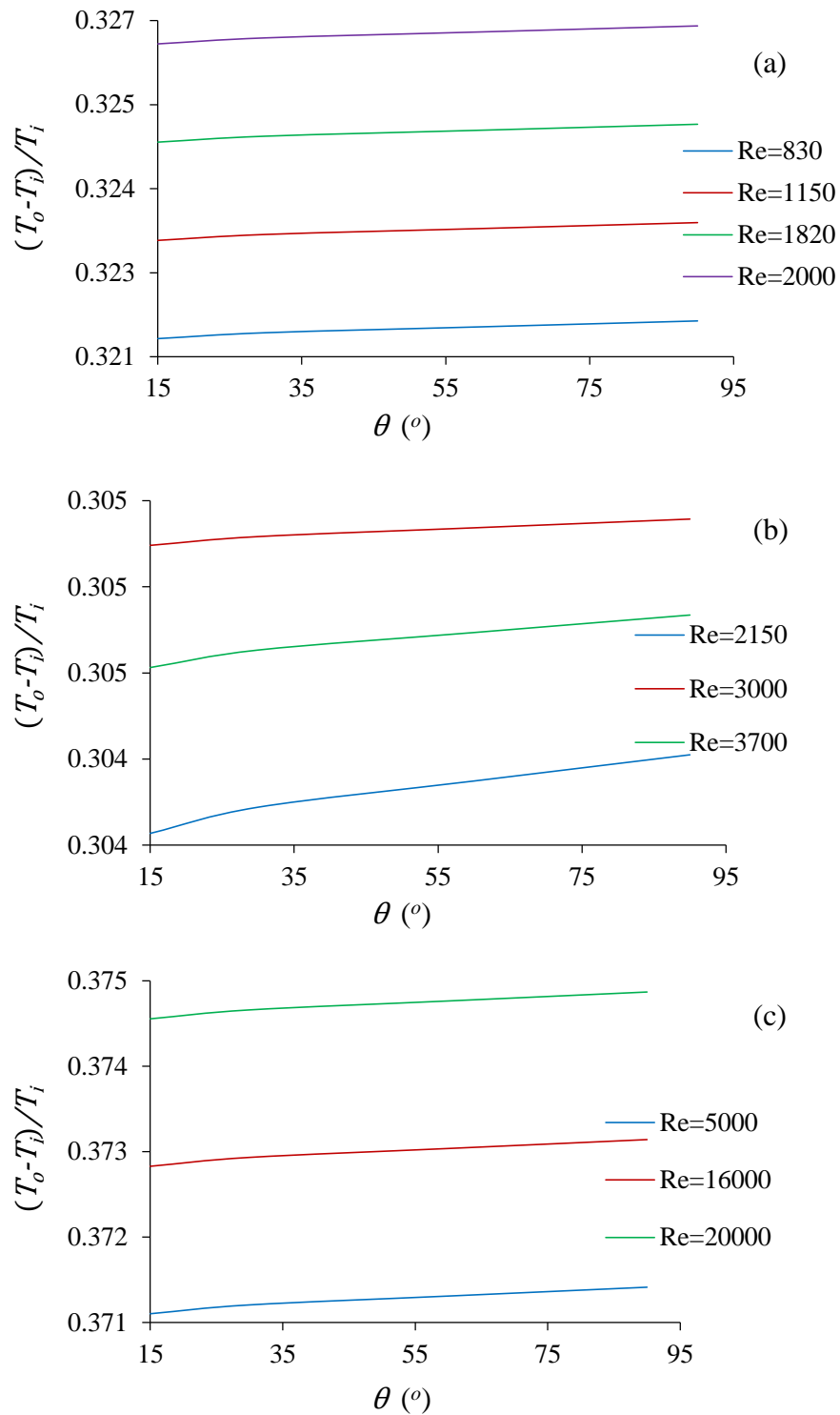


Figure 7.13: Effect of inclination on normalised outlet temperature for various Reynolds numbers of (a) laminar flow, (b) transitional flow and (c) turbulent flow.

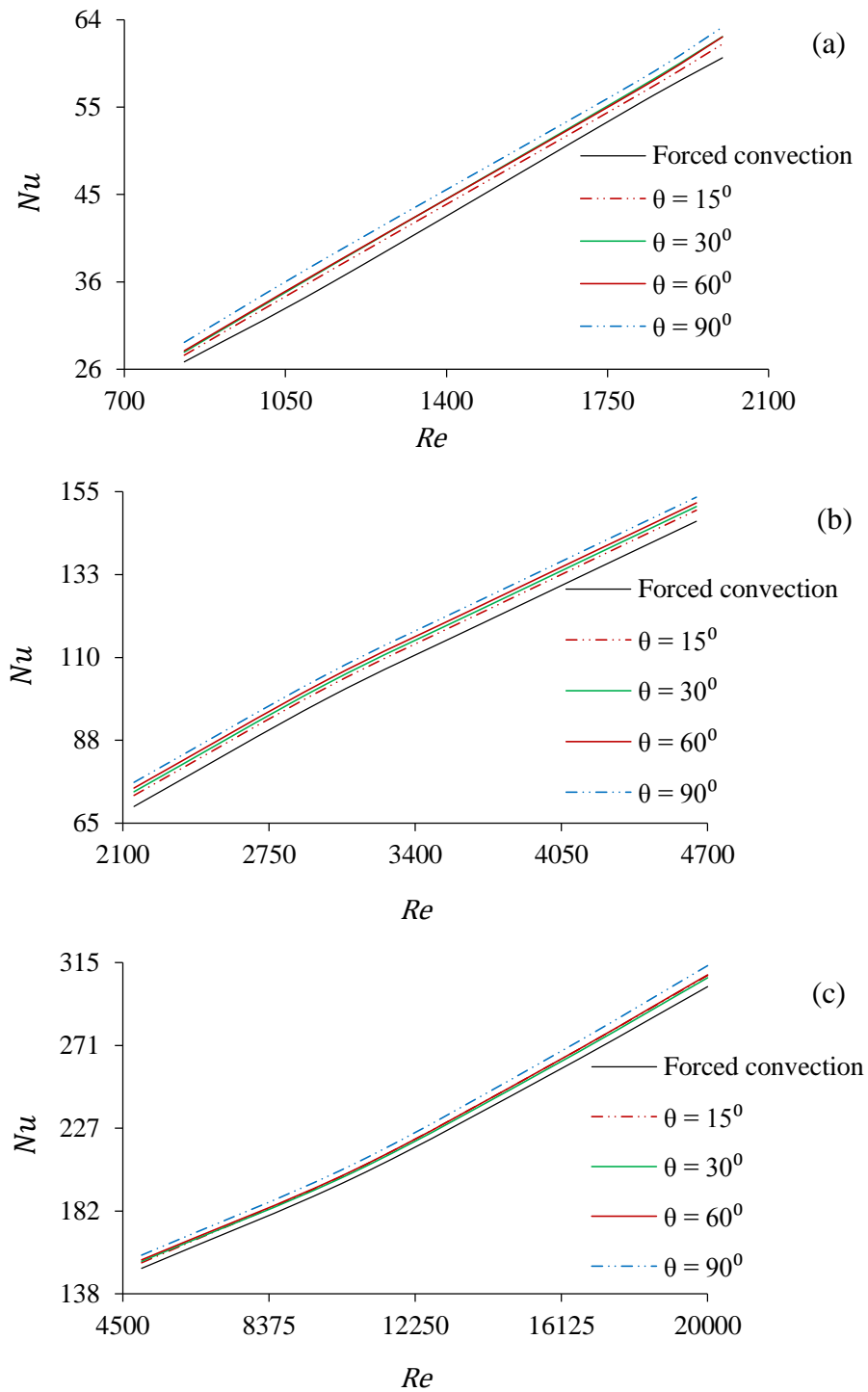


Figure 7.14: Impact of inclination on Nusselt number for various Reynolds numbers of (a) laminar flow, (b) transitional flow and (c) turbulent flow.

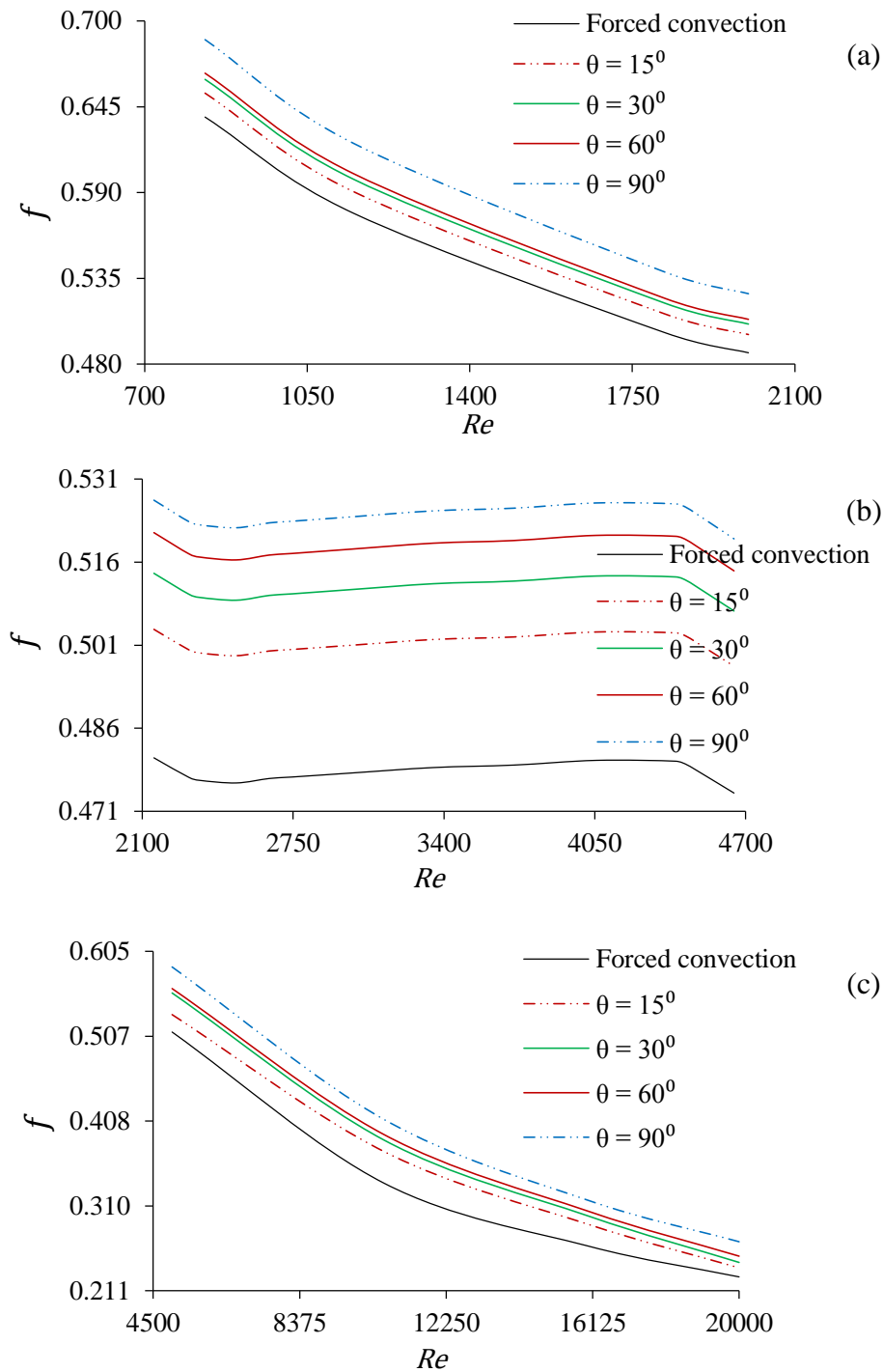


Figure 7.15: Impact of inclination on friction factor for various Reynolds numbers of (a) laminar flow, (b) transitional flow and (c) turbulent flow.

Chapter 8

CONCLUSIONS AND SUGGESTIONS FOR FURTHER RESEARCH

The findings of the work undertaken in this thesis are summarised in §8.1. In addition, some useful suggestions for future research are made in §8.2.

8.1 Conclusions

Heat transfer and fluid flow through tubes induced with twisted tape inserts were numerically investigated. The investigation was carried out for laminar, transitional and turbulent flows. Attention is also paid to the aspect of mixed convection. The findings of the thesis are presented below.

In Chapter 4, the tube design that gives the best performance in augmenting the heat transfer and thermal performance factor is numerically investigated for laminar flow of water through induced tubes of different designs. It was discovered that of all the tube designs considered, the tube fitted with alternate-axis triangular cut twisted tape (TATCT) gives the best performance. The Nusselt number and thermal performance index of the TATCT are up to 124.57% and 103.23% higher than those in the plain tube with plain twisted tape (TPT). This is attributed to improved swirl and superior mixing offered by the alternate-axis and triangular cuts on the twisted tape.

In Chapter 5, a numerical study was carried out on thermo-hydraulic

characteristic of turbulent flow through tube induced individually with different twisted tape insert. In the first part of the finding, it was revealed that the tube system with alternate-axis triangular cut twisted tape (TATCT) produced the highest enhancement in heat transfer and thermal performance factor when compared with those produced by the other induced tubes. Specifically, the Nusselt number and friction factor in the TATCT is up to 118.4% and 215.8% respectively higher than those in the tube system equipped with plain twisted tape. The second segment of the Chapter assesses the effects which the variations in the tape width, the tape pitch and the size of cut on the tape have on the thermo-hydraulic characteristics of the flow. The Nusselt number, friction factor and thermal performance factor were found to decrease as the tape pitch increases. Not only that, it was discovered that increasing the tape width and the size of the cuts on the tape is advantageous to the flow system because these enhance the heat transfer and thermal performance factor of the system.

In Chapter 6, the onset and end of transition in a flow of water through tubes induces individually with alternate-axis triangular cut twisted tape (TATCT), alternate-axis circular cut twisted tape (TACCT) and alternate-axis elliptical cut twisted tape (TAECT) were numerically studied. The heat transfer obtained in the TATCT is higher than that in the TAECT while the heat transfer in the TAECT is higher than that in the TACCT. It was observed that the transition occurs earlier and also ends earlier in the tube that has the highest Nusselt number. Thus, transition occurs first in the TATCT at $Re = 2300$ and ends at $Re = 4400$. For the TAECT, it occurs at $Re = 2550$ and ends at $Re = 4500$. Transition occurs in TACCT at $Re = 2780$ and ends at $Re = 4610$.

In Chapter 7, a numerical study of mixed convection in laminar, transitional and turbulent flows through a tube induced with TATCT was reported. As a

result of buoyancy force, the Nusselt number and friction factor of the mixed convection are higher than those in the forced convection. The inclination angle is varied from 15° to 90° with respect to the horizontal position. The Nusselt number and friction factor increases as the inclination angle increases, and the maximum enhancement is provided at an inclination angle of 90° . The Nusselt number obtained in the mixed convection is up to 8.9%, 10.1% and 6.4% higher than those in the forced convection for the laminar, transitional and turbulent flows. For the friction factor, the values obtained in the mixed convection is up to 9.25 10.8% and 18% higher than those in the forced convection for the laminar, transitional and turbulent flows. These findings indicate that the heat transfer and the friction factor increase as the inclination angle increases.

In all the cases considered for the laminar, transitional and turbulent flows operating under forced convection or mixed convection, the tube induced with alternate-axis triangular cut twisted tape (TATCT) proved to be the one with the best performance.

8.2 Suggestions for Future Research

The present research has investigated thermo-hydraulic performance of different enhanced tube with focus on heat transfer enhancement and has provided opportunity for future work which will create new insights into mechanisms of heat transfer enhancement. Thus, it is suggested that the future work should include the following:

- The impact of fouling in fluids with twisted tape should be investigated. Heat exchanger surface, piping flow channels, turbines, ship hulls, solar panels, etc., are some of the components

that may be subjected to fouling. As such, results of this suggested research work will be useful.

- The aspect of mixed convection flow on twisted tape-induced tube has not received adequate attention. Therefore, research on this area need to be expanded so that its practical significance can be utilized.
- In order to enrich the database on heat transfer enhancement, investigation should be conducted on a wider range of enhanced tube.
- Other fluids, aside from water that was investigated in the present work, should be subjected to investigation. This will definitely make it possible to compare the result that will be obtained with the present results on water.
- In addition, suitable experiment needs to be designed to further assess the simulated results of the best performing twisted tape (TATCT).

REFERENCES

- [1] L. M. Jiji, *Heat convection*, 2nd ed, New York: Springer Berlin Heidelberg, 2009.
- [2] J. P. Holman, *Heat transfer*, 10th ed, New York: McGraw-Hill, 2009.
- [3] S. V. Patil and P. V. Vijay-Babu, "Experimental studies on mixed convection heat transfer in laminar flow through a plain square duct," *Heat and Mass Transfer*, Vol. 48, pp. 2013-2021, 2012.
- [4] L. Wang and B. Sunden, "Performance comparison of some tube inserts," *International Communication in Heat Mass Transfer*, Vol. 29 (1), pp. 45-56, 2002.
- [5] A. E. Bergles, "The imperative to enhance heat transfer," in *Heat transfer enhancement of heat exchangers*, S. Kakac, A.E. Bergles, F. Mayinger and H. Yuncii, Editors. Kluwer: Dordrecht. pp. 13-29, 1999.
- [6] D. G. Kumbhar and N. K. Sane, "Heat transfer enhancement in a circular tube twisted with swirl flow generator." in *Proceedings of 3rd International Conference on Advances in Mechanical Engineering*, Gujarat, India, pp. 188-192, 2010.
- [7] K. M. Lunsford, *Increasing heat exchanger performance*, Texas: Bryan Research & Engineering Inc., 1998.
- [8] H. J. Lane and P. J. Heggs, "Extended surface heat transfer - the dovetail fin," *Applied Thermal Engineering*, Vol. 25, pp. 2555-2565, 2005.
- [9] A. G. Patil, "Laminar flow heat transfer and pressure drop characteristics of power-law fluids inside tubes with varying width twisted tape inserts," *Transaction of ASME Journal of Heat Transfer*, Vol. 122, pp. 143-149, 2000.

- [10] S. K. Saha, A. Dutta and S. K. Dhal, "Friction and heat transfer characteristics of laminar swirl flow through a circular tube fitted with regularly spaced twisted-tape elements," *International Journal of Heat and Mass Transfer*, Vol. 44, pp. 4211-4223, 2001.
- [11] V. Zimparov, "Enhancement of heat transfer by a combination of three-start spirally corrugated tubes with a twisted tape," *International Journal of Heat and Mass Transfer*, Vol. 44, pp. 551-574, 2001.
- [12] M. A. Akhavan-Behabadi, R. Kumar, A. Mohammadpour and M. Jamali-Asthiani, "Effect of twisted tape insert on heat transfer and pressure drop in horizontal evaporators for the flow of R-134a," *International Journal of Refrigeration*, Vol. 32, pp. 922-930, 2009.
- [13] A. E. Bergles, "Techniques to enhance heat transfer," in *Handbook of heat transfer*, W.M. Rohsenow, J.P. Hartnett and Y.I. Cho, Editors. McGraw-Hill: New York, 1998.
- [14] R. M. Manglik, "Heat transfer enhancement," in *Heat transfer handbook*, A. Bejan and A.D. Kraus, Editors. John Wiley & sons: New Jersey, 2003.
- [15] R. L. Webb, "Enhancement of single-phase heat transfer," in *Handbook of single-phase convective heat transfer*, S. Kakac, R.K. Shah and W. Aung, Editors. Wiley: New York, 1987.
- [16] Q. Liao and M. D. Xin, "Augmentation of convective heat transfer inside tubes with three-dimensional internal extended surfaces and twisted-tape inserts," *Chemical Engineering Journal*, Vol. 78, pp. 95-105, 2000.
- [17] R. M. Manglik and A. E. Bergles, "Heat transfer and pressure drop correlations for twisted-tape inserts in isothermal tubes: Part I - Laminar

- flows," *Transaction of ASME Journal of Heat Transfer*, Vol. 115 (4), pp. 881-889, 1993.
- [18] A. Dewan, P. Mahanta, K. S. Raju and P. S. Kumar, "Review of passive heat transfer augmentation techniques," *Proceedings of the Institutions of Mechanical Engineers, Part A: Journal of Power and Energy*, Vol. 218, pp. 509-527, 2004.
- [19] R. M. Manglik and A. D. Kraus, *Process, enhanced and multiphase heat transfer*, New York: Begell House, 1996.
- [20] A. E. Bergles, "The implications and challenges of enhanced heat transfer for the chemical process industries," *Transaction of Institution of Chemical Engineers*, Vol. 79, pp. 437-444, 2001.
- [21] R. M. Manglik and A. E. Bergles, "Heat transfer and pressure drop correlations for twisted -tape inserts in isothermal tubes: Part II - Transition and turbulent flows " *Transaction of ASME Journal of Heat Transfer*, Vol. 115, pp. 890-896, 1993.
- [22] S. Jaisankar, T. K. Radhakrishnan, K. N. Sheeba and S. Suresh, "Experimental investigation of heat transfer and friction factor characteristics of thermosyphon solar water heater system fitted with spacer at the trailing edge of left-right twisted tapes," *Energy Conversation Management*, Vol. 50, pp. 2638-2649, 2009.
- [23] J. P. Meyer and J. A. Oliver, "Heat transfer in the transitional flow regime," in *Condensation and heat transfer*, A. Ahsan, Editor. InTech. pp. 245-260, 2011.
- [24] T. Mullin, "Experimental studies of transition to turbulence in a pipe," *Annual Review of Fluid Mechanics*, Vol. 43, pp. 1-24, 2011.

-
- [25] ASHRAE, "Fluid flow," in *ASHRAE handbook - Fundamentals*. American Society of Heating, Refrigerating and Air-Conditioning Engineers, Inc.: Atlanta, 2009.
- [26] W. Yu-ting, L. Bin, M. Chong-fang and G. Hang, "Convective heat transfer in the laminar-turbulent transition region with molten salt in a circular tube," *Experimental Thermal and Fluid Science*, Vol. 33, pp. 1128-1132, 2009.
- [27] O. Reynolds, "An experimental investigation of the circumstances which determine whether the motion of water shall be direct or sinous, and of the law of resistances in parallel channels," *Philosophical Transactions of the Royal Society London*, Vol. 174, pp. 935-982, 1883.
- [28] O. Reynolds, "On the dynamical theory of incompressible viscous fluids and the determination of the criterion," *Philosophical Transactions of the Royal Society London*, Vol. 186A, pp. 123-164, 1895.
- [29] W. Pfenniger, *Boundary layer and flow control*: Pergamon, 1961.
- [30] V. W. Ekman, "On the change from steady to turbulent motion of liquids," *Arkiv för Matematik, Astronomi och Fysik*, 1910.
- [31] A. Meseguer and L. N. Trefethen, "Linearized pipe flow to Reynolds number 10^7 ," *Journal of Computational Physics*, Vol. 186, pp. 178-197, 2003.
- [32] K. V. Sharp and A. R. J., "Transition from laminar to turbulent flow in liquid filled microtubes," *Experiments in Fluids*, Vol. 36, pp. 741-747, 2004.
- [33] N. T. Obot, E. E.B. and R. T.J., "The role of transition in determining friction and heat transfer in smooth and rough passages," *International Journal of Heat and Mass Transfer*, Vol. 33 (10), pp. 2133-2143, 1990.

-
- [34] R. Royds, *Heat transmission by radiation, conduction and convection*, 1st ed, London: Constable and Co., 1921.
- [35] A. P. Colburn and W. J. King, "Heat transfer and pressure drop in empty, baffled and packed tubes III: Relationship between heat transfer and pressure drop," *Industrial and Engineering Chemistry*, Vol. 32, pp. 919-923, 1931.
- [36] N. Y. Kirov, "Turbulence promoter in boiler smoke tubes," *Journal of the Institute of Fuel*, Vol. 22, pp. 192-196, 1949.
- [37] S. W. Hong and A. E. Bergles, "Augmentation of laminar flow heat transfer in tubes by means of twisted-tape inserts," *Journal of Heat Transfer*, Vol. 98, pp. 251-256, 1976.
- [38] W. J. Marner and A. E. Bergles, "Augmentation of tubeside laminar flow heat transfer by means of twisted-tape inserts, static-mixer insert and internally-finned tubes " *Heat Transfer*, Vol. 2, pp. 583-588, 1978.
- [39] W. J. Marner and A. E. Bergles, "Augmentation of highly viscous laminar tubeside heat transfer by means of a twisted-tape insert and an internally finned tube," *Advances in Enhanced Heat Transfer*, Vol. 43, pp. 19-28, 1985.
- [40] Y. G. Nazmeev, "Intensification of convective heat exchange by ribbon swirlers in flow of anomalously viscous liquids in pipes," *Journal of Engineering Physics*, Vol. 37, pp. 910-913, 1979.
- [41] R. M. Manglik, A. E. Bergles and S. D. Joshi, "Augmentation of heat transfer to laminar flow of non-newtonian fluids in uniformly heated tubes with twisted-tape inserts," *Experimental Heat Transfer, Fluid Mechanics, and Thermodynamics*, pp. 676-684, 1988.

- [42] J. K. Dasmahapatra and M. Raja-Rao, "Laminar flow heat transfer to generalized power law fluids inside circular tubes fitted with regularly spaced twisted tape elements for uniform wall temperature condition," *Fundamentals of Heat Transfer in non-Newtonian Fluids*, Vol. 174, pp. 51-58, 1991.
- [43] S. K. Saha, U. N. Gaitonde and A. W. Date, "Heat transfer and pressure drop characteristics on laminar flow in a circular tube fitted with regularly spaced twisted-tape elements," *Experimental Thermal and Fluid Science*, Vol. 2, pp. 310-322, 1989.
- [44] W. J. Marner and A. E. Bergles, "Augmentation of highly viscous laminar heat transfer inside tubes with constant wall temperature," *Experimental Thermal and Fluid Science* Vol. 2, pp. 252-267, 1989.
- [45] P. Sivashanmham and S. Sundaram, "Improvement in performance of heat exchanger fitted with twisted tape," *Journal of Energy Engineering*, Vol. 125 (1), pp. 35-41, 1999.
- [46] S. Al-Fahed, L. M. Chamra and W. Chakroun, "Pressure drop and heat transfer comparison for both microfin tube and twisted-tape inserts in laminar flow," *Experimental Thermal and Fluid Science* Vol. 18, pp. 323-333, 1999.
- [47] S. K. Saha and A. Dutta, "Thermohydraulic study of laminar swirl flow through a circular tube fitted with twisted tapes," *Transaction of ASME Journal of Heat Transfer*, Vol. 123 (3), pp. 417-427, 2001.
- [48] A. Garcia, P. G. Vicente and A. Viedma, "Experimental study of heat transfer enhancement with wire coil inserts in laminar-transition-turbulent regimes at different prandtl numbers," *International Journal of Heat and Mass Transfer* Vol. 48, pp. 4640-4651, 2005.

- [49] A. Garcia, J. P. Solana, P. G. Vicente and A. Viedma, "Enhancement of laminar and transitional heat transfer in tubes by means of wire coil inserts," *International Journal of Heat and Mass Transfer*, Vol. 50, pp. 3176-3189, 2007.
- [50] S. I. Evans and R. J. Sarjant, "Heat transfer and turbulence in gases flowing inside tubes," *Journal of the Institute of Fuel*, Vol. 24, pp. 216-227, 1951.
- [51] F. Kreith and D. Margolis, "Heat transfer and friction in turbulent vortex flow," *Applied Scientific Research, Section A*, Vol. 8, pp. 457-473, 1959.
- [52] M. H. Ibragimov, E. V. Nomofelov and V. I. Subbotin, "Heat transfer and hydraulic resistance with swirl-type motion of liquid in pipes," *Teploenergetika*, Vol. 8 (7), pp. 57-60, 1961.
- [53] R. F. Lopina and A. E. Bergles, "Heat transfer and pressure drop in tape generated swirl flow of single-phase water," *Journal of Heat Transfer*, Vol. 91, pp. 434-442, 1969.
- [54] R. Brevi, M. Cumo, A. Palmieri and D. Pitimada, "Forced convection heat transfer and burn-out measurements with twisted tapes," *La Termotecnica*, Vol. 25 (12), pp. 619-625, 1971.
- [55] O. H. Klepper, "Heat transfer performance of short twisted tapes," *American Institute of Chemical Engineers*, Vol. 69, pp. 87-93, 1973.
- [56] N. V. Zozulya and I. Y. Shkuratov, "Effects of the length of a twisted-tape turbulence promoter and its initial twisting pitch on augmenting of heat transfer inside a tube," *Heat Transfer-Soviet Research*, Vol. 6 (6), pp. 98-100, 1974.

- [57] V. K. Migay and L. K. Golubev, "Friction and heat transfer in turbulent swirl flow with a variable swirl generator in a pipe," *Heat Transfer-Soviet Research*, Vol. 2 (3), pp. 68-73, 1970.
- [58] A. H. Algifri and R. K. Bhardwaj, "Prediction of heat transfer for decaying turbulent swirl flow in a tube," *International Journal of Heat and Mass Transfer*, Vol. 9, pp. 1637-1643, 1985.
- [59] D. Burfoot and P. Rice, "Heat transfer and pressure drop characteristics of short lengths of swirl flow inducers interspaced along a circular duct," *Chemical Engineering Research and Design*, Vol. 1, pp. 253-258, 1983.
- [60] Z. H. Ayub and S. F. Al-Fahed, "The effect of gap width between horizontal tube and twisted tape on the pressure drop in turbulent water flow," *International Journal of Heat and Fluid Flow*, Vol. 14 (1), pp. 64-67, 1993.
- [61] *Spirally corrugated tube*. Available from: https://www.google.co.uk/search?q=singlestart+spirally+corrugated+tube&biw=1366&bih=667&tbm=isch&source=lnms&sa=X&ei=kyEKVY2FDI2taaCagrAE&ved=0CAYQ_AUoAQ. [Accessed March 19, 2015].
- [62] V. Zimparov, "Enhancement of heat transfer by a combination of single-start spirally corrugated tubes with a twisted tape," *Experimental Thermal and Fluid Science*, Vol. 25, pp. 535-547, 2002.
- [63] A. Kumar and B. N. Prasad, "Investigation of twisted tape inserted solar water heaters - heat transfer, friction factor and thermal performance results," *Renewable Energy*, Vol. 19 (3), pp. 379-398, 2000.
- [64] P. Murugesan, K. Mayilsamy, S. Suresh and P. S. S. Srinivansan, "Heat transfer and pressure drop characteristics of turbulent flow in a tube fitted

- with trapezoidal-cut twisted tape insert," *International Journal of Academic Research*, Vol. 1, pp. 123-128, 2009.
- [65] P. Murugesan, K. Mayilsamy and S. Suresh, "Turbulent heat transfer and pressure drop in a tube fitted with square-cut twisted tape," *Chinese Journal of Chemical Engineering*, Vol. 18 (4), pp. 609-617, 2010.
- [66] S. W. Chang, Y. J. Jan and J. S. Liou, "Turbulent heat transfer and pressure drop in tube fitted with serrated twisted tape," *International Journal of Thermal Sciences*, Vol. 46, pp. 506-518, 2007.
- [67] S. Eiamsa-ard, S. Pethkool, C. Thianpong and P. Promvongse, "Turbulent flow heat transfer and pressure loss in a double pipe heat exchanger with louvered strip inserts," *International Communications in Heat and Mass Transfer*, Vol. 35, pp. 120-129, 2008.
- [68] S. Eiamsa-ard, C. Thianpong and P. Eiamsa-ard, "Turbulent heat transfer enhancement by counter/co-swirling flow in a tube fitted with twin twisted tapes," *Experimental Thermal and Fluid Science*, Vol. 34, pp. 53-62, 2010.
- [69] S. K. Saha, "Thermohydraulics of turbulent flow through rectangular and square ducts with axial corrugation roughness and twisted-tapes with and without oblique teeth," *Experimental Thermal and Fluid Science*, Vol. 34 (744-752), 2010.
- [70] A. W. Date and J. R. Singham, *Numerical prediction of friction and heat transfer characteristics of fully developed laminar flow in tubes containing twisted tapes*, ASME Paper No. 72-HT-17, 1972.
- [71] J. P. Du Plessis and D. G. Kroger, "Heat transfer correlation for thermally developing laminar flow in a smooth tube with a twisted-tape insert,"

International Journal of Heat and Mass Transfer, Vol. 30 (3), pp. 509-515, 1978.

- [72] J. P. Du Plessis and D. G. Kroeger, "Numerical prediction of laminar flow with heat transfer in a tube with a twisted tape insert ". in *International Conference on Numerical Methods in Laminar and Turbulent Flow*, pp. 775-785, 1983.
- [73] J. P. Du Plessis and D. G. Kroger, "Friction factor prediction for fully developed laminar twisted-tape flow," *International Journal of Heat and Mass Transfer*, Vol. 27 (11), pp. 2095-2100, 1984.
- [74] R. M. Manglik and A. E. Bergles, "Laminar flow heat transfer in a semi-circular tube with uniform wall temperature," *International Journal of Heat and Mass Transfer*, Vol. 31 (3), pp. 625-636, 1988.
- [75] A. W. Date and S. K. Saha, "Numerical prediction of laminar flow and heat transfer characteristics in a tube fitted with regularly spaced twisted-tape elements," *International Journal of Heat and Fluid Flow*, Vol. 11 (4), pp. 346-354, 1990.
- [76] A. W. Date and S. K. Saha, "Numerical prediction of laminar and heat transfer characteristics in a tube fitted with regularly spaced twisted-tape element," *International Journal of Heat and Fluid Flow*, Vol. 11 (4), pp. 346-354, 1990.
- [77] P. Sivashanmugam, S. Suresh and P. K. Nagarajan, "CFD simulation of heat transfer augmentation in a circular tube fitted with regularly spaced helical twist inserts in laminar flow under constant heat flux," *Advances in Energy Research*, pp. 478-473, 2006.

- [78] S. Ray and A. W. Date, "Friction and heat transfer characteristics of flow through square duct with twisted tape insert," *International Journal of Heat and Mass Transfer*, Vol. 46, pp. 889-902, 2003.
- [79] J. Guo, A. Fan, X. Zhang and W. Liu, "A numerical study on heat transfer and friction factor characteristics of laminar flow in a circular tube fitted with center-cleared twisted-tape," *International Journal of Thermal Sciences*, Vol. 50, pp. 1263-1270, 2011.
- [80] P. M. Kumar and R. V. Kumar, "Enhancement of heat transfer of laminar flow in a square ribbed duct with twisted tape," *International Journal of Engineering Science and Technology*, Vol. 4 (7), pp. 3450-3456, 2012.
- [81] X. Zhang, Z. Liu and W. Liu, "Numerical studies on heat transfer and flow characteristics for laminar flow in a tube with multiple spaced twisted tapes," *International Journal of Thermal Sciences*, Vol. 58, pp. 157-167, 2012.
- [82] A. W. Date, "Prediction of fully-developed flow in a tube containing a twisted-tape," *International Journal of Heat and Mass Transfer*, Vol. 17, pp. 845-859, 1974.
- [83] N. S. Gupte and A. W. Date, "Friction and heat transfer characteristics of helical turbulent air flow in annuli," *Transaction of ASME Journal of Heat Transfer*, Vol. 111, pp. 337-344, 1989.
- [84] R. J. Yadav and A. S. Padalkar, "CFD analysis for heat transfer enhancement inside a circular tube with half-length upstream and half-length downstream twisted tape," *Journal of Thermodynamics*, pp. 1-12, 2012.

- [85] Y. Chiu and J. Jang, "3D numerical and experimental analysis for thermal-hydraulic characteristics of air flow inside a circular tube with different tube inserts," *Applied Thermal Engineering*, Vol. 29, pp. 250-258, 2009.
- [86] S. Eiamsa-ard, K. Wongcharee and S. Sripattanapipat, "3-D numerical simulation of swirling flow and convective heat transfer in a circular tube induced by means of loose-fit twisted tapes," *International Communication in Heat and Mass Transfer*, Vol. 36, pp. 947-955, 2009.
- [87] Y. Cui and M. Tian, "Three-dimensional numerical simulation of thermohydraulic performance of a circular tube with edgefold-twisted-tape inserts," *Journal of Hydrodynamics*, Vol. 22 (5), pp. 662-670, 2010.
- [88] H. A. Mohammed, "Laminar mixed convection heat transfer in a vertical circular tube under buoyancy-assisted and opposed flows," *Energy Conversion and Management*, Vol. 49, pp. 2006-2015, 2008.
- [89] A. Ozsunar, S. Baskaya and M. Sivriogl, "Numerical analysis of Grashof number, Reynolds number and inclination effects on mixed convection heat transfer in rectangular channels," *International Communication in Heat and Mass Transfer*, Vol. 28 (7), pp. 985-994, 2001.
- [90] S. Piva, G. S. Barozzi and M. W. Collins, "Combined convection and wall conduction effects in laminar pipe flow: Numerical predictions and experimental validation under uniform wall heating," *Heat and Mass Transfer*, Vol. 30 (6), pp. 401-409, 1995.
- [91] W. L. Lin and T. F. Lin, "Unstable aiding and opposing mixed convection of air in a bottom-heated rectangular duct slightly inclined from the horizontal," *Transaction of ASME Journal of Heat Transfer*, Vol. 118 (1), pp. 47-55, 1996.

- [92] D. T. Chong, J. P. Liu and J. J. Yan, "Effects of duct inclination angle on thermal entrance region of laminar and transition mixed convection," *International Journal of Heat and Mass Transfer*, Vol. 51, pp. 3953-3962, 2008.
- [93] A. M. Abdelmeguid and D. B. Spalding, "Turbulent flow and heat transfer in pipes with buoyancy effects," *Journal of Fluid Mechanics*, Vol. 94, pp. 383-400, 1979.
- [94] B. Farouk and K. S. Ball, "Convective flows around a rotating isothermal cylinder," *International Journal of Heat and Mass Transfer*, Vol. 28, pp. 1921-1935., 1985.
- [95] C. T. Nguyen, G. Roy, M. A. Landry and S. E. B. Maiga, "Transient laminar mixed convection flow in a vertical tube under high Grashof number condition," *Transaction of ASME Journal of Heat Transfer*, Vol. 21 (3), pp. 133-139, 2004.
- [96] J. M. Jalil, Q. S. Mehdi and M. A. Ahmed, "Numerical study of laminar mixed convection heat transfer for flow over fixed and rotated cylinder," *Engineering Sciences*, Vol. 37 (1), pp. 83-96, 2010.
- [97] R. P. Benedict, *Fundermentals of pipe flow*, New York: John Wiley, 1980.
- [98] H. K. Versteeg and W. Malalasekera, *An introduction to computational fluid dynamics- the finite volume method*, 2nd ed, England: Pearson, 2007.
- [99] Fluent, *Fluent 6.3 user's guide*, , Lebanon, 2006.
- [100] W. M. Yan, "Mixed convection heat and mass transfer in inclined rectangular ducts," *International Journal of Heat and Mass Transfer*, Vol. 37 (13), pp. 1857-1866, 1994.

- [101] S. Baskaya, M. K. Aktas and N. Onur, "Numerical simulation of the effects of plate separation and inclination of heat transfer in buoyancy driven open channel," *Heat and Mass Transfer*, Vol. 35, pp. 273-280, 1999.
- [102] L. Davidson, "Calculation of the turbulent buoyancy driven flow in a rectangular cavity using an efficient solver," *Numerical Heat Transfer, Part A*, Vol. 18, pp. 129-147, 1990.
- [103] J. O. Hinze, *Turbulence*, New York: McGraw-Hill Publishing Co, 1975.
- [104] B. E. Launder and D. B. Spalding, *Lectures notes in mathematical models of turbulence*, London: Academic Press, 1972.
- [105] V. Yakhot and S. A. Orszag, "Renormalization group analysis of turbulence I: Basic theory," *Journal of Scientific Computing*, Vol. 1 (1), pp. 1-51, 1986.
- [106] A. J. Chorin, " Numerical solution of Navier-Stokes equations," *Mathematics of Computation*, Vol. 22, pp. 745-762, 1968.
- [107] J. P. Abraham, E. M. Sparrow and J. C. K. Tong, "Heat transfer in all pipe flow regimes: Laminar, transitional/intermittent and turbulent," *International Journal of Heat and Mass Transfer*, Vol. 52, pp. 557-563, 2009.
- [108] F. R. Menter, "Two-equation eddy-viscosity turbulence models for engineering applications," *The American Institute of Aeronautics and Astronautics*, Vol. 32 (8), pp. 1598-1605, 1994.
- [109] D. C. Wilcox, *Turbulence modeling for CFD*, La Canada, California: DCW Industries Inc, 1998.

- [110] P. H. Newell and A. E. Bergles, "Analysis of combined free and forced convection for fully developed laminar flow in horizontal tubes," *Transaction of ASME Journal of Heat Transfer*, Vol. 92, pp. 83-93, 1970.
- [111] C. Nonino and S. Del Giudice, "Laminar mixed convection in the entrance region of a horizontal rectangular duct," *International Journal of Numerical Methods in Fluids*, Vol. 12, pp. 33-48, 1991.
- [112] W. M. Kays and M. E. Crawford, *Convection heat and mass transfer*, 2nd ed, New York: McGrawHill, 1980.
- [113] H. Schlichting, *Boundary-layer theory*, 7th ed, New York: McGraw-Hill, 1979.
- [114] B. Kader, "Temperature and concentration profiles in fully turbulent boundary layers," *International Journal of Heat and Mass Transfer*, Vol. 24 (9), pp. 1541-1544, 1981.
- [115] R. F. Warming and R. M. Beam, "Upwind second-order difference schemes and applications in aerodynamic flows," *The American Institute of Aeronautics and Astronautics* Vol. 14, pp. 1241-1249, 1976.
- [116] C. T. Shaw, *Using computational fluid dynamics*, UK: Prentice Hall International Ltd., 1992.
- [117] S. V. Patankar and D. B. Spalding, " A calculation procedure for heat, mass and momentum transfer in three- dimensional parabolic flows," *International Journal of Heat Mass Transfer* Vol. 15, pp. 1787-1806, 1972.
- [118] D. F. Rogers, *Laminar flow analysis*: Cambridge University Press, 1992.
- [119] J. D. Anderson, *A history of aerodynamics and its impact on flying machines*: Cambridge University Press, 1997.

- [120] Gambit, *Gambit 2.4 user's guide*, Lebanon, 2006.
- [121] K. wongcharee and S. Eiamsa-ard, "Friction and heat transfer characteristics of laminar swirl flow through the round tubes inserted with alternate clockwise and counter-clockwise twisted-tapes," *International Communications in Heat and Mass Transfer*, Vol. 38, pp. 348-352, 2011.
- [122] P. Promvonge, "Thermal augmentation in circular tube with twisted tape and wire coil turbulent wire turbulators," *Energy Conversation and Management*, Vol. 49, pp. 2949-2955, 2008.
- [123] K. Wongcharee and S. Eiamsa-ard, "Heat transfer enhancement by twisted tapes with alternate-axes rectangular and trapezoidal wings," *Chemical Engineering and Processing*, Vol. 50, pp. 211 - 219, 2011.
- [124] B. R. Munson, T. H. Okiishi and W. W. Huebsch, *Fundamentals of fluid mechanics*, 6th ed, New Jersey: John Wiley & Sons, 2009.
- [125] F. P. Incropera, D. P. Dewitt, T. L. Bergman and A. S. Lavine, *Fundermentals of heat and mass transfer*, 6th ed, USA: John Wiley and sons, 2007.
- [126] M. Stoiber, C. Grasl, S. Pirker, L. Huber, P. Gittler and H. Schima, "Experimental validation of numerical simulations: A comparison of computational fluid dynamics and the oil film method," *International Journal of Artificial Organs* Vol. 30 (4), pp. 363 - 368, 2007.
- [127] B. Donevski and J. kulesza, "Friction in isothermal flow in tubes with twisted tapes," *Zeszyty Naukowe Politechniki Lodzkiej Mechanika*, Vol. 58 (358), pp. 5-25, 1980.

- [128] M. V. Casey, "Simulation of turbulent flows for industrial application: A fluid engineer's view," in *Advances in turbulence VI*, S. Garvrlakis, Editor. Kluwer Academic Publishers. pp. 157 - 162, 1996.
- [129] R. Narasimha, S. Rudra-Kumar, A. Prabhu and S. V. Kailas, "Turbulent flux events in a nearly neutral atmospheric boundary layer," *Philosophical Transactions of the Royal Society: Mathematical, Physical and Engineering Sciences*, Vol. 365 (1852), pp. 841-858, 2007.
- [130] M. Trevethan and H. Chanson, "Turbulence and turbulent flux events in a small estuary," *Environmental Fluid Mechanics* Vol. 10 (3), pp. 345-368, 2010.
- [131] P. Seemawute and S. Eiamsa-ard, "Thermohydraulics of turbulent flow through a round tube by peripherally-cut twisted tape with an alternate axis," *International Communication in Heat and Mass Transfer*, Vol. 37, pp. 652-659, 2010.
- [132] V. Gnielinski, "New equations for heat and mass transfer in turbulent pipe and channel flow," *International Chemical Engineering*, Vol. 16 (2), pp. 359-368, 1976.
- [133] G. J. Kidd, "Heat transfer and pressure drop for nitrogen flowing in tubes containing twisted tapes," *American Institute of Chemical Engineers*, Vol. 15, pp. 581-585, 1969.
- [134] M. R. Drizius, R. K. Shkema and A. A. Shlanciauskas, "Heat transfer in a twisted stream of water in a tube," *International Chemical Engineering*, Vol. 20, pp. 486-489, 1980.

- [135] B. S. Petukhov, "Heat transfer and friction in turbulent pipe flow with variable physical properties " in *Advances in heat transfer*, J.P. Hartnett and T.F. Irvine, Jr., Editors. Academic Press: New York. pp. 503-564, 1970.
- [136] Tecplot, *Tecplot 360 user's manual*, Bellevue, WA, 2009.
- [137] C. Thianpong, P. Eiamsa-ard and S. Eiamsa-ard, "Heat transfer and thermal performance characteristics of heat exchanger tube fitted with perforated twisted-tapes," *Heat and Mass Transfer*, Vol. 48, pp. 881-892, 2012.
- [138] P. R. Lang and F. S. Lombargo, *Atmospheric turbulence, meteorological modeling and aerodynamics*: Nova Science, 2010.
- [139] H. Blasius, "Grenzschichten in flüssigkeiten mit kleiner reibung," *Zeitschrift für angewandte Mathematik und Physik*, Vol. 56, pp. 1-37, 1908 (English translation).
- [140] W. R. Gambill and R. D. Bundy, "An investigation of the present status of swirl flow heat transfer," *American Society of Mechanical Engineer*, Vol. 62, 1962.
- [141] *Copper pipe sizes*. Available from: <http://www.screwfix.com/p/copper-pipe-22mm-x-2m/58277>. [Accessed December 27, 2014].
- [142] *Applications of transitional flows*. Available from: <https://www.craft-tech.com/applications/research/transitional-flows/>, . [Accessed March 22, 2015].
- [143] K. Y. Chien, "Prediction of channel and boundary layer flows with a low-Reynolds-number turbulence model," *The American Institute of Aeronautics and Astronautics*, Vol. 20, pp. 33-38, 1982.

- [144] A. Garcia, J. P. Solana, P. G. Vicente and A. Viedma, "Flow pattern assessment in tubes with wire coils inserts in laminar and transition regimes," *International Journal of Heat and Fluid Flow*, Vol. 28, pp. 516-525, 2007.
- [145] L. Tam and A. J. Ghajar, "Effect of inlet geometry and heating on the fully developed friction factor in the transition region of a horizontal tube " *Experimental Thermal and Fluid Science*, Vol. 15 (1), pp. 52-64, 1997.
- [146] D. D. Joye, J. P. Bushinsky and P. E. Saylor, "Mixed convection heat transfer at high Grashof number in a vertical tube," *Industrial and Engineering Chemistry Research*, Vol. 28 (12), pp. 1899-1903, 1989.
- [147] G. P. Paterson and A. Ortega, "Thermal control of electronic equipment and devices," *Advances in Heat Transfer*, Vol. 20, pp. 181-314., 1990.
- [148] S. Saha, G. Saha , M. Ali and Q. Islam, "Combined free and forced convection inside a two-dimensional multiple ventilated rectangular enclosure," *ARPJ Journal of Engineering and Applied Sciences*, Vol. 1 (3), pp. 23-35, 2006.
- [149] E. R. G. Eckert and A. J. Diaguila, "Convective heat transfer for mixed, free and forced flow through tubes," *ASME Transaction Journal of Heat Transfer*, Vol. 76, pp. 497-504, 1954.
- [150] M. Wang, T. N. Tsuji and Y. Nagano, "Mixed convection with flow reversal in the thermal entrance region of horizontal and vertical pipes," *International Journal of Heat and Mass Transfer*, Vol. 37 (15), pp. 2305-2319, 1994.

- [151] Y. Y. Hsu and J. M. Smith, "The effect of density variation on heat transfer in the critical region," *Transaction of ASME Journal of Heat Transfer*, Vol. 83, pp. 176-182, 1961.
- [152] M. J. Watts and C. T. Chou, "Mixed convection heat transfer to supercritical pressure water." in *7th International Heat Transfer Conference*, Munich, 1982.
- [153] J. R. Maughan and F. P. Incropera, "Experiments on mixed convection heat transfer for airflow in a horizontal and inclined channel," *International Journal of Heat and Mass Transfer*, Vol. 30 (7), pp. 1307-1318, 1987.
- [154] G. Wickern, "Mixed convection from an arbitrarily inclined semi-infinite flat plate - I. The influence of the inclination angle," *International Journal of Heat and Mass Transfer*, Vol. 34 (8), pp. 1935-1945, 1991.